

Quantitative Blood Flow  
as assessed by  
Intravascular Ultrasound

The studies presented in this dissertation were financially supported by the Interuniversity Cardiology Institute of the Netherlands (ICIN 18 and 32).

Front cover picture: Paula C. Delfos, AV Thorax, Rotterdam

ISBN : 90-9016030-2

©2002 Fermín A. Lupotti

# Quantitative Blood Flow as assessed by Intravascular Ultrasound

Kwantitatieve Bloedstroming  
waargenomen met  
Intravasculair Ultrageluid

PROEFSCHRIFT

ter verkrijging van de graad van doctor  
aan de Erasmus Universiteit Rotterdam  
op gezag van de rector magnificus  
Prof.dr.ir. J.H. van Bommel  
en volgens het besluit van het College voor Promoties

De openbare verdediging zal plaatsvinden op  
woensdag 11 September 2002 om 11.45 uur

door  
**Fermín Armando Lupotti**  
geboren te Santa Fe, Argentina

## PROMOTIECOMMISSIE

**PROMOTOREN:** Prof.dr.ir. N. Bom  
Prof.dr.ir. A.F.W. van der Steen

**OVERIGE LEDEN:** Prof.dr. P.W. Serruys  
Prof.dr. J.R.T.C. Roelandt  
Prof.dr.ir. A.P.G. Hoeks  
Prof.dr. P.D. Verdouw

Financial support by the Interuniversity Cardiology Institute of the Netherlands (ICIN) and the Netherlands Heart Foundation (NHS) for the publication of this thesis is gratefully acknowledged.

The financial contributions of the Interuniversity Cardiology Institute of the Netherlands (ICIN), Dutch Technology Foundation (STW) and JOMED Inc. are gratefully acknowledged.

Por María, Lucía  
and María Constanza

A mis padres y hermana  
Fermín, Rosa María e Inés María



# Contents

1	Introduction	1
1.1	The Heart: coronary arteries	1
1.2	Methods for assessing arteries	2
1.2.1	Imaging	2
1.2.2	Functional evaluation	6
1.3	Outline of the thesis	8
2	Flow Estimation using an Intravascular Imaging Catheter: <i>General Introduction</i>	11
2.1	Introduction	12
2.2	Methods	13
2.2.1	Decorrelation of blood echoes	13
2.2.2	Decorrelation-to-flow quantification	14
2.3	Results	15
2.3.1	Influence of catheter	16
2.3.2	Flow estimation using an array transducer	19
2.3.3	Automated boundary detection	20
3	Decorrelation of single Red Blood Cells	21
3.1	Introduction	22
3.2	Methods	24
3.2.1	IVUS transducer	24
3.2.2	Computer modeling	24
3.2.3	Statistical properties of the scattering medium	27
3.2.4	Decorrelation curves from beam theory	29
3.2.5	Decorrelation from point-scatterer media	29
3.3	Results and comparisons	29
3.4	Discussion	32
3.5	Conclusions	34

<b>4</b>	<b>Decorrelation of Aggregates of Red Blood Cells</b>	<b>35</b>
4.1	Introduction . . . . .	36
4.2	Methods . . . . .	38
4.2.1	IVUS transducer . . . . .	38
4.2.2	Computer modeling . . . . .	38
4.2.3	Statistical properties of the scattering medium . . .	41
4.3	Results . . . . .	42
4.4	Discussion . . . . .	44
4.5	Conclusions . . . . .	46
<b>5</b>	<b>Effects of Different Blood Velocity Profiles on the Correlation-based method</b>	<b>47</b>
5.1	Introduction . . . . .	48
5.2	Methods . . . . .	50
5.2.1	IVUS transducer . . . . .	50
5.2.2	Computer modeling . . . . .	50
5.2.3	Statistical properties of the scattering medium . . .	53
5.3	Results . . . . .	54
5.4	Discussion . . . . .	55
5.5	Conclusions . . . . .	60
<b>6</b>	<b>Effects of Aggregation of Red Blood Cells and Linear Velocity Gradients on the Correlation-based method:</b>	
	<i>In vitro</i> validation	<b>61</b>
6.1	Introduction . . . . .	62
6.2	Materials and Methods . . . . .	63
6.2.1	Blood samples . . . . .	63
6.2.2	Blood tests . . . . .	64
6.2.3	Experimental setup . . . . .	64
6.2.4	Protocol for the experiments . . . . .	66
6.2.5	Signal processing . . . . .	66
6.3	Outline of the results . . . . .	67
6.4	Results . . . . .	68
6.5	Discussion . . . . .	71
6.6	Conclusions . . . . .	74
<b>7</b>	<b>Line Spread Function as Calibration for the Correlation-based method</b>	<b>75</b>
7.1	Introduction . . . . .	76
7.2	Methods . . . . .	76
7.2.1	IVUS transducer . . . . .	76
7.2.2	Simulated LSF . . . . .	77



7.2.3	Experimental setup . . . . .	78
7.2.4	Experimental LSF and RF signals . . . . .	78
7.2.5	Second-order statistical properties of the experi- mental RF signals . . . . .	78
7.3	Results . . . . .	79
7.4	Discussion . . . . .	81
7.5	Conclusions . . . . .	81
<b>8</b>	<b>Dynamic Noise Correction for IVUS Blood Flow:</b> Methods and Numerical validation	<b>83</b>
8.1	Introduction . . . . .	84
8.2	Methods . . . . .	85
8.2.1	The IVUS array transducer . . . . .	85
8.2.2	Computer modeling . . . . .	86
8.2.3	Calibration method . . . . .	87
8.2.4	Statistical properties of the scattering medium . . . . .	87
8.2.5	Proposed method for noise correction . . . . .	88
8.3	Outline of the simulation experiments . . . . .	88
8.4	Results . . . . .	89
8.5	Discussion . . . . .	92
8.6	Conclusions . . . . .	95
<b>9</b>	<b>Quantitative IVUS Blood Flow:</b> Validation <i>in vitro</i> , in animal and in patient	<b>97</b>
9.1	Introduction . . . . .	98
9.2	Methods . . . . .	99
9.2.1	IVUS transducer . . . . .	99
9.2.2	Blood preparation . . . . .	100
9.2.3	<i>In vitro</i> setup for blood flow measurements . . . . .	100
9.2.4	Calibration method . . . . .	101
9.2.5	Noise correction method . . . . .	101
9.2.6	Ring-down obscuring . . . . .	102
9.2.7	Compensation for ring-down obscuring . . . . .	102
9.2.8	<i>In vitro</i> blood flow measurements . . . . .	102
9.2.9	In animal blood flow measurements . . . . .	103
9.2.10	In patient CFR measurements . . . . .	104
9.3	Results . . . . .	104
9.4	Discussion . . . . .	108
9.5	Conclusions . . . . .	111

<b>10 Coronary Flow Reserve versus Geometric Measurements of Coronary Dimensions</b>	<b>113</b>
10.1 Introduction	114
10.2 Rationale of coronary flow reserve	116
10.2.1 Induction of maximal hyperemia	117
10.2.2 Methods of measuring coronary flow reserve	118
10.2.3 Perfusion imaging and post-stenotic coronary blood flow	119
10.2.4 Variations in normal coronary vasodilatory reserve	120
10.2.5 Relative coronary flow reserve	121
10.3 The fractional coronary flow reserve	121
10.3.1 Clinical significance of pressure gradients	122
10.3.2 Limitations of $FFR_{myo}$	123
10.4 Optimization of a percutaneous intervention	123
10.5 Future directions	127
10.6 Conclusions	129
<b>11 Discussion and Conclusions</b>	<b>131</b>
11.1 Discussion	131
11.2 Computer simulations	131
11.3 <i>In vitro</i> experiments	132
11.4 In animal experiments	133
11.5 In patient recordings	133
11.6 Limitations and Future directions	134
11.7 Conclusions	135
<b>A Derivation of the Reference Curves</b>	<b>137</b>
<b>B The Fisher-Z transform</b>	<b>141</b>
<b>Bibliography</b>	<b>143</b>
<b>Summary</b>	<b>171</b>
<b>Samenvatting</b>	<b>175</b>
<b>Acknowledgements</b>	<b>179</b>
<b>Curriculum Vitae</b>	<b>183</b>
<b>List of Publications</b>	<b>185</b>





# Chapter 1

## Introduction

### 1.1 The Heart: coronary arteries

The human circulatory system is the transport system that supplies nutrients and oxygen ( $O_2$ ) to the tissues, returns carbon dioxide ( $CO_2$ ) to the lungs and other products of metabolism to the kidneys, regulates the body temperature and distributes hormones and other agents to regulate cell function. The myocardium is supplied with blood through the coronary arteries to fulfill its function. When the blood supply to a portion of the myocardium is reduced, the cells are partially deprived of oxygen, which is called ischemia. If the blood supply is severely compromised, muscle cells die and the region becomes necrotic ending in a myocardial infarction. The lack of oxygen can be caused by coronary artery diseases such as stenosis (reduction of the free lumen of an artery by an atherosclerotic plaque).

Currently, many interventional techniques have been developed to treat coronary artery diseases. Most of them are based on increasing the free lumen to reestablish the blood flow to the myocardium (Waller 1989). Angioplasty balloons are used to stretch the lumen area or to crack a calcified part of the vessel wall. However, restenosis of the vessel can occur at a rate of about 30% after angioplasty, which can end in a new obstruction in the vessel (Serruys et al. 1998b). At this point, stents become an important technique to avoid restenosis. Stents are metallic wire frames folded around a balloon. When the balloon is expanded against the vessel wall, the balloon is then deflated and the stent is deployed keeping the vessel lumen open. Although restenosis after stent implantation can occur, the rate of restenosis is low (10-30%) (Serruys et al. 1998b). Brachytherapy is a possible technique to reduce restenosis; radioactive sources are moved in the treatment site to reduce pathologic process (King III et al. 1998). Using radioactive (Wardeh et al. 2002) stents can reduce the restenosis. However, radioactive stents could not prevent from the restenosis at the edge of

the implanted stent (Wardeh et al. 2002). First trials using eluting stents for local drug delivery in patients to prevent restenosis showed a rate of restenosis of 13% (Rensing et al. 2001; Serruys et al. 1996). However, the latest results from the randomized study RAVEL, using the rapamycin coated BX velocity balloon expandable stent, showed at six months' follow up a rate of restenosis of 0% (Serruys et al. 2002). Intravascular sonotherapy was found to decelerate cellular proliferation and decrease in-stent hyperplasia (Fitzgerald et al. 2001). In other techniques such as laser (Hamburger et al. 1997), atherectomy and spark-erosion (Slager et al. 1985), the obstruction is removed. When removing the obstruction, the particles are collected through the catheter. However, before and after any intravascular intervention, the key factors for making decisions are based on imaging of the artery lumen and the evaluation of a functional parameter of the myocardium such as blood flow reserve measured by Doppler wire, pressure devices, thermodilution or IVUS blood flow.

## 1.2 Methods for assessing arteries

### 1.2.1 Imaging

#### Angiography

Coronary artery diseases are assessed by measurement of lumen diameter and cross-sectional area by coronary angiography. A commonly used variable used in the assessment of atherosclerosis is percentage of stenosis. However, the arterial lumen often includes noncircular cross-section areas at the site of the stenoses introducing an image projection angle-dependent error. Digital angiography can be used to measure lumen volume by geometric and video densitometry techniques. The geometric techniques consist of vessel diameter measurement and arterial length measurement by 3D reconstruction of the arterial center line (Wellnhofer et al. 1999); these techniques require biplane images and assume a circular or elliptical cross section, which sometimes does not apply in the presence of obstructive atherosclerosis (Thomas et al. 1986). Furthermore, since digital angiography can detect only the free lumen of a vessel by means contrast agent, any positive remodeling of the artery cannot be observed (Sgura & Di Mario 2001).

#### Magnetic Resonance Imaging

The understanding that many nuclei possess an angular momentum and a magnetic moment -that they behave like small, charged, spinning spheres- was first observed in 1924, when Pauli demonstrated the existence of hyperfine splitting in atomic spectra. The full potential of this technique went largely unnoticed until several decades. Later, it was demonstrated that the precise frequency at which magnetic resonance occurs is a function of the specific chemical environment in

which the nuclei reside. This behavior, called chemical shift, makes it possible to use nuclear magnetic resonance measurements as a nondestructive probe of chemical structure. Jasper Johns who had measured nuclear magnetic resonance from live animals proposed the first human applications in 1967. However, it was Lauterbur who produced the first images of an inhomogeneous object (two tubes of water) providing the first demonstration of magnetic resonance imaging (MRI).

MRI has the potential to non-invasively image the human coronary artery wall and define the degree and nature of coronary artery diseases (Fayad et al. 2000). It provides morphological features of atherosclerotic and normal human coronary arteries. Recent *in vivo* studies of atherosclerotic plaques in animal models (Fayad et al. 1998a), carotid arteries (Toussaint et al. 1996), and aorta (Fayad et al. 1998b) demonstrate that high-resolution MRI can non-invasively image the artery wall and assess plaque composition. The major difficulties of MR coronary wall imaging are due to the combination of cardiac and respiratory motion artifacts, the nonlinear course of the coronary arteries, and their relatively small size and location (Worthley et al. 2000). Thus, an effective *in vivo* MRI technique for coronary artery imaging must overcome artifacts related to blood flow and cardiac, respiratory, and vessel wall motion to achieve high-resolution and high-contrast imaging.

### Computed Tomography (CT) and Electron Beam CT (EBCT)

Cardiac imaging is a highly demanding application for any cross sectional imaging modality. For the last decade CT investigation of the heart was the domain of electron beam CT (EBCT) exclusively. In these cardiac CT scanners, electrons are accelerated in a vacuum tunnel and focused on four 210 tungsten target rings underneath the patient. X-ray radiation is emitted, passing through the patient, and is detected by two 240 detector rings above the patient. The design of these scanners was primarily chosen to allow for perfusion and cine imaging of the myocardium at eight levels combined with a minimal exposure time of 50 ms per slice. Morphological assessment of cardiac structures became possible with EBCT by a slice-by-slice acquisition and prospective ECG triggering at 100 ms temporal resolution. Nevertheless, ECG triggering is of limited use in patients with arrhythmia. A technique using the retrospective ECG-gating is able to overcome this limitation.

Unenhanced scans of the heart clearly display any calcifications of the coronary artery tree. As arterial calcifications almost always represent atherosclerosis, EBCT was shown to be the most sensitive tool to detect coronary atherosclerosis and is even superior to fluoroscopy (Agatston et al. 1990) for this application. Quantitative assessment of coronary calcium was first introduced by Agatston et al. (1990). Contrast-enhanced EBCT has been reported to permit

visualization of the coronary arteries and detection of significant stenoses (Budoff et al. 1999). In a blinded study of patient with and without coronary anomalies, Ropers et al. (2001) demonstrated that contrast-enhanced EBCT permits reliable detection and classification of anomalous coronary arteries. Three-dimensional reconstructions, which can be generated based on the volume data set acquired by EBCT, provided clear visualization of the anomalous vessels. De Feyter et al. (2000) performed a study on non-invasive coronary imaging with electron beam computed tomography and magnetic resonance imaging. Although electron beam computed tomography seemed more robust than magnetic resonance for visualizing coronary arteries and venous bypass, magnetic resonance is superior for study left ventricular function and perfusion and for measuring blood flow (still in early phase of development).

### Intravascular Ultrasound (IVUS)

Arteries can be imaged from outside the body or from inside the lumen. Carotid arteries are accessible for ultrasound since they are located just under the skin. Using a 5 MHz ultrasound transducer, quantitative information about the vessel lumen and wall (*e.g.* plaque) can be obtained. However, small arteries -that are not superficial- such as coronary arteries must be imaged from inside the lumen. The movement of the heart may introduce distortions in the images and complicate the diagnosis. IVUS is a technique to acoustically survey arteries

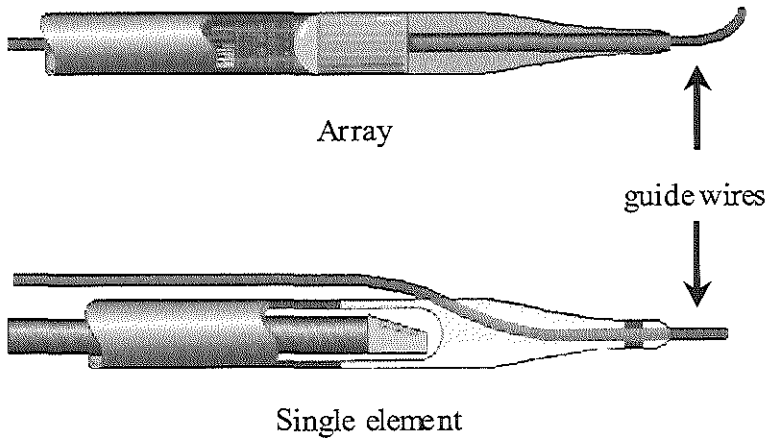


**Figure 1.1:** Intravascular Ultrasound catheters. Top: electronically switched phased array catheter consisting of 64 elements (JOMED Inc., Rancho Cordova, CA, USA). Bottom: mechanical rotating single-element catheter



from within the lumen by means of a catheter. Cross-sectional images of a vessel are generated by sweeping the ultrasound beam sequentially in a 360 scan angle. Since the ultrasound transducer is closer to the imaging target, high frequencies can be used and thus high-resolution images from the vessel lumen and wall can be obtained. However, increasing the used frequency will cause increase of backscatter signal from blood, which decreases delineation between lumen and vessel wall.

Currently, two types of IVUS catheters to generate real-time imaging are commercially available a mechanical and an electronic catheter (Fig. 1.1). The mechanical system, consist of a rotating a single element transducer mounted on a flexible drive shaft (Fig. 1.1, bottom). Alternatively, a rotating mirror can be used to direct the ultrasound beam to all angular positions. An advantage of this system is that the water path between the transducer and the dome minimizes the ring-down effect and interference in the extreme near field. However, the mechanical nature of these two methods may introduce image artifacts caused by non-uniform rotations. This occurs especially when the catheter is bended in a severely curved vessel such as coronary arteries. A disadvantage of mechanical system is that catheters have to be advanced over a guide-wire that goes outside the catheter introducing a strong reflection with a distal shadowing of part of the image (Bom et al. 1972). With the advances in integrated circuits, it was possible to construct an IVUS array catheter small enough to be situated in coronary arteries (Fig. 1.1, top) (Bom et al. 1989; Eberle 1997). The ultrasound beam is then steered electronically to produce a cross-sectional image of the vessel. This type of IVUS catheter does not present any image distortion caused by rotation as mentioned above.

For many years, IVUS has been used for various clinical purposes as it provides real-time cross-sectional images of blood vessels at high spatial resolution (Roelandt et al. 1993; Siegel 1998). As an imaging tool, IVUS allows to measure the lumen and vessel wall (von Birgelen et al. 1998), to study the progression of arterioscleroses and restenosis (Di Mario et al. 1998), to evaluate intravascular interventions (de Jaegere et al. 1998) such as Percutaneous Transluminal Coronary Angioplasty (PTCA) (Serruys et al. 1998b), stents (Rensing et al. 2001), and atherectomy (Mehran et al. 2000). IVUS can be combined with angiography in order to produce a true 3D reconstruction of the lumen of a coronary artery, called ANGUS (Slager et al. 2000). A biplane angiography is used to produce the 3D shape of the coronary artery whereas the IVUS images are used to trace the lumen contours. IVUS has also been focused on obtaining information concerning the acoustic and elastic properties of the vessel wall and plaque for the purpose of vascular tissue characterization (Céspedes et al. 1999; de Korte et al. 2000).

## 1.2.2 Functional evaluation

### Doppler

An observer moving toward a sound source hears a tone with higher frequency than at rest; if the observer moves away from the sound source he hears a tone of lower frequency. This phenomenon was described by Christian Johan Doppler and is called Doppler effect (Doppler 1843). This principle is applied to measure blood velocity using a piezoelectric crystal that emits and receives high frequency sound on the tip of a catheter. Doppler catheters have been used extensively in cardiac catheterization laboratories, mainly for assessing relative changes of coronary velocities. Doppler has several advantages for the assessment of the coronary circulation. Doppler catheters directly measure the red blood cell velocity and since the catheter is small, measurements of blood velocity can be performed in epicardial vessels.

Volumetric blood flow can be measured using a Doppler catheter (volume flow = cross-sectional area  $\times$  blood velocity), however, the cross-sectional area of the vessel needs to be measured by a method such as IVUS or angiography. Intracoronary Doppler catheters have also several limitations. The angle between the ultrasound beam and the main stream of blood flow is critical for the estimation of flow velocity and may be affected by the stenoses geometry as well as by the intracoronary velocity profile (Kilpatrick & Webber 1986). The catheter itself changes the velocity profile, and this velocity profile is not constant during the pulsatile-flow condition of a cardiac cycle. This is of concern if velocities close to the transducer have to be measured. With the advent of the Doppler guidewire, a 0.0355 cm in diameter, 175 cm long, flexible and steerable guidewire with handling characteristics similar to traditional angioplasty guidewires, the disturbance of the flow profile distal to its tip when placed within a vessel is minimized. The Doppler guidewire can also be passed into small coronary arteries or stenoses without creating significant stenosis.

### Pressure

Pressure-wires are used to sense the blood pressure in the spot where the treatment is about to happen. The sensor, a piezo resistive pressure sensor, is located just before the tip of the wire proximal to a radiopaque tip. The signal is transmitted to a small interface, which can be then connected to an ordinary pressure monitoring system in the cardiac catheterization laboratory. Since pressure wires are of very small diameters (0.014 in), the pressure monitoring guidewire can be advanced through a stenotic segment (Briguori et al. 2001). Pressure measurements proximal and distal to the stenotic lesion can be performed at rest and during maximal hyperemia induced by the injection of adenosine. Fractional

Flow Reserve (FFR) can be then calculated as the ratio between the pressure at rest and at peak hyperemia; which can be obtained from the distal and proximal part of the lesion.

De Bruyne et al. (2000) derived and validated in animals 2 equations to calculate FFR by means of pressure measurements. The equations used the hyperemic coronary pressure measurements and the interaction between stenoses. Recently, Pijls (2000) developed and experimentally validated in humans two equations for determining the FFR of individual stenosis; these equations use the hyperemic coronary pressure measurements and account for interactions among stenoses. This approach facilitates the selection of lesions for PTCA and assesses the functional result of each intervention, thereby minimizing unnecessary additional procedures on hemodynamically insignificant lesions or diffuse disease, which increases the risk of complications or restenosis without patient benefit.

### **Thermodilution**

The method for measuring blood flow is derived from earlier techniques using indicator dye-dilution. In the dye dilution technique, a green dye is injected by a catheter into the artery, where it mixes with the blood. Its concentration is then measured by a photo-absorbance detector using a catheter tipped with a light and the photo detector. The faster the blood flow, the more diluted the dye becomes, and so the lower the absorbance measured. Thermodilution works on a similar principle, except the fluid injected is saline at a significantly different temperature than the blood (Meier & Zierler 1954). The temperature of the downstream blood is then measured to determine the dilution of the cold saline, and therefore measure blood flow. Because the bolus of tracer is injected and disperses within the blood volume, the concentration of tracer at the downstream sample point varies with time following the injection.

Typically, the tracer first appears at the sample point at the time following injection point and the sample point, and the fluid flow rate. The concentration of the tracer at the sample point increases rapidly and then decreases exponentially as the injectate bolus passes the sampling point. An exponential decay is observed due to the fact that the injectate bolus does not remain as a lump, but it mixes and dilutes over a longer path due to the fluid flow. For accurate thermodilution measurements there should be a large temperature difference between the injectate and the blood, the injectate must mix thoroughly within the flow stream, and the injectate must be injected quickly and consistently so the fluid enters as a bolus of liquid. Coronary thermodilution to assess flow reserve has been experimentally validated (de Bruyne et al. 2001). Cardiac output, defined as the volume at which the heart pumps blood, can also be measured by thermodilution (Ganz et al. 1971a; Nishikawa & Dohi 1993).

## IVUS Flow

Radio Frequency (RF) data processing has significantly enhanced the potential of IVUS (van der Steen et al. 1998a). IVUS gives not only morphological information of coronary artery but also functional assessment such as blood flow (Li et al. 1998b; Carlier et al. 1998d), palpography (Céspedes et al. 2000; Doyley et al. 2001) and elastography (Céspedes 1993; de Korte et al. 1998), and characterization of plaques components (Bridal et al. 1997a; Spencer et al. 1997b; de Korte et al. 2000). This is an advantage since all functional evaluations can be performed with only one device. Current methods to assess blood flow using intravascular techniques include Doppler processing and time-domain correlation techniques (Chou et al. 1994; Isner et al. 1993). IVUS has been applied to measure qualitatively (Crowe et al. 2000) and quantitatively (Li et al. 1998b) blood flow velocity and volumetric flow. For intravascular volumetric blood flow measurements, the cross-sectional vessel area and the blood velocity must be assessed simultaneously. Using an IVUS catheter can solve this. Recently, Li et al. (1997, 1998b) proposed to measure blood velocity and quantify intravascular volume flow using a correlation-based method in a burst of ultrasound beam that were transmitted in the same direction. The measurements were performed from cross-sectional IVUS RF signals and the results showed this method capable to measure blood velocity profiles and volumetric blood flow. Céspedes et al. (1998a) have presented initial *in vivo* evaluations of blood flow assessment based on correlation with a rotating single-element catheter.

### 1.3 Outline of the thesis

The aim of the present study was to develop the correlation-based method for quantitative blood flow for intravascular ultrasound purposes. The feasibility of the technique was studied by means of computer simulations, *in vitro* and in animal measurements, and in patient validation. A general overview in IVUS flow is presented (Chapter 2). Computer simulations were implemented for the study of the decorrelation characteristics of the ultrasound beam from the IVUS array catheter. First, blood was mimicked as a collection of randomly located point scatterers as single red blood cells (Chapter 3). Second, strings of point scatterers were used as aggregates of red blood cell (Chapter 4). Different blood flow profiles were also studied by means of computer simulation (Chapter 5). *In vitro* measurements were performed to validate the results presented in Chapter 3, 4 and 5 (Chapter 6). *In vitro* measurements of the ultrasound beam of the IVUS array catheter were performed to calibrate the correlation-based method for quantitative blood flow method (Chapter 7). Noise in the radio frequency signals is of major importance in the correlation-based blood velocity method; therefore, a technique was needed to correct the correlation coefficients for noise. Numerical

validation, and *in vitro* and in animal measurements were performed to validate the correlation-based method for blood velocity estimation and quantitative volume blood flow, and the new technique that corrects for noise (Chapter 8 and 9). Finally, a functional parameter such as coronary flow reserve (CFR, ratio between high flow and low flow) of the heart was evaluated in patients (Chapter 9). In another series of patients CFR was compared with Geometric Measurements of Coronary Dimensions (Chapter 10).



## Chapter 2

# Flow Estimation using an Intravascular Imaging Catheter: *General Introduction*

### Abstract

*Coronary flow assessment can be useful for determining the hemodynamic severity of a stenosis and evaluate the outcome of interventional therapy. We developed a method for measuring the transverse flow through the imaging plane of an intravascular ultrasound catheter. This possibility has raised a great clinical interest since it permits simultaneous assessment of vessel geometry and function with the same device. Furthermore it should give more accurate information than combination devices, because lumen diameter and velocity are determined at the same location. Flow velocity is estimated, based on correlation estimation from sequences of radiofrequency (RF)-traces acquired at (nearly) the same position. Signal gating yields a local estimate of the velocity. Integrating the local velocity over the lumen gives the quantitative flow. This principle has been calibrated and tested through computer modeling, in vitro measurements using a flow phantom and in vivo experiments in a porcine animal model, and validated against a Doppler flowwire in humans. Originally the method has been developed and tested for a rotating single element device. Currently the method is being developed for an array system. The great advantage of an array over the single element approach would be that*

---

based on the Publication: "Flow estimation using an intravascular imaging catheter" by Antonius F.W. van der Steen, E. Ignacio Céspedes, Stephane G. Carlier, Frits Mastik, Fermín A. Lupotti, Jerome M.G. Borsboom, Wenguang Li, Patrick W. Serruys and Nicolaas Bom, *Ultrasonics*; 2000: 38(1-8): 363-368.

*the transducer has no intrinsic motion. This intrinsic motion sets a minimal threshold in the detectable velocity components. Although the principle is the same, the method needs some adaptations through the inherent different beamforming of the transducer.*

## 2.1 Introduction

Currently, IVUS is the only clinically available technique, capable of providing real time cross-sectional images *in vivo*. It delivers information that is not available from X-ray angiography. Since the number of available interventional techniques for treatment of atherosclerotic luminal narrowing increases, specific diagnostic information that can aid in the selection becomes increasingly important. For this reason, IVUS is more and more routinely used for guiding interventional procedures (Baptista et al. 1996) and for studying the mechanisms for restenosis (Mintz et al. 1996). In the last couple of years the possibilities to access a sufficient amount of RF data at adequate speed have improved significantly. This has given the possibility to study IVUS data in a totally different way (Bom et al. 1998; van der Steen et al. 1998a). In the traditional way the emphasis was always on imaging itself while RF-analysis also allows tissue characterization (Spencer et al. 1997a; Bridal et al. 1997b), elasticity imaging (de Korte et al. 1998; de Korte 1999; Céspedes et al. 1997a; van der Steen et al. 1998b), flow estimation and enhanced boundary detection. Assessment of blood flow has long been recognized as an important approach to evaluate the functional status of a diseased artery. Intracoronary Doppler is a conventional ultrasonic method for measurement of blood velocities and has been applied for coronary flow reserve assessment and to evaluate the severity of coronary lesion (Doucette et al. 1992; Carlier et al. 1998c). The use of Doppler velocimetry alone, however, does not allow direct measurement of flow volume. For quantitative measurement of flow volume, the vessel cross-sectional area and the blood velocity must be assessed coincidentally in time and space. Intravascular ultrasound (IVUS) is a tomographic imaging technique that allows accurate measurement of the vessel cross-sectional area, irrespective of vessel geometry (Di Mario et al. 1992). Several studies have demonstrated the feasibility of simultaneous use of intracoronary Doppler for velocity measurement and IVUS imaging for area measurement to estimate blood flow (Chou et al. 1994). One potential limitation of this approach is that the flow volume is estimated from the mean Doppler velocity with an assumed velocity profile. Additionally, the simultaneous use of multiple ultrasound transducers could cause possible interference between devices, for instance, cross-talk between the Doppler and IVUS transducer (Isner et al. 1993). A unique feature of IVUS techniques is that the direction of blood flow is almost normal to the imaging plane. As blood particles move across the imaging plane, the received echo signals decorrelate at a rate proportional to flow velocities. The temporal



correlation properties of the radio frequency (RF) blood scattering signals *in vivo* have been documented extensively (Li et al. 1996). In this chapter, we review the principles of a method that allows a direct measure of local velocity as well as volume flow by means of analysis of the intravascular RF echo signals. The flow measurements obtained with the correlation-based method (IVUS-flow) are compared to the data of an electromagnetic flow meter (EM-flow) *in vivo* under various flow conditions in an animal model. Furthermore clinical data are presented. Since a rotating single element transducer suffers from some inherent motion artifacts we are currently developing the method for an array transducer system. These transducers get to their inherent resolution and image quality by synthetic aperture focussing techniques. Since this is based on reconstructing of the image from multiple pulses from different directions towards the same "static" object, this technique is not directly suited for flow estimation, because the blood particles are moving in the time course of the acquisition. The scanning protocol of the array had to be changed. In this chapter another scanning protocol is described, based on a computer model of the array and included in an intravascular ultrasound system. Preliminary patient data using this catheter are presented. Furthermore possibilities to use this method for automatic boundary detection in IVUS are discussed.

## 2.2 Methods

### 2.2.1 Decorrelation of blood echoes

The displacement of an ultrasound-scattering material such as blood moving through the beam of an ultrasound transducer results in concomitant changes (decorrelation) in the received echo signal. The decorrelation phenomenon can be clearly observed in the intravascular environment in which the ultrasound beam is transmitted perpendicularly to the arterial tissue and blood flow (Fig. 2.1). In IVUS, it is commonly observed from real-time display that the scattering pattern of flowing blood varies rapidly over time. This is due to the fact that the flow stream drives the randomly distributed blood particles constantly washing in/out of the image plane, causing the received echo signals to decorrelate as a function of time delay. The speed of the blood decorrelation process has proven to be related to the flow velocity. In other words, the faster blood particles move across the ultrasound beam, the higher the decorrelation rate of the received signals will be. The relationship between echo decorrelation and flow velocity is approximately linear. This result suggests that if the velocity-correlation relation is pre-quantified for the type of transducers used, the measured decorrelation value from blood scattering signals can be converted into flow velocity.

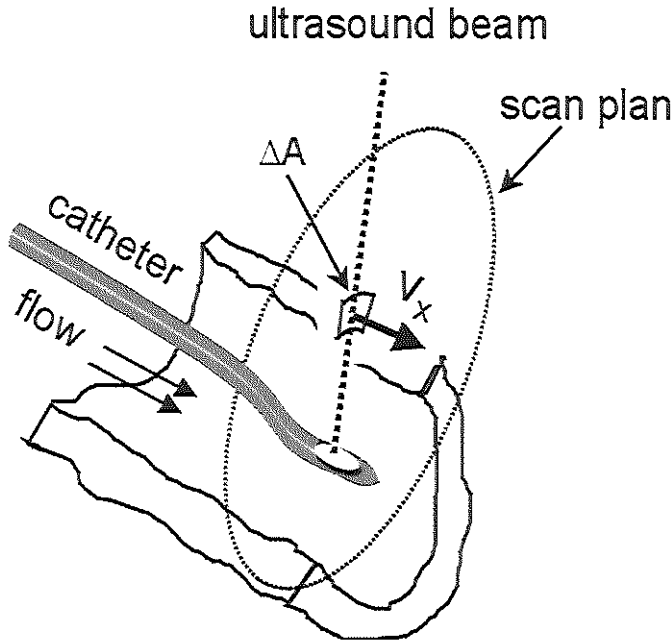


**Figure 2.1:** The coordinates of the IVUS imaging set up. The scanning plane is perpendicular to the direction of blood flow.

### 2.2.2 Decorrelation-to-flow quantification

The method is based on correlation processing of a series of RF signals (time RF sequence) acquired approximately at the same transmission angle.

#### *Spatial decorrelation model:*

Unlike most other medical imaging techniques, majority of IVUS signals is acquired in the near field of the ultrasound beam (0.1~4 mm). The relationship between the correlation of echo signals and the scatterer motion across the ultrasound beam (lateral decorrelation) can be approximated with a linear model in the near field (Li et al. 1998a, 1998b). The slope, termed the displacement decorrelation slope ( $\text{mm}^{-1}$ ), is characterized by the beam pattern. The linear dependence of signal correlation upon the scatterer lateral displacement has been validated in both computer simulation and *in vitro* with a flow phantom. Our results show that, because the beam pattern may change significantly in the near field, the slope is a beam dependent factor that requires to be calibrated for the type of transducer used (Li et al. 1998a, 1998b).

*Time decorrelation measurement:*

At each transmission angle, a sequence of RF traces separated by a fixed time interval is acquired at a high pulse repetition rate. The decorrelation rate of the range-gated echo is evaluated in two steps:

1. Shifting over the time delay where the cross-correlation function reaches maximum first aligns the RF-traces. This is a phase matching procedure that removes the decorrelation due to the axial displacement (along the ultrasound beam) of blood scatterers.
2. Then the correlation coefficient between pairs of traces in the aligned RF windows are calculated. A slope is obtained by fitting a linear model through the correlation versus displacement. The slope, termed the time decorrelation slope ( $s^{-1}$ ), is related to the transverse blood velocity (normal to the ultrasound beam) for a given beam position.

*Velocity estimation:*

Thus, the transverse velocity can be estimated at each window position from the ratio between the *calibrated* decorrelation function and the *measured* decorrelation slope from a time RF sequence. Note that the calibration procedure needs to be carried out only once for a specific type of transducer.

*Volume flow integration:*

The local velocity measurement in a number of small, consecutive range windows can be repeated over the lumen cross-section to provide two-dimensional flow mapping. As illustrated in Figure 2.1, the volume flow is calculated by integrating the local transverse velocity with its corresponding area element over the complete imaging plane. Because the lateral motion of wall tissues has a much lower velocity than blood, the contribution of tissue velocities can be automatically removed by setting a threshold. Thus, no contour tracing of the arterial lumen is needed.

## 2.3 Results

The methods described above have been implemented on a rotating single element IVUS system (DuMed/JOMED Inc.) and validated in a number of ways. *In vitro* data showed good agreement with a calibrated EM-flow (Li et al. 1998b). In the carotid artery of a pig the IVUS flow showed good agreement with EM-flow estimation (Fig. 2.2) (Céspedes et al. 1998a; van der Steen et al. 1997). The relation under a variety of flow conditions approached unity. In patient studies

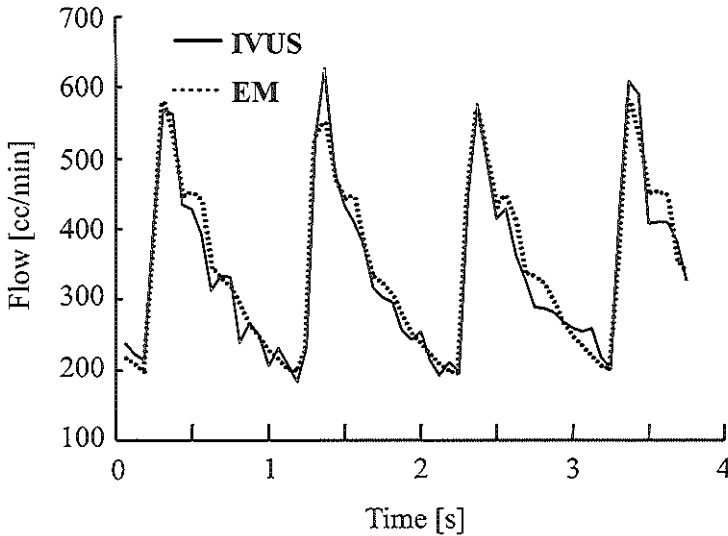


**Figure 2.2:** Flow curves of phasic EM-flow (dotted line) and IVUS-flow (solid line) in a pig carotid artery, showing an almost identical beat-to-beat change in blood volume flow (Li et al., 1997, 1998).

the IVUS flow is compared to the values obtained by a Doppler flow wire (Carlier et al. 1998d, 1997). Again a good agreement was found. This method has been evaluated extensively in the Catheterization laboratory (Fig. 2.3) (Céspedes et al. 1998a; Carlier et al. 1998a).

### 2.3.1 Influence of catheter

One important issue in this flow measurement is the question if the flow measurement with the catheter inside is a good representation of the flow as if the catheter were not there. There are three important aspects that should be addressed:

1. Is the flow profile changed by the catheter?
  2. Does the catheter cause secondary flow?
  3. Does the catheter impede the flow?
1. This is indeed the case, but this does not affect the flow estimation, since the values of the transverse velocity profile are integrated over the full cross section and the exact profile is not important.
  2. The method is able to discriminate between axial and transverse flow, but incapable of discriminating transverse motion through the plane from in

plane transverse motion. The latter one is referred to as secondary flow and a significant presence of this could cause a bias on the flow estimation. This secondary flow has been studied using Finite Element Modelling (Wentzel et al. 1997). The flow through a curved vessel with a catheter inside at a variety of positions is compared to the flow without a catheter present. The main conclusion of the study was that the secondary flow with a catheter inside is of minor influence on the flow estimation (Krams et al. 1999). A peculiar fact is that secondary flow with a catheter inside is even less than without catheter. The catheter seems to have a regulating effect on the secondary flow.

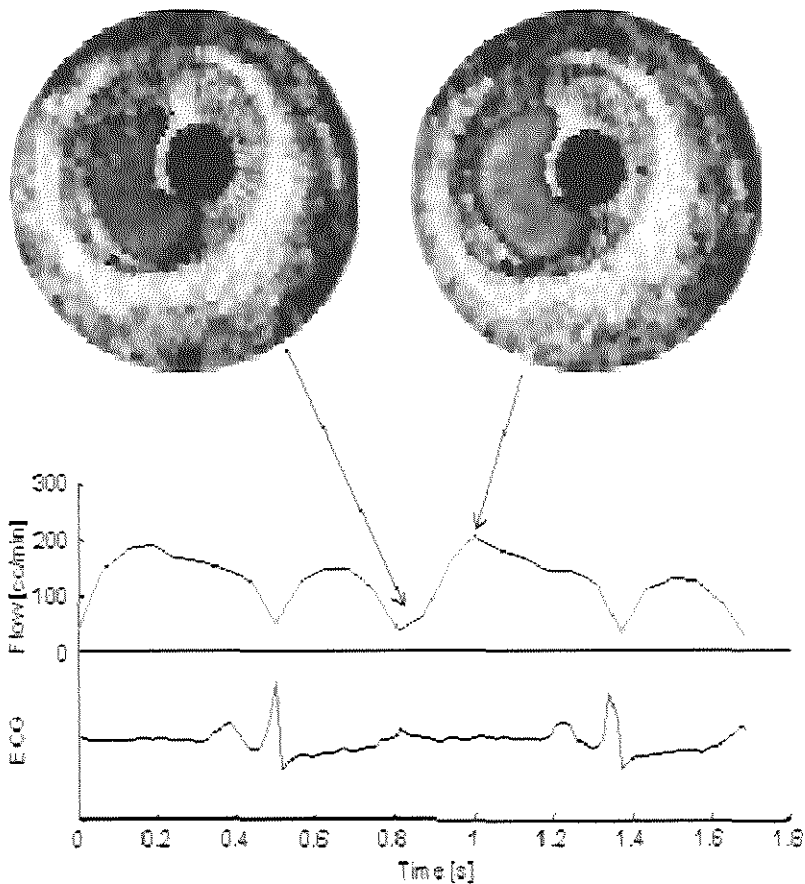


**Figure 2.3:** Upper panel: Coronary flow mapping obtained in patient for low (left) and high (right) flow rates during the cardiac cycle. Lower panel: IVUS flow curve showing a typical 2-phasic diastolic flow pattern of a coronary artery.

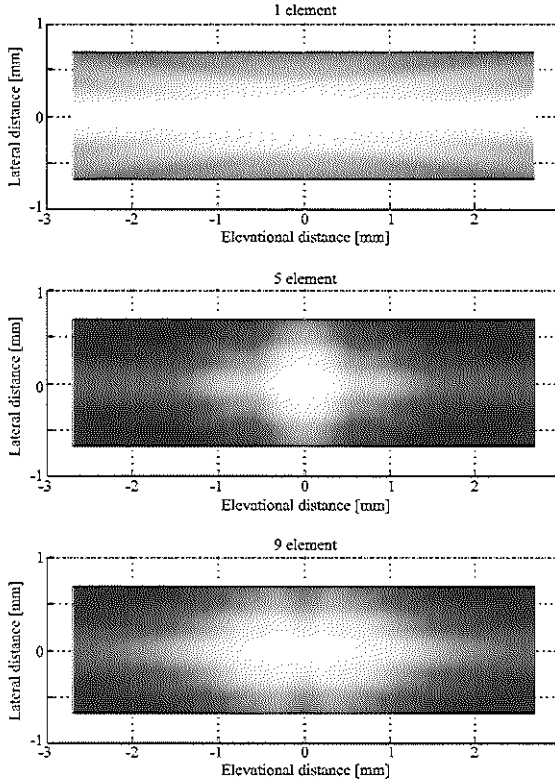


Figure 2.4: Intensity plots at a distance of 2 mm from an array transducer that is operated in linear array mode using 1,5 or 9 elements (Borsboom et al., 2000).

3. The impediment of the catheter on the flow is also under study. This is done in an *in vitro* set up where tubes with several stenoses are studied. The pressure drop over the stenosis is established without catheter, with a guide wire and with a catheter there. This pressure drop is a direct measure of the impedance of the flow. Preliminary results show that if the stenosis is severe enough, there is an influence of the catheter on the flow. One should bear in mind that the impedance in human subjects at baseline is mainly determined by the resistance of the vascular bed. In normal subjects, the vascular bed may well compensate the enhanced impedance in flow through the stenosis. However, in hyperemia, this is not the case. For the calculation of the coronary flow reserve, which is an indicator for the severity of a stenosis, the flow needs to be assessed at baseline and at hyperemia. Since the calculation of coronary flow reserve is one of the envisioned application,

the *in vitro* study is accompanied by measuring the pressure drop over a stenosis in human subjects in the presence of a catheter.

### 2.3.2 Flow estimation using an array transducer

Although the flow estimation seems to work well on a rotating single under a number of circumstances element catheter, there are certain disadvantages to it. One of them is the fact that motion of the catheter with respect to the blood can not be separated from motion of blood with respect to the catheter. In principle the decorrelation due to element rotation can be corrected for, but two problems remain.

1. If the flow becomes very slow the relative decorrelation due to rotation becomes significant. Therefore only velocity components above a certain threshold can be used.
2. The correction is based on a uniform rotation of the element. If this is not the case the results may be biased.

For these reasons the methods are currently evaluated on a solid state system. The tip of the catheter consists of 64 static elements. The image is constructed using Synthetic Aperture Focusing Techniques (SAFT) (O'Donnell et al. 1997a). This is based on multiple excitation and receiving of individual elements. For the reconstruction it is essential that the imaged object does not move during the acquisition time. For blood flow estimation this mode is not suitable. The array needs to be operated in linear array mode. This means that a number of elements are excited simultaneously and the same elements are used for receiving. The influence of the number of elements that need to be used for this is studied extensively (Fig. 2.4) (Borsboom et al. 2000). If the number is too low, the resolution is poor and the ultrasound energy will be concentrated close to the transducer. If the number is too high the ultrasound beam will split. This is due to the fact that due to the curvature of the surface, the far field of the transducer can never be reached. An optimal number would be 4 or 5 elements. Another aspect is the shape of the decorrelation curve of the array system in linear array mode. For the near field of the single element transducer it had proven to be close to linear (Li et al. 1998b), but for the array transducer this is not necessarily the case. Computer modelling has shown that for 4 elements the decorrelation at varying distance is fairly linear, although a different calibration has to be performed at different distances to the transducer (Chapter 3 and 7). It seems that in principle the array is suited for flow estimation. Currently it is evaluated in the catheterization laboratory (Fig. 2.5) (Carrier et al. 1998a).

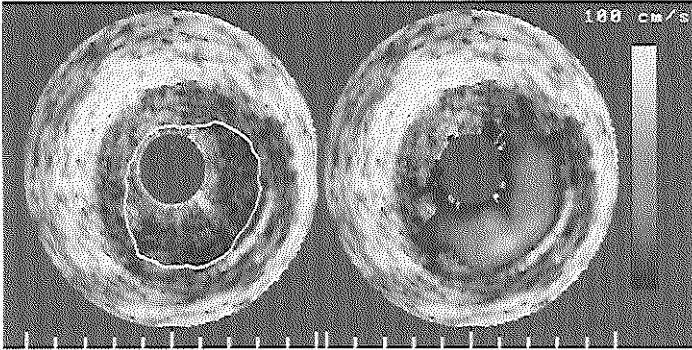


Figure 2.5: IVUS flow image (right) and automated detected boundary from flow (left) obtained with an array catheter. Note that the resolution of the image is limited because no SAFT was used (Li et al., 1998).

### 2.3.3 Automated boundary detection

Because the flow usually has a higher velocity than wall motion, blood echo signals decorrelate significantly faster than those of tissues do. The different correlation time in the received RF signals between blood and tissue has been documented *in vivo* in our earlier studies (Li et al. 1996). The time in which the blood RF signals remains correlated is approximately 1 ms, which is significantly shorter in that measured in wall echoes ( $\gg 6$  ms). In this way the regions that are potentially identified as blood are distinguished from those that are potentially identified as vascular wall. After this addition, image filtering is applied (van der Steen et al. 1998a). The result of this automated detection of the arterial lumen boundary based on RF-processing technique is illustrated in Figure 2.5. Other methods of assessing the flow area have recently been described (Céspedes et al. 1997c; Crowe et al. 1996; O'Donnell et al. 1997b). Although not capable of quantitative flow measurement, these are very well capable for detecting areas with flow or not, making it very well suited for guidance of stent placement (Céspedes et al. 1998b).



## Chapter 3

# Decorrelation of single Red Blood Cells

### Abstract

*In recent years, a new method to measure transverse blood flow, based on correlation of the Radio Frequency (RF) signals has been introduced. In this chapter, we investigated the decorrelation characteristics of transverse blood flow measurement using an intravascular ultrasound (IVUS) array catheter by means of computer modeling. Blood was simulated as a collection of randomly located point scatterers. Moving this scattering medium transversally across the acoustical beam represented flow. First-order statistics from the RF signals were evaluated and the mean-to-standard deviation ratio measured. The correlation coefficient method was used to present the results. The decorrelation patterns for RF and for envelope signals were studied. The decorrelation patterns from the RF signals were in good agreement with those obtained from theoretical beam profiles. This agreement suggests that the decorrelation properties of an IVUS array catheter for measuring quantitative transverse blood flow can be assessed by measuring the ultrasound beam. A line of point scatterers, moved transversally across the acoustical beam (Line Spread Function), can determine this decorrelation behaviour.*

---

based on the Publication: "Decorrelation Characteristics of Transverse Blood Flow along an Intravascular Array Catheter" by Fermín A. Lupotti, E. Ignacio Céspedes and Antonius F.W. van der Steen, *IEEE Transactions on Ultrasonics, Ferroelectrics, and Frequency Control*; 2000: 47(6): 1582-1592.

### 3.1 Introduction

Intracardiac and intracoronary array catheters have been in development since the '70s (Bom et al. 1972). With the advances in integrated circuits, it was possible to construct an Intravascular Ultrasound (IVUS) array catheter small enough to be situated in coronary arteries (Bom et al. 1989; Eberle 1997). For many years, IVUS has been used for various clinical purposes as it provides real-time cross-sectional images of blood vessels at high spatial resolution (Tobis & Yock 1992; Roelandt et al. 1993; Siegel 1998; Schwarzacher et al. 1997a).

As an imaging tool, IVUS allows to measure the lumen and vessel wall (von Birgelen et al. 1998), to study the progression of atherosclerosis and restenosis (Di Mario et al. 1998; Schwartz et al. 1998), to implant and examine coronary stents (de Jaegere et al. 1998; Schiele et al. 1998) and to evaluate intravascular interventions (Schatz 1989; Schwarzacher et al. 1997b; Blasini et al. 1997). RF-data processing has significantly enhanced the potential of IVUS (van der Steen et al. 1998a). Recent research in IVUS has been focusing on obtaining information concerning the acoustic and elastic properties of the vessel wall and plaque for the purpose of vascular tissue characterization (Spencer et al. 1997b; Bridal et al. 1997a; Céspedes et al. 1997b, 1999; de Korte et al. 1998). Also, IVUS has been applied to measure blood flow velocity and volumetric flow (Li et al. 1998b; Embree & O'Brien 1990; Foster et al. 1990; Hoeks et al. 1993; Crowe et al. 1996; O'Donnell et al. 1997b).

Current methods to assess blood flow using intravascular techniques include Doppler processing and time-domain correlation techniques (Chou et al. 1994; Isner et al. 1993). For intravascular volumetric blood flow measurements, the cross-sectional vessel area and the blood velocity must be assessed simultaneously. Flow velocity could be measured using a Doppler Flowire<sup>TM</sup> (JOMED Inc., Rancho Cordova, CA, USA) and the lumen area using IVUS or Quantitative Coronary Angiography (QCA) (Blasini et al. 1997). A Doppler Flowire<sup>TM</sup> is a guide wire with a Doppler transducer in the tip. When IVUS is used in combination with a Doppler Flowire<sup>TM</sup>, however, blood velocity and lumen area can not be assessed simultaneously and at the same location. When using QCA, the lumen area detection is limited to a projection of the vessel and the area calculation is based on the assumption of a circular vessel lumen. All these problems could be solved if blood velocity and the lumen area were assessed simultaneously using only an IVUS catheter.

Recently, Li et al. (1998b, 1997) proposed to measure blood velocity and quantify intravascular volume flow using a correlation-based method in a burst of ultrasound beam that were transmitted in the same direction. The measurements were performed from cross-sectional IVUS RF signals and the results showed that this method is capable of obtaining blood velocity profiles and volumetric blood flow. Céspedes et al. (1998a) have presented initial *in vivo* evaluations of blood

flow assessment based on correlation with a rotating single-element catheter. The rotating single-element catheter has an extra component of decorrelation due to the inherent and constant rotation of the transducer element. This rotation induces an additional lateral displacement with respect to the RBCs motion (Li et al. 1998b). With the advent of array technology in IVUS applications, this extra component of decorrelation is not present since the array transducer is capable of transmitting and receiving a multitude of echoes at exactly the same angle with respect to the array.

In the current chapter, the response of the IVUS array catheter to transverse blood flow was studied using a computer simulation program. The principle of blood flow assessment is based on lateral decorrelation, which depends on the beam profile of the transducer. More specifically, decorrelation is related to the auto-convolution of the ultrasound beam in the direction of blood flow and decorrelation was proven to be proportional to the transverse blood flow velocity. The decorrelation of the received IVUS RF signals can be evaluated as a function of time using a sequence of RF signals acquired at a fixed pulse interval from the same angular position. After gating the RF signals with a fixed window length, the sequence of RF signal windows was phase-matched to remove the axial motion of the scatterers and then the correlation coefficients were calculated as a function of time. Next, in a controlled experimental environment, the correlation coefficients as a function of transverse displacements of the scatterers were obtained to calibrate the method. Thus, after the time and displacement decorrelation functions are known, the correlation coefficients can be converted into velocity. Assuming that the only cause of decorrelation is the transverse displacement of the scatterers (*i.e.* noise-less RF signals), the velocity was obtained from the ratio of the correlation coefficient as a function of displacement (calibration) and the correlation coefficient as a function of time (measured). The volumetric flow can be calculated by integrating the local transverse velocity with the area element over the complete vessel cross-section. Thus, quantitative volume blood flow was assessed with a single IVUS catheter that measured the cross-sectional vessel area and the transverse blood velocity simultaneously and at the same location (Li et al. 1998b).

Early studies have documented that correlation-based techniques can be used to measure axial and transverse blood flow. The transverse and axial directions correspond to displacement across the acoustical beam and along the beam, respectively. Wagner et al. (1983) have studied the decorrelation in axial and transverse directions in the focal zone. For the transverse direction, the mean of six experimental auto-covariance functions was compared with the reference magnitude and intensity curves from beam theory. In a later study, Wagner et al. (1988) showed that their previous theoretical curves (auto-covariance of the intensity) were in good agreement with experimental data for magnitude from Zagzebski et al. (1985). Smith et al. (1988) assumed the auto-covariance function to

be separable into transverse and axial directions and studied the transverse auto-covariance function in the focal zone experimentally. The results were similar to the theoretical curves from Wagner et al. (1983).

For the present study, we used a computer program that simulates transverse blood flow by moving a scattering medium transversally across the acoustical beam of an IVUS array catheter. Axial blood flow (*i.e.* displacement along the ultrasound beam) was not addressed during the present study. The backscattered RF signals were used to observe the relationship between the mean decorrelation pattern and the acoustical beam properties. The acoustical beam properties were evaluated and presented as five reference curves. For the analysis, we utilized both RF signals and envelope signals. The decorrelation patterns and the reference curves were assessed for the near field ( $\approx 1$  mm) and for the far field ( $\approx 3$  mm) because of the dependence of the decorrelation on the axial direction of the ultrasound beam.

## 3.2 Methods

### 3.2.1 IVUS transducer

We simulated an IVUS array catheter with 64 elements mounted on the circular surface of the catheter tip with a diameter of 1.2 mm. The array operates at a central frequency of 20 MHz and the -20 dB bandwidth is 7.5 MHz. The element size of the array under study is 0.7 mm in length ( $L$ ) and 0.028 mm in width ( $W$ ); the pitch of the elements was 0.059 mm (Fig. 3.1). This configuration was similar to commercially available coronary IVUS catheters (Eberle 1997; O'Donnell et al. 1997a).

The IVUS array catheter uses synthetic aperture focusing mode for imaging and linear mode for flow imaging. Synthetic aperture focusing is not suitable for flow assessment since the acoustical beam is formed over a time frame on the order of milliseconds, during which, the red blood cells will move through the beam. This will influence flow assessment based on correlation. Therefore, in flow imaging, four elements are electronically tied together and produce a burst of ultrasound pulses in linear array mode (Borsboom et al. 2000). Then, the system will be shifted one element and the next burst will be generated; this is repeated 64 times to produce a full frame.

### 3.2.2 Computer modeling

#### The simulation program

A computer model was developed to investigate the response of this IVUS array catheter to transverse blood flow. The mathematical development to simulate ultrasound signals was based on pressure field calculations using the impulse

response method. The four elements were considered as one curved (convex) single element and its area divided into a grid of small areas with dimensions around quarter of a wavelength ( $20 \mu\text{m}$  for a wavelength of  $75 \mu\text{m}$ ). Thus, each small area transmits an echo and the backscattered response is received by the entire transducer and summed with the responses from other scatterers (Borsboom et al. 2000). In general, the pressure field along the acoustical axis of an ultrasound transducer exhibited rapid fluctuations in the near field and a gradual decay in the far field. The transition from the near field to far field could be defined to occur at the last axial maximum of the pressure response (Christensen 1988). For the IVUS array catheter, this last maximum was located around 1.5 mm away from the transducer surface (Borsboom et al. 2000). The coordinate system, as defined in Figure 3.1, was used for all the calculations in this chapter. The origin of this system was on the surface and in the middle of these four elements. This simulation program had been developed and validated separately (Borsboom et al. 2000). The axial sampling frequency was 200 MHz to over-sample the response to the correlation function.

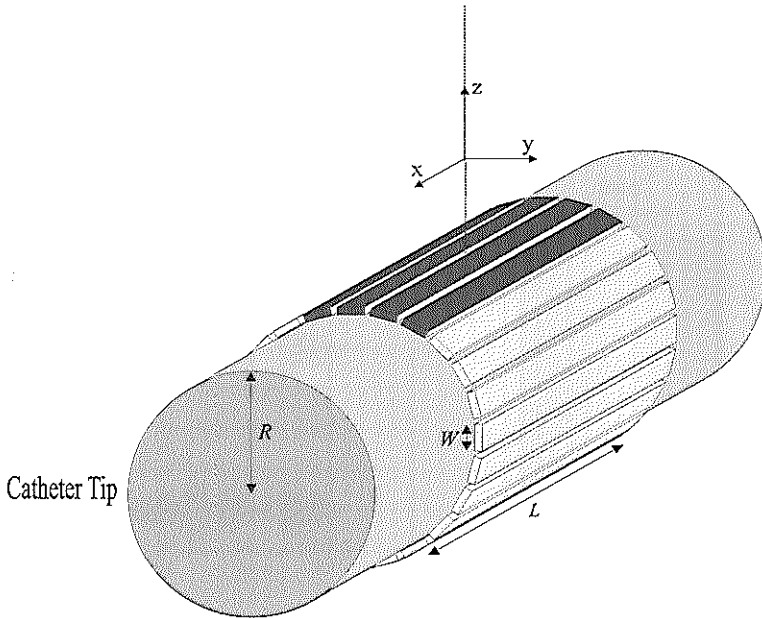


**Figure 3.1:** The IVUS array catheter with a radius ( $R$ ) of 0.6 mm, and the transducer elements and their dimensions, the length ( $L$ ) and the width ( $W$ ). In linear mode, four elements are electronically tied together. The conventional axes  $x$ ,  $y$  and  $z$  are used as references axis for all the calculations.

### The scattering medium

The scattering medium was defined as a collection of randomly positioned point scatterers in a three-dimensional space. This is the simplest way to mimic blood; a more realistic approach (*e.g.* aggregates of Red Blood Cells) will be discussed later in the thesis (Chapter 4 and 6). The locations of the point scatterers were measured with respect to the origin of the reference axis (Fig. 3.1) and a function that contains the point scatterers coordinates was used (section Computer Modeling: Blood Flow Simulation). For computational efficiency, the beam profile and its decorrelation properties were evaluated at two depths, first in the near field ( $\approx 1$  mm) and second in the far field ( $\approx 3$  mm).

For both near and far fields, the  $x$  size of the scattering medium was defined as the summation of the length of the transducer element plus the displacements of the scattering medium. The  $y$  size of the scattering medium was determined by the -20 dB beam-width (Wendling et al. 1992). The  $z$  size of the scattering medium was set to 1 mm around the axial distance of interest. In the near field, the volume sizes of the scattering medium were  $-2.2$  mm  $\leq x \leq 0.5$  mm,  $-0.6$  mm  $\leq y \leq 0.6$  mm and  $0.5$  mm  $\leq z \leq 1.5$  mm (Fig. 3.1 for the coordinate system). In the far field, the volume sizes of the scattering medium were  $-2.2$  mm  $\leq x \leq 0.5$  mm,  $-1$  mm  $\leq y \leq 1$  mm and  $2.5$  mm  $\leq z \leq 3.5$  mm. The scatterer density was chosen to meet the Rayleigh criterion (section Computer Modeling: Statistical Properties of the Scattering Medium): 1800 per mm<sup>3</sup>.

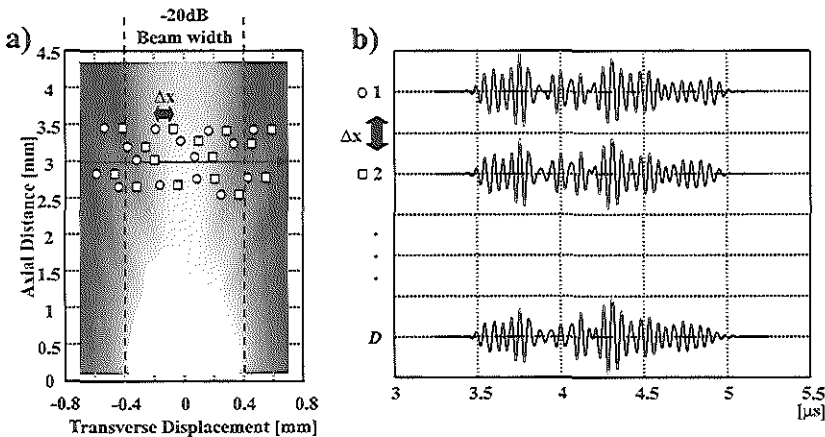


**Figure 3.2:** a) A two-dimensional ( $xz$ -plane,  $y=0$ ) representation of transverse blood flow. The beam profile is formed by four elements electronically tied together (linear mode operation) as a single element and a cloud of point scatterers in two positions (circles and rectangles) during a transverse displacement ( $\Delta x = 0.02$  mm); the considered -20 dB beam-width is also shown. b) RF signals received from the point scatterers within the -20 dB beam-width at each position of the cloud. The discrete time window length ( $N$ ) and the number of RF signals ( $D$ ) are shown.

### Blood flow simulation

To simulate blood flow, the scattering medium was moved transversally across the acoustical beam with regular steps ( $\Delta x$ ) of 0.02 mm. Similarly to Wendling et al. (1992), we considered the echo response or RF signals from point scatterers within the -20 dB beam-width. A schematic representation of transverse blood flow is presented in Figure 3.2. Figure 3.2a shows the ultrasound beam formed by four elements tied together (linear mode). The function  $P_k(x, y, z)$  for all the point scatterers coordinates was used, where  $k=1, 2, \dots, K_{tot}$  and  $K_{tot}$  was the total number of point scatterers within the medium. When the scattering medium was transversally moved (*i.e.* transverse blood flow), only the  $x$ -coordinates changed for all the point scatterers coordinates:

$$P_k(x_d, y_0, z_0) = P_k(x_0 + d\Delta x, y_0, z_0), \quad (3.1)$$

where  $d=0, 1, \dots, D$  and  $D$  was the total number of displacements. The  $x$ -coordinates were used to determine which point scatterers, from the whole scattering medium, were within -20 dB beam-width. At each displacement, the backscattered RF signals from the point scatterers within the -20 dB beam-width were summed and saved as one RF signal (Fig. 3.2b). At the selected scatterer density, the average number of point scatterers inside the -20 dB beam-width was approximately constant ( $\approx 4100$  point scatterers).

Let  $e(P, n)$  be the backscattered (RF) signal from a point scatterer located in  $P_k(x, y, z)$  where  $n$  is discrete time. Let  $s(n)$  be the summation of backscattered RF signals from  $K_{-20dB}$  point scatterers, within the -20 dB beam-width, when the scattering medium was transversally moved  $d$  steps:

$$s_d(n) = \sum_{k=1}^{K_{-20dB}} e(P_k(x + d\Delta x, y, z), n), \text{ for } d = 0, 1, 2, \dots, D, \quad (3.2)$$

where  $K_{-20dB} < K_{tot}$  and  $d\Delta x$  was the transverse displacement.

### 3.2.3 Statistical properties of the scattering medium

The backscattered RF signals from the scattering medium were evaluated. The first-order statistics were studied to determine the scatterer density of the scattering medium. Subsequently, the second-order statistics (correlation coefficients) were assessed for the RF and for the envelope signals. The envelope was defined as the absolute value of the Hilbert transform of the RF signal.

#### First-order statistics

The speckle of an ultrasound B-mode image depends on the scatterer density (Wagner et al. 1983, 1988; Smith et al. 1988). If there are many scatterers inside

a resolution cell, the pattern of the speckle is independent of the scattering itself; it depends exclusively on the physical properties of the transducer, its spectral properties (dimension, spectrum, distance, etc.) (Wagner et al. 1983).

The mean-to-standard deviation ratio of the envelope of the RF signals was used to verify that the first-order statistics of the backscattered signals were consistent with the theory, where the theoretical mean-to-standard deviation ratio of the sub-sampled envelope should be 1.91 (Wagner et al. 1983; George et al. 1976). The mean-to-standard deviation ratio of the sub-sampled envelope of the backscattered RF signals from the 50 independent scattering media was tested for the used scatterer density and the result ( $1.88 \pm 0.18$ ) was close to the theoretical value.

### Second-order statistics

The second-order statistics were used to examine the variations between backscattered signals, when a scattering medium was transversally moved across the acoustical beam. The correlation coefficient  $\rho_{i,j}$  between two signals (RF or envelope),  $s_i(n)$  and  $s_j(n)$ , received from positions of the scattering medium corresponding to  $d=i$  and  $d=j$  is:

$$\rho_{i,j} = \frac{\sum_{n=1}^N (s_i(n) - \bar{s}_i(n)) \cdot (s_j(n) - \bar{s}_j(n))}{\sqrt{\sum_{n=1}^N (s_i(n) - \bar{s}_i(n))^2 \cdot \sum_{n=1}^N (s_j(n) - \bar{s}_j(n))^2}} \quad (3.3)$$

where the subscript  $i=1,2,\dots,D$  and  $j=1,2,\dots,D$  being  $D$  the number of displacements (*i.e.* number of signals). For RF and envelope signals,  $N$  is the length in time (Fig. 3.2) and  $\bar{s}$  is the mean value. The  $\rho_{i,j}$  are the correlation coefficients for the signal pair,  $s_i$  and  $s_{i+m}$ , which are spaced  $m=(j-i)$  steps and  $m=0,1,\dots,D-1$ .

Let  $\rho_{i,i+m}$  be the correlation coefficient between the signals  $s_i$  and  $s_{i+m}$  when the space is zero (*i.e.*  $m=0$ ). Thus, the average correlation coefficients when  $m=0$  is  $\rho_0$ . In such a case,  $m=0$ , the correlation coefficient is equal to one when no other source of decorrelation is present (*e.g.* electronic noise). For the case of  $m=1$ ,  $\rho_{i,i+1}$  is the correlation coefficient between the signals  $s_i$  and  $s_{i+1}$ , and the average correlation coefficients when  $m=1$  is  $\rho_1$ . In a more general equation, the average correlation coefficient in the signal set for a space of  $m$  steps between signals is:

$$\rho_m = \frac{\sum_{i=1}^{D-m} \rho_{i,i+m}}{D-m} \quad (3.4)$$

and thus  $\rho_m$  describes the transducer decorrelation pattern as a function of transverse displacements of a scattering medium.



### 3.2.4 Decorrelation curves from beam theory

Five reference curves, representative of the ultrasound beam characteristics, were assessed to compare with the mean decorrelation patterns from blood flow simulations. The reference curves were obtained for the near field and for the far field, separately. The definitions of these curves are given in Appendix A. In brief,  $A_{1D}$  (Eq. A.3) is the amplitude and  $E_{1D}$  (Eq. A.6) the energy of a backscattered RF signal from a point scatterer that is transversally moved across the ultrasound beam.  $A_{2D}$  (Eq. A.9) is the amplitude,  $E_{2D}$  (Eq. A.13) the energy and  $Envelope_{2D}$  (Eq. A.17) the envelope of a line of point scatterers that is transversally moved across the ultrasound beam.

### 3.2.5 Decorrelation from point-scatterer media

The decorrelation pattern from the RF signals when the scattering medium was transversally moved across the ultrasound beam was assessed. The correlation coefficients were calculated (Eq. 3.3 and Eq. 3.4) from a set of 30 independent scattering media in the near field and 25 in the far field. More realizations were needed in the near field to reach acceptable standard deviations. Because the correlation coefficients were not normally distributed, the Fisher-Z transform (Appendix B) was used to present the results as the mean and 95% confidence intervals (Céspedes et al. 1999).

Next, the decorrelation patterns were assessed for the envelope of the RF signals. The envelope detection process produced boundary effects with a strong influence in the correlation process. To remove the edge effects, the first and last half a wavelength ( $\lambda/2$ ) of the envelope signals were not considered in the calculations.

## 3.3 Results and comparisons

The point spread function (PSF) and a two-dimensional gray-scale representation of the RF signals are shown in Figures 3.3 and 3.4 for the near field and for the far field, respectively. In the near field (Fig. 3.3), the intensity shows a double peak as previously described (Borsboom et al. 2000). However, in the far field (Fig. 3.4), the acoustical beam has a single main lobe (Fig. 3.4a) with side lobes.

Four reference curves are plotted in Figure 3.5 as a function of transverse displacements and in comparison to each other in the near field and in the far field, separately. In both near and far fields, the convolution of the RF signals from a point scatterer (1-D) is similar to that one from a line of point scatterers (2-D). Even so, in the far field, there is a slight difference when the convolution approaches zero (Fig. 3.5b). The mean decorrelation patterns of a scattering medium are shown in Figure 3.6 in comparison with the reference curves  $A_{1D}$ ,

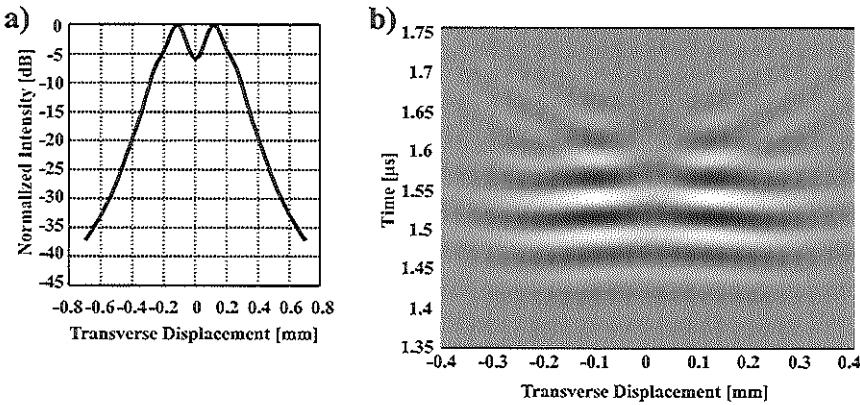


Figure 3.3: a) Self-normalized intensity from a point scatterer transversally moved across the ultrasound beam in the near field (1 mm). b) Two-dimensional representation of the RF signals versus transverse displacements.

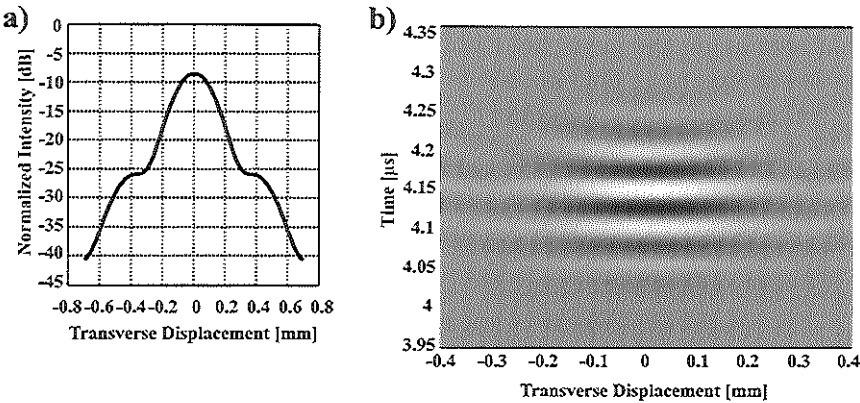
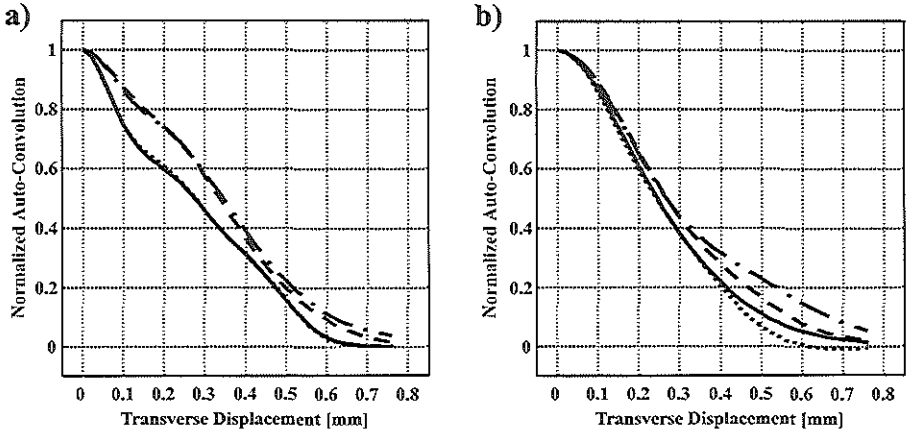


Figure 3.4: a) Intensity from a point scatterer transversally moved across the ultrasound beam in the far field (3 mm); normalized with respect to the intensity in the near field. b) Two-dimensional representation of the RF signals versus transverse displacements.

$A_{2D}$  and  $E_{2D}$ . In the near field (Fig. 3.6a), the mean decorrelation pattern is in agreement with the reference curves  $A_{1D}$  and  $A_{2D}$ . However, in the far field (Fig. 3.6b), the mean decorrelation pattern only follows the  $A_{2D}$  reference curve.

In order to examine the decorrelation pattern from the envelope of the RF signals, the reference curve  $Envelope_{2D}$  was calculated (Fig. 3.7). The  $Envelope_{2D}$  reference curve was plotted together with  $A_{2D}$  and  $E_{2D}$ . An agreement with the  $E_{2D}$  for both near and far fields was observed. Next, the mean decorrelation patterns from the envelope as a function of transverse displacement are shown in Figure 3.8 for both near and far fields. These mean decorrelation patterns are



**Figure 3.5:** Comparison between the Amplitude ( $A_{1D}$  (dotted line) and  $A_{2D}$  (solid line) and Energy ( $E_{1D}$  (dash dotted line) and  $E_{2D}$  (dashed line)) reference curves. a) Near field (1 mm) and b) Far field (3 mm).

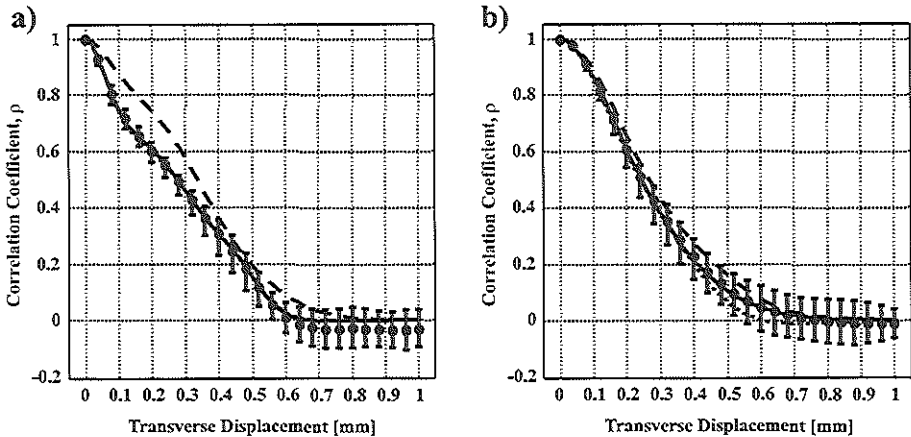


**Figure 3.6:** Mean decorrelation pattern from RF signals as a function of transverse displacements (error bars); a comparison with three reference curves the  $A_{1D}$  (dotted line) and the  $A_{2D}$  (solid line) and  $E_{2D}$  (dashed line). a) Near field (1 mm) and b) Far field (3 mm).

between the same number of curves as for the RF signals in each field and the error bars are plus and minus two standard deviations (95% confidence interval, see Fisher-Z transform in Appendix B).

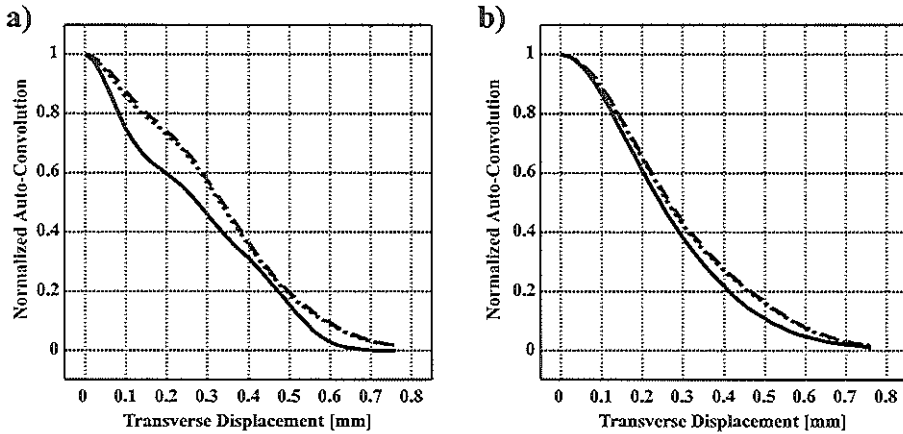


Figure 3.7: Comparison between the  $A_{2D}$  (solid line),  $E_{2D}$  (dashed line) and  $Envelope_{2D}$  (dotted line) curves. a) Near field (1 mm) and b) Far field (3 mm).

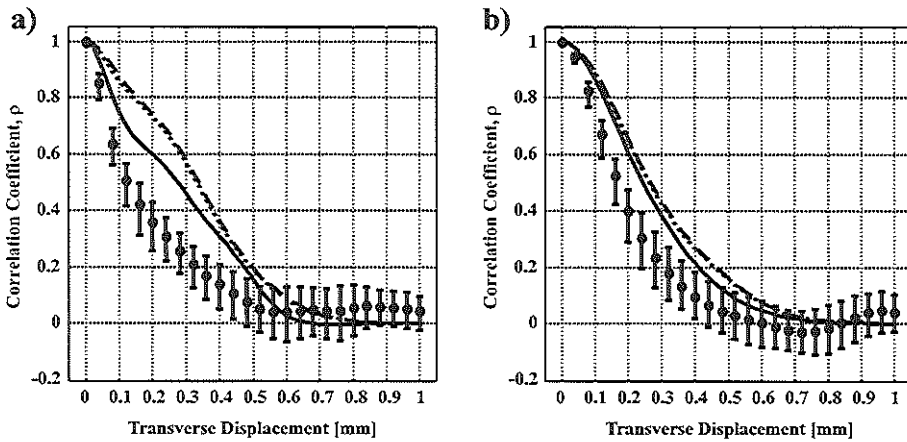


Figure 3.8: Mean decorrelation pattern for the envelope of the RF signals (errorbars), as a function of transverse displacements, in comparison with the  $A_{2D}$  (solid line),  $E_{2D}$  (dashed line) and  $Envelope_{2D}$  (dotted line) reference curves. a) Near field (1 mm) and b) Far field (3 mm).

### 3.4 Discussion

For the IVUS array transducer in linear mode operation, the ultrasound beam showed a strong influence of the irregularity of the ultrasound beam in the near field (Fig. 3.3a) and in the far field this influence starts to disappear (Fig. 3.4a). The irregularity can be also observed in the two-dimensional gray-scale representation of the RF signals (Fig. 3.3b). Note that this rectangular transducer

has maximum intensity in the near field (Borsboom et al. 2000). The reference curves in the near field  $A_{1D}$ ,  $E_{1D}$ ,  $A_{2D}$  and the  $E_{2D}$  also show the presence of the irregularity of the ultrasound beam (Fig. 3.5a). In this figure, it is notable that the amplitude and energy curve pairs nearly coincide in the near field. However, in the far field, the irregularity of the ultrasound beam is not present (Fig. 3.5b). The presence of side lobes in the far field is notable and the reference curves diverge as the lateral translation exceeds about 0.4 mm.

The analysis of the characteristic decorrelation pattern of the ultrasound beam during transverse blood flow shows that for RF signals, the mean decorrelation pattern has a monotonic decay as a function of transverse displacement (*i.e.* transverse blood flow) in both near and far fields (Fig. 3.6). In the near field (Fig. 3.6a), the mean decorrelation pattern shows a hump due to the changes in the intensity levels of the ultrasound beam (Fig. 3.3a). Moreover, the mean decorrelation pattern falls to zero before the length of the array element. In the far field (Fig. 3.6b), the mean decorrelation pattern does not suffer too much influence from side lobes and falls to zero beyond the length of the array element. A main result from Figure 3.6 is the agreement between the mean decorrelation pattern for the RF signals and the reference curves. In the near field (Fig. 3.6a), the agreement is with the reference curves  $A_{1D}$  and  $A_{2D}$ . However, in the far field, the mean decorrelation pattern from the RF signals follows only the reference curve  $A_{2D}$ .

We also examined the decorrelation patterns from the envelope of the RF signals. In both near and far fields (Fig. 3.8), poor agreement was found between the decorrelation patterns and their reference curves  $Envelope_{2D}$ . Furthermore, the rate of the mean decorrelation pattern for the envelope was faster than the one for the RF signals and the standard deviations (95% confidence interval) were increased (Fig. 3.6a and 3.6b). The faster rate of decorrelation could be explained the loss of phase information by the envelope; the phase information contributes to an increase in the probability of finding the best match between RF signals. Thus, this faster decorrelation will overestimate the measurements of transverse blood flow and the probability of finding the right velocity is decreased due to the increment of the variance. The increment in the standard deviations (Fig. 3.8) was due to the decrement in the signal bandwidth by the envelope detection process; the variance is inversely related to the signal bandwidth (Bendat & Piersol 1986).

As it was explained in the introduction, the correlation-based method needs to be calibrated in order to convert the measured correlation coefficients as a function of time into transverse velocity. Obtaining the correlation coefficients as a function of transverse displacements does this. The process to obtain such a calibration is time consuming since many experimental realizations have to be performed. From our findings, we have shown that the calibration of an ultrasound beam for measuring quantitative volume blood flow using the correlation-

based method could be assessed by only a theoretical evaluation of the acoustical beam such as the reference curve  $A_{2D}$ .

The model presented in this study assumed bulk motion of the scattering medium, such as would be produced by moving tissue or plug blood flow. A more realistic approach should include velocity gradients in the motion of the scattering medium (Ferrara & Algazi 1994). Li et al. (1997) have shown, for a rotating single-element catheter, that axial velocity gradients do have a significant effect on decorrelation. However, transverse velocity gradients have a minimal effect on the decorrelation of RF signals. Other source of RF signal decorrelation, such as electronic and quantization noise, was also not assessed. Nevertheless, if noise were added to the RF signals, the rate of decorrelation would become faster than the rate of decorrelation for noise-less RF signals.

### 3.5 Conclusions

A computer program to simulate the acoustical beam and transverse blood flow for an intravascular array transducer catheter was developed. Through this computer model, the user can manipulate all the parameters involved in such a study, *e.g.*, width and length of the transducer elements, number of elements tied together in linear mode, the blood flow velocity, central frequency and bandwidth, and the length of the RF signals and sampling frequency. This study has shown the feasibility to assess transverse blood flow using the RF signals and the correlation-based method with an IVUS array catheter. In both near and far fields, the mean decorrelation pattern from RF signals fully agreed with the reference curve  $A_{2D}$ . This agreement suggests that the decorrelation properties of an IVUS array catheter for measuring quantitative transverse blood flow can be assessed by measuring the ultrasound beam. Therefore, only a line of point scatterers (line target) that is transversally moved across the ultrasound beam is needed to determine the behaviour of an intravascular array catheter to transverse blood flow.

## Chapter 4

# Decorrelation of Aggregates of Red Blood Cells

### Abstract

*A method to measure transverse blood flow, based on correlation between consecutive Radio Frequency (RF) signals, has been introduced. This method was validated for an intravascular (IVUS) rotating single element catheter. Currently, we are implementing the method for an IVUS array transducer catheter. The decorrelation characteristics during transverse blood flow using the IVUS array catheter are investigated using computer modeling. Up to now, blood was simulated as a collection of randomly located point scatterers, and by moving this scattering medium transversally across the acoustical beam, blood flow is produced. This chapter presents a more realistic scattering media by simulating aggregates of Red Blood Cells (RBCs) as strings of point scatterers. Three configurations of aggregates of RBCs were simulated. First, aggregates of RBCs were strings with different lengths and parallel to the catheter axis. Second, the strings were with a fixed length and angles of plus or minus  $45^\circ$  with respect to the catheter axis. Third, the strings were with different lengths and random angles ranging from  $-45^\circ$  to  $+45^\circ$ . The decorrelation characteristics for these configurations of aggregates of RBCs were investigated and compared with point scatterers. The decorrelation characteristics were shown to be influenced by the scattering medium properties depending on the size and orientation of the particles within the medium. Results suggests that the presence of aggregates of RBCs will probably not affect the measurements of transverse blood flow using the correlation-based method and an IVUS array catheter.*

---

based on the Publication: "Decorrelation Characteristics of Transverse Blood Flow along an Intravascular Array Catheter: Effects of Aggregation of Red Blood Cells" by Fermín A. Lupotti, E. Ignacio Céspedes and Antonius F.W. van der Steen, *Ultrasound in Medicine and Biology*; 2001: 27(3): 409-417.

## 4.1 Introduction

Intravascular ultrasound (IVUS) has been used for many purposes as it provides real-time cross-sectional images of blood vessels at a high-resolution (Tobis & Yock 1992; Roelandt et al. 1993; Siegel 1998). As an imaging tool, IVUS allows to measure the lumen and vessel wall (von Birgelen et al. 1998) and the progression of atherosclerosis and restenosis (Di Mario et al. 1998; Schwartz et al. 1998). Furthermore, important applications of IVUS are the guidance of therapeutic interventions such as coronary stents implantation (Schatz 1989; de Jaegere et al. 1998; Schiele et al. 1998) and the evaluation of intravascular intervention (Schwarzacher et al. 1997b; Blasini et al. 1997). Current research in IVUS has focused on obtaining information concerning the acoustic and elastic properties of the vessel wall and plaque for the purpose of vascular tissue characterization (Spencer et al. 1997b; Bridal et al. 1997a). RF-data processing has significantly enhanced the potential of IVUS (van der Steen et al. 1998a). IVUS RF-data processing is now aiming to obtain information concerning vessel wall and plaque properties and vascular tissue characterization (Céspedes et al. 1997b; de Korte et al. 1998; Spencer et al. 1997b; Bridal et al. 1997a; de Korte et al. 2000). In addition, IVUS has been applied to measure blood flow velocity and volumetric flow (Li et al. 1998b).

Current methods to assess blood flow include Doppler processing and time-domain correlation techniques (Chou et al. 1994; Isner et al. 1993). For intravascular volumetric blood flow measurements, the cross-sectional vessel area and the blood velocity must be assessed simultaneously. Flow velocity could be measured using a Doppler-Flowire<sup>TM</sup> (JOMED Inc., Rancho Cordova, CA, USA) and the lumen area using an IVUS catheter or Quantitative Coronary Angiography (QCA). A Doppler-Flowire<sup>TM</sup> is a guide wire with a Doppler transducer in the tip. For these configurations, Doppler-Flowire<sup>TM</sup>-IVUS and Doppler-Flowire<sup>TM</sup>-QCA, blood velocity and lumen area are not assessed simultaneously and in the same location.

Recent research has shown that transverse blood flow velocity and quantitative volume blood flow can be measured using a correlation-based method in a burst of ultrasound beams that were transmitted in the same direction (Li et al. 1997, 1998b). The measurements were performed from cross-sectional IVUS RF signals. The correlation of the received IVUS RF signals can be evaluated as a function of time using a sequence of RF signals acquired at a fixed pulse interval from the same angular position. After gating the RF signals with a fixed window length, the sequence of RF signal windows was phase-matched to remove the axial motion of the scatterers and then the correlation coefficients were calculated as a function of time. Next, in a controlled experimental environment, the correlation coefficients were obtained as a function of transverse displacements of the scatterers to calibrate the method. Thus, after the time and displacement decorrelation



functions are known, the correlation coefficients can be converted into velocity. Assuming that the only cause of decorrelation is transverse displacement of the scatterers with respect to the ultrasound beam (*i.e.* noise-less RF signals), the velocity was obtained from the ratio of the correlation coefficient as a function of displacement (calibration) and the correlation coefficient as a function of time (measured). The volumetric flow can be calculated by integrating the local transverse velocity with the area element over the complete vessel cross-section. Thus, quantitative volume blood flow was assessed with a single IVUS catheter that measured the cross-sectional vessel minus the catheter area and the transverse blood velocity simultaneously and at the same location (Li et al. 1998b). Initial *in vivo* evaluations of quantitative volume blood flow assessment based on this method with a rotating-single-element catheter have been presented by Céspedes et al. (1998a) and Carlier et al. (1998b).

The rotating single-element catheter has an extra component of decorrelation due to the inherent and constant rotation of the transducer element. This rotation induces an additional lateral displacement with respect to the RBCs motion (Li et al. 1998b). With the advent of array technology in IVUS applications (O'Donnell et al. 1997a), this extra component of decorrelation is not present since the array transducer is capable of transmitting and receiving a multitude of echoes at exactly the same angle with respect to the array. Recently, a study of the decorrelation characteristics of the IVUS array catheter during transverse blood flow was performed (Chapter 3). Blood was simulated as a collection of omnidirectional and randomly located point scatterers as single RBCs; this medium was then transversally moved across the acoustical beam to produce blood flow.

However, when RBCs flow through the vessel they can form aggregates known as rouleau (Chien 1974; Fung 1993). The process of RBCs aggregation depends basically on three conditions: a sufficient concentration of RBCs (*i.e.* Hematocrit), a sufficient concentration of macromolecules (*i.e.* Fibrinogen and others) and a shear rate in blood low enough to leave the aggregates intact (Chien 1974). Since the IVUS array catheter is in direct contact with blood, the ultrasound beam is not attenuated or deflected by any other structure (*e.g.* tissue). Van der Heiden (van der Heiden et al. 1995) showed, for a rotating-single element IVUS catheter with a central frequency of 30 MHz, that when RBCs aggregation goes on during blood flow, the integrated backscatter power increases. Thus, since IVUS catheters operate at a central frequency between 20-30 MHz, the rate of decorrelation could be affected by the presence of aggregates of RBCs during blood flow. The objective of the present study is to quantify the effect of the aggregates of RBCs on the rate of decorrelation during transverse blood flow and judge how the aggregates of RBCs could affect the measurements of quantitative blood flow using the RF signal and the correlation-based method.

In the current chapter, the response of the IVUS array catheter to transverse blood flow for scattering media formed by aggregates of RBCs was studied

using a computer simulation program. Our principle of blood flow assessment depends on the acoustical beam characteristics of the transducer; the decorrelation has proven to be proportional to the transverse blood velocity and related to the characteristic of the acoustical beam (Li et al. 1997, 1998b) (Chapter 3). In the present study, different RBCs aggregation formulations were used to investigate the effects of these formulations on the blood flow estimation using the correlation-based method. Within the scattering media, aggregates of RBCs were simulated as lines or strings of point scatterers under a variety of lengths and angles. Three-dimensional distribution of these strings was used to form a more general scattering medium.

## 4.2 Methods

### 4.2.1 IVUS transducer

The IVUS array catheter is formed by 64 elements mounted on a circular surface of a catheter tip with a diameter of 1.2 mm. The element size of the array under study is 0.7 mm in length ( $L$ ) and 0.028 mm in width ( $W$ ); the pitch of the elements was 0.059 mm (Fig. 3.1). The array transducer operates at a central frequency of 20 MHz and with a -20 dB bandwidth of 7.5 MHz (Eberle 1997; O'Donnell et al. 1997a). The array transducer operates in synthetic aperture focusing mode for imaging and linear mode for flow imaging. Synthetic aperture focusing mode is not suitable for flow assessment since the acoustical beam is formed over a time frame on the order of milliseconds, during which, the red blood cells will move through the beam and will influence flow assessment based on correlation. Therefore, in flow imaging, four elements are electronically tied together and produce a burst of ultrasound pulses in linear array mode (Borsboom et al. 2000). Then, the system shifts one element and the next burst is generated; this is repeated 64 times to produce a full frame.

### 4.2.2 Computer modeling

#### General settings

In order to perform this study, a computer simulation program extended from Chapter 3 was used. In the computer simulation program, four elements were considered as one curved (convex) single element and its area was divided into a grid of small areas with dimensions around a quarter of a wavelength ( $20 \mu m$  for a wavelength of  $75 \mu m$ ). Thus, each small area transmits an echo and the entire transducer receives the backscattered response. In the coordinate system (Fig. 3.1), the  $x$ -axis is the transverse direction, the  $y$ -axis is the lateral direction and the  $z$ -axis is the axial direction. The center of coordinates is on the surface and in the center of the group of four elements. The mathematical development

to simulate ultrasound signals was based on pressure field calculations using the impulse response method (Borsboom et al. 2000). The axial sampling frequency was 200 MHz to over sample the response to the correlation function.

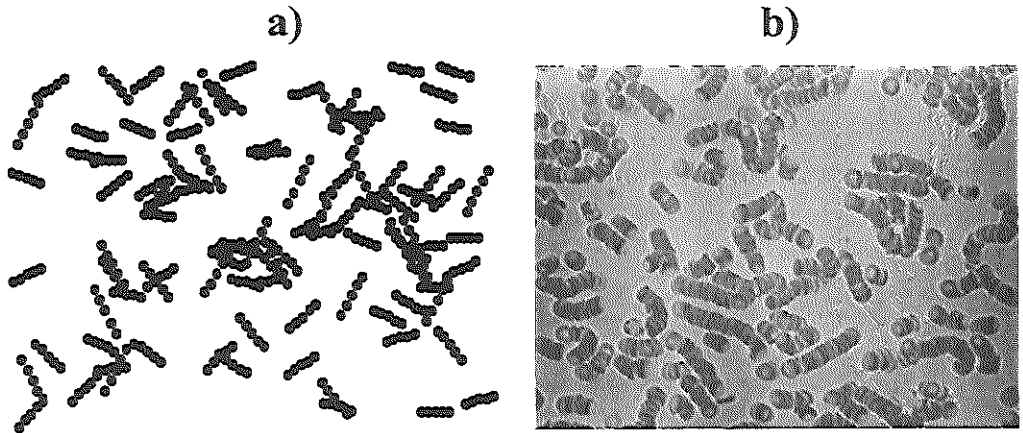


Figure 4.1: a) Light microscopic image of whole human blood compared to b) simulated aggregates of Human RBCs (van der Heiden et al., 1995).

### Scattering medium: aggregates of RBCs

Two scattering media volumes were used in this simulation, one for the near field ( $\approx 1$  mm) and one for the far field ( $\approx 3$  mm). For both near and far fields, the  $x$  size of the scattering medium was defined as the summation of the length of the transducer element ( $L$  in Fig. 3.1) plus the displacements of the scattering medium (36 times  $\Delta x$  0.02 mm). The  $y$  size of the scattering medium was determined by the -20 dB beam-width (Wendling et al. 1992). The  $z$  size of the scattering medium was set to 1 mm around the axial distance of interest. In the near field, the volume sizes of the scattering medium were  $-2.2 \text{ mm} \leq x \leq 0.5 \text{ mm}$ ,  $-0.6 \text{ mm} \leq y \leq 0.6 \text{ mm}$  and  $0.5 \text{ mm} \leq z \leq 1.5 \text{ mm}$  (Fig. 3.1, the coordinate system). In the far field, the volume sizes of the scattering medium were  $-2.2 \text{ mm} \leq x \leq 0.5 \text{ mm}$ ,  $-1 \text{ mm} \leq y \leq 1 \text{ mm}$  and  $2.5 \text{ mm} \leq z \leq 3.5 \text{ mm}$ .

For the present study, the scattering media were formed by different sets of strings of point scatterers. The computer simulation program allowed us to change the string lengths and angles (*i.e.* angle with respect to the catheter axis) and thus three different formulations of strings of point scatterers were generated. The first formulation had angle  $0^\circ$  between the strings and the catheter axis (*i.e.* strings perpendicular to the acoustical beam). The lengths of the strings were  $2.5\lambda$ ,  $5.0\lambda$  and  $7.5\lambda$ ; such string lengths were used in order to observe the changes in the rate of decorrelation when the length of the strings was increased.

The second formulation had strings with angles of  $-45^\circ$  or  $+45^\circ$  with respect to the catheter axis and the decision between the angles was a random process. The length of the strings was fixed to  $2.5\lambda$  in order to observe and compare, with the correspondent string size from the first formulation, the effect of the string angle on the rate of decorrelation. Third, to simulate aggregates of RBCs in a more proper way (*i.e.*, string lengths and angles), the scattering media were formed by strings with random angles ranging from  $-45^\circ$  to  $+45^\circ$  with respect to the catheter axis and the lengths of the strings were  $0.75\lambda$ ,  $1.25\lambda$  and  $1.75\lambda$ . For all the formulations, the distance between the point scatterers forming the strings was  $\lambda/4$ , which was selected based on the axial and lateral resolution of the transducer. Figure 4.1 shows an example of a simulated scattering medium containing strings of point scatterers (Fig. 4.1a) and of a light microscopic image of whole blood from a healthy volunteer (Fig. 4.1b) (van der Heiden et al. 1995) compared to each other.

In order to analyze if the scattering medium mimics blood, the mean-to-standard deviation ratio of the sub-sample envelope could be used to verify if the statistics of the backscattered signals are consistent with the theory (Wagner et al. 1983). In a previous study (Chapter 3), the used scatterer density was chosen to meet the Rayleigh criterion (1800 point scatterers per  $\text{mm}^3$ ). However, when aggregates of red blood cells are considered, the scattering size increases ( $r > \lambda/2\pi$  where  $r$  is the length of the strings) and the scattering medium become non-Rayleigh (Morse & Ingard 1968; Narayanan et al. 1994). Nevertheless, the scattering density remained as in the previous study (Chapter 3).

### Blood flow simulation

A function,  $P_k(x,y,z)$ , was used for all point scatterer coordinates forming the strings, where  $k=1,2,\dots,K_{tot}$  and  $K_{tot}$  was the number of point scatterers within the whole scattering medium. The location of the first point scatterer from each string was randomly decided and the string lengths and angles were determined using polar coordinates. In order to compare the results, the mean decorrelation patterns were obtained from 16 independent scattering media for each formulation of strings and for both near and far fields. These scattering media were transversally moved across the acoustical beam (*i.e.* transverse blood flow) with regular steps ( $\Delta x$ ) of 0.02 mm to produce blood flow.

As in previous studies (Chapter 3) (Wendling et al. 1992), at each displacement, the backscattered RF signals from the strings within the -20 dB beam-width were summed and then saved as one RF signal. The  $x$ -coordinates were used to determine which point scatterers (part of a string) or which strings were within -20 dB beam-width. Let  $e(P,n)$  be the backscattered RF signal from a string  $q$  located at  $P_q(x,y,z)$ . Then, the summation of the backscattered RF signals from the strings within the -20 dB beam-width, when the scattering medium was

transversally moved, is:

$$s_d(n) = \sum_q e(P_q(x + d\Delta x, y, z), n) \text{ for } d = 0, 1, \dots, D, \quad (4.1)$$

where  $d\Delta x$  was the transverse displacement and  $D$  was the number of transverse displacements. The average number of strings moving through the ultrasound beam was approximately constant.

### 4.2.3 Statistical properties of the scattering medium

In order to evaluate the RF signals coming from the scattering medium, only the second-order statistics were used. The correlation coefficient  $\rho_{i,j}$  between two RF signals,  $s_i(n)$  and  $s_j(n)$ , received from positions of the scattering medium corresponding to  $d=i$  and  $d=j$  is:

$$\rho_{i,j} = \frac{\sum_{n=1}^N (s_i(n) - \bar{s}_i(n)) \cdot (s_j(n) - \bar{s}_j(n))}{\sqrt{\sum_{n=1}^N (s_i(n) - \bar{s}_i(n))^2 \cdot \sum_{n=1}^N (s_j(n) - \bar{s}_j(n))^2}} \quad (4.2)$$

where the subscript  $i=1, 2, \dots, D$  and  $j=1, 2, \dots, D$  being  $D$  the number of displacements (*i.e.* number of signals). For the RF signals,  $N$  is the length in time and  $\bar{s}$  is the mean value. The  $\rho_{i,j}$  are the correlation coefficients for the signal pair,  $s_i$  and  $s_{i+m}$ , which are spaced  $m=(j-i)$  steps and  $m=0, 1, \dots, D-1$ .

Let  $\rho_{i,j}$  be the correlation coefficient between the signals  $s_i$  and  $s_{i+m}$  when the space is zero (*i.e.*  $m=0$ ). Thus, the average correlation coefficients when  $m=0$  is  $\rho_0$ . In such a case,  $m=0$ , the correlation coefficient is equal to one when no other source of decorrelation is present (*e.g.* electronic noise). For the case of  $m=1$ ,  $\rho_{i,i+1}$  is the correlation coefficient between the signals  $s_i$  and  $s_{i+1}$ , and the average correlation coefficients when  $m=1$  is  $\rho_1$ . In a more general equation, the average correlation coefficient in the signal set for a space of  $m$  steps between signals is:

$$\rho_m = \frac{\sum_{i=1}^{D-m} \rho_{i,i+m}}{D - m} \quad (4.3)$$

and thus  $\rho_m$  describes the transducer decorrelation pattern as a function of transverse displacements of a scattering medium. Because the correlation coefficients were not normally distributed, the Fisher-Z transform (Appendix B) was used to present the results. To get an impression of the standard deviations, they are presented in one of the curves.

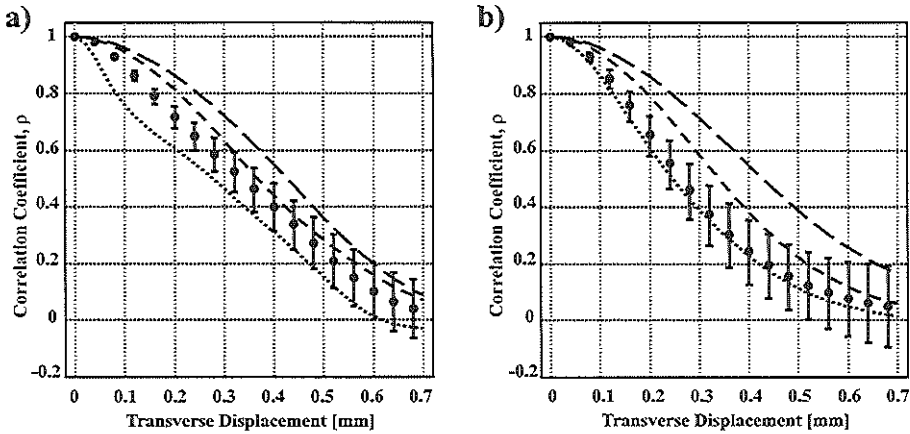


**Figure 4.2:** Mean decorrelation patterns from point scatterers (dotted line) and from aggregates of RBCs parallel to the catheter axis, the string lengths are  $2.5\lambda$  (error bars),  $5.0\lambda$  (short dashed line) and  $7.5\lambda$  (long dashed line), a) Near field and b) far field. Decorrelation patterns from point scatterers were obtained from Chapter 3.

## 4.3 Results

### *Decorrelation pattern from parallel aggregates of RBCs*

Figure 4.2 shows the mean decorrelation patterns as a function of transverse displacements where the scattering media were formed by strings of point scatterers parallel to the catheter axis and for string lengths of  $2.5\lambda$ ,  $5.0\lambda$  and  $7.5\lambda$ . The results are compared with the mean decorrelation pattern from transverse blood flow simulations for scattering media containing point scatterers (Chapter 3), for both near (Fig. 4.2a) and far (Fig. 4.2b) fields, separately. As can be observed, for both near and far fields, when the length of the string or aggregate of RBCs increases, the rate of decorrelation becomes slower.

### *Decorrelation pattern from aggregates of RBCs with fixed angles*

Figure 4.3 shows the decorrelation function with a string angle of plus or minus  $45^\circ$  as a function of transverse displacements and compared with the decorrelation pattern from point scatterers and from strings ( $2.5\lambda$  in length) parallel to the catheter axis. A similar decorrelation rate compared with the one from point scatterers is observed showing that the rate of decorrelation also depends on the angle between the strings and the acoustical beam. Even so, in the near field (Fig. 4.3a), there is a slight difference when the mean correlation coefficient goes below  $\rho < 0.5$ .

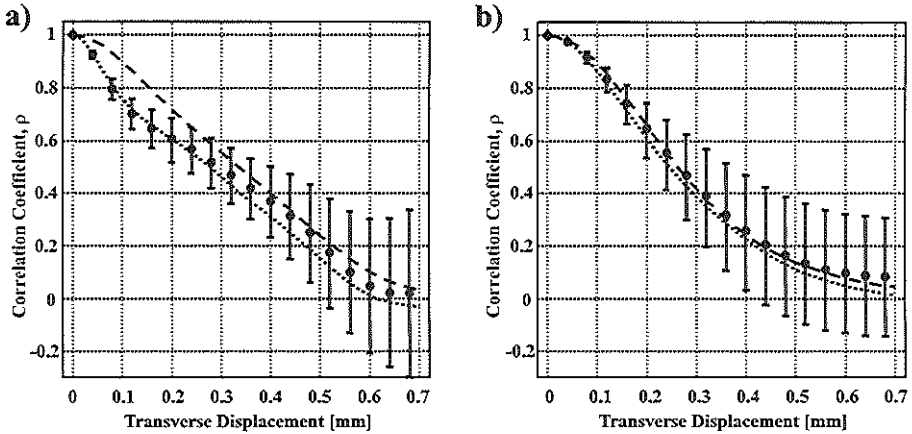


Figure 4.3: Mean decorrelation pattern from strings of point scatterers with angles of  $-45^\circ$  or  $+45^\circ$  and a string length of  $2.5\lambda$  (error bars). The results are compared to the mean decorrelation patterns from point scatterers (dotted line)(Chapter 3) and parallel aggregates of RBCs of  $2.5\lambda$  (dashed line). a) Near field and b) far field.

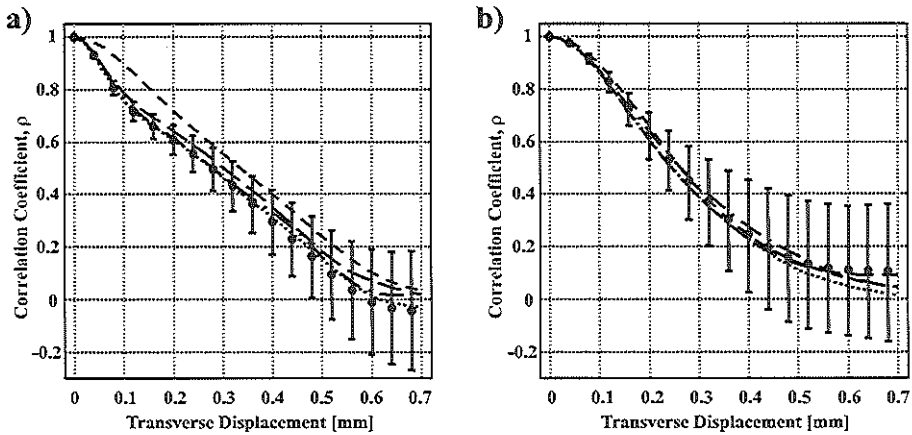


Figure 4.4: Mean decorrelation pattern from strings of point scatterers with random angles ranging from  $-45^\circ$  to  $+45^\circ$  and for string lengths of  $0.75\lambda$  (error bars),  $1.25\lambda$  (dash dotted line) and  $1.75\lambda$  (long dash line). A comparison with the mean decorrelation patterns from point scatterers (dotted line)(Chapter 3) and parallel aggregates of RBCs of  $2.5\lambda$  (short dashed line). a) Near field and b) far field.

#### *Decorrelation pattern from aggregates of RBCs with random angles*

Figure 4.4 shows the mean decorrelation patterns as a function of transverse displacements for strings of  $0.75\lambda$ ,  $1.25\lambda$  and  $1.75\lambda$  in length at random angles

between  $-45^\circ$  and  $+45^\circ$ , for both near (Fig. 4.4b) and far (Fig. 4.4b) fields. These results are compared with the mean decorrelation pattern from point scatterers (Chapter 3) and from strings ( $2.5\lambda$  in length) parallel to the catheter axis. As can be seen, the mean decorrelation patterns for aggregates of RBCs with random angles and different lengths are close to the mean decorrelation patterns from point scatterers in both near and far fields.

## 4.4 Discussion

An example of a scattering medium containing strings of point scatterers as aggregates of RBCs is presented in Figure 4.1a compared with a light microscopic image of human whole blood (Fig. 4.1b), and a reasonable resemblance between the strings and the aggregates of RBCs was observed. The results from the first formulation, presented in Figure 4.2, showed the effect from the interaction between the acoustical beam and the scattering medium characteristics on the decorrelation pattern. In both near and far fields, the mean decorrelation rate became slower when the length of the strings was increased. Thus, each string or aggregate of RBCs was a more directional reflector and had its own impulse response. When the scattering medium resembles a unidirectional medium, the decorrelation pattern as a function of transverse displacements would tend to be closer to 1 for small displacements; if no other source of decorrelation were present (*e.g.* additive noise). Derode et al. (1998) have used the correlation technique in order to compare sets of data from a unidirectional composite made of long and thin fibers perfectly aligned and randomly distributed. When this medium was moved across the ultrasound beam (focal zone from a circular transducer), the decorrelation rate became slower when the scan angle went from  $90^\circ$  (*i.e.* fibers perpendicular to the displacement) to  $0^\circ$  (*i.e.* fibers parallel to the displacement). Thus, through this method, they were able to characterize the scattering medium properties by using the rate of decorrelation.

The results presented in Figure 4.3 show the effect on the rate of decorrelation when strings with random angles ( $-45^\circ$  or  $+45^\circ$ ) were included in the scattering medium. These results compared with the mean decorrelation from strings ( $2.5\lambda$  in length) parallel to the catheter axis, showed that the string angle also defines the rate of decorrelation when the scattering medium contains particles larger than a wavelength; this effect is clearly observed in the near field (Fig. 4.3a). Next, random angles between the strings and the catheter axis ranging from  $-45^\circ$  to  $+45^\circ$  were considered. The results are shown in Figure 4.4 where the mean decorrelation patterns for different string lengths approached the mean decorrelation pattern from point scatterers for both near and far fields. As can be seen, a good agreement between these decorrelation patterns was found in both near and far fields. Thus, the ultrasound reflected from a string depended on the angle



between the acoustical beam and the string and on the string length. Recently, Ledoux et al. (1998) studied the correlation behavior from analytic RF signals received from moving structures where the particle sizes were  $5\ \mu\text{m}$  (Carborundum),  $50\ \mu\text{m}$  (Sephadex) and sponge with 2 pores/mm. The transducer used was a circular single-element transducer with a central-wavelength of  $300\ \mu\text{m}$ ; during both transverse and axial motion, the decorrelation curves showed to be independent from particle sizes within the scattering medium.

As shown in the present study, if strings or aggregates of RBCs flow parallel to the catheter axis, the rate of decorrelation depends on the length of them. Thus, since we are interested in measuring blood flow velocity using a correlation-based method, the aggregation process will affect the velocity measurements. Fortunately, only during laminar flow (*i.e.* blood flowing in a long straight tube and no entrance and outcome effects present) the aggregates of RBCs could be large and flow parallel to the IVUS catheter axis. Qin et al. (1998b) have indicated a cone-shaped orientation of rouleau around the center of the tube with an angle of about  $\pm 25^\circ$ . The experiments were performed with horse blood and under steady flow. Later on, they presented new results describing the rouleau orientations before and after a sudden reduction of the blood flow (Qin et al. 1998a). In both situations, their findings showed the same rouleau orientation pattern as the previous study. Moreover, according to Goldsmith (Goldsmith & Mason 1962), aggregates of RBCs and individual blood cells tend to align to the applied shear stress. For our interest, coronary arteries (usually curved arteries), the conditions for laminar flow are hardly reached; the only presence of an IVUS catheter inside the lumen of the arteries disturbs the blood flow profile. All phenomena that disturb the velocity profile (*e.g.* shear rate  $> 100\ \text{s}^{-1}$ ) will result in a reduction of the RBCs aggregate formation (van der Heiden et al. 1995). Thus, when the IVUS catheter is placed inside the lumen only RBCs and small size of aggregates of RBCs at random angles will be present.

The model presented in this study assumed bulk motion of the scattering medium, such as would be produced by moving tissue or plug blood flow. A more realistic approach should include velocity gradients in the motion of the scattering medium (Ferrara & Algazi 1994). However, Li et al. (1997) have shown, for a rotating single-element catheter, that transverse velocity gradients have a minimal effect on the decorrelation of RF signals. A factor, which was not considered here, is blood flow pulsatility highly present in coronary arteries that produces changes in the shear rates across the vessel lumen. In pulsatile flow, the velocity profile within a vessel changes significantly as a function of the timing within the cardiac cycle (Milnor 1989). The velocity profile is flat during early systole, becomes almost parabolic at peak systole (depending on the hematocrit), and then flattens again during diastole. Results from Cloutier et al. (1993) suggested that prolonged diastole is necessary to observe an aggregate size enlargement in systole because no cyclic variation on the doppler power was found

during pulsatile flow at 70 beats/min and using whole porcine blood. Rouleau formation, during systole and at 70 beats/min, was not observed probably because the red cells do not have enough time in diastole to be brought into contact and to align themselves. As flow accelerates with a flat and more parabolic profile in late systole, the aligned red cells then probably form rouleau until the shear rate within the doppler-sample volume becomes sufficient to break them totally or partly. When the shear rate increases ( $> 100 \text{ s}^{-1}$ ), the aggregation of RBCs ceases and the blood cells tend to become elongated and aligned with the streamline of flow to reduce the blood viscosity (van der Heiden et al. 1995). The aggregation is a reversible process and when the shear rate ceases ( $< 100 \text{ s}^{-1}$ ) the rouleau can be formed again. As suggested by Kitamura et al. (1995), the aggregates of RBCs reduces their resistance to flow through the vessel by placing the rouleau centrally and using a few cells (fluid layer) as a lubricant between the aggregates and the vessel wall. They also presented results for the effective scatterer diameter using washed red cells from healthy males. For three hematocrit levels (20%, 40% and 60%) and a constant level of fibrinogen, the effective scatterer diameter was around  $70 \mu\text{m}$ . Then, where the sample volume within the vessel lumen is considered, single RBCs or aggregates of them can be found. Close to vessel wall, where the shear rates are high, single RBCs are present, and around the center of the vessel lumen where shear rates are low, aggregates of RBCs can be found. Other sources of RF signal decorrelation such as electronic and quantization noise were also not assessed. Nevertheless, if noise were added to the RF signals, the rate of decorrelation would become faster than the rate of decorrelation for noise-less RF signals. The present study was validated *in vitro* and the results are presented in Chapter 6.

## 4.5 Conclusions

In this chapter, we have assessed the ultrasound beam decorrelation characteristics of an IVUS array catheter during transverse blood flow using a computer simulation program. The scattering media were a general representation of blood that included strings of point scatterers as aggregates of RBCs of different lengths and angles. The correlation characteristics were shown to be influenced by the scattering medium properties; the size and orientation of the particles within the medium influenced the rate of decorrelation. When the string angle ranged from  $-45^\circ$  to  $+45^\circ$ , the decorrelation patterns were in agreement with the mean decorrelation pattern from point scatterers. Therefore, only randomly located and omnidirectional point scatterers would be needed to perform such study. From our findings, we suggest that the presence of aggregates of RBCs would probably not affect the measurements of transverse blood flow using the IVUS array catheter, the RF signals and the correlation-based method.

## Chapter 5

# Effects of Different Blood Velocity Profiles on the Correlation-based method

### Abstract

*In recent years, a new method to measure transverse blood flow, based on correlation between consecutive Radio Frequency (RF) signals has been developed. In this chapter, we investigated the influence of non-uniform flow on the velocity estimation. The decorrelation characteristics of transverse blood flow using an intravascular ultrasound (IVUS) array catheter are studied by means of computer modeling. Blood was simulated as a collection of randomly located point scatterers; moving this scattering medium transversally across the acoustical beam represented flow. First-order statistics, the mean-to-standard deviation ratio from the signals, were evaluated. The correlation coefficient method was used to present the results. Three velocity profiles were simulated: random spread of blood-flow velocity, linear blood-flow velocity gradient and parabolic blood flow. RF and envelope signals were used to calculate the decorrelation pattern. The results were compared to the mean decorrelation pattern for plug blood flow. RF signals decorrelation patterns were in good agreement with those obtained for plug blood flow. Envelope decorrelation patterns show a close agreement with the one for plug blood flow. For axial blood flow, there is a discrepancy between decorrelation patterns. The results presented here suggest that the decorrelation properties of an IVUS array catheter for measuring quantitative transverse blood flow will probably be not affected by different transverse blood-flow conditions.*

---

based on the Publication: "Decorrelation-based Blood Flow Velocity estimation: Effect of Spread of Flow Velocity, Linear Flow Velocity Gradients, and Parabolic Flow" by Fermín A. Lupotti, Antonius F.W. van der Steen, Frits Mastik and Chris L. de Korte, *IEEE Transactions on Ultrasonics, Ferroelectrics, and Frequency Control*; 2002: 49(6): 705-714.

## 5.1 Introduction

Commercially available IVUS echo systems produce only conventional B-plane images of the vessel lumen and the surrounding tissue but no blood velocity information is shown; they are unable to measure transverse blood velocity and therefore quantitative volume blood flow can also not be estimated. This will be of great interest for interventional cardiologists using flow information to guide therapy. RF-data processing has significantly enhanced the potential of IVUS (van der Steen et al. 1998a), which is now aiming to obtain information concerning vessel wall and plaque properties and vascular tissue characterization (Céspedes et al. 1997b; de Korte et al. 1998; Spencer et al. 1997b; Bridal et al. 1997a; de Korte et al. 2000). In addition, IVUS has been applied to measure blood flow velocity and volumetric flow (Li et al. 1998b). Crowe et al. (2000) recently introduced qualitative blood flow information by means of a frequency domain method of decorrelation processing using a FIR filter bank.

Li et al. (1997) have previously introduced a time domain technique to measure quantitative blood velocity and blood flow; transverse blood flow velocity and quantitative volume blood flow can be measured using a correlation-based method in a burst of ultrasound beams that were transmitted in the same direction. The measurements were performed from cross-sectional IVUS RF signals. The correlation of the received IVUS RF signals was evaluated as a function of time using a sequence of RF signals acquired at a fixed pulse interval from the same angular position. After gating the RF signals with a fixed window length, the sequence of RF signal windows was phase-matched to remove the axial motion of the scatterers and then the correlation coefficients were calculated as a function of time. Next, in a controlled experimental environment, the correlation coefficients were obtained as a function of transverse displacements of the scatterers to calibrate the method. Blood velocity was then obtained from the ratio of the correlation coefficient as a function of displacement (calibration) and the correlation coefficient as a function of time (measured). The volumetric flow can be calculated by integrating the local transverse velocity with the area element over the complete vessel cross-section (Li et al. 1998b).

Initial *in vivo* evaluations of quantitative volume blood flow assessment based on this method with a rotating-single-element catheter have been presented by Céspedes et al. (1998a) and Carlier et al. (1998b). The rotating single-element catheter has an extra component of decorrelation due to the inherent and constant rotation of the transducer element, which induces an additional lateral displacement with respect to the red blood cells (RBCs) motion (Li et al. 1998b). With the advent of array technology in IVUS applications (O'Donnell et al. 1997a), this extra component of decorrelation is not present since the array transducer is capable of transmitting and receiving a multitude of echoes at exactly the same angle with respect to the array. Using a computer simulation program, the

decorrelation characteristics of the IVUS array catheter during transverse blood flow was assessed (Chapter 3). The mean decorrelation pattern from scattering media containing only point scatterers, as RBCs, agreed with a reference curve based on the auto-convolution of the acoustical beam (Chapter 3). Results, from simulated and *in vitro* measurements for aggregation of RBCs, showed the mean decorrelation pattern in close agreement with the auto-convolution of the acoustical beam, which suggests that the correlation behavior of the IVUS array-catheter ultrasound beam would not be affected by the presence of aggregates of RBCs (Chapter 4 and 6).

In previous studies (Chapter 3 and 4), the transverse decorrelation pattern for plug blood flow was addressed. The present study evaluates the effect of random spread of blood-flow velocity, linear blood-flow velocity gradients and parabolic blood flow on the correlation-based method. Placing the IVUS catheter in the lumen of an artery disturbs the blood flow profile producing blood flow turbulence. This turbulence leads red blood cells to move at different velocities and directions, which means a random distribution of red blood cell velocities. A velocity gradient always exists because blood flow velocities are non-uniformly distributed over the vessel cross section and due to the size and shape of the ultrasound sample volume. For IVUS imaging, the blood velocity changes significantly along the scan depth, leading to a high velocity gradient near the wall and the catheter. RF or envelope decorrelation due to flow gradients or spread of flow is primarily caused by scatterers moving relative to one another within the resolution cell. Blood-flow pulsatility in coronary arteries also produces changes in the shear rate across the vessel lumen. In pulsatile flow, the velocity profile within a vessel changes significantly as a function of the time within the cardiac cycle (Milnor 1989). The velocity profile is flat during early systole, becomes almost parabolic at peak systole, depending on the hematocrit, and then flattens again during diastole.

Friemel et al. (1998), have assessed transverse and axial blood-flow gradients using a point-spread function convolved with an array of random numbers in the frequency domain to produce RF signals. Tilting the point-spread function in the direction of flow simulated flow gradient. They showed the speckle decorrelation due to flow gradients to be highly dependent on the direction of flow; transverse flow was shown to be less susceptible to relative scatterer motion than axial flow. Early studies have also documented that envelope correlation-based techniques, used to estimate axial blood velocity, suffer from velocity spread or gradient. Ferrara et al. (1994), showed the axial velocity spread or gradient as a limiting factor for velocity estimation; the duration of the correlated signal was inversely related to the velocity gradient. The experimental and simulated results, compared to axial blood flow with a constant velocity, showed a faster decorrelation rate when axial velocity spread was considered.

In the current study, a computer program that simulates blood flow by moving a scattering medium across and along the ultrasound beam of an IVUS array catheter was used. Simulation of transverse (*i.e.* displacement across the ultrasound beam) and axial (*i.e.* displacement along the ultrasound beam) blood flow were performed. The backscattered RF and envelope signals were used to observe the influence on the mean decorrelation pattern from different blood velocity profiles. For random spread of blood-flow velocity and linear blood-flow velocity gradients, the decorrelation patterns were assessed for the near field ( $\approx 1$  mm) and for the far field ( $\approx 3$  mm), separately, because of the range dependence of the rate of decorrelation. For parabolic blood flow, the decorrelation pattern was assessed for the full beam depth.

## 5.2 Methods

### 5.2.1 IVUS transducer

The simulated IVUS array catheter is formed by 64 elements mounted on a circular surface of a catheter tip with a diameter of 1.2 mm. The element size of the array under study is 0.7 mm in length ( $L$ ) and 0.028 mm in width ( $W$ ); the pitch of the elements was 0.059 mm (Fig. 3.1). The array transducer operates at a central frequency of 20 MHz and with a -20 dB bandwidth of 7.5 MHz (Eberle 1997; O'Donnell et al. 1997a). The array transducer works in synthetic aperture focusing mode for grayscale imaging and linear mode for color flow imaging. Synthetic aperture focusing mode is not suitable for flow assessment since the acoustical beam is formed over a time frame on the order of milliseconds, during which, the red blood cells will move through the beam and will influence flow assessment based on correlation. Therefore, in flow imaging, four elements are electronically tied together and produce a burst of ultrasound pulses in linear array mode (Borsboom et al. 2000). Then, the system will be shifted one element and the next burst will be generated; this will be repeated 64 times to produce a full frame.

### 5.2.2 Computer modeling

#### General settings

In order to perform the present study, a computer simulation program extended from Chapter 3 was used. In the computer simulation program, four elements were considered as one curved (convex) single element and its area was divided into a grid of small areas with dimensions less than quarter of a wavelength ( $17 \mu m$  for a wavelength of  $75 \mu m$ ). Thus, each small area transmits an echo and the backscattered response received by the entire transducer. In the coordinate system (Fig. 3.1), the  $x$ -axis is the transverse direction, the  $y$ -axis is the lateral

direction and the  $z$ -axis is the axial direction. The center of coordinates is on the surface and in the center of the four elements. The mathematical development to simulate ultrasound signals was based on pressure field calculations using the impulse response method (Borsboom et al. 2000). The ultrasound beam is assumed to be separable in the axial and transverse directions and symmetric with respect to its axis. The axial sampling frequency was 200 MHz to over-sample the response to the correlation function.

### Blood flow simulation

As proposed by Wendling et al. (1992), we considered the echo response or backscattered RF signals from point scatterers within the -20 dB beam-width. Three blood velocity profiles were simulated for which the pulse repetition interval (PRI) used was  $37.4 \mu\text{s}$ . Firstly, for both transverse and axial flow, a random spread of blood-flow velocities was implemented as point scatterers moving at random normally distributed velocities within the scattering medium (Fig. 5.1). Secondly, for transverse flow, a linear blood-flow velocity gradient was simulated where the point scatterers' velocities were defined as a linear function of depth considered only within scattering medium. Thus, the scatterers at the edge of the scattering medium nearest to the transducer were assumed to have the lowest velocity and the scatterers at the distant edge were assumed to have the highest velocity. For both random spread of blood-flow velocity and linear blood-flow velocity gradient, the scatterer velocity distribution is described as follows. For transverse displacements, the velocity ranged from 26.7 cm/s to 80.1 cm/s with a mean velocity of 53.4 cm/s. For axial displacements, the velocities were 10% of the transverse velocities. Third, transverse plug blood flow was simulated for the full beam depth where the velocity was 53.4 cm/s; and transverse parabolic blood flow was also simulated where the velocity ranged from 0 cm/s to 80.1 cm/s with a mean velocity of 53.4 cm/s. According to Wentzel et al. (1997), the ratio of the maximal velocity in the direction of blood flow normalized by the mean velocity should be close to 1.5. The geometry of the parabolic blood-flow profile was defined as 1 minus the squared of the ratio between the distances from the center of the lumen ( $r$ ) over the total radius of the lumen vessel ( $R$ ) all multiply by the peak velocity ( $V_{\text{peak}}$ ) (*i.e.*  $(1-(r/R)^2) * V_{\text{peak}}$ ). The blood velocities used during this study included high physiological blood velocities and velocities beyond them in order to evaluate the entire correlation function.

At each displacement of the scattering medium, the backscattered RF signals from the point scatterers within the -20 dB beam-width were summed and saved as one RF signal. As the scattering medium was moved, the  $x$ - and  $z$ -coordinates changed for all the point scatterers' coordinates representing transverse and axial blood flow, respectively. For the used scatterer density, the average number of point scatterers inside the -20 dB beam-width was approximately constant.

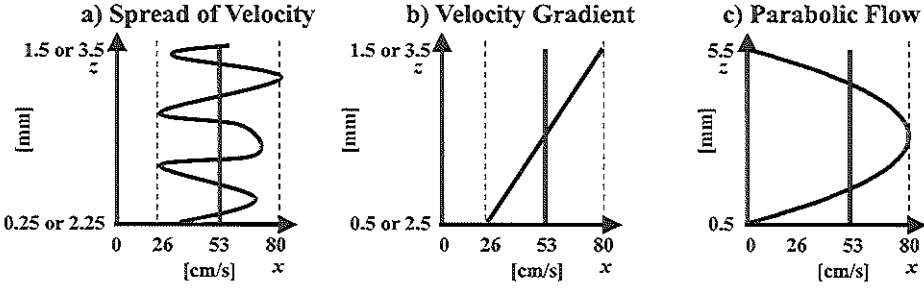


Figure 5.1: Different blood flow conditions: a) spread of blood-flow velocity, b) linear blood-flow velocity gradients and c) parabolic blood flow. The spread of blood-flow velocity shown here is just an example; this was not used during the study. Plots a) and b) show two scales on  $z$ -axis, which means scale for the near field and for the far field, respectively.

The locations of the point scatterers were measured with respect to the origin of the reference axis. Let  $e(P, n)$  be the backscattered (RF) signal from a point scatterer located in  $P_k(x, y, z)$  where  $n$  is discrete time and  $k=1, 2, \dots, K_{tot}$ . Let  $s(n)$  be the summation of backscattered RF signals from  $K_{-20dB}$  point scatterers, within the -20 dB beam-width, when the scattering medium was transversally moved  $d$  steps:

$$s_d(n) = \sum_{k=1}^{K_{-20dB}} e(P_k(x + d\Delta x, y, z + d\Delta z), n) \text{ for } d = 0, 1, \dots, D, \quad (5.1)$$

where  $K_{-20dB} < K_{tot}$ ,  $d\Delta x$  and  $d\Delta z$  were the transverse and axial displacements, respectively, and  $D$  was the total number of displacements. The envelope was defined as the absolute value of the Hilbert transform of the  $s(n)$  signal.

### Scattering medium

The scattering medium was defined as a collection of omnidirectional and randomly positioned point scatterers in a three-dimensional space. This is the simplest way to mimic blood; a more realistic approach, *e.g.* strings of point scatterers at random angles and lengths as aggregates of RBCs was already studied, suggesting that there is no effect on the decorrelation pattern (Chapter 4 and 6). For computational efficiency, the beam profile and its decorrelation properties were evaluated at two depths, first in the near field ( $\approx 1$  mm) and second in the far field ( $\approx 3$  mm).

For both near and far fields, the  $x$  size of the scattering medium was defined as the summation of the length of the transducer element (0.7 mm) plus the number of displacements of the scattering medium by the maximum step size ( $\Delta x_{max}$ ),



which depends on the blood flow conditions under study. By measuring the -20 dB beam-width, as suggested by (Wendling et al. 1992), the  $y$  size of the scattering medium was determined. The  $z$  size of the scattering medium was set around the axial distance of interest. In the near field, the volume sizes of the scattering medium were  $-2.5 \text{ mm} \leq x \leq 0.5 \text{ mm}$ ,  $-0.6 \text{ mm} \leq y \leq 0.6 \text{ mm}$  and  $0.25 \text{ mm} \leq z \leq 1.5 \text{ mm}$  (Fig. 3.1 for the coordinate system). In the far field, the volume sizes of the scattering medium were  $-2.5 \text{ mm} \leq x \leq 0.5 \text{ mm}$ ,  $-1 \text{ mm} \leq y \leq 1 \text{ mm}$  and  $2.25 \text{ mm} \leq z \leq 3.5 \text{ mm}$ . The  $x$  and  $z$  size of the scattering media are asymmetric since the scattering medium have to be moved transversally or axially respect to the acoustical beam; new point scatterers need to be brought into the acoustical beam to produce blood flow. For transverse parabolic blood flow simulation, the  $x$  size of the scattering medium remained as for previous cases and the  $y$  size of the scattering medium was determined using an average of the -20 dB beam-width along the ultrasound beam. The  $z$  size of the scattering medium ranged from 0.5 mm to 5.5 mm. For all flow conditions, the scatterer density was chosen to meet the Rayleigh criterion: 1800 per  $\text{mm}^3$  (Chapter 3).

### 5.2.3 Statistical properties of the scattering medium

#### First-order statistics

The mean-to-standard deviation ratio of the sub-sampled envelope of the RF signals was used to verify that the first-order statistics of the backscattered signals were consistent with the theory, where the theoretical mean-to-standard deviation ratio should be 1.91 (Wagner et al. 1983; George et al. 1976). The mean-to-standard deviation ratio of the sub-sampled envelope of the RF signals was tested and the result ( $1.92 \pm 0.17$ ) was close to the theoretical value.

#### Second-order statistics

In order to evaluate the RF signals coming from the scattering medium, the second-order statistics were used. The correlation coefficient  $\rho_{i,j}$  between two RF signals,  $s_i(n)$  and  $s_j(n)$ , received from positions of the scattering medium corresponding to  $d=i$  and  $d=j$  is:

$$\rho_{i,j} = \frac{\sum_{n=1}^N (s_i(n) - \bar{s}_i(n)) \cdot (s_j(n) - \bar{s}_j(n))}{\sqrt{\sum_{n=1}^N (s_i(n) - \bar{s}_i(n))^2 \cdot \sum_{n=1}^N (s_j(n) - \bar{s}_j(n))^2}} \quad (5.2)$$

where the subscript  $i=1,2\dots D$  and  $j=1,2\dots D$  being  $D$  the number of displacements (*i.e.* number of signals). For the RF signals,  $N$  is the length in time and  $\bar{s}$  is the mean value. The  $\rho_{i,j}$  are the correlation coefficients for the signal pair,  $s_i$  and  $s_{i+m}$ , which are spaced  $m=(j-i)$  steps and  $m=0,1\dots D-1$ .

Let  $\rho_{i,i+m}$  be the correlation coefficient between the signals  $s_i$  and  $s_{i+m}$  when the space is zero (*i.e.*  $m=0$ ). Thus, the average correlation coefficients when  $m=0$  is  $\rho_0$ . In such case,  $m=0$ , the correlation coefficient is equal to one when no other source of decorrelation is present (*e.g.* electronic noise). For the case of  $m=1$ ,  $\rho_{i,i+1}$  is the correlation coefficient between the signals  $s_i$  and  $s_{i+1}$ , and the average correlation coefficients when  $m=1$  is  $\rho_1$ .

In a more general equation, the average correlation coefficient in the signal set  $\rho_m$  for a space of  $m$  steps between signals is calculated. Thus,  $\rho_m$  describes the transducer decorrelation pattern as a function of transverse displacements of a scattering medium (Chapter 3). Because the correlation coefficients were not normally distributed, the Fisher-Z transform (Appendix B) was used to present the results.

### 5.3 Results

The mean decorrelation pattern as a function of transverse displacements for spread of blood-flow velocity is shown in Figure 5.2 for the near field and for the far field, separately. In both near (Fig. 5.2a) and far (Fig. 5.2c) fields, the mean decorrelation pattern from RF signals is in agreement with the one for plug blood flow (Chapter 3). Similar results for the envelope are presented in Figures 5.2b and 5.2d, for both near and far fields, where a close agreement between mean decorrelation patterns is observed for the near field. However, for the far field (Fig. 5.2d), the mean decorrelation pattern occurs at a faster rate than the one for plug blood flow.

For blood-flow velocity gradients, the mean decorrelation pattern as a function of transverse displacements is shown in Figure 5.3. In both near (Fig. 5.3a) and far (Fig. 5.3c) fields, the mean decorrelation pattern for blood-flow velocity gradients is in agreement with the one for plug blood flow. However, in the near field, the rate of decorrelation is slower when the mean decorrelation pattern is below 0.5 (Fig. 5.3a). Similar results for the envelope are presented in Figures 5.3b and 5.3d where close agreements between mean decorrelation patterns are also observed.

Full depth blood-flow simulations were also performed for plug blood flow and parabolic blood flow. The mean decorrelation pattern for parabolic blood flow showed agreements with the one for plug blood flow for both RF and envelope signals, Figures 5.4a and 5.4b, respectively. However, one could observe, especially in Figure 5.4b, that the rate of decorrelation became slower with respect to previous results.

A mean decorrelation pattern as a function of axial displacements for random spread of blood-flow velocity is shown in Figure 5.5. Using the RF signals in both near and far fields, Figures 5.5a and 5.5c, respectively, the mean decorrelation

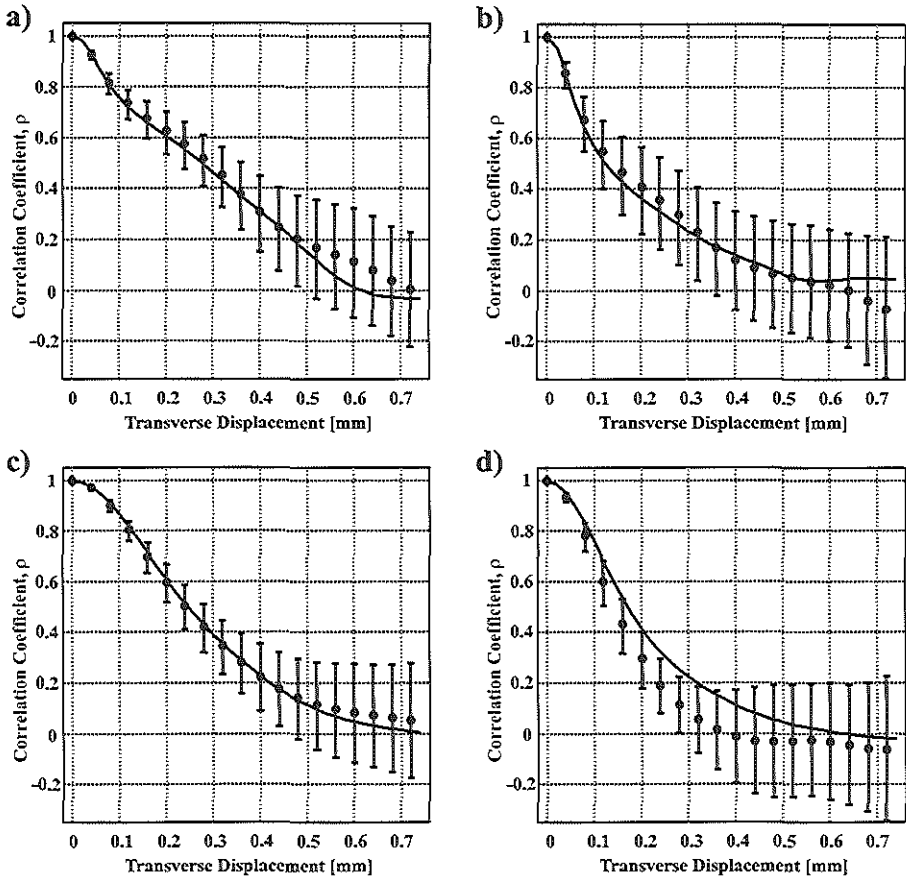


**Figure 5.2:** Transverse blood-flow, mean decorrelation pattern for plug blood flow (solid line) compared with the one for spread of blood-flow velocity (error bars). For the RF signals, a) near field and c) far field; and for the envelope, b) near field and d) far field.

pattern for spread of blood-flow velocity is similar to the one for plug blood flow before the first zero crossing where the mean decorrelation patterns start to diverge. Similar results for the envelope are presented, for both near (Fig. 5.5b) and far (Fig. 5.5d) fields, where discrepancies between mean decorrelation patterns are observed. The envelope mean decorrelation pattern for axial spread of blood-flow velocity is faster than the one for axial plug blood flow.

## 5.4 Discussion

In previous studies (Chapter 3 and 4), RF signal decorrelation pattern for plug blood flow was shown in agreement with the auto-convolution of the acoustical

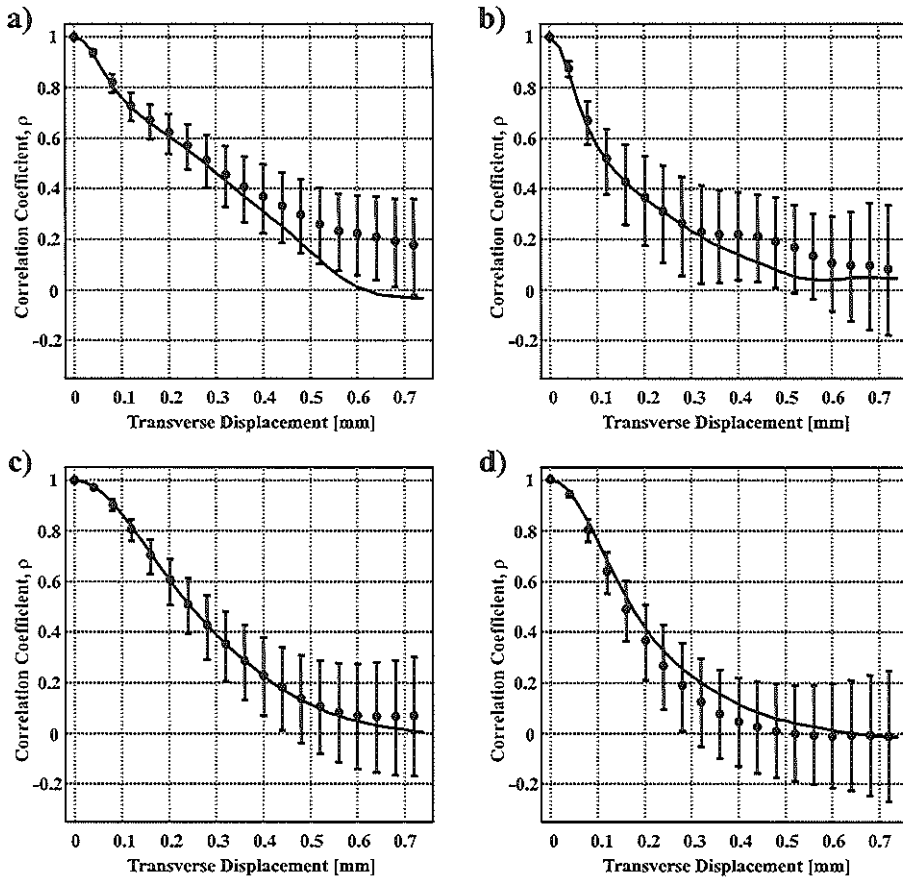


**Figure 5.3:** Transverse blood-flow, mean decorrelation pattern for plug blood flow (solid line) compared with the one for linear blood-flow velocity gradients (error bars). For the RF signals, a) near field and c) far field; and for the envelope, b) near field and d) far field.

beam; such agreement was not found when using the envelope signal. The analysis of the decorrelation patterns presented here, for the RF and the envelope signals and for different blood flow conditions, showed the mean decorrelation pattern to have a monotonic decay as a function of transverse or axial displacements before the first zero crossing, in both near and far fields (Fig. 5.2-5.5). The RF decorrelation patterns showed smaller standard deviations and better agreements between curves than for the envelope; which suggests that RF decorrelation is less sensitive to different blood flow conditions than envelope decorrelation. The only deviation for RF decorrelation was found in the near field for lateral displacements above 0.4 mm. The decorrelation was below 0.3 at this point (Fig. 5.3a). The reason for this deviation could be explained as follows. First, when groups of

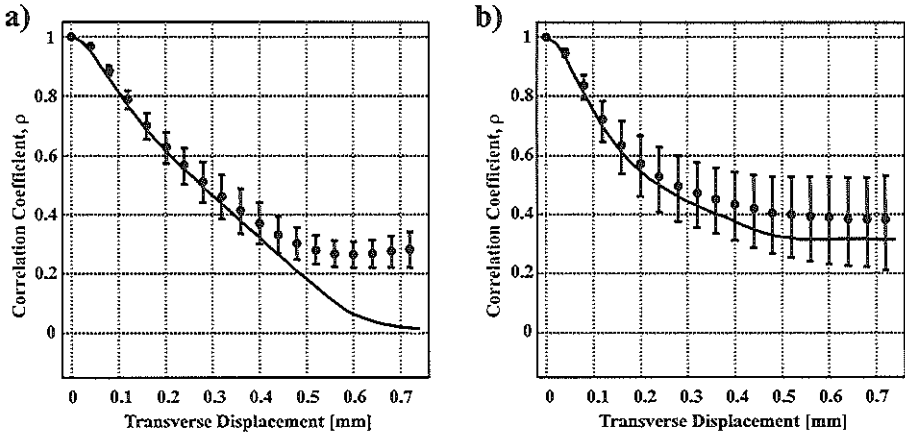


**Figure 5.4:** Transverse blood-flow, mean decorrelation pattern for plug blood flow (solid line) compared with the one for parabolic blood flow (error bars) for the full beam depth, a) for the RF signals and b) for the envelope.

scatterers enter the sample volume with higher amplitude than the rest, these scatterers may dominate the correlation function and so the velocity estimation. In general, the pressure field along the acoustical axis of an ultrasound transducer exhibits rapid fluctuations in the near field and gradually decay in the far field. The transition from the near field to the far field could be defined to occur at the last axial maximum of the pressure response (Christensen 1988). Borsboom et al. (2000) have shown that the maximum amplitudes for this array catheter are located in the near field with a last axial maximum located around 1.5 mm away from the transducer surface. Since the scatterers with low velocities were close to the transducer, the backscattered RF signals had maximum amplitude and thus they will govern the correlation function. Secondly, for displacements larger than 0.4 mm, the scatterers distant from the transducer, which were moving at high velocity, remain for a short period of time within the sample volume. Note that this deviation was not present in the far field (Fig. 5.3c), which could correspond to the uniform beam profile. For quantitative blood flow measurements using the correlation-based method, correlation values ranging from 1 to 0.7 are used and so this deviation will have no influence on the measurements. In case of using the envelope, a faster rate of decorrelation was shown compared to the one for the RF signals, which could be explained by the loss of phase information. The phase information contributes to an increase in the probability of finding the best match between RF signals. An increase in the standard deviations (Fig. 5.2b, 5.2d, 5.3b and 5.3d) due to the decrement in the signal bandwidth by the envelope detection process is observed; the variance is inversely related to the signal bandwidth (Bendat & Piersol 1986).

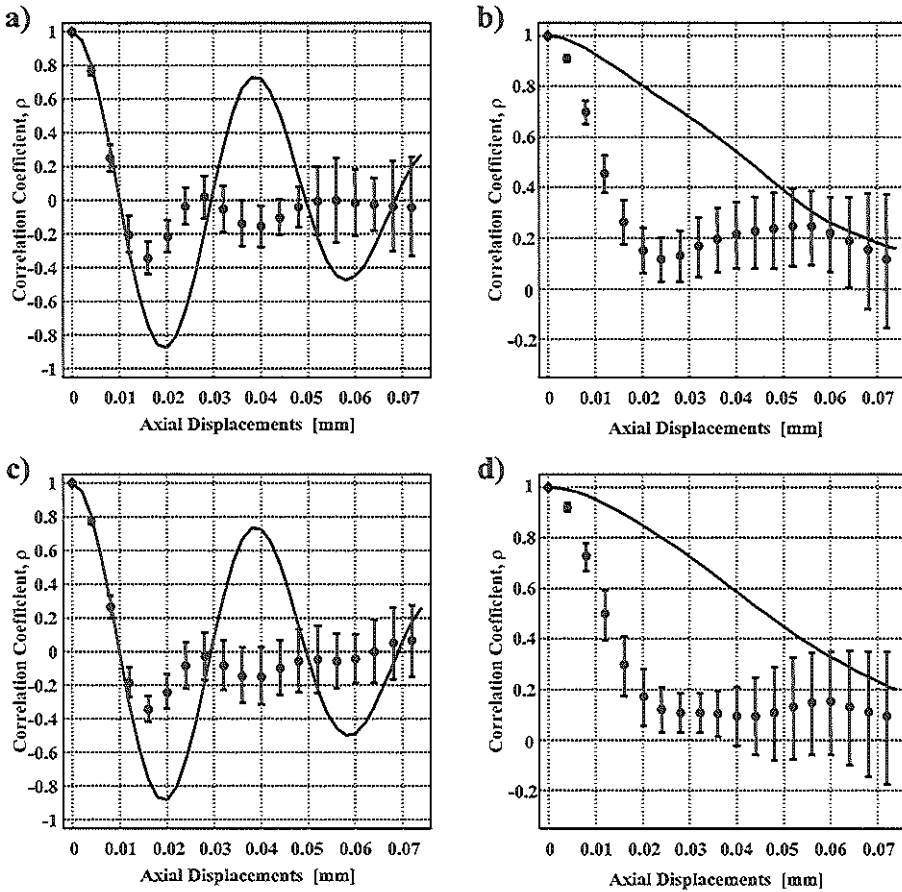


**Figure 5.5:** Axial blood flow, mean decorrelation pattern for plug blood flow (solid line) compared with the one for spread of blood-flow velocity (error bars). For the RF signals, a) near field and c) far field; and for the envelope, b) near field and d) far field.

For the full depth blood flow simulation, the decorrelation pattern for plug blood flow and for parabolic blood flow were in close agreement (Fig. 5.4a). Here, a deviation was also observed for displacements larger than 0.4 mm, which can be explained as for the case of linear blood-flow velocity gradient (Fig. 5.3a).

In the case of axial blood flow (Fig. 5.5), and for the RF signals (Fig. 5.5a and 5.5c), the mean decorrelation pattern for random spread of blood-flow velocity was shown in close agreement to the one for plug blood flow in both near and far fields until the first zero-crossing. The RF decorrelation pattern decreases quickly when the phase is shifted as a result of the axial blood flow. For plug blood flow, and in both near and far fields, a sinusoidal pattern was observed which clearly depends on the phase of the RF signals. This sinusoidal pattern was hardly seen

when there is a spread of blood-flow velocity, which may be produced by the changes in phase due to the relative motion between point scatterers. Another observation is that the decorrelation patterns, in both near and far fields, were similar to each other meaning that there is no difference between the near and far field in terms of decorrelation patterns. These results are in accordance with the ones shown by Friemel et al. (1998), who showed the axial RF decorrelation pattern to be affected by the presence of axial velocity gradient. Their results showed a significantly smaller overlap between the pre- and post-gradient spectra for axial flow than for lateral flow; the degree of overlap between the Fourier transforms of the two functions represented the similarity between signals. The band-pass nature of the axial component of the spectrum causes the images to be susceptible to axial flow gradients; however, the low-pass nature of the lateral component guarantees some overlap between the spectrums.

Envelope decorrelation patterns for axial blood flow were presented in Figures 5.5b and 5.5d. The mean decorrelation pattern for axial spread of blood-flow velocity was much faster than the one for axial plug blood flow, in both near and far fields. This discrepancy between curves suggests that axial blood flow could not be measured using the envelope if axial spread of blood-flow velocity is present in the stream of flow. Therefore, the size of a correlation window should be sufficiently small to reduce velocity differences within the correlation window in order to limit the error caused by the presence of axial spread of blood-flow velocity when using the envelope. Thus, there is a trade-off in the window length between variations in decorrelation estimate and the resolution of velocity measurement or the error caused by velocity gradients. Alternatively, several decorrelation values should be obtained for one window position to reduce the variation of the measurements. These results agree with those from Ferrara et al. (1994) who noted that the decrease in the signal correlation can be predicted as a function of the mean lateral velocity and axial velocity spread within the sample volume.

A factor, which was not considered here, is blood flow pulsatility such as that present in coronary arteries that produces changes in the shear rates across the vessel lumen. In pulsatile flow, the velocity profile within a vessel changes significantly as a function of the timing within the cardiac cycle (Milnor 1989; Cloutier & Shung 1993). The velocity profile is flat during early systole, becomes almost parabolic at peak systole, depending on the hematocrit, and then flattens again during diastole. In the case of transverse blood flow, the change in blood velocity profile produces significant velocity gradients, which it is suggested here to may not affect the blood flow measurements using the correlation-based method. However, in the case of axial blood flow, the change in blood velocity profile could affect the blood flow measurements. Aggregation of RBCs was also not considered here, results from other studies suggest that aggregation of RBCs, at random lengths and angles, does not affect the rate of decorrelation (Chapter 4 and 6).

Results from Cloutier et al. (1993) suggested that prolonged diastole is necessary to observe an aggregate size enlargement in systole because no cyclic variation on the Doppler power was found during pulsatile flow at 70 beats/min using whole porcine blood. Rouleau formation, during systole and at 70 beats/min, was not observed probably because the red cells do not have enough time in diastole to be brought into contact and to align themselves. As flow accelerates with a flat and more parabolic profile in late systole, the aligned red cells then probably form rouleau until the shear rate within the doppler-sample volume becomes sufficient to break them either totally or partly.

From the results presented here, for the RF and envelope signals, one can observe that during transverse blood flow there is no significant effect on the decorrelation pattern when random spread of blood-flow velocity, linear blood-flow velocity gradient or parabolic blood flow were present in the stream of flow. A similar result can be seen for axial blood flow and for the RF signals when spread blood-flow velocity was considered.

## 5.5 Conclusions

In the present study, we have assessed the ultrasound beam decorrelation characteristics of an IVUS array catheter under representative transverse and axial blood flow conditions. The scattering media were a simple representation of blood that included only omnidirectional and randomly located point scatterers as red blood cells. In the case of spread of blood-flow velocity, linear blood-flow velocity gradient or parabolic blood flow, the decorrelation patterns were in good agreement with the mean decorrelation pattern for plug blood flow when using the RF signals. For the envelope, close agreement was found between decorrelation patterns for different flow conditions. From our findings, we can conclude that the presence of different flow conditions will probably not affect the measurements of transverse blood-flow with an IVUS array catheter using the correlation-based method. In the case of axial blood flow, the measurements of blood flow using the correlation-based method will be affected by the presence of spread of blood-flow velocity.



## Chapter 6

# Effects of Aggregation of Red Blood Cells and Linear Velocity Gradients on the Correlation-based method: *In vitro* validation

### Abstract

*Recent computer simulations suggested that the presence of aggregates of red blood cells (RBCs), at random angles and lengths, does not affect the measurements of transverse blood flow using a correlation-based method and an IVUS array catheter. However, in case of aggregates of RBCs aligned with the flow, the measurements of simulated blood velocity are affected. Blood velocity gradients were also shown not to influence the correlation-based method for blood velocity estimation. The objective of this study is to quantify the influence of aggregates of RBCs and blood velocity gradients on the correlation-based method during in vitro experiments. For this purpose, measurements were performed on washed RBCs (no aggregation), normal human blood and two types of diseased blood in which a lower or a higher level of aggregation was present. The decorrelation pattern of a circular ultrasound transducer as a function of transverse blood flow was studied using a Couette system. Changing the shear rate of the Couette system modified the aggregation level of RBCs and the velocity gradient. With the exception of the results at low shear rates and abnormally high aggregation levels, agreements were found between the auto-*

---

based on the Publication: "Effects of Aggregation of Red Blood Cells and Linear Velocity Gradients on the Correlation-based method for Quantitative IVUS Blood Flow at 20 MHz" by Fermín A. Lupotti, Audrey Zimmer, Michel Daronat, F. Stuart Foster, Antonius F.W. van der Steen and Guy Cloutier, *Ultrasound in Medicine and Biology*, submitted; 2002

*convolution of the acoustical beam and the RF decorrelation patterns. For the high shear rate present in coronary arteries, the correlation-based method for blood flow estimation should not be influenced by these phenomena.*

## 6.1 Introduction

Intravascular ultrasound (IVUS) imaging has become a valuable diagnostic tool in interventional cardiology (Siegel 1998). RF-data processing has significantly enhanced the potential of IVUS (van der Steen et al. 1998a). In addition, IVUS has been applied to measure blood flow velocity and volumetric flow (Li et al. 1998b). The principle of blood flow assessment depends on the acoustical beam characteristics of the transducer; the decorrelation has proven to be proportional to the transverse blood velocity and related to the characteristic of the acoustical beam.

When RBCs flow through a vessel, they can form aggregates known as rouleau (Chien 1974; Fung 1993). Depending on the characteristics of the blood sample and flow rate, complex 3D networks also can be formed. Red blood cell aggregation has been associated with diabetes (Le Devehat et al. 1990), dyslipidemia (Razavian et al. 1992), hypertension (Zannad et al. 1988), cardiac and cerebral vascular diseases (Neumann et al. 1991), thromboembolic events (Chabanel et al. 1994), carcinoma and inflammation (Weng et al. 1996). The process of RBC aggregation depends basically on three conditions: a sufficient concentration of RBCs (*i.e.* Hematocrit), a sufficient concentration of macromolecules (*i.e.* fibrinogen and others) and a shear rate in blood low enough to leave the aggregates intact (Chien 1974). When the shear rate increases ( $> 100 \text{ s}^{-1}$ ), the aggregation of RBCs ceases to be important and the blood cells tend to become elongated and aligned with the streamline of flow to reduce the blood viscosity (Fung 1993). Aggregation is a reversible process and when the shear rate is lowered ( $< 100 \text{ s}^{-1}$ ) the rouleau can be formed again.

Weng et al. (1996, 1998) studied the influence of acute-phase proteins (group of plasma glycoproteins synthesized by the liver) on erythrocyte aggregation. The proteins such as haptoglobin (Hp), C-reactive protein (CRP) and ceruloplasmin (Cp) had an effect on the aggregation kinetics and adhesive forces between erythrocytes; more specifically, abnormal high levels of Hp and Cp induced a significant increase in the reversible erythrocyte rouleau formation, while CRP and Cp increased the adhesive forces of the aggregates. In patients with unstable angina pectoris, abnormal RBC aggregation levels were found to be predictive of subsequent acute myocardial infarction (Neumann et al. 1991).

During human IVUS interventions, the ultrasound transducer is in direct contact with blood; the ultrasound beam is not attenuated or deflected by any other structure such as tissue. Van der Heiden et al. (1995) showed, for a

rotating-single element IVUS catheter with a central frequency of 30 MHz, that when RBCs aggregation goes on during blood flow, the integrated backscatter power increases. Recently, a study of the decorrelation characteristics of an IVUS array catheter during transverse blood flow was performed (Chapter 3 and 4). First, blood was simulated as a collection of omnidirectional and randomly located point scatterers as single RBCs; and second, strings of point scatterers at random angles and lengths as normal physiological aggregates of RBCs simulated blood in a more general way. Agreements were found between decorrelation patterns from both scattering media and the auto-convolution of the acoustical beam. However, when the aggregates of RBCs were aligned with the flow, the rate of decorrelation became lower. Simulation of blood flow with a linear blood velocity gradient or shear rate (*e.g.* near the wall boundaries in case of a parabolic blood flow) was performed, which showed to produce no effect on the mean decorrelation pattern (Chapter 5). In that last study, point scatterers were considered and the possible effect of rouleau was ignored.

In the present study, *in vitro* experiments were performed to corroborate previous simulation studies on the influence of aggregates of RBCs and of linear blood velocity gradients on the correlation-based method for blood velocity estimation. The decorrelation pattern of the RF signals caused by transverse blood flow was studied using a circular ultrasound transducer in a Couette system. Whole human blood samples and washed RBCs drawn from healthy volunteers and from patients were used. The Couette system produces a stable linear velocity gradient or shear rate that, when varied, modified the level of aggregation of RBCs in the whole blood. The objective of this study was to quantify the influence of aggregates of RBCs and linear blood velocity gradients on the correlation-based method during transverse blood flow, and judge how this could affect the measurements of quantitative blood flow.

## 6.2 Materials and Methods

### 6.2.1 Blood samples

Whole blood was freshly drawn from 20 individuals and immediately anticoagulated with ethylenediamine tetra acetic acid (EDTA, 3 g/L); 8 blood samples were from healthy volunteers from our institutional staff, 2 were from a blood bank, and 10 were from patients with a disease that could increase the aggregation of RBCs such as cardiovascular disease, diabetes, hypercholesterolemia, hypertension, hyperlipidemia, thrombosis or heavy smoking. The hematocrit of the donor was not adjusted and thus remained to its physiological value for the 8 normal and 10 diseased blood samples. The blood samples of patients collected during peripheral interventions represent a typical population normally prescribed for an IVUS exam of their coronary arteries.

The 2 larger blood volumes, obtained from the blood bank, were used to produce washed blood samples where the hematocrit was set as close as possible to 40%. These 2 blood samples were centrifuged and the plasma was replaced with a saline solution; this washing procedure was repeated three times to remove any plasma proteins promoting aggregation. The three groups of sample blood are identified here on as normal blood, diseased blood and washed RBCs, respectively. The diseased blood samples were subdivided in two subgroups according to the aggregation level measured with an erythroaggregameter.

### 6.2.2 Blood tests

Blood tests, such as the hematocrit and the aggregation level, were performed on all blood samples used in this study. The hematocrit was measured using a micro-centrifuge system (Haemofuge, Heraeus Instruments) at 12000 rpm for 10 min. The RBC aggregation level was determined with an erythroaggregameter based on a Couette flow arrangement (Regulest, France) (Houbouyan et al. 1997). A blood volume of 1.5 ml was needed to perform these measurements. The instrument provides information on the aggregation time (sec), the mean kinetic index at 10 sec or aggregation index ( $S_{10}$ , no unit), partial ( $\gamma_D$  in  $s^{-1}$ ) and total dissociation thresholds ( $\gamma_S$  in  $s^{-1}$ ). The aggregation time was obtained from the inverse of the slope of the scattered light intensity variation between 0.3 and 1.9 sec after stoppage of the flow rotation.

The index  $S_{10}$  was calculated as the ratio of the area above the light intensity curve during the first 10 sec following flow stoppage to the total area within the same period of time. The partial dissociation threshold ( $\gamma_D$ ) was obtained from the intersection of a regression line computed for shear rates below  $20 s^{-1}$  and a horizontal line intercepting the maximum of the scattered light intensity, and the total dissociation threshold ( $\gamma_S$ ) corresponded to the shear rate at the maximum scattered light intensity. These last two parameters provide information about the adhesive force between red blood cells. A low value of  $S_{10}$ ,  $\gamma_D$  and  $\gamma_S$  indicate a low level of aggregation and vice versa (Cloutier & Qin 2000). The aggregation time is inversely proportional to the kinetics of rouleau formation.

### 6.2.3 Experimental setup

The experimental setup was formed by a Couette system, an echo system (VS40 Ultrasound BioMicroscope (UBM), VisualSonics Inc., Toronto, ON, Canada) and a PC-based acquisition system (Fig. 6.1).

#### The Couette system

The Couette system was used to produce linear blood velocity gradient profiles at a given shear rate (Whorlow 1980; van der Heiden et al. 1995). It requires

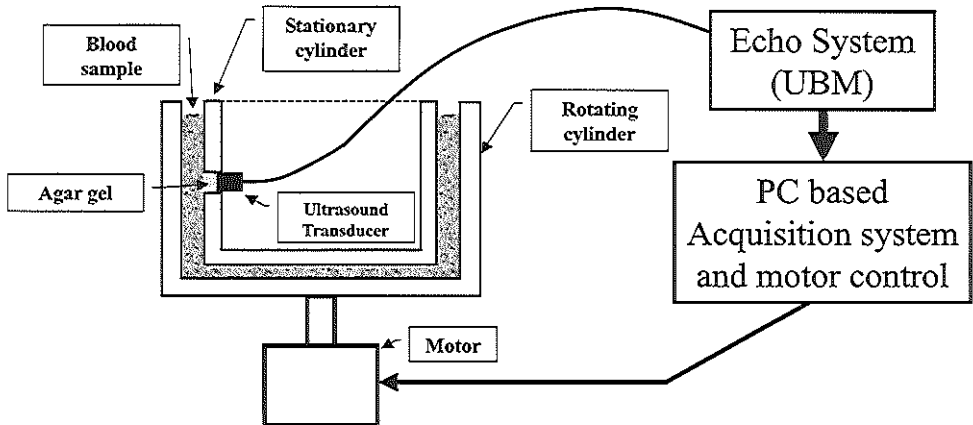


**Figure 6.1:** Experimental setup, the Couette system formed by 2 cylinders. The outer cylinder rotates at a given angular velocity driven by the motor while the inner one is fixed and holds the ultrasound transducer. The blood sample ( $\approx 50$  ml) flows in the 2 mm gap between the coaxial cylinders.

only 50 ml of blood. The system consisted of a stationary inner cylinder and a rotating outer cylinder (Fig. 6.1). The gap between cylinders was 2 mm, where the blood shear rate was approximately constant. The Couette flow system of the current study was originally designed for ultrasound high frequency blood backscattering measurements (Foster et al. 1994).

### The ultrasound transducer and the echo system

The ultrasound transducer, a 36 MHz 3-mm circular PVDF transducer (-6 dB bandwidth of 18-54 MHz and focused at 6 mm), was excited at a pulse repetition frequency (PRF) of 5 KHz. The transducer was placed in the stationary inner cylinder (Fig. 6.1). The positioning of the transducer, perpendicular to the area of interest and at the right focal length, was important to obtain the best RF signals for measuring the decorrelation patterns. The transducer was screwed within the inner cylinder made of plexiglas. Agar gel was used to fill the acoustic window between the transducer surface and the blood sample. The UBM echo system provides controls of the gain, filters, and central frequency that were adjusted to optimize the signal-to-noise ratio. The ultrasound system fired bipolar square wave pulses at a central frequency of 19 MHz, the UBM band-pass filter was set to 10-80 MHz; and a receiving gain around 23 dB was used for all the experiments. The location of the measurement window ranged from 4.5 to 7.5 mm from the face of the transducer (around the focal depth) and the length of the window was 2 mm (gap between cylinders).

## The PC-based acquisition system

The acquisition system was based on a PC with an acquisition board (CS 8500 GageScope board, Gage Applied Sciences Inc., Montreal, QC, Canada) and the Compuscope software that allows the acquisition of multiple sets of RF signals. RF data were digitized at a sampling frequency of 250 MHz into 8 bits; sets of RF signals at the PRF of 5 KHz were acquired with a time interval of 5 seconds between sets and this was performed for each shear rate in order to reach the steady state plateau of aggregation. A computer program implemented in LabView (National Instruments, Austin, TX, USA) was used to control the rotational speed (*i.e.* the shear rate) of the outer cylinder of the Couette system.

### 6.2.4 Protocol for the experiments

All experiments were performed at room temperature ( $\approx 22$  °C). Prior to each experiment, the blood hematocrit and aggregation level were measured as mentioned above. After the blood sample was placed in the Couette system, the measurements were performed as follows. In the first 120 s, a shear rate of  $600 \text{ s}^{-1}$  was applied to break RBC aggregates. The shear rate was then reduced to values of 1, 5, 20, 40 or  $80 \text{ s}^{-1}$  and acquisition was performed for 240 s. The measurements were repeated twice for each blood sample and shear rate. Thirty-six sets of 120, 90 and 60 RF signals were acquired for shear rates of 1, 5 and  $20 \text{ s}^{-1}$ , respectively; and 36 sets of 30 RF signals were acquired for shear rates of 40 and  $80 \text{ s}^{-1}$ . One set of RF signals, from the 36 sets, was acquired during the disaggregation phase just before the beginning of the aggregation phase, which is considered to be acquired at time 0.

### 6.2.5 Signal processing

#### Relative backscattered signal power

The relative backscattered signal power (in dB) as a function of time was calculated to follow the aggregation kinetic of the red blood cells. Since all measurements were performed at the same distance from the transducer using the same window length as a setting of the system, no correction was made for the beam characteristics of the transducer for the assessment of the backscattered power. The relative backscattered signal power is defined as 10 times the  $\log_{10}$  of the summation of the squared backscattered RF signal components normalized by the number of sample points. The mean raising slopes of the relative backscattered signal power as a function of time was calculated (in dB/s) based on measurements at time 0 and at 20 sec in the aggregation phase.

### Statistical analysis

The correlation coefficient  $\rho_{i,j}$  between two RF signals,  $s_i$  and  $s_j$ , was calculated using a standard method as described in Chapter 3. The relative backscattered signal from blood (about 2 mm in length) was used for the calculation of the correlation coefficients. Because the correlation coefficients are not normally distributed, the Fisher-Z transform was used to present the results. The sets of RF signals used for the calculation of the decorrelation patterns were those acquired after 60 seconds of the aggregation phase; at the plateau of the of the aggregation process.

### Noise correction method

A correction for noise -in the RF signals- method was used during this study (Chapter 8). Briefly, the method uses the fact that the decorrelation pattern should be 1 at lag 0; however, this does not occur in the presence of noise in the RF signals. Noise produces an offset in the decorrelation pattern -by shifting the decorrelation pattern down- and thus the correlation coefficient at lag 0 may not be 1 in some acquisitions (Fig. 8.1). The correlation coefficient at lag 0 or offset is then estimated by curve fitting of the correlation coefficients. Since the entire decorrelation pattern was studied, all correlation coefficients were normalized by the intercept value to correct them for noise.

### Acoustical beam

The acoustical beam of the used transducer was measured in order to calculate its auto-convolution, which is used as a reference curve; the device used for the measurements is described in Chapter 7. Briefly, a line target is moved transversally across the ultrasound beam at the depth of interest; then the auto-convolution of the measured acoustical beam is performed and normalized by the maximum. The mean auto-convolution of the measured ultrasound beam is based on measurements performed at 5.5, 6 and 6.5 mm from the transducer.

## 6.3 Outline of the results

Considering the fact that some patients were under medication, the patient's group was subdivided into two subgroups, the low (LA) and high (HA) aggregation level groups. The parameter used to discriminate between groups was the aggregation time measured with the erythroaggregameter. As shown next, the relative backscattered signal power is plotted as a function of time for the normal and diseased blood samples. Results for relative backscattered signal power with the washed RBCs are not presented since no increase in the relative backscattered

signal power was observed due to any cell aggregation as results of the washing procedure. The decorrelation patterns for all experiments are presented and compared with the auto-convolution of the acoustical beam, which is considered the reference curve.

Blood type	Normal	WRBCs	LA	HA
Age (years)	26.1 ± 2.5	not known	60.4 ± 11.1*	69.8 ± 9.5*†
Hematocrit (%)	41.8 ± 2.6	38.5 ± 0.7	33.0 ± 3.2*	35.0 ± 2.3*†
Agg. time (sec)	3.7 ± 0.6	1410 ± 1668	5.6 ± 2.0*	2.87 ± 0.56*†
S <sub>10</sub> (no unit)	17.9 ± 2.0	0.43 ± 0.02	13.3 ± 3.3*	20.7 ± 2.7*†
γ <sub>D</sub> (s <sup>-1</sup> )	40.9 ± 7.4	17.7 ± 2.2	56 ± 25*	82 ± 43*†
γ <sub>S</sub> (s <sup>-1</sup> )	117 ± 21	20.0 ± 2.8	239 ± 148*	275 ± 92*†

Table 6.1: Values, as mean ± standard deviations, for the age (years), hematocrit (%), aggregation time (sec), aggregation index S<sub>10</sub> (no unit), and the partial (γ<sub>D</sub>, in s<sup>-1</sup>) and total dissociation threshold (γ<sub>S</sub>, in s<sup>-1</sup>), from the normal, washed RBCs (WRBCs) and diseased blood samples LA and HA.\* P < 0.0001 (T-test); normal blood group vs. combined diseased blood groups. †P < 0.005 (T-test); diseased blood LA vs. HA. ‡P = 0.023 (T-test); diseased blood LA vs. HA.

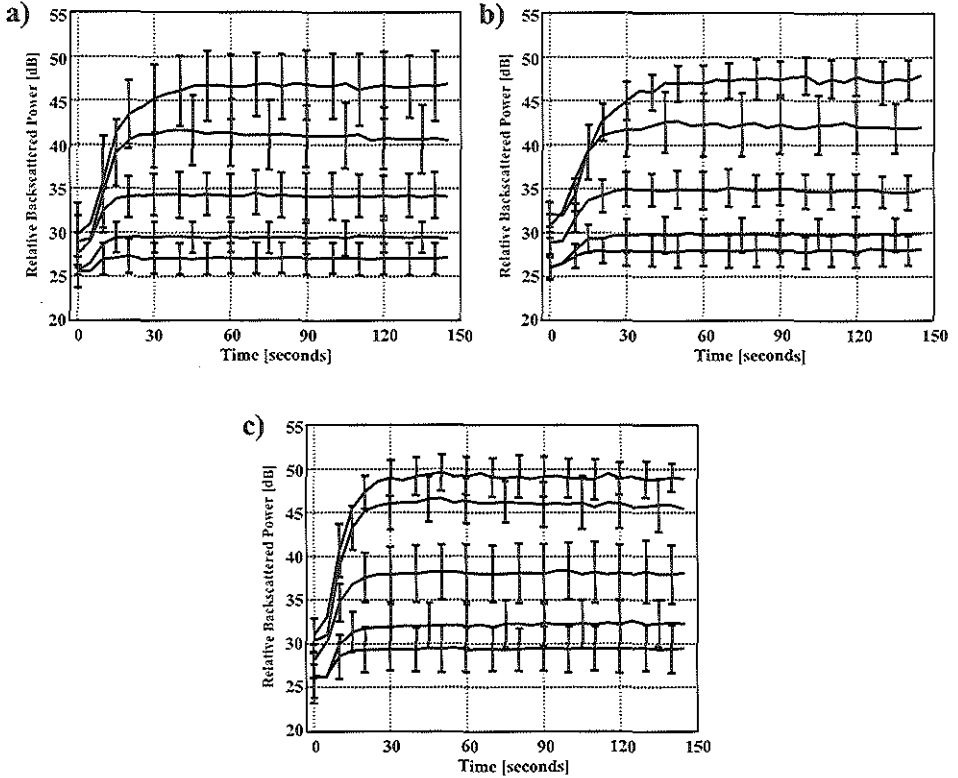
Blood type	Normal	LA	HA
Shear rate (s <sup>-1</sup> )	(dB/s)	(dB/s)	(dB/s)
1	0.67	0.52	0.81
5	0.57	0.51	0.74
20	0.32	0.26	0.48
40	0.19	0.16	0.26
80	0.09	0.09	0.16

Table 6.2: Mean raising slope values (dB/s) of the aggregation kinetic measured from time 0 to 20 sec for normal, LA and HA blood samples.

### 6.4 Results

Means and standard deviations of the physiological parameters such as age (years), hematocrit (%), aggregation time (sec), aggregation index S<sub>10</sub> (no unit), and partial (γ<sub>D</sub>, in s<sup>-1</sup>) and total (γ<sub>S</sub>, in s<sup>-1</sup>) dissociation thresholds are presented in Table I. Highly significant differences were observed between normal blood and the combined diseased blood groups for all parameters as well as between diseased blood groups. The aggregation time for diseased blood LA was higher than the one from the normal blood; however, lower values for S<sub>10</sub>, γ<sub>D</sub>, and γ<sub>S</sub> were found for the LA group compared to those from the HA group.





**Figure 6.2:** Means and standard deviations for the relative backscattered signal power (in dB) as a function of time for shear rates of 1, 5, 20, 40 and  $80 \text{ s}^{-1}$ , from top to bottom, respectively; a) for normal blood, b) for diseased blood LA and c) for diseased blood HA.

Figure 6.2 shows the relative backscattered signal power (in dB) as a function of time for shear rates of 1, 5, 20, 40 and  $80 \text{ s}^{-1}$ , from top to bottom, respectively, for normal (Fig. 6.2a) and for diseased blood LA (Fig. 6.2b) and HA (Fig. 6.2c). The kinetic of aggregation becomes faster for diseased blood samples mainly for the group HA as expected by the low aggregation time and high indexes such as  $S_{10}$ ,  $\gamma_D$  and  $\gamma_S$ . Table II presents the values of the mean raising slopes of the kinetic of aggregation for normal, LA and HA blood samples.

Figure 6.3 shows the measured mean decorrelation pattern and standard deviations as a function of transverse displacements, as well as the mean auto-convolution of the acoustical beam, for a) 1 and  $5 \text{ s}^{-1}$  and b) 20, 40 and  $80 \text{ s}^{-1}$  for washed RBCs. Similar results are presented in Figures 6.4, 6.5 and 6.6 for normal blood, diseased blood LA and HA groups, respectively.

Decorrelation patterns are compared with the auto-convolution of the acoustical beam used as a reference curve. Close agreements between mean decorrelation

patterns and the auto-convolution of the acoustical beam for all blood samples and shear rates are observed, except for the HA blood samples where the decorrelation patterns for low shear rates (1 and 5 s<sup>-1</sup>) are slower than the expected theoretical values.

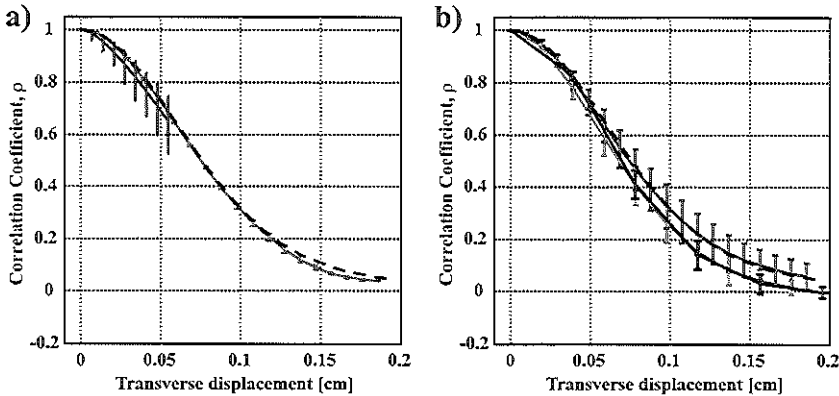


Figure 6.3: Mean decorrelation patterns and standard deviations as a function of transverse displacements for washed RBCs at shear rates of a) 1 (blue errorbars) and 5 (red errorbars) s<sup>-1</sup> and b) 20 (green errorbars), 40 (magenta errorbars) and 80 (black errorbars) s<sup>-1</sup>, in comparison with the auto-convolution of the acoustical beam (dashed black line).

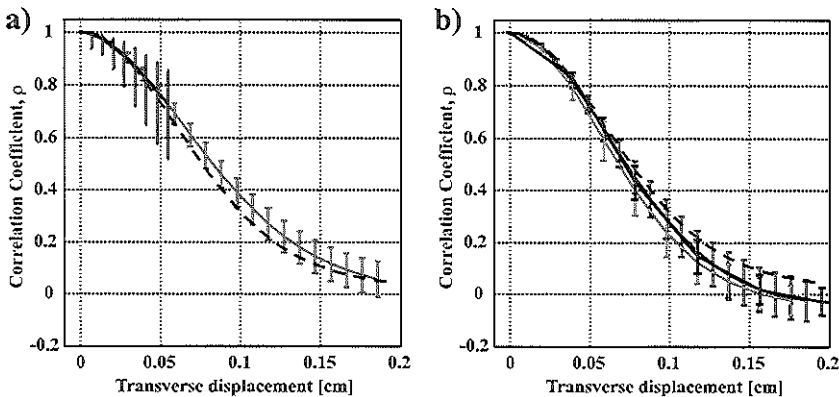


Figure 6.4: Mean decorrelation patterns and standard deviations as a function of transverse displacements for normal blood samples at shear rates of a) 1 (blue errorbars) and 5 (red errorbars) s<sup>-1</sup> and b) 20 (green errorbars), 40 (magenta errorbars) and 80 (black errorbars) s<sup>-1</sup>, in comparison with the auto-convolution of the acoustical beam (dashed black line).

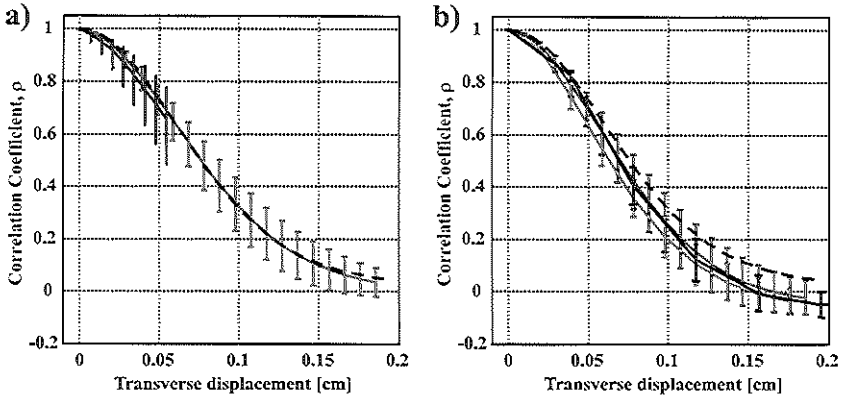


Figure 6.5: Mean decorrelation patterns and standard deviations as a function of transverse displacements for diseased blood LA at shear rates of a) 1 (blue errorbars) and 5 (red errorbars)  $s^{-1}$  and b) 20 (green errorbars), 40 (magenta errorbars) and 80 (black errorbars)  $s^{-1}$ , in comparison with the auto-convolution of the acoustical beam (dashed black line).

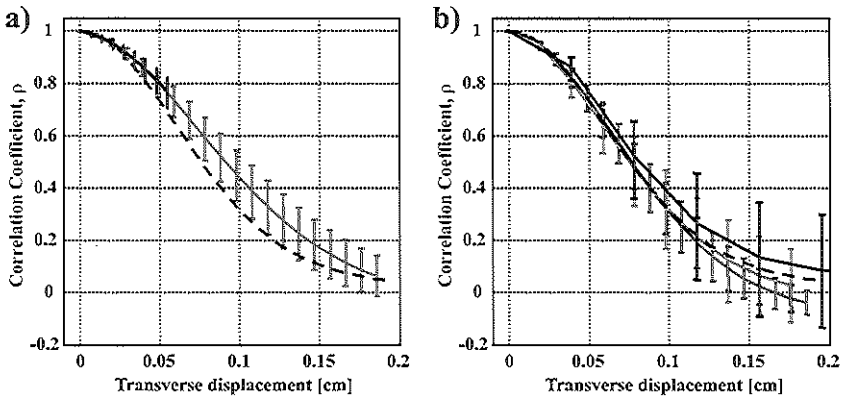


Figure 6.6: Mean decorrelation patterns and standard deviations as a function of transverse displacements for diseased blood HA at shear rates of a) 1 (blue errorbars) and 5 (red errorbars)  $s^{-1}$  and b) 20 (green errorbars), 40 (magenta errorbars) and 80 (black errorbars)  $s^{-1}$ , in comparison with the auto-convolution of the acoustical beam (dashed black line).

## 6.5 Discussion

From the parameters presented in Table I, a difference on the hematocrit and age between groups was found, which could influence the aggregation level. For the diseased groups LA and HA, the hematocrit is lower than for the one from normal blood; a slight difference is also observed between hematocrits from LA and HA. Other research groups already studied the influence of the hematocrit on the

aggregation of RBCs. Kitamura et al. (1995) showed for three hematocrit levels (20%, 40% and 60%) and a constant level of fibrinogen, an effective scatterer diameter of approximately 70 nm was reached; the effective scatterer diameter was measured by using the power spectrum computed as the squared magnitude of the Fast Fourier transform of the windowed signal. However, the rate at which this occurred varied with the hematocrit; a lower rate of aggregation for the low hematocrit was found. This could explain the higher aggregation time for diseased blood LA compared to diseased blood HA. Regarding the mean age of the groups of blood samples, Linderkamp et al. (1984) studied the red blood cell aggregation in pre-term and term neonates, and adults by means of a rheoscope (increase in light transmission during blood stasis). Both the rate and extent of RBC aggregation were low in the premature infants, increased with gestational age, and reached the highest values in the adults. Based on that study and since for the present study all blood samples were drawn from adult volunteers and patients, no influence in the aggregation level due to difference in age can be expected.

During the present study, the *in vitro* measurements were performed at room temperature ( $\approx 22\text{ }^{\circ}\text{C}$ ) and not at the physiological temperature of  $37\text{ }^{\circ}\text{C}$ , which could affect the process of formation and size of aggregates of RBCs. Neumann et al. (1987) studied the effect of temperature on the level of aggregation of RBCs at 3, 10, 20, 30 and  $37\text{ }^{\circ}\text{C}$  from normal donors and blood samples of patients with venous ulcers of the leg. Although red cell aggregate formation as an overall process is retarded by a decrease in temperature and the aggregates become more resistant to hydrodynamic dispersion, they become more prone to growing under low shear stress. Neumann et al. concluded that as a whole red cell aggregation is favored by temperature lowering.

The results presented in Figure 6.2 showed an increase in the mean raising slope of the aggregation kinetic from the normal and diseased blood LA to the HA group for all shear rates (Table II), which corresponds with the shorter aggregation time -measure by the erythroaggregameter- from diseased blood sample HA (Table I). The relative backscattered signal power from diseased blood HA is higher than other blood samples for all shear rates, which suggests larger formation of aggregates of RBCs. This is also expected from the high indexes  $S_{10}$ ,  $\gamma_D$  and  $\gamma_S$  from this group. During the disaggregation phase (high shear rate,  $600\text{ s}^{-1}$ ), red cell aggregation is expected to fully cease and thus similar relative backscattered signal power should be observed. However, the relative backscattered signal power at the disaggregation phase shows a slight difference depending on the shear rates.

The results presented in Figure 6.3 for washed RBCs suggest that a linear velocity gradient does not affect the measurements of blood velocity using the correlation-based method even when a large window size (2 mm in this case) is used for the calculations, which includes a large range of blood velocities. Never-

theless, most of blood velocity estimator methods use a window length of about a wavelength. For IVUS blood flow measurements, at a central frequency from 20 MHz, the wavelength is about 0.075 mm, which covers a small range of blood velocities. Consequently, the current study may be conservative and the broad range of velocities within the region of interest may explain the tendency toward a faster decorrelation than expected at the higher shear rates of 20, 40 and 80  $s^{-1}$ . For quantitative IVUS blood flow measurements using the correlation-based method, correlation values ranging from 1 to 0.5 are normally used. Correlation coefficients lower than 0.5 means a signal-to-noise ratio below 0 dB (Céspedes et al. 1997d); for such transverse displacements, the scatterers remain for a short period of time within the ultrasound sample volume, which produces a large decorrelation between RF signals.

Generally, close agreements between the mean decorrelation pattern and the theoretical values were observed at all shear rates, for the normal and diseased blood groups (Figs. 6.4, 6.5 and 6.6), except at shear rates of 1 and 5  $s^{-1}$  for HA blood samples. The lower rate of decorrelation may be explained by the size and orientation of the aggregates of RBCs, as previously described by a theoretical study (Chapter 4). When the scattering medium resembles a unidirectional medium, the rate of decorrelation tended to be closer to 1 for small displacements. In a Couette system, since both cylinders are concentric, aggregates of RBCs could be aligned with the flow (Chien et al. 1970), which causes the RF signals to remain correlated for longer period of time as observed by the decorrelation patterns for the HA blood sample at these very low shear rates (1 and 5  $s^{-1}$ ) (Fig. 6.6).

The high indexes  $S_{10}$ ,  $\gamma_D$  and  $\gamma_S$  -aggregation index, partial and total dissociation threshold, respectively- from diseased blood HA indicate the formation of large aggregates of RBCs. The standard deviations of the measurements increase from the washed RBCs to diseased blood samples. Aggregates of RBCs are large structures that are coming in and out of the acoustical beam introducing large changes in the RF signals, which contributes to an increase of the standard deviations of the decorrelation patterns. The fact that the ultrasound transducer must be removed and cleaned after each experiment may introduce some variations between experiments too.

In clinical practice interventional cardiologists are most interested in blood flow through coronary arteries, which are usually curved; the conditions for laminar flow are in these arteries hardly ever reached. The presence of an IVUS catheter inside the lumen of an artery also disturbs the blood flow profile. All phenomena that disturb the velocity profile (e.g. shear rate  $> 100 s^{-1}$ ) will result in a reduction of the RBC aggregate formation (van der Heiden et al. 1995). He et al. (1996) studied the pulsatile flow in the human left coronary artery bifurcation by a numerical study for realistic *in vivo* anatomic and physiologic conditions. It was shown that the mean wall shear stress during an entire car-

diac cycle at the root and downstream of the left coronary artery is around 20 dyne/cm<sup>2</sup> ( $\approx 2$  Pa). This indicates that, for a non-Newtonian fluid where the viscosity at infinite (shear rates  $> 100$  s<sup>-1</sup>) is 3.5 cP, the mean wall shear rate is around 570 s<sup>-1</sup>. Similar results were found by Lee et al. (2001) for coronary and aortic circulation. A mean wall shear stress of 19.84 dyne/cm<sup>2</sup> was obtained through a numerical analysis based on *in vivo* hemodynamic parameters. A shear rate close to 0 s<sup>-1</sup> is expected at the center of the vessel and thus a mean shear rate across the vessel can be estimated as being around 250 s<sup>-1</sup>.

Blood flow pulsatility, highly present in coronary arteries, produces changes in the shear rate across the vessel lumen as a function of the timing within the cardiac cycle (Milnor 1989). The velocity profile is flat during early systole (*i.e.* low shear rates), becomes almost parabolic at peak systole (depending on the hematocrit) (*i.e.* high shear rates), and then flattens again during diastole. Using a 30 MHz IVUS catheter, De Kroon et al. (1991) measured a cyclic variation of the backscattered power at 70 beats/min in the Iliac artery of three patients, which suggests that at higher frequency, dynamic changes in aggregate size between systole and diastole can be observed. However, Cloutier et al. (1993) suggested that a prolonged diastole is necessary to observe, at 10 MHz, an aggregate size enlargement in systole because no cyclic variation on the Doppler power was found during pulsatile flow at 70 beats/min by using whole porcine blood. Rouleau formation, during systole and at 70 beats/min, was not observed probably because the red cells do not have enough time in diastole to be brought into contact and to align themselves. As flow accelerates with a flat and more parabolic profile in late systole, the aligned red cells then probably form rouleau until the shear rate becomes sufficient to break them totally or partly.

## 6.6 Conclusions

In this chapter, the influence of the aggregation of RBCs and of linear velocity gradients on the correlation-based method for blood velocity estimation was assessed. Whole human blood and a Couette system were used for this purpose. The decorrelation patterns showed to be not affected by linear velocity gradients when washed RBCs were used. Aggregation of RBCs showed no effect on the decorrelation patterns, except at very low shear rates and for high aggregating blood (*i.e.* large aggregates of RBCs). Overall, for the high shear rate present in coronary arteries, the correlation-based method for blood flow estimation should not be influenced by these phenomena when a small window length is used for the evaluations. However, the impact of the ultrasound frequency selected and that of dynamic changes in aggregate sizes as a function of time are factors that may need additional consideration since their effects on the decorrelation patterns have not been studied yet.

## Chapter 7

# Line Spread Function as Calibration for the Correlation-based method

### Abstract

*A method to measure transverse blood flow, based on correlation between consecutive Radio Frequency (RF) signals, has been developed. Currently, we are implementing the method for an intravascular (IVUS) array catheter. In this chapter, the acoustical beam (Line Spread Function, LSF) was experimentally measured and compared with the simulated one. Next, the experimental  $LSF_E$  was convolved with a matrix of white noise to produce  $RF_E$  signals. Decorrelation pattern from the  $RF_E$  signals was compared with the correspondent auto-convolution of the  $LSF_E$  and a good agreement was found. We conclude that the transverse decorrelation pattern of the IVUS array catheter can be assessed from the properties of the acoustical beam.*

---

based on the Publication: "IVUS Flow measurements: Line Spread Function and Decorrelation Pattern" by Fermín A. Lupotti, E. Ignacio Céspedes, Frits Mastik and Antonius F.W. van der Steen, *Ultrasonics*; 2002: 40: 843-847.

## 7.1 Introduction

Intravascular ultrasound (IVUS) has been used for many purposes as it provides real-time cross-sectional images of blood vessels at a high-resolution (Tobis & Yock 1992). Recent research in IVUS has been focused on obtaining information from RF data (van der Steen et al. 1998a) concerning the acoustic and elastic properties of the vessel wall and plaque for the purpose of vascular tissue characterization (de Korte et al. 2000). IVUS has also been applied to measure blood flow velocity and volumetric flow (Li et al. 1998b; van der Steen et al. 2000). First initial *in vivo* evaluations of volumetric blood flow assessment based on this method using a rotating-single-element catheter have been presented by Céspedes et al. (1998a) and Carlier et al. (1998b). This type of catheter has an extra component of decorrelation, the angular displacement of the ultrasound beam (Li et al. 1998b). The use of array technology in IVUS applications removes this limitation in the intravascular measurements of blood flow.

In the current chapter, experiments were performed to evaluate the response of the IVUS array catheter to transverse blood flow. Many techniques are currently used for acoustical-beam characterization, the Schlieren and Raman-Nath diffraction technique (Schneider & Shung 1996), the hydrophone (Bacon 1982) and a spherical or line target moved across the ultrasound beam (Walker et al. 1999). The first two techniques have the disadvantage that is not possible to measure the two-way response to evaluate the transducer reception and the receive-electronic behavior. This is an important issue for our study since we are interested in evaluating the backscattered RF signals. Therefore, a line target is an adequate technique for acoustical beam characterization of this IVUS array catheter. The objective of the present study was to experimentally measure the acoustical beam properties and to compare the result with simulations. The LSF from computer simulations and from experimental realizations will be compared. Power Spectral Density (PSD) curves from experimental and simulated results are also compared. Second-order statistics from the experimental ( $RF_E$ ) signals are compared with the auto-convolution of the  $LSF_E$ . The results are presented for the near ( $\approx 1$  mm) and for the far ( $\approx 3$  mm) fields, separately.

## 7.2 Methods

### 7.2.1 IVUS transducer

The IVUS array catheter is formed by 64 elements mounted on a circular surface of a catheter tip with a diameter of 1.2 mm. The array transducer operates at a central frequency of 20 MHz and with a -20 dB bandwidth of 7.5 MHz (Eberle 1997). The element size of the array under study is 0.7 mm in length ( $L$ ) and 0.028 mm in width ( $W$ ); the pitch of the elements was 0.059 mm (Fig. 3.1).



The array transducer operates in synthetic aperture focusing mode for imaging and linear mode for flow imaging. In linear mode, four elements are electronically tied together and produce a burst of ultrasound pulses in linear array mode. Then, the system will be shifted one element and the next burst will be generated; this will be repeated 64 times to produce a full frame. In order to perform the present study, a computer simulation program extended from Chapter 3 was used. The mathematical development to simulate ultrasound signals was based on pressure field calculations using the impulse response method. The axial sampling frequency was 200 MHz to over-sample the response to the correlation function.

### 7.2.2 Simulated LSF

The scattering target, a line of point scatterers, was transversally moved across the acoustical beam. The distance between the point scatterers was based on the resolution of the ultrasound beam in the elevation direction. Half a wavelength ( $\lambda/2$ ) is a distance well below the distance for which the transducer ultrasound beam cannot distinguish each individual point scatterer and could only see them as a thin line. At each displacement of 0.02 mm, the backscattered RF signals were summed and saved as one  $RF_S$  signal and thus producing the two-dimensional 2-D  $LSF_S$ . The one-dimensional 1-D  $LSF_S$  comes from the auto-convolution of the summation in time of each  $RF_S$  from the 2-D  $LSF_S$ .

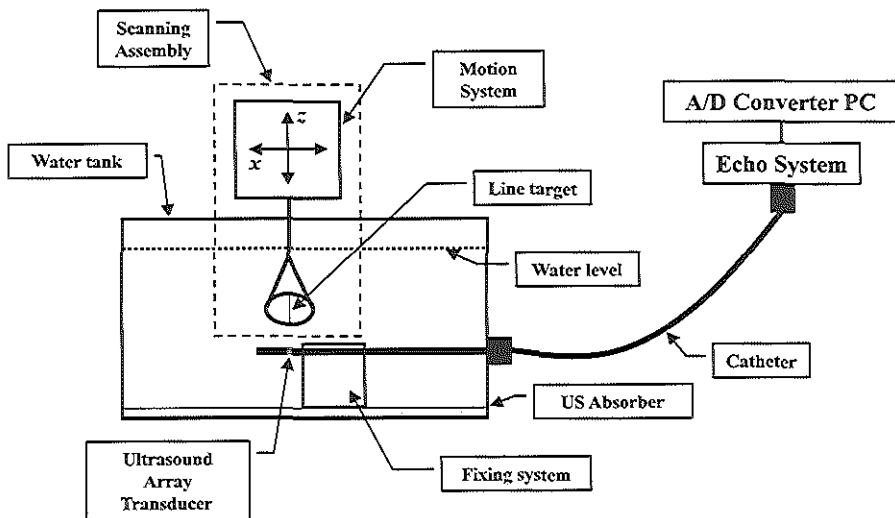


**Figure 7.1:** A block diagram of the used set-up; the echo-system, the A/D-converter-PC and the water tank with the motion system; the IVUS array catheter connected to the echo-system and placed into the water tank.

### 7.2.3 Experimental setup

The measurement system was formed by a water tank, which held the motion system, the echo system (JOMED Inc., Rancho Cordova, CA, USA) with the IVUS array catheter (20 MHz Vision 64F/X<sup>TM</sup>, JOMED Inc.), and the A/D-converter-PC (Fig. 7.1). The A/D-converter-PC contained a Pentium computer with an acquisition board (Signatec, Corona, CA, USA) with 128 Mbytes to store the RF data at a sampling frequency of 200 MHz in 8 bits. The water tank was filled with degassed water at room temperature ( $\approx 22$  °C) and ultrasound absorber was placed on the bottom and both sides of the tank to reduce the ultrasound reflections from the tank wall. The motion system was a manual micrometer fixed to the water tank wall; the micrometer was capable of moving the target in  $x$  (transverse across the ultrasound beam) and  $z$  (along the ultrasound beam) directions. A line target of 8  $\mu\text{m}$  in diameter (Kevlar, Du Pont de Nemours Int. S.A., Geneva, Switzerland) was held in a ring fixed to the motion system and placed under the water level. Supported by a fixing system, the IVUS array catheter was placed under the water level between the ultrasound absorber and the line target.

### 7.2.4 Experimental LSF and RF signals

The line target was moved across the ultrasound beam using the micrometer ( $x$  direction in Fig. 7.1 and 3.1). At each displacement of 0.02 mm, three frames containing the backscattered RF signals (16 RF signals per angle for 64 angles) were acquired by the A/D-converter-PC and then saved to hard-disc (Fig. 7.1). In order to produce the 2-D LSF<sub>E</sub>, the 16 RF signals from the angle - from all three frames- containing the ultrasound reflection from the line target with maximum amplitude were averaged to reduce the electronic noise. The experiment was performed for 8 and 5 different catheters for the near and for the far fields, respectively. The 1-D LSF<sub>E</sub> comes from the summation in time of the auto-convolved RF signals -from the 2-D LSF<sub>E</sub>- over the displacements and then normalized by its maximum. Experimental RF<sub>E</sub> signals were generated by convolving the 2-D LSF<sub>E</sub> with a matrix of white-noise signals (WNS). The RF<sub>E</sub> signals were correlated to each other since the white noise matrix was moved across the LSF<sub>E</sub>. The convolution process was repeated for 20 independent WNS matrixes for both near and far fields.

### 7.2.5 Second-order statistical properties of the experimental RF signals

The temporal correlation was used to examine the variations between backscattered signals when a scattering medium is transversally moved across the acoustical beam. The correlation coefficient  $\rho_{i,j}$  between two RF signals,  $s_i(n)$  and  $s_j(n)$ ,

received from positions of the scattering medium corresponding to  $d=i$  and  $d=j$  is:

$$\rho_{i,j} = \frac{\sum_{n=1}^N (s_i(n) - \bar{s}_i(n)) \cdot (s_j(n) - \bar{s}_j(n))}{\sqrt{\sum_{n=1}^N (s_i(n) - \bar{s}_i(n))^2 \cdot \sum_{n=1}^N (s_j(n) - \bar{s}_j(n))^2}} \quad (7.1)$$

where the subscript  $i=1,2,\dots,D$  and  $j=1,2,\dots,D$  being  $D$  the number of displacements. For the RF signals,  $N$  is the length in time and  $\bar{s}$  is the mean value. The  $\rho_{i,j}$  are the correlation coefficients for the signal pair,  $s_i$  and  $s_{i+m}$ , which are spaced  $m=(j-i)$  steps and  $m=0,1,\dots,D-1$ . Next, the average correlation coefficient in the signal set for a space of  $m$  steps between signals is calculated. Thus  $\rho_m$  describes the transducer decorrelation pattern as a function of transverse displacements of a scattering medium. Because the correlation coefficients were not normally distributed, the Fisher-Z transform was used to present the results (Appendix B).

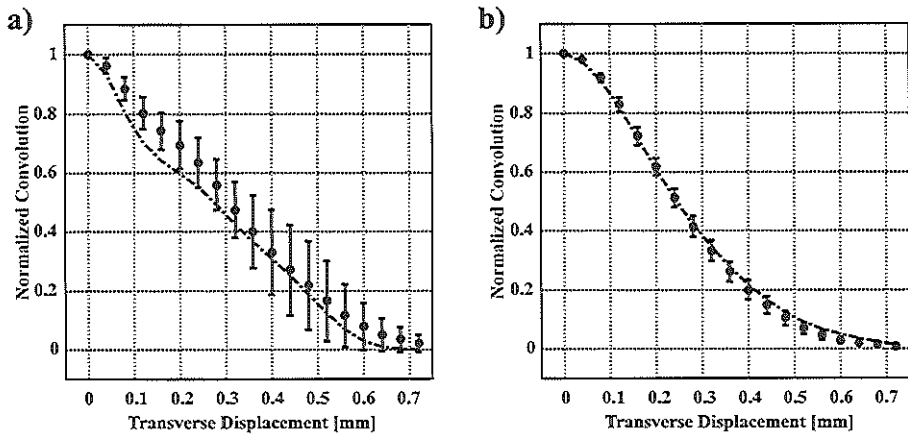


**Figure 7.2:** Comparison between the reference curve 1-D.LSF<sub>S</sub> (dashed line) and the averaged experimental line spread function (1-D.LSF<sub>E</sub>) (error bars). a) Near field and b) far field.

## 7.3 Results

The 1-D.LSF<sub>S</sub> is compared to the averaged experimental 1-D.LSF<sub>E</sub> for both near (Fig. 7.2a) and far (Fig. 7.2b) fields where close agreement is observed between curves; the 1-D.LSF<sub>S</sub> is almost everywhere within the standard deviations. Next, two 2-D.LSF<sub>E</sub> were selected, one from the near field and one from the far field, in order to produce RF<sub>E</sub> signals. Figure 7.3 shows the PSD in decibels as a function of the normalized frequency of a signal from the WNS matrix, from an RF<sub>E</sub> and

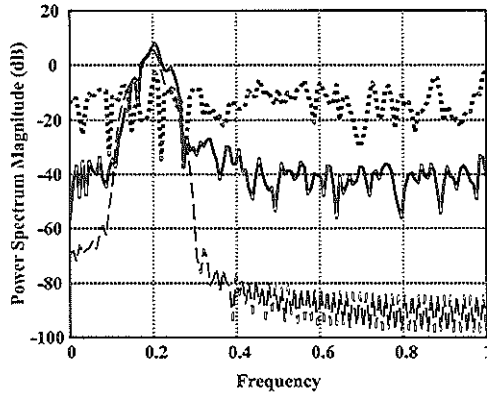


Figure 7.3: The Power Spectrum Density (PSD) from a signal from the WNS matrix (dotted line) compared to the PSD from an experimental (solid line) and simulated (dashed line) RF signal.

$RF_S$  signal compared to each other. The  $RF_E$  signals were normalized to obtain the PSD. The mean decorrelation patterns, for both near and far fields, from the sets of  $RF_E$  signals were obtained as a function of transverse displacements. Figure 7.4 shows the mean decorrelation patterns in good agreement with the 1-D  $LSF_E$  in the near field (Fig. 7.4a) and in the far field (Fig. 7.4b).

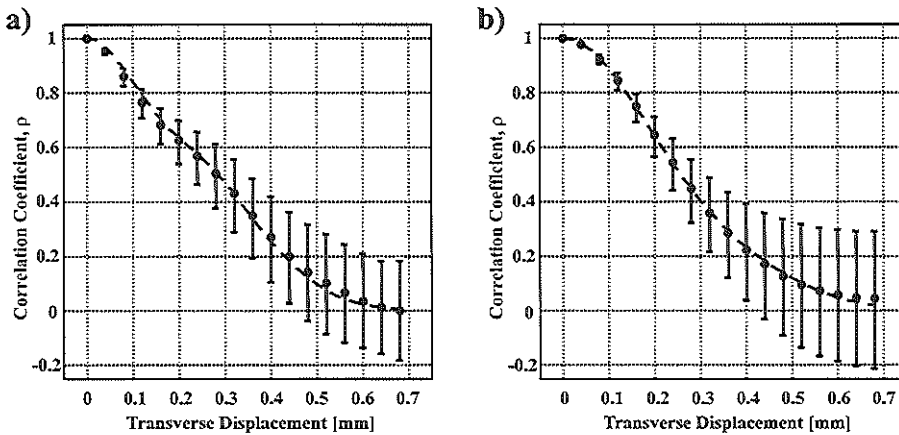


Figure 7.4: Mean decorrelation pattern from experimental  $RF_E$  signals as a function of transverse blood flow (error bars) compared to the 1-D  $LSF_E$  (solid line). a) Near field and b) far field.

## 7.4 Discussion

In the present study, we have shown the averaged 1-D  $\text{LSF}_E$  to agree with the 1-D  $\text{LSF}_S$  (Fig. 7.2a and 7.2b) in both near and far fields. In the near field, the agreement is not present for the full curve; the reason of the widening of the averaged experimental 1-D  $\text{LSF}_E$  could be explained by the presence of the ring-down (ultrasound reverberations from the array transducer) at the distance of interest ( $\approx 1$  mm). The ring-down acts as a DC offset, widening the auto-convolution. In general, the pressure field along the acoustical axis of an ultrasound transducer exhibited rapid fluctuations in the near field and a gradual decay in the far field (Christensen 1988). The standard deviations also showed an increase that could correspond to the irregularity of the ultrasound beam in the near field (Fig. 7.2a). However, in the far field (Fig. 7.2b), the agreement is almost full for the complete 1-D  $\text{LSF}_E$ ; the 1-D  $\text{LSF}_S$  is within all the standard deviations. The convolution of the 2-D  $\text{LSF}_E$  with the WNS matrix used for the present study is of easy implementation and faster than pressure field calculations. The  $\text{RF}_E$  signals produced through this method showed a power spectrum magnitude with a peak centered at 20 MHz that corresponds to the central frequency of the used transducer (Fig. 7.3). The peak is around 40 dB above the noise level; the higher noise level, compared to the simulated one (80 dB), could be due to the noise presents in the  $\text{LSF}_E$ . The agreement shown in Figure 7.4 between the mean decorrelation pattern as a function of transverse displacements and the 1-D  $\text{LSF}_E$  confirms our results introduced in Chapter 3.

## 7.5 Conclusions

The experiments conducted here to characterize the ultrasound beam of the IVUS array catheter agreed with simulated results. These agreements are of great interest since the process to characterize the ultrasound beam for measuring quantitative volume blood flow using the correlation-based method has become more efficient and more robust. We could conclude that the mean decorrelation pattern due to transverse blood flow will agree with the auto-convolution of the  $\text{LSF}$ .



## Chapter 8

# Dynamic Noise Correction for IVUS Blood Flow: Methods and Numerical validation

### Abstract

*In recent years, a new method to measure transverse blood flow, based on correlation between consecutive Radio Frequency (RF) signals has been developed. Transverse blood flow estimation may be influenced by noise. In this chapter, we investigated a new correlation-based method for noise correction. The decorrelation characteristics of transverse blood flow using an intravascular ultrasound (IVUS) array catheter are studied by means of computer modeling. Blood was simulated as a collection of randomly located point scatterers; moving this scattering medium transversally across the acoustical beam represented flow. Parabolic blood flow was simulated. Additive noise was added to the RF signals at a given signal-to-noise ratio. Next, a new method to dynamically estimate and suppress the decorrelation due to noise is presented. The decorrelation due to noise is estimated from the correlation coefficients from flowing blood obtained at increasing time lags. The correlation graphs are corrected for the decorrelation due to noise, leaving the decorrelation due to blood flow. The method shows to estimate and correct the correlation coefficients for noise well.*

---

based on the Publication: "Dynamic Noise Correction for IVUS Quantitative Volume Blood Flow: Methods and Numerical validation" by Fermín A. Lupotti, Chris L. de Korte, Frits Mastik and Antonius F.W. van der Steen, *accepted for publication in Ultrasound in Medicine and Biology*; 2002.

## 8.1 Introduction

Commercially available IVUS echo systems produce conventional B-mode images of the vessel lumen and the surrounding tissue and qualitative blood flow. However, they are unable to measure transverse blood velocity and therefore quantitative volume blood flow can also not be estimated. This will be of great interest for the interventional cardiologist in guiding the therapy (Tobis et al. 1993; Carlier et al. 1998d, 1998b). Crowe et al. (2000) recently introduced qualitative blood flow information by means of a frequency domain method of decorrelation processing using a FIR filter bank. Rubin et al. (2001) have been measuring volumetric flow using Doppler and gray-scale decorrelation with a limited accuracy.

RF-data processing has significantly enhanced the potential of IVUS (van der Steen et al. 1998a), which is now aiming to obtain information concerning vessel wall and plaque properties and vascular tissue characterization (Spencer et al. 1997b; Bridal et al. 1997a; de Korte et al. 2000). In addition, IVUS has been applied to measure blood flow velocity and volumetric flow (Li et al. 1998b). Transverse blood flow velocity and quantitative volume blood flow can be measured using a correlation-based method in a burst of ultrasound beams that were transmitted in the same direction (Li et al. 1997, 1998b). Céspedes et al. (1998a) have presented initial *in vivo* evaluations of blood flow assessment based on correlation with a rotating single-element catheter.

The principle of blood flow assessment is based on lateral decorrelation, which depends on the beam profile of the transducer. More specifically, decorrelation is related to the auto-convolution of the ultrasound beam in the direction of blood flow and decorrelation was proven to be proportional to the transverse blood flow velocity. The range of blood flow that can be estimated with the correlation-based method basically depends on the pulse repetition interval (PRI) of the echo system, the vessel lumen and the blood velocity profile. The decorrelation of the received IVUS RF signals can be evaluated as a function of time using a sequence of RF signals acquired at a fixed pulse lag from the same angular position. After gating the RF signals with a fixed window length, the sequence of RF signal windows was aligned to remove the axial motion of the scatterers (this motion does not contribute to the flow) and then the correlation coefficients were calculated as a function of time. Next, in a controlled experimental environment, the correlation coefficients as a function of transverse displacements of the scatterers were obtained to calibrate the method. Thus, when the time and displacement decorrelation functions are known, the correlation coefficients can be converted into velocity. The volumetric flow can be calculated by integrating the local transverse velocity with the area element over the complete vessel cross-section.



Thus, quantitative volume blood flow was assessed with a single IVUS catheter that measured the cross-sectional vessel area and the transverse blood velocity simultaneously and at the same location (Li et al. 1998b).

Electronic and quantization noise are well-known sources of signal decorrelation (Friemel et al. 1998). In correlation based flow imaging, the decrease in signal correlation produces an overestimation of the blood flow velocity (Ledoux et al. 1998). Céspedes et al. (1997d) described a method to measure signal-to-noise ratio (SNR) by means of correlation coefficients calculated from RF signals in tissue for the purpose of elastography and blood flow. Stationary tissue will produce a correlation coefficient for lag 1 close to the one for lag 0. Then, the SNR level can be obtained from the ratio of correlation coefficient over 1 minus the correlation coefficient. Using simulated data, Céspedes et al. showed that for a SNR of 20 dB the correlation decreases to 0.98 and then the correlation decreases rapidly for SNR's below 20 dB. Li et al. (1997) described the correlation coefficient from RF signals with a given SNR to be reduced by a weighting factor, which is related to the SNR. However, these techniques are based on SNR estimations from static tissue, which do not correspond to the SNR from flowing blood.

In this chapter, we present a new method to dynamically estimate and suppress the decorrelation due to noise from the total decorrelation. The decorrelation due to noise is estimated from the correlation coefficients from flowing blood obtained at increasing time lags. Presuming additive noise, the relation between these correlation coefficients will be dominated by the flow, and the decorrelation due to noise can be estimated. This chapter presents results from simulated data with known velocities and noise level. The method showed to estimate and correct the correlation coefficients for noise well.

## 8.2 Methods

### 8.2.1 The IVUS array transducer

The simulated IVUS array catheter is formed by 64 elements mounted on a circular surface of a catheter tip with a radius of 0.6 mm ( $R$ ). The element size of the array under study is 0.7 mm ( $L$ ) in length and 0.028 mm in width ( $W$ ); the pitch of the elements is 0.059 mm (Fig. 3.1). The array transducer operates at a central frequency of 20 MHz and with a -20 dB bandwidth of 7.5 MHz (Eberle 1997; O'Donnell et al. 1997a). The array transducer works in synthetic aperture focusing mode for imaging and linear mode for color flow imaging. Synthetic aperture focusing mode is not suitable for flow assessment since the acoustical beam is formed over a time frame on the order of milliseconds, during which, the

red blood cells will move through the beam and will influence flow assessment based on correlation. Therefore, in flow imaging, four elements are electronically tied together and produce a burst of 8 ultrasound pulses in linear array mode (Borsboom et al. 2000). Then, the system will be shifted one element and the next burst will be generated; this will be repeated 64 times to produce a full frame.

## 8.2.2 Computer modeling

### General settings

In order to perform the present study, a computer simulation program extended from Chapter 3 was used. In the computer simulation program, four elements were considered as one curved (convex) single element and its area was divided into a grid of small areas with dimensions less than quarter of a wavelength ( $17 \mu\text{m}$  for a wavelength of  $75 \mu\text{m}$ ). Thus, each small area transmits an echo and the backscattered response received by the entire transducer. In the coordinate system (Fig. 3.1), the  $x$ -axis is the transverse direction, the  $y$ -axis is the lateral direction and the  $z$ -axis is the axial direction. The center of coordinates is on the surface and in the center of the four elements. The mathematical development to simulate ultrasound signals was based on pressure field calculations using the impulse response method (Borsboom et al. 2000). The axial sampling frequency was 200 MHz to obtain a better estimation of the peak of the correlation function.

### Scattering medium

The scattering medium was defined as a collection of omnidirectional and randomly positioned point scatterers in a three-dimensional space. This is the simplest way to mimic blood; a more realistic approach, *e.g.* aggregates of red blood cells, was already studied suggesting to have no effect on the decorrelation pattern (Chapter 4 and 6). For blood flow simulations, the  $x$  and  $y$  lengths of the scattering medium remained as for previous cases (Chapter 3). The  $z$  length of the scattering medium ranged from 0.5 mm to 5.5 mm. The locations of the point scatterers were measured with respect to the origin of the reference axis. The used scatterer density was chosen to meet the Rayleigh criterion: 1800 per  $\text{mm}^3$  (Chapter 3).

### Blood flow simulation

Transverse parabolic blood flow was simulated where the velocity ranged from 0 cm/s to 32 cm/s (*i.e.* peak velocity), which includes the range of normal human blood flow velocities. At each displacement of the scattering medium, the backscattered RF signals, from point scatterers within the -20 dB beamwidth,

were summed and saved as one RF signal. At the selected scatterer density, the average number of point scatterers inside the -20 dB beamwidth was approximately constant. The geometry of the parabolic blood flow profile was defined as follows:

$$V=(1-(r/R)^2) * V_{peak},$$

where  $r$  is the distance to the center of the lumen,  $R$  is the total radius of the lumen vessel and  $V_{peak}$  is the peak velocity. For the transverse parabolic blood flow, only 8 RF signals were used for the calculation of the correlation coefficients for lags of 1, 2, 3 and 4, and 64 sets of 8 RF signals were used to produce to results presented in this study.

### 8.2.3 Calibration method

The correlation-based method needs to be calibrated to convert the measured correlation coefficients as a function of time into transverse velocity. The calibration for the correlation-based method was based on the auto-convolution of the acoustical beam. The simulated acoustical beam was measured for depths ranging from 0.5 mm to 6 mm with steps of 0.5 mm and then the calibration file was produced (Chapter 7).

### 8.2.4 Statistical properties of the scattering medium

#### First-order statistics

The mean-to-standard deviation ratio of the sub-sampled envelope of the RF signals was tested and the result ( $1.95 \pm 0.23$ ) was close to the theoretical value (1.91) (Wagner et al. 1983; George et al. 1976).

#### Second-order statistics

The correlation coefficient  $\rho_{i,j}$  between two RF signals,  $s_i$  and  $s_j$ , was calculated using a standard method as described in Chapter 3. Because the correlation coefficients are not normally distributed, the Fisher-Z transform was used to present the results (Appendix B). The 64 sets of 8 RF signals were used to calculate the correlation coefficient for lags of 1, 2, 3 and 4 signals. Then, the correlation coefficient for lag 1 is the mean over the 7 estimates and so on. The correlation coefficients are obtained from windowed RF signals for windows of 40 samples -about one wavelength- and an overlap of 20 samples.

### 8.2.5 Proposed method for noise correction

Independent broadband (*i.e.* white) noise was added to each RF signal to obtain a given signal-to-noise ratio (SNR). The SNR is defined as the ratio of the average signal power to the average noise power. It should be realized that the signal is only present in the bandwidth of the array transducer, while broadband noise is present for 0 to 100 MHz. The noise level was based on the mean amplitude of the RF signal so the SNR in the near field is higher than in the far field as it is the case in the real situation. The method proposed here uses the fact that the correlation pattern should be 1 at lag 0; however, this does not occur when noise is present in the RF signals. Correlation coefficients from the windowed RF signals were calculated for lags of 1, 2, 3 and 4 signals. Noise produces an offset in the correlation pattern -by shifting the correlation pattern down- and thus the correlation coefficient at lag 0 is not 1 any more (Fig. 8.1a,  $\rho_{SN}$ ). In other words: if 2 times the same scatterer distribution is insonified, the correlation coefficient is smaller than 1 due to noise.

In the method proposed here, the correlation coefficients at lag 0 is estimated by curve fitting in order to measure the shift in the correlation pattern. Adding 1 minus the intercept value at lag 0 to each correlation value corrects the correlation pattern for noise (Fig. 8.1a,  $\rho_S$ ). The acoustical beam is symmetric with respect to the direction of transverse blood flow and thus the auto-correlation function is symmetric too. A quadratic curve fitting was then used to represent the shape of the auto-correlation function. The fitted curve, a parabola, can be based on either 2, 3 or 4 points using the least square method and at lag 0 the derivative (*i.e.* slope of the curve) of the parabola was forced to 0.

## 8.3 Outline of the simulation experiments

Transverse parabolic blood flow with a peak velocity of 32 cm/s was simulated. Correlation versus distance from the ultrasound transducer was studied individually for lags of 1, 2, 3, and 4 signals. First, the noise correction method was tested for RF signals with infinite SNR to evaluate if the method introduces an error in the correlation coefficients. Second, independent broadband (*i.e.* white) noise was added to each RF signal to obtain a SNR of 15 dB. The noise correction method was then used; the estimated correlation coefficients at lag 0 during noise correction are presented. Next, the noise corrected correlation coefficients of the RF signals at an SNR of 15 dB were compared with the ones at an infinite SNR, and the relative error between these correlation coefficients is presented. Similar measurements were performed for SNRs of 5 dB and 10 dB. Blood velocity profiles (in cm/s) as a function of depth were obtained for RF signals at infinite SNR, and for a 15 dB SNR before and after corrected for noise. All measurements were assessed for a PRI of 37  $\mu$ s and of 74  $\mu$ s, separately.

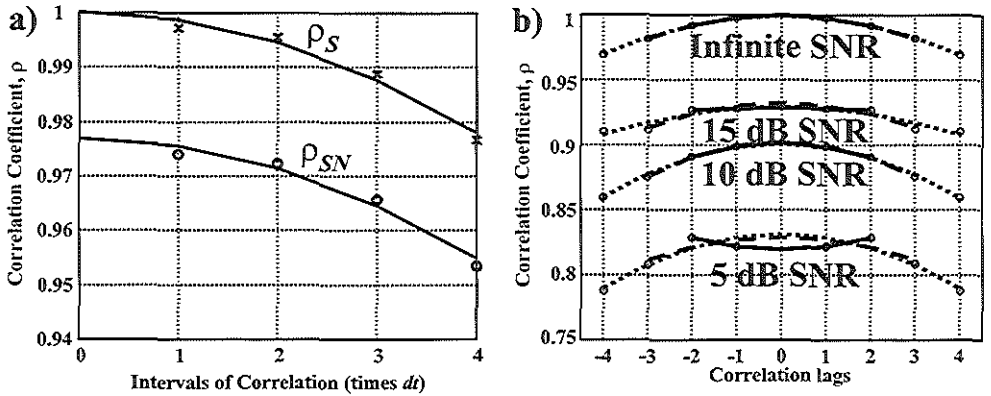


Figure 8.1: a) An example of the noise correction method; measured correlation coefficients at an unknown SNR before ( $\rho_{SN}$ ) and after ( $\rho_S$ ) correcting for noise. b) An example of the 2-points (solid line), 3-points (dashed line) and 4-points (dotted line) curve fitting process through measured correlation coefficients from simulated transverse blood flow for 5 dB, 10 dB, 15 dB and for infinite SNR.

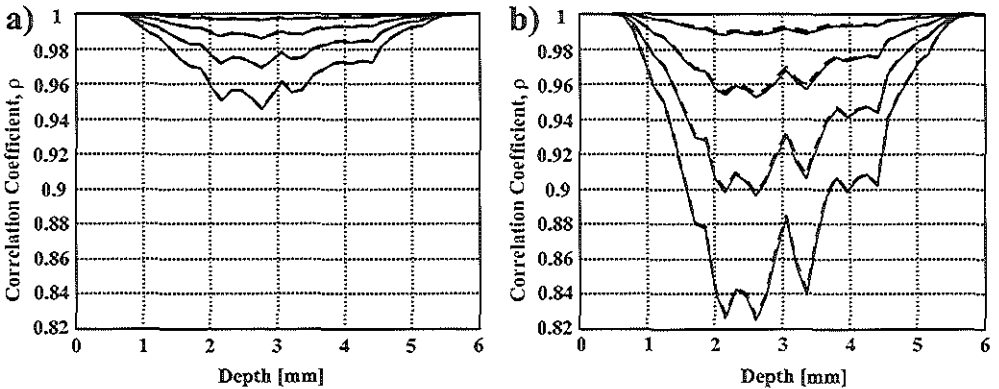
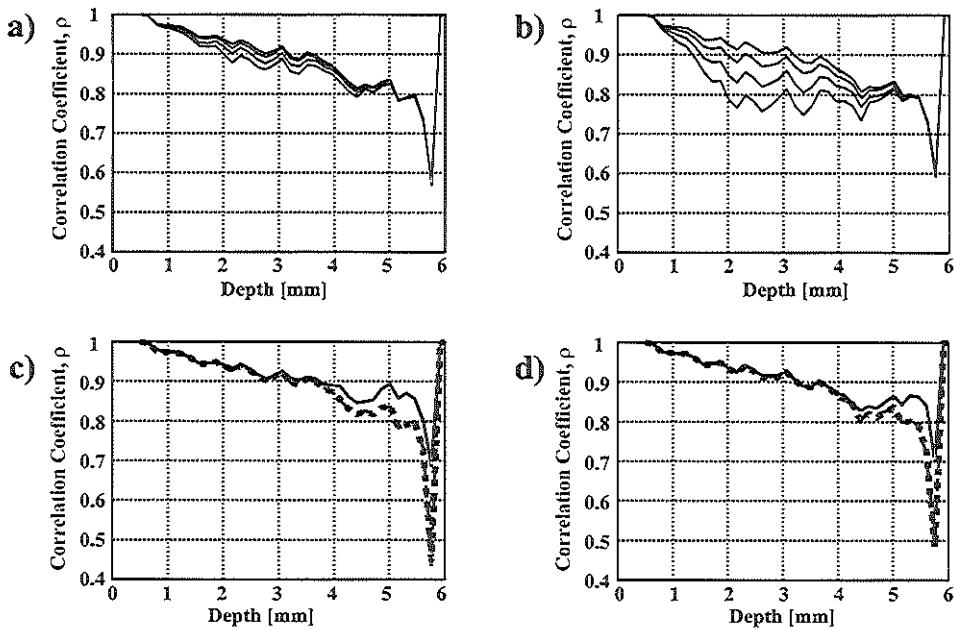


Figure 8.2: Correlation coefficients as a function of depth for a parabolic blood flow profile with a peak velocity of 32 cm/s and for infinite SNR; comparison between correlation coefficients for lags of 1, 2, 3 and 4 signals (from top to bottom) before (solid line) and after (dashed line) a 3-points curve fitting noise correction for a PRI between Rf signals of a) 37  $\mu$ s and of b) 74  $\mu$ s.

## 8.4 Results

In practice, the expected SNR from the used IVUS array catheter is usually around 15 dB when an optimal gain setting is used for blood scattering signals. An example of the noise correction method is presented in Figure 8.1a. The measured correlation coefficients at an unknown SNR (Fig. 8.1a,  $\rho_{SN}$ ) are shown



**Figure 8.3:** Correlation coefficients for lags of 1, 2, 3 and 4 signals (from top to bottom) as a function of depth for a parabolic blood flow profile with a peak velocity of 32 cm/s and for a SNR of 15 dB. Result before noise correction for a PRI of a)  $37 \mu s$  and of b)  $74 \mu s$ . Correlation coefficients at lag 0 as a function of depth obtained from the evaluation of the 2-points (solid line), 3-points (dashed line) and 4-points (dotted line) noise correction method for a PRI of c)  $37 \mu s$  and of d)  $74 \mu s$ .

with an intercept value at lag 0 lower than 1. Next, after correcting for noise, the correlation coefficients (Fig. 8.1a,  $\rho_S$ ) are shown with an intercept value of 1 at lag 0. The symmetry of the correlation function with respect to the intervals (*i.e.* transverse blood flow) is shown in Figure 8.1b for the 2, 3 and 4 points curve fitting process through estimated correlation coefficients for a SNR of 5 dB, 10 dB and 15 dB. Figure 8.2 shows the correlation coefficients for lags of 1, 2, 3 and 4 signals (from top to bottom) as a function of depth for RF signals with infinite SNR before and after noise correction, compared to each other for a PRI of  $37 \mu s$  (Fig. 8.2a) and of  $74 \mu s$  (Fig. 8.2b). The results show the noise correction method for noiseless RF signals to have a minor negative effect on the correlation coefficients.

Figures 8.3a and 8.3b show the correlation coefficients for lags of 1, 2, 3 and 4 signals (from top to bottom) for RF signals with a SNR of 15 dB before noise correction for the two PRIs,  $37 \mu s$  and  $74 \mu s$ , respectively. As can be observed, the correlation coefficients clearly deviate from the results showed in Figure 8.2. Figures 8.3c and 8.3d show the correlation coefficients at lag 0 as estimated by the

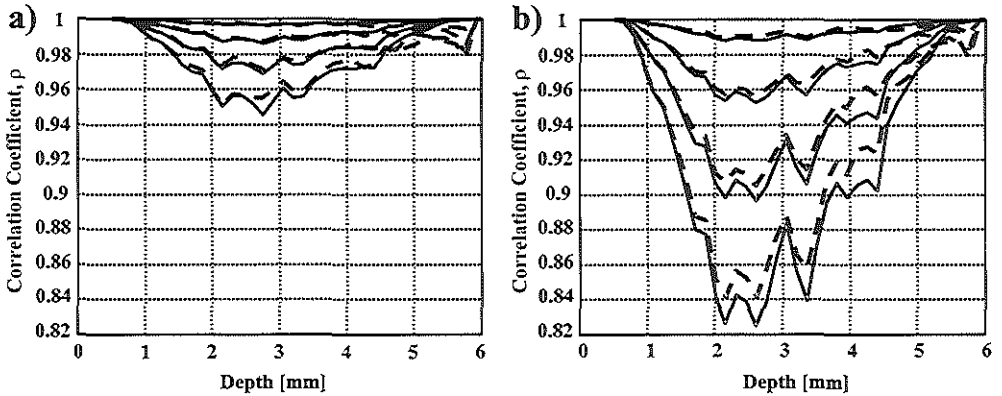


Figure 8.4: The 3-points curve fitting noise correction, correlation coefficients for lags of 1, 2, 3 and 4 signals (from top to bottom) as a function of depth from RF signals with a 15 dB SNR after noise correction (dashed lines) and compared to the correlation coefficients from the infinite SNR RF signals (solid lines). Results for a PRI of a)  $37 \mu\text{s}$  and of b)  $74 \mu\text{s}$ .

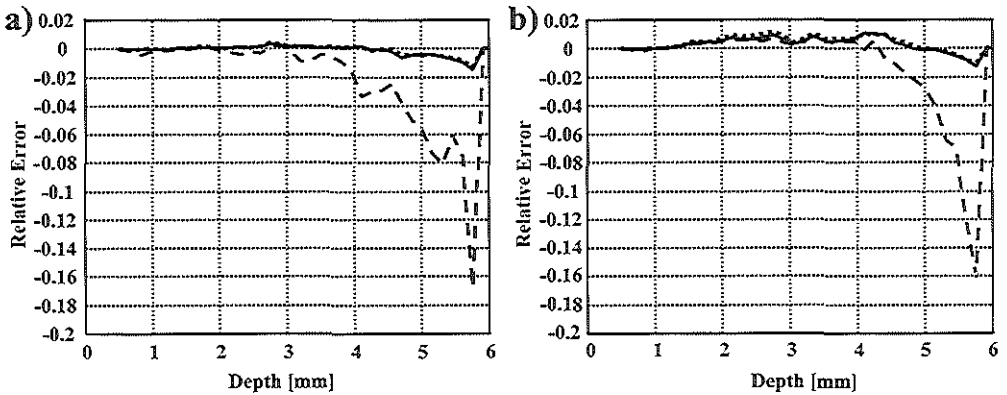
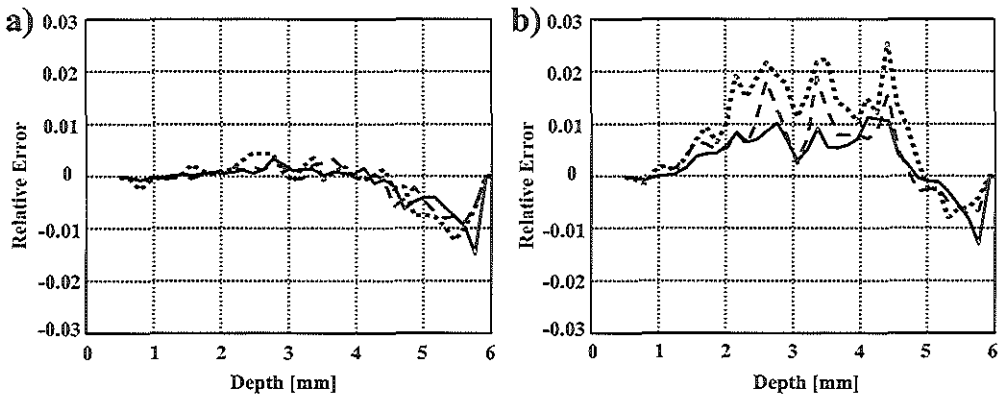


Figure 8.5: Mean -over lags 1, 2, 3 and 4 signals- relative error between correlation coefficients before and after correction for noise. The results are presented for the 2- (dashed line), 3- (solid line) and 4-points (dotted line) curve fitting for a PRI of a)  $37 \mu\text{s}$  and of b)  $74 \mu\text{s}$ .

2, 3 and 4 points curve fitting noise correction method based on the correlation coefficients from Figures 8.3a and 8.3b. Using the correlation coefficient at lag 0 estimated by the 3-point curve fitting method, the corrected for noise correlation coefficients from Figures 8.3a and 8.3b are presented in Figure 8.4, for the two PRIs -a) for  $37 \mu\text{s}$  and b) for  $74 \mu\text{s}$ - compared to the correlation coefficients from noiseless RF signals. The noise corrected correlation coefficients clearly approach the original ones up to a depth of 4 mm where a slight deviation from the original

correlation coefficients is observed for both PRIs. Although the relative error is large at depth of 4 mm, the contribution of this part of the blood velocity profile to the total flow is small compared to the rest of the velocity profile. It should be realized that normal coronary arteries have a free lumen diameter ranging from 3 to 4.5 mm. Figure 8.5 shows the mean -over lags of 1, 2, 3 and 4 signals- relative error between correlation coefficients for RF signals with an infinite and 15 dB of SNR, for a PRI of a)  $37 \mu s$  and b)  $74 \mu s$ . For both PRIs,  $37 \mu s$  and  $74 \mu s$ , the curve fitting based on 3 and 4 points show a better performance than that based on 2 points. Figure 8.6 shows similar results to Figure 8.5 for the 3-points noise correction method used on correlation coefficients from RF signals with a SNR of 5 dB, 10 dB and 15 dB; small relative errors are observed for both PRIs of a)  $37 \mu s$  and of b)  $74 \mu s$ . Figure 8.7 shows blood velocity profiles -based on correlation coefficient for a lag of 3 signals converted into velocity (cm/s) by the calibration- as a function of depth for a parabolic flow profile with a peak velocity of 32 cm/s; results for RF signals at infinite SNR, and for a 15 dB SNR before and after correction for noise, for a PRI of a)  $37 \mu s$  and of b)  $74 \mu s$ . Close agreement between the velocity profile for RF signals at infinite SNR and the one at 15 dB SNR corrected for noise is observed for both PRIs.



**Figure 8.6:** The 3-points method to correct the correlation coefficients for noise, results of relative error for SNR of 5 dB (dotted line), 10 dB (dashed line) and 15 dB (solid line) are presented for a PRI of a)  $37 \mu s$  and of b)  $74 \mu s$ .

## 8.5 Discussion

Noise correction is crucial when measuring intravascular transverse blood flow using the correlation-based method; if no correction for noise is applied, an over-estimation of the blood velocity will occur. The noise within the RF signals is



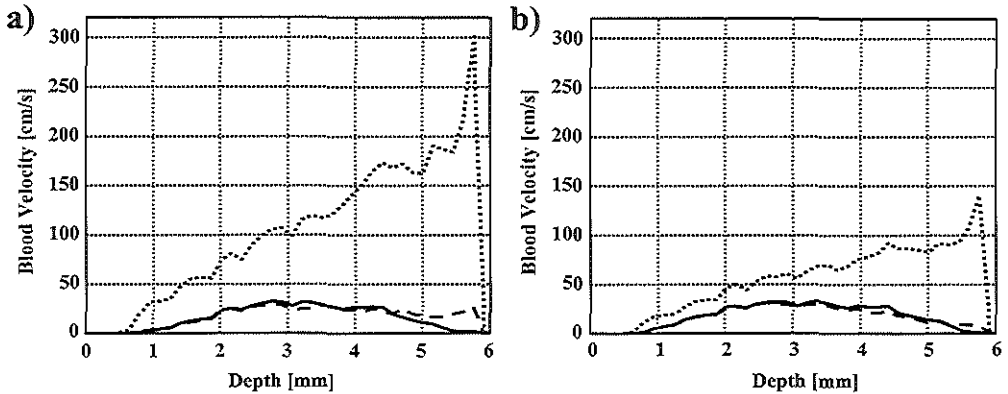


**Figure 8.7:** Blood velocity profiles -based on correlation coefficient at lag of 3 signals- as a function of depth for a parabolic blood flow profile with a peak velocity of 32 cm/s. Results for RF signals at infinite SNR (solid line), and for a 15 dB SNR before (dotted line) and after (dashed line) correction for noise, for a PRI of a) 37  $\mu$ s and of b) 74  $\mu$ s.

system-dependent and is band-limited, which has an impact on the shape of the correlation function especially the correlation coefficients at lag 0 (Ledoux et al. 1998); however, by normalizing the correlation function by the correlation coefficient at lag 1, Ledoux et al. (1998) showed the shape of the correlation function to be similar for different SNRs. This also shows that the correlation coefficients for different lags are equally affected by noise. Noise outside the signal band can be reduced by band pass filter the RF signals with a corresponding increase of the SNR. In case of band-limited noise in the RF signals, for the same noise level, the measured SNR is higher than the SNR when using broadband noise. What matters is the SNR for the coinciding spectral distribution (Hoeks et al. 1994).

The method for noise correction presented in this chapter is easy to implement and not computationally time consuming. A general example was introduced in Figure 8.1a; the 2, the 3 and the 4 points noise correction methods were presented in Figure 8.1b. The 2-points method is less computationally time consuming since only correlation coefficients for lags 1 and 2 are needed. However, the 3 and 4 points curve fittings are more robust since they are based on more correlation coefficient estimates and prevent the curve fitting on estimate a wrong correlation coefficient at lag 0 (Fig. 8.1b, 2-points fit for a SNR of 5 dB).

It can also be observed that the 3-points and the 4-points methods, for SNR of 5 dB, 10 dB and 15 dB, are nearly the same. Correlation coefficients at lag 0 (Fig. 8.1b) closely correspond to the results presented by Céspedes et al. (1997d) where correlation coefficient at lag 0 was plotted as a function of SNR showing that SNRs above 20 dB produce almost no influence in the correlation coefficients. However, for SNRs below 20 dB, the correlation coefficient decreases drastically.

The SNR is not measured by our method; however, when the correlation coefficient at lag 0 is determined the SNR can be obtained as described by Céspedes et al. (1997d).

Figure 8.3 showed that the correlation coefficients from RF signals with a SNR of 15 dB, before noise for correction, clearly deviate from the parabolic profile shown in Figure 8.2. The decay of the correlation coefficients as a function of depth corresponds not only to transverse blood flow but also to the decreasing SNR in the far field of the ultrasound beam, similar decay is also observed for the correlation coefficients at lag 0 as a function of depth (Fig. 8.3c and 8.3d). It can be observed that the 3 and 4 points give similar noise decorrelation estimates while the 2-points gives an underestimation. When using the 3-points curve fitting, the correlation coefficients corrected for noise clearly approached the original one (Fig. 8.4). The relative error introduced by the 3 and 4 points curve fitting is very low; however, for the 2-points curve fitting a large error will be introduced (Fig. 8.5). This can be explained by the fact that the quadratic function, based on only two correlation coefficients, does not represent the true decorrelation pattern as a function of transverse flow.

Although the relative error introduced by the 3-points fitting noise correction method is very small ( $< \pm 3\%$ ) for all SNRs, results from Figure 8.6 suggests that the noise correction method performs better for a shorter PRI; the relative error in this case is lower than  $\pm 1\%$  up to a depth of 4 mm, which is an acceptable error. However, Figure 8.7 suggested that the noise correction method performs better for a larger PRI, which can be explained by the shape of the calibration. The calibration has a parabolic shape for correlation coefficients close to 1; however, for lower correlation coefficients the calibration becomes more linear. A small error in estimating correlation coefficients for low velocities, and for a short PRI, may introduce an error in the noise correction method and in the process to convert correlation into blood velocity. Nevertheless, the relative error in volumetric blood flow estimation will be in the same order as those for correlation coefficients. The results presented here suggest that the noise correction method is not influenced by the blood velocity profile. The method for noise correction is expected to work during transverse blood flow, under any blood flow condition (*e.g.* laminar, turbulent flow or linear velocity gradient) and especially during *in vivo* blood flow measurements.

In case of stationary tissue or not moving red blood cells (*i.e.* no transverse blood flow), the correlation coefficients for lags of 1, 2, 3 and 4 will only decorrelate due to noise and thus the correlation coefficients will be similar. When correcting for noise, the four correlation coefficients will then be shifted close to 1 and considered as stationary tissue or no blood flow condition. A trade off appears when measuring high velocities; in case of long PRI and high blood flow, the particles or red blood cells will cross almost the entire ultrasound beam between excitations and thus producing uncorrelated RF signals.

A previous study (Chapter 5) suggested that RF decorrelation is less sensitive to different blood flow conditions than envelope decorrelation, which could be explained by the loss of phase information. The phase information contributes to an increase in the probability of finding the best match between RF signals. An increase in the standard deviations due to the decrement in the signal bandwidth by the envelope detection process was also observed; the variance is inversely related to the signal bandwidth (Bendat & Piersol 1986).

Other methods for noise estimation when measuring blood flow and elastography are based on estimation of the signal-to-noise ratio in stationary tissue (Céspedes et al. 1997d; Li et al. 1997). Although the methods could be implemented for blood flow measurements, they will be biased because the SNR in flowing blood is lower than the SNR in stationary tissue due to scattering amplitude differences. Thus, an overestimation of the blood flow velocity will occur. Another factor is that RF signals are acquired at a high gain setting to achieve sufficient blood scattering power, which produces saturation of the RF signals from tissue that produces an under estimation of the SNR from tissue. Additionally, the backscattered RF signal from blood is strongly influenced by the formation of rouleau or aggregates of red blood cells, which is also flow dependent (de Kroon et al. 1991; Cloutier & Qin 2000). Further *in vitro* and *in vivo* validation of the noise correction method is presented in Chapter 9.

## 8.6 Conclusions

The analysis of the noise correction method presented here showed the method to work for a wide variety of SNRs. Even SNRs below 15 dB gives good results. Dynamic noise correction is now feasible by only observing the decorrelation properties of the RF signals from flowing blood. The set of RF signals are windowed and since the decorrelation due to noise is estimated and corrected per window, the noise correction method is dynamic and not dependent on previous measurements.



## Chapter 9

# Quantitative IVUS Blood Flow: Validation *in vitro*, in animal and in patient

### Abstract

*In recent years, a new method to measure transverse blood flow based on correlation between consecutive Radio Frequency (RF) signals of Intravascular Ultrasound (IVUS) rotating single-element scanners was introduced. We report here in vitro, in animal and in patient testing to evaluate the correlation-based method using an IVUS array catheter. A new correlation-based method to dynamically correct for noise the correlation coefficients is implemented. The decorrelation due to noise was estimated from the correlation coefficients from flowing blood obtained at increasing time lags. First, blood flow experiments were carried out with different catheters in a tissue mimicking flow phantom with an inner diameter ranging from 3.0 to 5.0 mm. A calibrated Electromagnetic Flow meter (EMF, range: 0 to 250 cc/min) was used as a reference. Good linear relationships were found between the IVUS derived flow and the calibrated EMF (all  $R^2 > 0.96$ ). The catheter position within the flow phantom and the size of the ring-down were theoretically analyzed. These elements, and noise in the RF signals, have an important influence on the IVUS blood flow measurements reflected by the offset and the slope of the linear relationships. By placing the IVUS catheter outside the flow phantom, parabolic blood flow profiles were also measured. Second, IVUS blood flow measurements were performed in the carotid artery of two Yorkshire pigs, which showed linear relationships (all  $R^2 > 0.85$ ) between the IVUS derived flow and the calibrated EMF. Experimentally, the offset was*

---

based on the Publication: "Quantitative IVUS Blood Flow: Validation *in vitro*, in animals and in patients" by Fermín A. Lupotti, Frits Mastik, Chris L. de Korte, Stephane G. Carlier, Willem J. van der Giessen, Patrick W. Serruys and Antonius F.W. van der Steen, *Ultrasound in Medicine and Biology*, submitted; 2002.

lower than 3 cc/min and the slope was close to 1. Third, IVUS blood flow measurements were performed in coronary arteries in patients. Preliminary results for the Coronary Flow Reserve (CFR= high flow / baseline flow) in patients using the decorrelation method of RF signals of an array IVUS scanner were comparable with CFR based on Doppler measurements.

## 9.1 Introduction

Intravascular ultrasound (IVUS) has been used for many purposes as it provides real-time cross-sectional images of blood vessels at a high-resolution (Nissen & Yock 2001). RF-data processing has significantly enhanced the potential of IVUS (van der Steen et al. 1998a) and aims now at obtaining information concerning vessel wall and mechanical plaque properties (de Korte et al. 2000). In addition, IVUS has been applied to measure blood velocity and volumetric flow (Li et al. 1998b; Carlier et al. 1998d).

Methods to assess blood flow include Doppler processing and time-domain correlation techniques (Chou et al. 1994; Isner et al. 1993; Carlier et al. 1998c). Intravascular volumetric blood flow can be assessed with configurations such as combined Doppler Flowire<sup>TM</sup> and IVUS or Doppler Flowire<sup>TM</sup> and Quantitative Coronary Angiography (QCA) (Sudhir et al. 1993; Serruys et al. 1993; Doriot et al. 2000). A Doppler Flowire<sup>TM</sup> is a guide wire with a Doppler transducer in the tip (Doucette et al. 1992). However, these configurations do not easily allow the operator to assess blood velocity and lumen area simultaneously and at the same location. Moreover, the mean blood velocity is derived from the assumption of a parabolic flow profile that is rarely encountered in human coronary arteries (Carlier et al. 1999). Recent research has rendered the measurement of blood velocity and the quantification of volume blood flow using a correlation-based method with a rotating single-element catheter (Li et al. 1997, 1998b). First initial in patient evaluations of volumetric blood flow assessment based on this method using a rotating single-element catheter have been reported (Céspedes et al. 1998a; Carlier et al. 1998d).

The use of mechanically rotated transducer to measure flow requires compensation for the intrinsic decorrelation due to rotation. This could be cumbersome if the rotation is not uniform. IVUS array catheters are not hampered by rotational problems. The array transducer is capable of transmitting and receiving many echoes at a fixed angle. The array is scanned electronically (Eberle 1997). The decorrelation properties of the IVUS array catheter during transverse blood flow have been studied and recently reported (Chapter 3, 4 and 5). The mean decorrelation pattern for scattering media containing scatterers, as red blood cells (RBCs) and as aggregates of them, corresponded to the auto-convolution of the

acoustical beam. Therefore, the auto-convolution of the acoustical beam was used during the present study as calibration of the method (Chapter 7).

Electronic and quantization noise are well-known sources of decreasing the signal correlation. In correlation based flow imaging, the decrease in signal correlation produces an overestimation of the blood velocity. Different methods to estimate and suppress noise from the RF signals for measuring blood velocity, tissue motion and elasticity imaging, have been proposed (Li et al. 1997; Céspedes et al. 1997d). However, these methods are normally based on measurements of the signal-to-noise ration in stationary tissue such as vessel wall, which does not correspond well for noise in flowing blood. Dynamic noise correction in flowing blood was shown to be feasible by observing the decorrelation properties of the RF signals. When measuring transverse blood flow using an IVUS catheter in human arteries, the set of RF signals are windowed and the correlation coefficients are calculated per window. Decorrelation due to noise is then estimated and corrected per window, which makes this method dynamic and not dependent on previous measurements. This method was tested using computer simulations (Chapter 8) and is now implemented for measurements performed during the present study.

During the present study, *in vitro*, in animal and in patient recordings were performed to evaluate the correlation-based estimation of quantitative volume blood flow using the noise correction method together with the auto-convolution of the measured acoustical beam as a calibration file. *In vitro* measurements were carried out for different flow phantom lumen diameters and for several catheters; parabolic blood flow was measured. Using a computer program, the influence of the catheter position and the ring-down size on the blood flow measurements was also studied. A compensation method was implemented to work out the obscuring of blood flow by the ring-down. IVUS blood flow measurements were performed at the carotid artery of two Yorkshire pigs and compared to a calibrated EMF connected in line with the artery. IVUS blood flow measurements and CFR were obtained during in patient recordings. Preliminary results from patient recordings demonstrate the feasibility of this approach showing good agreement with CFR based on Doppler blood velocity measurements.

## 9.2 Methods

### 9.2.1 IVUS transducer

The IVUS array catheter is formed by 64 elements mounted on a circular surface of a catheter tip with a diameter of 1.2 mm. The array transducer operates at a central frequency of 20 MHz and with a -20 dB bandwidth of 7.5 MHz (Eberle 1997; O'Donnell et al. 1997a). The element size of the array under study is 0.7 mm in length and 28 mm in width; the pitch of the elements is 59  $\mu\text{m}$  (Fig. 3.1).

The array transducer operates in synthetic aperture focusing mode for imaging and linear mode for flow imaging. Synthetic aperture focusing mode is not suitable for flow assessment since the acoustical beam is formed over a time frame on the order of milliseconds, during which, the red blood cells will move through the beam and will influence flow assessment based on correlation. Therefore, in flow imaging, four elements are electronically tied together (Borsboom et al. 2000) and produce a burst of ultrasound pulses in linear array mode at a pulse repetition rate of  $74 \mu\text{s}$ . The selected elements are then electronically shifted by one element and the next burst is generated. The circular array is linearly scanned and pulsed 64 times to produce a frame.

### 9.2.2 Blood preparation

Packs of concentrated red blood cells (RBCs) from the blood bank of our hospital were used during the experiments. The blood sample was diluted with Haemacel solution to reach normal hematocrit and preserved normal blood viscosity. During the experiments, blood manipulation was performed in such way to avoid cellular damage and changes in the hematocrit and in the mean corpuscular volume (MCV). The blood temperature was kept at room temperature ( $\approx 22^\circ\text{C}$ ) to avoid red blood cell destruction. A blood test for the RBC counts, hematocrit, and MCV was performed just before and after the experiments and the results showed almost no change in both parameters. For the first experiments, the hematocrit was 0.345 L/L and 0.339 L/L and the MCV was 92.2 fL and 93.4 fL, pre and post-experiments, respectively. For the second experiments, the hematocrit was 0.43 L/L and 0.42 L/L and the MCV was 101.9 fL and 100.7 fL, pre and post-experiments, respectively.

### 9.2.3 *In vitro* setup for blood flow measurements

The experimental setup was based on a water-tank, an echo system (JOMED Inc., Rancho Cordova, CA, USA) and the IVUS array catheter (20 MHz Vision 64F/X<sup>TM</sup>, JOMED Inc.), an acquisition PC and an EMF (Fig. 9.1). The water tank was filled with degassed water at room temperature ( $\approx 22^\circ\text{C}$ ) and an ultrasound absorber was placed on the bottom and at both sides of the tank to reduce ultrasound reflections. The EMF was connected to the tubing system after the exit of the water tank. The valve was used to regulate the blood flow. Fifteen full frames for each blood flow condition were saved to hard disk and then used to calculate quantitative volume blood flow using the correlation-based method. The axial sampling frequency of the RF signals was 100 MHz. The EMF was calibrated before and after the experiments using the same human blood sample and for a range of volumetric blood flow from 0 up to 250 cc/min using the conventional time-volume approach.



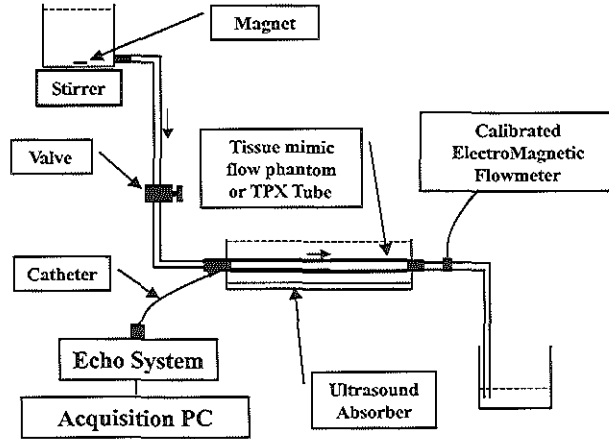


Figure 9.1: Block diagram of the blood flow setup used during the experiments; the echo system, the A/D converter PC and the water tank; the IVUS array catheter connected to the echo system and placed within the flow phantom.

#### 9.2.4 Calibration method

The correlation-based method needs to be calibrated in order to convert the measured correlation coefficients as a function of time into transverse velocity. The calibration for the correlation-based method was based on the auto-convolution of the acoustical beam. For the *in vitro* measurements, a Gaussian fit through the auto-convolution of the acoustical beam was used as a calibration. For the animal and patient recordings, the mean auto-convolution of the acoustical beam was used as a calibration. The acoustical beam was experimentally measured for depths ranging from 0.5 mm to 6 mm with steps of 0.5 mm and then the calibration file was produced; these measurements were performed for several catheters (Chapter 7).

#### 9.2.5 Noise correction method

The noise correction method introduced in Chapter 8 was implemented during the present study. Briefly, the method uses the fact that the decorrelation pattern should be 1 at lag 0; however, this does not occur in the presence of noise in the RF signals. Noise produces an offset in the decorrelation pattern -by shifting the correlation pattern down- and thus the correlation coefficient at lag 0 is not 1 any more (Fig. 8.1a,  $\rho_{SN}$ ). The correlation coefficient at lag 0 or offset is then estimated by curve fitting the correlation coefficients; a Gaussian fit was used for this purpose. Adding 1 minus the offset to each correlation value corrects the correlation coefficients for noise (Fig. 8.1a,  $\rho_S$ ). For blood flow calculations, correlation coefficients from the windowed RF signals were calculated for lags

of 1, 2 and 3 signals; the fitted curve, was then based on these 3 correlation coefficients using the least square method.

### 9.2.6 Ring-down obscuring

The ring-down of the IVUS catheter (formed by ultrasound reverberations from the array transducer) obscures part of the vessel lumen and thus blood flow too. The level of obscuring is dependent on the ring-down length and on the eccentricity of the IVUS catheter. Through a computer program, we studied both effects. The radius of the IVUS catheter was 0.6 mm and the ring-down sizes were assumed to be 0.3 and 0.6 mm in depth. These ring-down sizes are representative of the limits in ring-down size from an IVUS array catheter. The vessel lumen was considered circular with radius ranging from 3.0 mm to 5.0 mm. The eccentricity of the catheter, in %, is defined as the distance between the center of the lumen and the center of the IVUS catheter divided by the radius of the lumen. Eccentricity 0 means that the catheter is located in the center of the vessel lumen and thus maximum obscuring of the vessel lumen will occur.

### 9.2.7 Compensation for ring-down obscuring

A method was derived to estimate the blood flow that cannot be measured in the ring-down. Through a numerical simulation and assuming a parabolic blood flow profile; a factor ( $\alpha$ ) was obtained as the ratio between the blood flow that cannot be measured in the ring-down to the blood flow in the free lumen (outside the ring-down) normalized by the respective areas. A linear relationship was found between  $1/\alpha$  and the lumen radius (based on a contour detection and considering the center of the catheter as the origin). With this fixed ratio, by entering the curve with the lumen radius, the  $\alpha$  was obtained. Next, the blood flow missed in the ring-down is  $\alpha$  times the blood flow in the free lumen. The blood flow compensation process is performed per angle in those angles where a minimum free lumen is present. All IVUS blood flow measurements presented in this study are compensated for the ring-down obscuring.

### 9.2.8 *In vitro* blood flow measurements

First, the IVUS array catheter was placed inside a 40-cm long tissue mimic flow phantom (Polyvinyl Alcohol (PVA) Cryogel) with an inner diameter ranging from 3.0 to 5.0 mm. The location of the catheter inside the flow phantom was chosen to be preferably eccentric with respect to the lumen of the flow phantom (*i.e.* against the wall). Measurements were performed for a range of flows from 0 to 250 cc/min.

Second, the IVUS array catheter was placed outside a 40-cm long tube (TPX tube, Mitsui Chemicals, Tokyo, Japan) of 2 mm of inner diameter to reach a

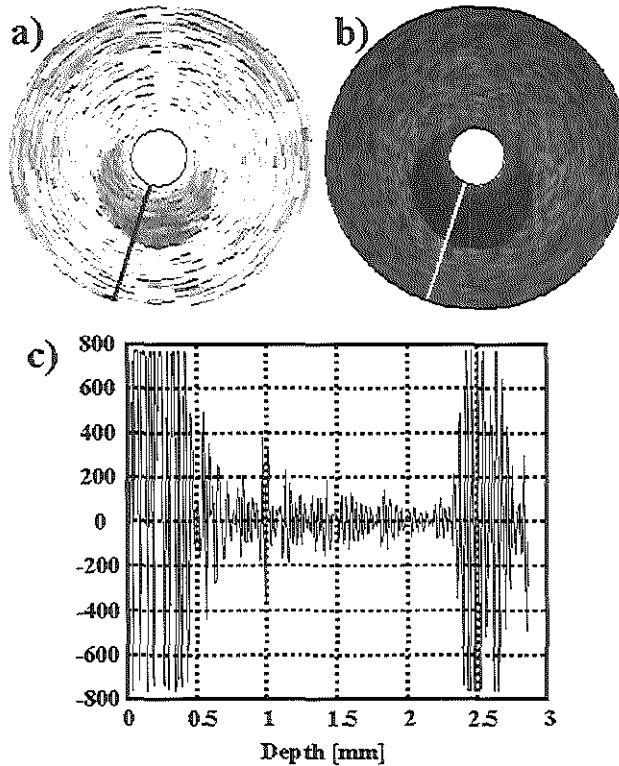


**Figure 9.2:** Echograms from the same IVUS catheter, a) in linear mode for blood flow measurements and b) synthetic aperture mode for imaging; c) an IVUS RF signal in linear mode where the ring-down produces signal amplitude saturation and no blood flow can be measured there.

laminar flow condition. The IVUS catheter was placed about 0.75 mm away from the tube to perform the blood velocity measurements outside the ring-down. Measurements were performed for three peak blood velocities, 20 cm/s, 103 cm/s and 209 cm/s. The correlation-based blood velocity estimates are compared with the parabolic blood flow profiles derived from the mean blood flow from the EMF (reference flow profile). The geometry of the reference flow profile was defined as 1 minus the squared of the ratio between the distances from the center of the lumen ( $r$ ) over the total radius of the lumen vessel ( $R$ ) all multiply by the peak velocity ( $V_{peak}$ ) (*i.e.*  $(1-(r/R)^2) * V_{peak}$ ).

### 9.2.9 In animal blood flow measurements

IVUS blood flow measurements were performed in two Yorkshire pigs at the Experimental Echocardiology department, Erasmus University, Rotterdam.

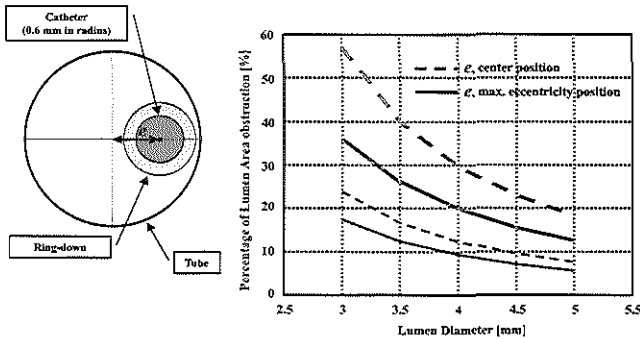


**Figure 9.3:** Percentage of obscured area due to catheter eccentricity for different tube diameters and for two eccentricity values, minimum (dashed line) and maximum eccentricity (solid line). Result for a catheter radius of 0.6 mm and ring-down sizes of 0.3 (thin black lines) and 0.6 (thick gray lines) mm in depth.

The IVUS catheter was pushed from the femoral artery up to the right carotid artery. A shunt was made between the right carotid artery and the right jugular vein by connecting the side parts of two introducer sheaths then the EMF was connected in line with the shunt. By clamping the shunt distal to the EMF, the blood flow was changed. The pig heart rates were ranging from 100 to 120 beats/min. The EMF was calibrated at the end of each experiment using the conventional time-volume approach.

### 9.2.10 In patient CFR measurements

Coronary flow reserve in patients is measured as the ratio of the hyperemic flow measured during *e.g.* an infusion of adenosine over the baseline flow. This parameter evaluates the physiological significance of a coronary stenosis (Gould et al. 1990). IVUS blood flow measurements were performed in 5 patients at the department of Interventional Cardiology at the Thoraxcentre, Rotterdam. The hyperemia cycle could be followed by acquiring the RF data every 30 seconds from the moment of the adenosine injection. Blood velocity measurements, obtained with a Doppler Flowire<sup>TM</sup>, were also performed during a hyperemia cycle and the CFR was calculated using the average peak velocity in baseline and in peak hyperemia. All IVUS blood flow and Doppler blood velocity measurements were performed with the IVUS catheter and Doppler Flowire<sup>TM</sup> in place.

## 9.3 Results

Figure 9.2 illustrates the effect of the transducer ring-down in masking blood flow near the surface of the catheter. IVUS echograms are presented in the

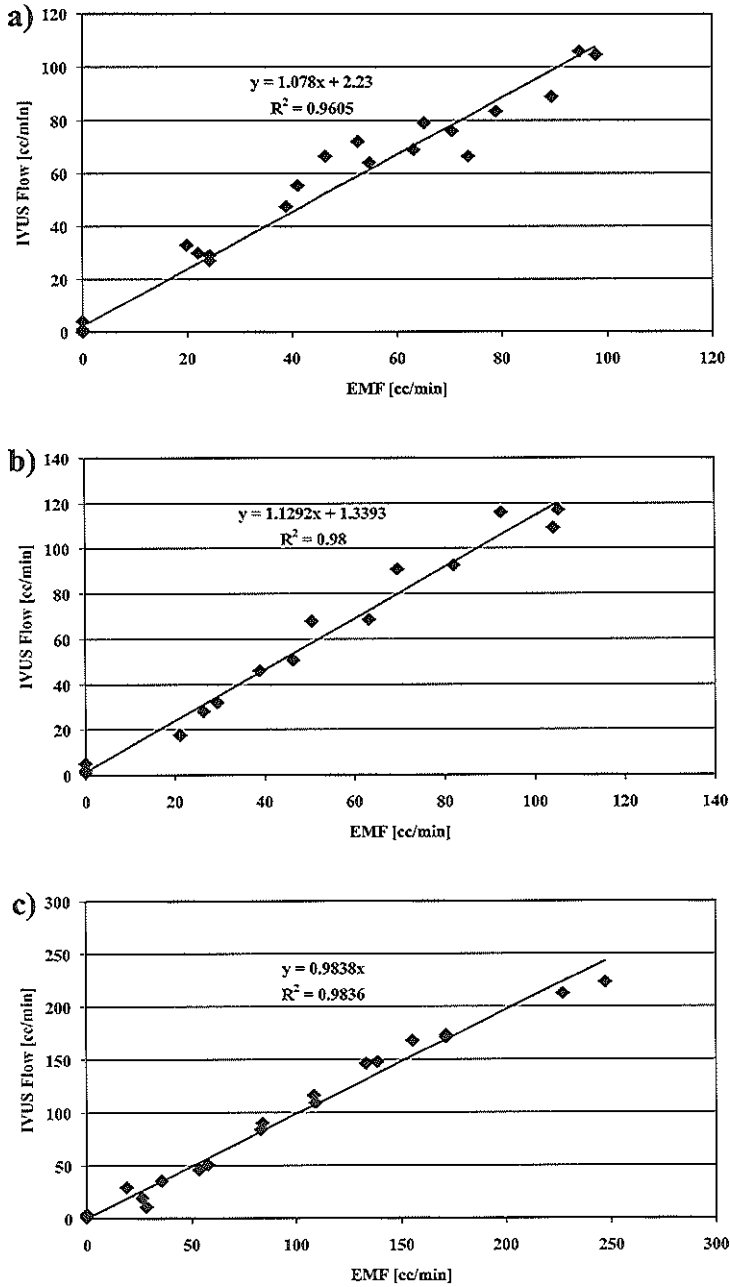


Figure 9.4: IVUS blood flow versus calibrated EMF for the catheter placed inside the lumen with an eccentricity as maximum as possible; results for different lumen diameters, a) 3.0, b) 4.0 and c) 5.0 mm. Linear polynomial approximates to the points with a high  $R^2$  ( $> 0.96$ ).

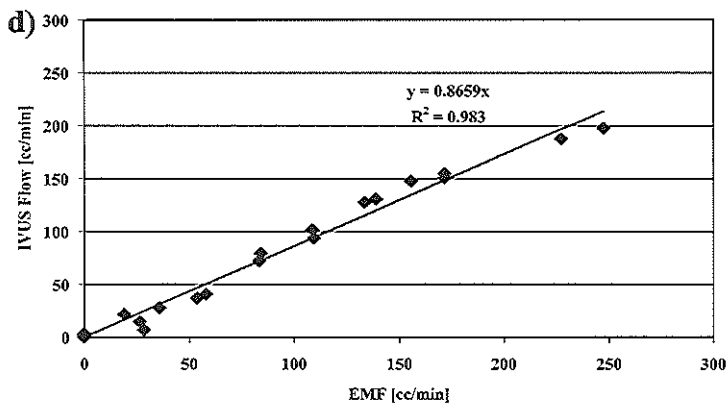


Figure 9.4: d) shows IVUS blood flow versus calibrated EMF for a lumen diameter of 5.0 mm before ring-down compensation.

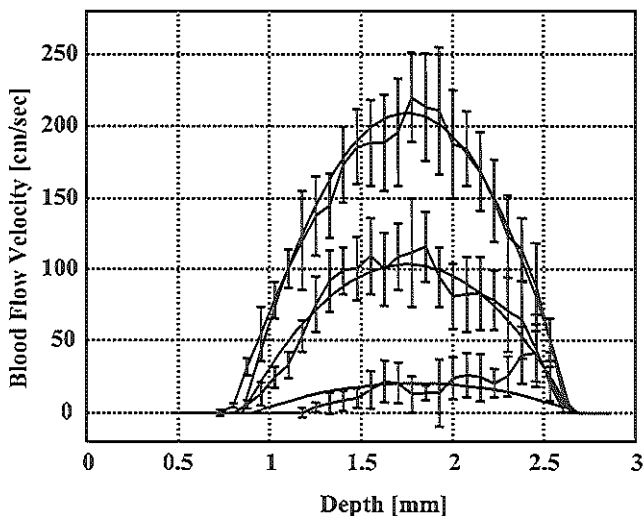
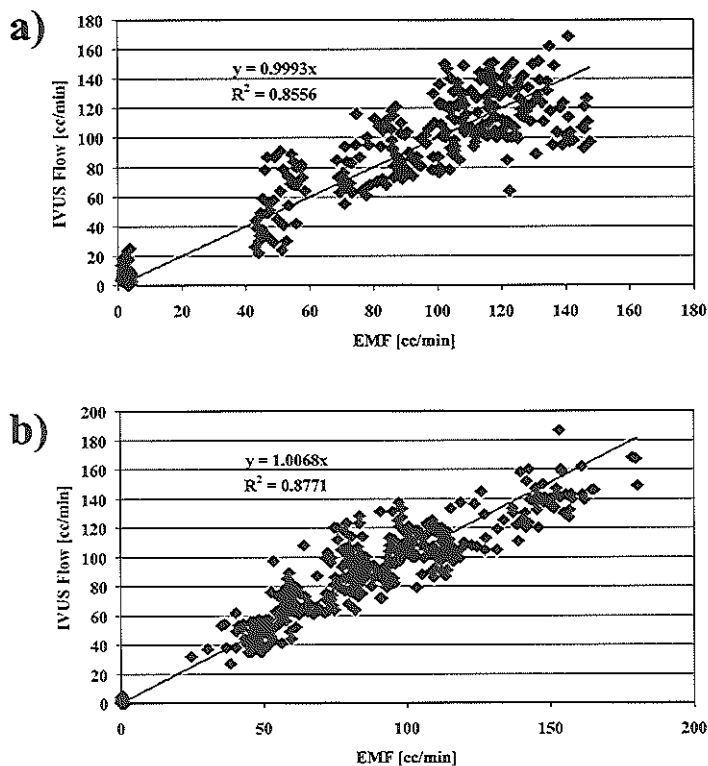


Figure 9.5: IVUS blood velocity measurements (mean and standard deviations) as a function of depth during parabolic blood flow condition compared with parabolic blood flow (solid line) based on EMF for peak blood velocities of 20 cm/s, 103 cm/s and 209 cm/s. Results for a tube of lumen diameter of 2 mm; the IVUS catheter was placed outside the lumen with maximum eccentricity.

top of the figure for color flow mode (linear mode, Fig. 9.2a) and for imaging mode (synthetic aperture mode, Fig. 9.2b). A RF signal in color flow mode is shown (Fig. 9.2c), where the beginning of the RF signal shows signal amplitude saturation due to the ring-down effect. The ring-down estimated thickness is in

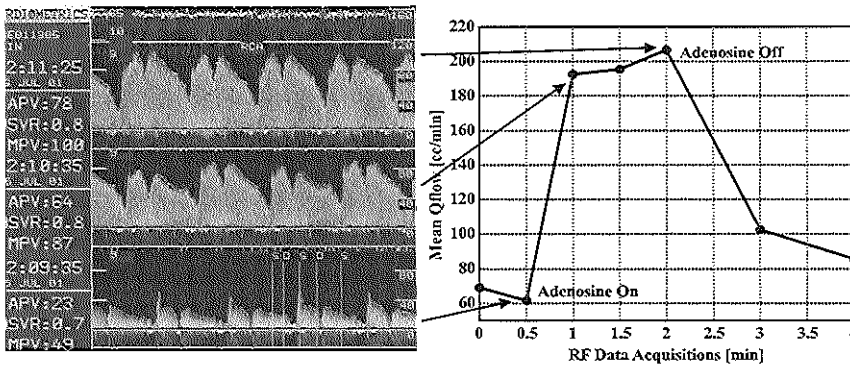
this case of 0.4 mm. The results of percentage of the lumen area obscured by ring-down as a function of lumen diameter are presented in Figure 9.3 for lumen diameters ranging from 3.0 to 5.0 mm and for two ring-down sizes (0.3 and 0.6 mm in depth). In case of an artery of 3.5 mm in diameter, and for a catheter ring-down of 0.6 mm, the obstructed area by the ring-down goes from 25 up to 40% of the lumen when moving the catheter from the most eccentric position (thick solid line) to a centric (thick dashed line).

Figure 9.4 shows the IVUS blood flow measurements versus flow measurements from the calibrated EMF for a range of flow from 0 to 250 cc/min. The data is presented for three different flow phantom lumen diameters, 3.0 mm (Fig. 9.4a), 4.0 mm (Fig. 9.4b) and 5.0 mm (Fig. 9.4c). Good linear relationships (all  $R^2 > 0.96$ ) are observed for all lumen diameters. The slope is in all cases around 1 and the offset is lower than 3 cc/min. Figure 9.4d presents the same data as for Figure 9.4c (5.0 mm) before ring-down compensation, showing a slope 0.865.



**Figure 9.6:** IVUS blood flow measurements versus calibrated EMF during in animal recordings; linear polynomial approximates to the points with a high  $R^2$  ( $> 0.85$ ). a) first and b) second Yorkshire pig recordings.

For the case of 3.0 and 4.0 mm, the slopes before ring-down compensation are 0.837 and 0.938, respectively. Results for parabolic blood flow measurements are shown in Figure 9.5; the measured parabolic blood flow profiles are in good agreement with the reference flow profile based on the EMF for the three blood velocities, 20 cm/s, 103 cm/s and 209 cm/s. The results from the IVUS blood flow measurements versus flow measurements from the calibrated EMF performed in two Yorkshire pigs are presented in Figure 9.6. Good linear relationships (all  $R^2 > 0.85$ ) are observed with a slope of 1. Figure 9.7 shows an example of CFR in patients; the CFR IVUS (*i.e.* blood flow ratio of 3.0) shows a close agreement with the CFR based on Doppler measurements (*i.e.* blood velocity ratio of 3.3) during a hyperemia cycle. Each point in the IVUS blood flow measurements is the mean blood flow over 2 or 3 cardiac cycles. Table I shows the results for CFR based on IVUS close to those based on Doppler for 5 patient recordings.



**Figure 9.7:** An in patient example of CFR based on Doppler blood velocity measurements (3.3) compared to CFR based on IVUS blood flow measurements (3.0) during a hyperemia cycle. The hyperemia cycle can be followed by the IVUS blood flow measurements.

## 9.4 Discussion

The eccentricity of the catheter was shown to have an important effect on the blood flow measurements when ring-down is present. The ring-down, formed by ultrasound reverberations from the array transducer, obscures part of the lumen vessel area where blood is flowing, which will produce an under estimation of the measurements if the system is not compensated for it. When the amplitude of the RF signals is saturated (Fig. 9.2c), no change due to blood flow can be detected by the correlation-based method. Flow estimated in that region is then zero. When the ring-down is maximal (0.6 mm) and the vessel is small (3.5 mm), and the IVUS catheter is located in the center, the obscured area can be up to 40% (Fig. 9.3). It should be realized that close to the catheter the flow



Doppler CFR (Velocity Ratio)	IVUS CFR (Flow Ratio)
3.3	3
3.6	3.4
1.9	1.9
2.3	2.2
1.2	1.2

**Table 9.1:** CFR based on Doppler blood velocity measurements compared to CFR based on IVUS blood flow obtained during a hyperemia cycle.

is low. Eccentricity  $e$  is expected to increase as a function of lumen diameter. The average eccentricity of the IVUS catheter during the *in vitro* measurements were 45%, 52% and 46% where the possible maximum eccentricities are 60%, 70% and 75% for lumen diameters of 3.0, 4.0 and 5.0 mm, respectively. However, the compensation for ring-down obscuring method implemented during the present study estimates the volume flow in the ring-down well. IVUS blood flow versus EMF flow measurements *in vitro* showed a good linear relationship with slopes close to 1 for all lumen diameters (Fig. 9.4). The correlation-based method works well for volume flows ranging from 0 up to 250 cc/min. Small offsets compared to the normal human mean blood flow (50 cc/min to 300 cc/min) were observed.

For parabolic blood flow measurements, good agreements in the results were shown (Fig. 9.5). However, for low blood flows (Fig. 9.5, peak velocity of 20 cm/s), the measured profile did not correspond well with the reference flow profile, which can be pointed as a limitation of the method on measuring very low velocities in a noisy environment. The results presented here for parabolic blood flow validates a previous study from this group (Chapter 5), where spread of blood-flow velocity, linear blood-flow velocity gradient and parabolic blood flow were studied by means of computer simulations showing to have no influence in the correlation-based method for blood velocity estimation. Figure 9.5 showed for high flows (209 cm/s) the correlation-based method to be not influenced by large velocity gradients present in the parabolic blood flow. The Gaussian fit used as calibration of the correlation-based method for the *in vitro* measurements performed well. The agreements found in Figure 9.5 between blood velocity profiles showed the blood flow correlation-based method to be calibrated for the full depth well. These *in vitro* measurements were performed as close as possible under laminar flow. Therefore, aggregation of RBCs might occur.

Qin et al. have indicated rouleau orientation with the flow under steady or laminar flow (Qin et al. 1998b) and before and after a sudden reduction of the blood flow (Qin et al. 1998a). Moreover, according to Goldsmith et al. (1962),

aggregates of RBCs and individual blood cells tend to align to the applied shear stress. During the present study, the *in vitro* measurements were performed at room temperature ( $\approx 22^\circ\text{C}$ ). Neumann et al. (1987) studied the effect of temperature on the level of aggregation of RBCs at 3, 10, 20, 30 and  $37^\circ\text{C}$  from normal donors and blood samples of patients with venous ulcers of the leg. Although, red cell aggregate formation as an overall process is retarded by a decrease in temperature and the aggregates become more resistant to hydrodynamic dispersion, they become more prone to growing under low shear stress. Neumann et al. concluded that as a whole red cell aggregation is favored by temperature lowering. Previous study showed that when the scattering medium resembles a unidirectional medium, the rate of decorrelation becomes lower for small displacements (Chapter 4). Thus, the aggregates of RBCs will align with the flow and produce a lower rate of RF decorrelation, and in consequence a blood flow underestimation. At correlation coefficients close to 1 the Gaussian fit is broader than the mean correlation coefficients. This broadening of the calibration seemed to compensate the lower rate of decorrelation of the aligned aggregates of RBCs.

However, in pulsatile flow, the velocity profile changes significantly as a function of the cardiac cycle preventing long aggregates of RBCs to occur (Milnor 1989). Since almost no aggregation of RBCs is expected in coronary arteries during pulsatile flow, the mean auto-convolution of the acoustical beam as calibration of the correlation-based method is the best suited for animal and patient recordings; this was confirmed from the results in Figure 9.6. In the case of transverse blood flow, the change in blood velocity profile produces significant velocity gradients, which in the present situation seem to have no effect on the blood flow measurements using the correlation-based method.

Noise estimation from tissue is possible (Céspedes et al. 1997d; Li et al. 1997); however, for blood flow measurements, the amplitude gain setting of the echo system is normally set for high blood scattering power, which produces saturation of the RF signals from tissue. This signal saturation will produce an under estimation of the SNR from tissue. The saturation effect can be observed in the RF signals for color flow shown in Figure 9.2c around 2.5 mm from the transducer. The noise correction method described in Chapter 8 was implemented here. From the *in vitro*, in animal and in patient measurements presented in this study the method showed to perform well. Dynamic noise correction is now feasible by only observing the decorrelation properties of the RF signals from flowing blood. The set of RF signals are windowed and since the decorrelation due to noise is estimated and corrected per window, the noise correction method is dynamic and not dependent on previous measurements.

Absolute coronary blood flow is the optimal parameter for intracoronary physiological studies. However, intracoronary flow measurements have been simplified for clinical practice. The most useful index at the end of an intervention such as a stent implantation is the coronary flow reserve estimated from the ratio of the

maximum flow velocity measured with a Doppler Flowwire<sup>TM</sup> during hyperemia to the baseline velocity (Serruys et al. 2000; Di Mario et al. 2000). Figure 9.7 shows an example of CFR in patient based on IVUS blood flow compared to the CFR based on Doppler blood velocity; the hyperemia cycle can be followed by both methods and the peak hyperemia was obtained at about 2 min after the injection of adenosine. Table I showed the CFR values obtained in patients where the CFR IVUS values are very close to the CFR based on Doppler measurements. IVUS blood flow measurements were acquired every 30 sec, which could lead to miss the peak of the hyperemia cycle and thus produce an underestimation of the CFR. It would also be very interesting to assess the reduction of the maximal flow through moderate coronary stenosis, beside their conventional morphological IVUS assessment. However, presently, the relatively large diameter of the IVUS catheter ( $> 1$  mm) may cause a noticeable increase of the pressure gradient across the stenosis, since many of these lesions may have a minimal lumen diameter ranging between 1.5 and 2.5 mm. Further miniaturization of the IVUS device would be desirable for this application.

## 9.5 Conclusions

We have characterized experimentally the IVUS quantitative blood flow assessment method. The results clearly indicate dependence of the measured flow on the magnitude of the inevitable ring-down artifact as well as noise present in the RF signals. Additionally, the severity of the ring-down artifact is dependent on the eccentricity of the IVUS catheter within the lumen. Noise is a crucial issue in the correlation-based method; however, dynamic noise correction of the correlation coefficients is now feasible. These combined deleterious effects were experimentally solved. From the *in vitro* and in animal measurements, the correlation-based method showed to estimate quantitative IVUS blood flow well; from the coronary flow reserve in patients, CFR-IVUS values were very close to the CFR-Doppler measurements.



## Chapter 10

# Coronary Flow Reserve versus Geometric Measurements of Coronary Dimensions

### Advantages and Limitations of the Functional Stenosis Assessment

#### Abstract

*This chapter reviews the physiopathological background of invasive functional assessment of coronary artery stenoses and the recent developments for clinical-decision making based on intracoronary flow and pressure measurements. Limitations of these recordings are stressed, as well as their present clinical application to guide the decision of performing an intervention, or to assess the results of a percutaneous procedure. The additional value over (quantitative) angiography and intravascular ultrasound is discussed. Finally, the potentials of a new method of coronary flow measurement, based on the processing of the radiofrequency IVUS signal, offering combined simultaneous morphological and physiological assessments, are briefly introduced.*

---

based on the Publication: "Coronary Flow Reserve versus Geometric Measurements of Coronary Dimensions: Advantages and Limitations of the Functional Stenosis Assessment" by Stephane G. Carlier, Glen van Langenhove, Fermín A. Lupotti, Mariano Albertal, Frits Mastik, Nicolaas Bom and Patrick W. Serruys, *Journal of Interventional Cardiology*, 1999; 12: 411-424.

## 10.1 Introduction

The development of selective coronary angiography in the 1960s by Sones (Proudfit et al. 1966) offered a dramatic improvement in the management of ischaemic heart disease. Technological advances and methodological improvements boosted clinical decision-making for medical versus surgical management. However, decisions were only based on 'shadow'grams of coronary stenoses. Early invasive assessment of stenosis severity and coronary flow have been developed, based on the Doppler effect, using piezoelectric crystal mounted at the tip of standard Sones catheters (Hartley & Cole 1974), on suction-mounted epicardial probes for intraoperative use (Wright et al. 1980) and on intraluminal, rather large, probes (Wilson et al. 1985), since no conventional experimental method like radiolabelled microspheres are applicable in the catheterization laboratory. However, the partial obstruction of the coronary ostium by these devices limited their clinical use (Carlier et al. 1998c). With the next breakthrough in patient care, when Grüntzig performed his first Percutaneous Transluminal Coronary Angioplasty (PTCA) in 1977, the concept of physiological assessment of the results of percutaneous interventions was already introduced (Grüntzig et al. 1979). The double-lumen 4-French dilatation catheters permitted on one side balloon inflation, and on the other side the recording of the distal coronary pressure. Trans-stenotic pressure gradients were a guide to follow the progression of the dilatation: a residual trans-stenotic gradient less than 20 mmHg was considered optimal (Rothman et al. 1982). However, with technical developments like the flexible-tipped guidewires introduced in the lumen previously used to measure pressure, and the introduction of low-profile balloons, pressure recordings were more difficult to perform. Moreover, the relations between the measured pressure gradient, the diameter stenosis and the lesion length were imprecisely known, and dependent on the presence of the catheter itself in the stenosis (Anderson et al. 1986).

Pressure gradient had finally a limited prognostic value and distal pressure recordings were abandoned, in parallel with the advent of quantitative computerized angiography (QCA). With the development of parameters to assess the functional significance of a stenosis from its geometry (Gould et al. 1982), many interventional cardiologist considered that the available anatomical information was sufficient and that these attempts to perform physiological pressure and flow recordings were only for research purposes. Nowadays, the angiogram is still considered by most physicians to be the "gold standard" for defining coronary anatomy. However, its resolution is limited and numerous confounding factors (vessel tortuosity, overlap of structures, effects of lumen shape) result in a marked disparity between the apparent severity of a lesion and its physiological effect (White et al. 1984; Topol & Nissen 1995).

The limitations of QCA for the physiological assessment of intermediate coronary lesions in unselected patients with extensive coronary atherosclerosis have been recognized (Legrand et al. 1986; Miller et al. 1994). The hazziness of the borders of the vessel after PTCA limits also the use of QCA to assess the acute results of an intervention. In the late 1980s, intravascular ultrasound (IVUS) emerged as a promising imaging modality to assess vascular disease (Yock & Linker 1990). IVUS provides real-time tomographic images of vessel wall cross sections, elucidating the true morphology of the lumen and transmural components of atherosclerotic arteries, on the contrary to angiography which can only demonstrate lumen narrowings. Early atheromatous thickening of the arterial wall, partly due to vascular remodeling that permits plaque to occupy up to 40% of the vessel cross section before luminal encroachment occurs (Glagov et al. 1987) could finally be demonstrated *in vivo*. IVUS has led to improvements in the understanding of atherosclerotic disease and the response to various therapeutic interventions (Hodgson et al. 1993). However, a main thrust of this technique is the guidance of therapeutic interventions, and controversial data exist in the literature on the value of IVUS parameters to predict and/or to lower the restenosis rate.

Development of miniaturized pressure and Doppler transducers, mounted now on 0.014-inch guide wires, has resolved the initial fluid dynamics problems of flow impediment. The clinical importance of the coronary flow reserve (CFR) distal to a stenosis, derived from Doppler recordings, or of the myocardial fractional flow reserve ( $FFR_{myo}$ ), derived from pressure recordings, has been extensively demonstrated and will be reviewed. The combination of morphological and physiological parameters ( $CFR > 2.5$  and diameter stenosis  $\leq 35\%$ ) is now a demonstrated prognostic factor of beneficial outcome after angioplasty (Serruys et al. 1997). The safety of not performing an angioplasty for intermediate stenoses without a functional significant severity assessed by flow or pressure measurements has also been demonstrated (Kern et al. 1995; Pijls et al. 1996; Ferrari et al. 1999; Bech et al. 1999b, 1999a). This new interest for pressure and flow recordings illustrates one more example of the swinging back of the pendulum, a commonly seen process in interventional cardiology. However, these recent developments should be critically reviewed, and the limitations of these measurements stressed, in order to define what is the potential role of (quantitative) angiography, intravascular ultrasound and pressure and flow measurements in the field of interventional cardiology nowadays.

Finally, a recent development from our laboratory will be overviewed, which demonstrates that by the processing of the radiofrequency IVUS signals, a new approach combining morphological and physiological assessment of the results of an intervention might be the ideal tool in the catheterization laboratory in the years 2000 (Carlier et al. 1998b).

## 10.2 Rationale of coronary flow reserve

The clinical status of a patient presenting a coronary stenosis depends on the maximum amount of O<sub>2</sub> that can be delivered to the downstream myocardial territory. When the maximum blood flow is no more able to meet the metabolic demand, which is almost totally dependent on aerobic metabolism, ischemia and/or angina occur. The decision to perform a coronary intervention should be based on objective evidence of ischemia (Ryan et al. 1993). However, a large survey has showed that a stress test prior to catheterization had been performed in less than 30% of the investigated cohort (Topol et al. 1993).

The possibility to assess the functional significance of a lesion in a catheterization laboratory appears thus of paramount interest, and is also a cost-saving alternative to required exercise thallium testing (Kern et al. 1997a). Major epicardial coronary vessels contribute to the coronary vascular resistance, but they act primarily as conductance vessels, and most of the resistance to coronary blood flow arises from the intramural arterioles of less than 200  $\mu\text{m}$  in diameter (Spaan 1991). Gould has demonstrated that the resting coronary flow does not decrease until there is a 90% diameter stenosis of the epicardial vessel. On the contrary, the maximal achievable flow begins to decrease when the percent diameter stenosis exceeds 50%. The coronary flow reserve, defined as the ratio of coronary flow at maximum vasodilatation to flow at rest has been proposed as a measure of stenosis severity (Gould et al. 1974). This assumption is derived from the complex hemodynamic principles regulating the coronary circulation. At rest, flow is independent from the driving pressure over a wide range (60 to 180 mmHg) of physiologic pressures, a phenomenon classically described as autoregulation of the coronary circulation (Fig. 10.1). During maximal vasodilation, flow becomes linearly related to the driving pressure (Klocke 1987; Hoffman & Spaan 1990).

The presence of a flow-limiting stenosis in a major epicardial vessel generates a pressure drop across the stenotic lesion that is the result of viscous and turbulent resistances, so that the driving pressure distal to the stenosis decreases exponentially in response to the flow increase (Sugawara 1989). The coronary flow reserve concept is appealing to the clinician because it constitutes a functional surrogate to the anatomic description of the lesions located in the epicardial vessels. Many investigators have shown in animal experiments that a decrease in flow reserve may discriminately detect lesions of increasing severity (Gould et al. 1990). Although the concept may be easily applied in humans, conflicting results have been reported (White et al. 1984; Harrison et al. 1984; Wilson et al. 1987; Uren et al. 1994). It should be recognized that CFR is influenced by several factors independent from the hydrodynamic characteristics of the stenotic lesion. Being a ratio, similar values may be obtained at very different levels of resting and hyperemic flow. Changes in basal resting flow without changes in hyperemic flow will considerably affect the ratio (Fig. 10.1).



Since coronary blood flow is linearly related to myocardial oxygen consumption, determined by heart rate, contractility and wall stress (Braunwald 1971), these parameters should remain constant during successive CFR assessments. Furthermore, any factors affecting the hyperemic pressure-flow relationship would likewise modify the flow reserve and thereby change the assessment of the severity of the coronary lesion under study. This relationship is influenced by factors such as heart rate, preload, myocardial hypertrophy, contractility (Marcus et al. 1981b; McGinn et al. 1990; Rossen & Winniford 1993; Hongo et al. 1994; de Bruyne et al. 1996), rheological factors (*e.g.* polycythemia), and diseases of the microvasculature, as initially described by Cannon et al. (1983), and which may exist in various pathological conditions such as diabetes mellitus, myocardial infarction or syndrome X (Strauer 1990).

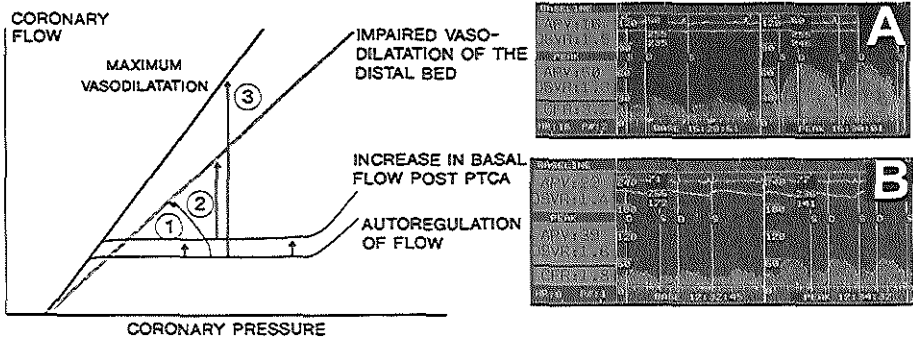


**Figure 10.1:** The pressure flow relationship in coronary arteries and the principle of coronary flow reserve. Baseline flow (thin line) presents a plateau over the physiological normal driving pressure range (60 to 180 mmHg), whereas hyperemic flow (thick line) is linearly related to the driving pressure. Coronary flow reserve (CFR) is the ratio of maximal hyperemic flow to baseline flow. After PTCA, CFR may change with (1) an increase in basal flow, (2) a change in the pressure drop over the residual stenosis and (3) an impaired vasodilatation of the distal bed (adapted from Serruys et al., 1993) Panel A demonstrates a normal CFR of 3.2 measured with the Doppler Flowwire, as the ratio of peak to baseline average peak velocities (APV). Panel B demonstrates a typical recording obtained after a suboptimal balloon angioplasty in DEBATE I, combining a higher baseline flow and lower hyperemic flow.

### 10.2.1 Induction of maximal hyperemia

Maximal coronary flow can be measured in the catheterization laboratory after transient coronary occlusion (Marcus et al. 1981a), or with pharmacologically induced hyperemia obtained with intracoronary or intravenous administration of dipyridamole (Voudris et al. 1996), papaverine (Wilson & White 1986), adenosine (Wilson et al. 1990) or adenosine 5'-triphosphate (Sonoda et al. 1998).

Kern and colleagues have shown that a continuous intravenous infusion of 140  $\mu\text{g}/\text{kg}/\text{min}$  induces maximal coronary vasodilation in the vast majority of patients (Kern et al. 1991). Development of mild hypotension, bradycardia, first- or second-degree atrioventricular block or symptoms (flushing, chest discomfort, headache, dyspnea) rarely requires discontinuation of the infusion (Abreu et al. 1991). In view of the extremely high safety profile of adenosine, this agent is the pharmacological stimulus of choice.

### 10.2.2 Methods of measuring coronary flow reserve

Pioneering invasive methods developed to measure coronary blood flow were timed venous collection from the great cardiac vein (Rayford et al. 1959) or coronary sinus thermodilution (Ganz et al. 1971b). Presently, besides established non-invasive nuclear techniques (Berman et al. 1990; Muzik et al. 1998), methods under development are based on transesophageal (Hutchison et al. 1997) or transthoracic (Hozumi et al. 1998) echocardiography, magnetic resonance imaging (Passariello & De Santis 1998) or computed beam tomography (Bell et al. 1999). However, we will focus our interest on the invasive method based on the Doppler guidewire (Flowire<sup>TM</sup>, JOMED Inc., Rancho Cordova, CA, USA), a 0.014-inch diameter, 175-cm-long, flexible and steerable device with handling characteristics similar to traditional angioplasty guidewires. It has a minimal cross-sectional area of 0.1 mm<sup>2</sup>, causing only a 9 per cent area reduction of a circular lumen of 1.2 mm diameter. An optimal and stable signal is obtained by directing the tip towards the lumen center, avoiding strong artifacts from the vessel wall. Finding of the best position can now be improved with a method based on the normalized first Doppler moment (Jenni et al. 1998a). The latest "wide-beam" model has a 12-MHz piezoelectric ultrasound transducer integrated onto the tip, and the forward-directed ultrasound beam diverges at 35 degrees. This broad beam provides a relatively large area of insonification of the flow-velocity profile. Real-time spectral analysis provides a scrolling gray scale spectral display. The frequency response of this system calculates approximately 90 spectra per second. The spectral analysis of the signal and the Doppler audio signals are videorecorded for later review. Simultaneous electrocardiogram and blood pressure are displayed with the spectral velocity. We have demonstrated the feasibility of recording the quadrature signals with an independent PC based A/D acquisition system for archiving and post-processing of such Doppler spectra and use this approach now routinely in our laboratory for combined flow/pressure recordings (Carlier et al. 1996).

The Flowire has been validated in model tubes with pulsatile blood flow and in canine circumflex coronary arteries (Doucette et al. 1992). *In vivo* studies (Ofili et al. 1992; Serruys et al. 1993) have established that the Flowire can be easily steered in the proximal and distal branches of the coronary arterial tree

and prolonged monitoring periods are possible. Safety of the instrumentation is now widely demonstrated (Kern et al. 1997a). Among all the available indices based on the velocity measurements (systolo-diastolic ratio, proximal-to-distal ratio,...) (Carlier et al. 1998c), coronary flow reserve is the only index reflecting the stenosis severity. The Doppler sample should be positioned at least 2 cm distal to the stenosis to avoid turbulences. The Doppler velocity reserve (ratio of average peak velocity (APV) during hyperemia to baseline) is used as a surrogate of the true coronary flow reserve (Fig. 10.1). *In vitro* experiments and computer simulations have indicated that because the guidewire alters the flow profile, the Doppler velocity reserve may underestimate the true flow reserve (Porenta et al. 1999). This has not been confirmed by other investigators (Jenni et al. 1998b), but all these experiments have clearly demonstrated that the velocity profile can not be assumed parabolic, so that the computation of the true coronary blood flow as the cross-sectional area at the level of the Doppler tip (measured by IVUS or QCA) times APV times 0.5 is an invalid oversimplification. Another potential error when measuring the Doppler velocity reserve is related to coronary vasodilatation occurring during hyperemia (Lupi et al. 1997). The administration of an intracoronary bolus of nitroglycerin (100-300  $\mu\text{g}$ ) or isosorbide dinitrate (1-3 mg) 2-3 min before velocity measurements assures maximally vasodilated vessel and improves measurement reproducibility (Di Mario et al. 1995; Hasdai et al. 1998). The coefficient of variation of Doppler CFR measurements is  $\sim 10\%$  (de Bruyne et al. 1996). Several technical factors may influence the measurements. A possible flow obstruction may be due to a large (8 Fr) guiding catheter engaged in the coronary ostium. This can be detected by the recording of a pressure damping and avoided by pulling back the guiding catheter. However, most of the interventions are presently performed with smaller guiding catheters (6 Fr). There is also an unpredictable amount of adenosine being lost in the aorta during intracoronary bolus injection of adenosine with guiding catheter presenting side holes, which influences the measurement of CFR (Abizaid et al. 1997). A larger dose (up to 36  $\mu\text{g}$ ) should then be used.

### 10.2.3 Perfusion imaging and post-stenotic coronary blood flow

The correlation between poststenotic coronary flow reserve and hyperemic myocardial perfusion scintigraphic imaging has been thoroughly investigated. Miller et al. (1994) compared  $^{99m}\text{Tc}$  sestamibi and poststenotic CFR in 33 patients with angiographically intermediate stenoses. QCA stenosis severity ( $> 50\%$  diameter stenosis (DS)) and CFR  $> 2.0$  were correlated in 20/27 patients. Perfusion imaging abnormalities and DS were correlated in 28/33 patients. The strongest correlation was noted between CFR and perfusion imaging in 24/27 patients. Nearly all patients with abnormal distal hyperemic flow velocity values had corresponding reversible myocardial perfusion tomographic imaging de-

fects. Similar data have been described by Joye et al. (1994) using single-photon emission-computed tomographic (SPECT) thallium imaging in 30 patients with intermediate coronary stenoses. The sensitivity, specificity, and overall predictive accuracy of a Doppler-derived CFR  $< 2$  and an abnormal stress SPECT thallium-201 were 94, 95 and 94 percent, respectively. More recently, Miller et al. have correlated in 11 patients regional myocardial blood flow measured by positron emission tomography (PET) with invasive CFR, using dipyridamole-induced hyperemia (Miller et al. 1996). There was a highly significant correlation between Doppler-derived and PET-derived myocardial perfusion reserve. There was a trend toward a correlation between Doppler-derived CFR and minimal luminal diameter (MLD), but no correlation was found between PET-derived CFR and MLD or DS. These data demonstrate that the correlation of two physiological end points of coronary blood flow more accurately reflects the functional severity of coronary stenoses than angiography alone. Physiological techniques provide thus objective evidence of lesion significance, which is useful to support the decision for coronary revascularization interventions.

#### 10.2.4 Variations in normal coronary vasodilatory reserve

Variations of CFR in multiple arteries in large numbers of patients in the cardiac catheterization laboratory has led to controversy regarding normal values. This issue is especially pertinent for assessing the significance of intermediate ( $\sim 50\%$ ) coronary stenoses in patients who may have concomitant impairment of their microcirculation. To assess the spectrum of CFR responses found in adult patients undergoing cardiac catheterization, CFR was measured in 410 coronary arteries in 214 patients comprising 3 groups: atypical chest pain syndrome and angiographically normal coronary arteries ( $n=85$ ); coronary artery disease and angiographically normal vessels ( $n=21$ ); and angiographically normal transplant recipients ( $n=108$ ) (Kern et al. 1996). CFR, on average, in normal patients with chest pain syndromes was approximately  $2.9 \pm 0.6$ , and similar in the angiographically normal artery in patients with coronary artery disease ( $2.5 \pm 0.95$ ), both values were higher than in the post-stenotic diseased vessel CFR ( $1.8 \pm 0.6$ ). Transplant arteries had the highest CFR ( $3.1 \pm 0.9$ ). Among different normal arteries, there was no difference in CFR for circumflex, right, or left coronary arteries. Regional differences were not present suggesting that relative CFR should be  $1.0 \pm 0.2$ .

Erbel et al. (1996) have reported CFR values in angiographically normal coronary arteries in which IVUS was performed to further classify patients with early atherosclerosis. Of 44 patients, 16 (group 1) had a normal coronary morphology by IVUS, and a CFR  $> 3.0$  (mean= $5.3 \pm 1.8$ ), and 7 (group 2) had a normal IVUS appearance but a reduced CFR ( $2.1 \pm 0.4$ ). Plaque formation was found in a total of 21 patients. Mean plaque sizes were  $3.6 \pm 1.6 \text{ mm}^2$  for the patients with

a  $CFR > 3$  (group 3), and  $5.0 \pm 2.3 \text{ mm}^2$  in those having a reduced CFR (group 4). The authors concluded that only 36% of the patients with normal angiograms were true normal, that 48% exhibited early stage of coronary atherosclerosis, and that the patients in group 2 might be considered as syndrome X. These data were in agreement with earlier reports of abnormal CFR in patients with angina but normal coronary angiography (Cannon et al. 1987; Holdright et al. 1993; Chauhan et al. 1994). Baumgart has recently extensively reviewed the different studies reported over "normal" CFR values and has stressed the confounding factors related to the different techniques, unstandardized procedures and uncomparable populations (Baumgart et al. 1998b).

### 10.2.5 Relative coronary flow reserve

Absolute CFR is the summed response of the conduit and microcirculatory response. Relative CFR ( $CFR_{\text{target}}/CFR_{\text{reference}}$  - RCFR) in patients with coronary artery disease should exclude the differences attributable to microvascular disease and different hemodynamic states for serial studies. Baumgart et al. (1998a) compared  $FFR_{\text{myo}}$ , RCFR and QCA measurements in 21 patients. Reference diameter was  $3.0 \pm 0.4 \text{ mm}$ , and area stenosis was  $74 \pm 15\%$ . CFR in the target and reference vessels were  $2.1 \pm 0.5$  and  $2.6 \pm 0.7$ , respectively. FFR ranged from 0.49 to 0.99 and RCFR from 0.53 to 1.0. Poststenotic CFR did not correlate with either percent area stenosis or FFR. In contrast, FFR as well as RCFR showed a curvilinear relation to percent area stenosis ( $R = 0.89$ ,  $P = 0.0001$  and  $R = 0.79$ ,  $P = 0.0001$ , respectively). There was a close linear correlation between FFR and RCFR ( $R = 0.91$ ,  $P = 0.0001$ ). Uren et al. (1997) have reported similar data obtained in an experimental canine model. These data indicate that RCFR has an excellent correlation with  $FFR_{\text{myo}}$  and that absolute CFR had a poor correlation due to the unexpected and unpredictable abnormalities of microcirculation. The RCFR seems to be more appropriate to assess lesion specificity than absolute CFR. However, these multiple measurements are cumbersome and require a normal reference vessel. The use of the  $FFR_{\text{myo}}$  is an easier method to determine the individual significance of a stenosis.

## 10.3 The fractional coronary flow reserve

From translesional pressure measurements made with a guidewire transducer during maximal hyperemia, Pijls et al. have developed a new concept for the determination of coronary blood flow: the fractional flow reserve of the myocardium ( $FFR_{\text{myo}}$ ) (Pijls et al. 1993). When blood flows from the proximal to the distal part of the normal epicardial coronary artery, virtually no energy is lost and, therefore, the pressure remains constant throughout the conduit. In the case of epicardial coronary narrowing, potential energy is transformed in kinetic energy

and in heat when blood traverses the lesion. The resultant pressure drop reflects the total loss of energy. In order to maintain resting myocardial perfusion at a constant level, a decrease in arteriolar resistance compensate for any resistance of flow due to the epicardial narrowing. The maximal myocardial blood flow in the presence of a stenosis is reduced relative to expected normal flow in the absence of a stenosis and can be expressed as a percentage of its expected value, if there was no lesion. This percentage is the myocardial fractional flow reserve ( $FFR_{myo}$ ). It can be derived from pressure data alone considering several assumptions regarding translesional pressure measured during maximal hyperemia (Pijls et al. 1995). The proposed equations have been derived from a theoretical model of the coronary circulation, and have been validated experimentally in instrumented dogs and recently *in vitro* (Segers et al. 1997). In humans,  $FFR_{myo}$  has been compared to relative flow reserve measured by PET (de Bruyne et al. 1994). With the mean venous pressure assumed low and constant,  $FFR_{myo}$  can be estimated as the ratio between the mean distal coronary blood pressure (measured with a pressure guide wire) to the mean aortic blood pressure (measured by the guiding catheter). For a normal vessel,  $FFR_{myo}$  is unequivocally equal to 100%. Since each myocardial territory serves as its own control, it is a lesion-specific index independent of the microcirculation, heart rate, blood pressure, and other hemodynamic variables and it can be applied in multivessel disease. QCA and  $FFR_{myo}$  data obtained before and after an angioplasty procedure have been compared in 105 patients (Bartunek et al. 1995). A curvilinear relation was found between DS and MLD and  $FFR_{myo}$ . A linear equation was also found between the angiographic stenosis flow reserve and  $FFR_{myo}$ . There was a rather large dispersion of the data, nevertheless, the diagnostic accuracy of a MLD < 1.5 mm and a DS > 50% in detecting lesions associated with a  $FFR_{myo}$  < 0.72 were 92% and 89% respectively.

### 10.3.1 Clinical significance of pressure gradients

The risks of abrupt closure and restenosis were rapidly associated with high residual pressure gradients after angioplasty (Anderson et al. 1986; Hodgson et al. 1986). However, several limitations exist when using the resting pressure gradient only to predict ischemia (Serruys et al. 1985). The threshold of  $FFR_{myo}$  of 0.75 below which inducible ischemia is present has been extensively assessed (Pijls et al. 1995; de Bruyne et al. 1995). In 45 patients with moderate coronary stenoses and chest pain syndromes (Pijls et al. 1996), when  $FFR_{myo}$  was lower than 0.75 (21 patients), reversible myocardial ischemia was demonstrated unequivocally on at least one non invasive test (bicycle exercise testing, thallium scintigraphy, stress echocardiography with dobutamine) and all these positive test results were reverted after PTCA or CABG. In 21 of 24 patients with a  $FFR_{myo}$  greater than 0.75, all test were negative, with no demonstration of is-

chemia, and no revascularization procedure was performed. None were required after 14 months of follow-up. The sensitivity of  $FFR_{myo}$  in the identification of reversible ischemia was 88%, the specificity 100%, the positive predictive value 100%, the negative predicted value 88% and the accuracy 93%.  $FFR_{myo}$  has also been compared to dobutamine echocardiography in 75 patients with normal left ventricular function and single vessel coronary artery disease (Bartunek et al. 1996): the degree of dobutamine-induced dyssynergy correlated significantly with the quantitative coronary data but the correlation was markedly better with myocardial fractional flow reserve. All but one patient with a  $FFR_{myo} > 0.75$  had a normal stress test result. De Bruyne et al. have demonstrated that in humans  $FFR_{myo}$  is independent of hemodynamic conditions: changes in heart rate by pacing, in contractility by dobutamine infusion, in blood pressure by nitroprusside infusion did not alter  $FFR_{myo}$  (de Bruyne et al. 1996). The coefficient of variability between two consecutive measurements was 4.2%. The DEFER study has recently investigated the outcome of 303 patients admitted for PTCA of one stenosis without previously documented ischemia.  $FFR_{myo}$  was measured prior to the intervention, and when it was  $< 0.75$ , the intervention was performed ( $n=140$ ). The patients with a  $FFR_{myo} \geq 0.75$  ( $n=163$ ) were randomly assigned to PTCA or deferral of angioplasty. The event-free survival at 1-year was 67%, 81% and 81%, respectively, demonstrating that for the patients without inducible ischemia, performance, as compared to deferral of PTCA did not improve event-free survival (Bech et al. 1999a).

### 10.3.2 Limitations of $FFR_{myo}$

After myocardial infarction or in the presence of left ventricular hypertrophy, the threshold for inducible ischemia of 0.75 may not hold true. Exercise induced spasms or to some degree, microvascular disease, where the maximal epicardial flow may be limited, are other potential problems for the assessment of  $FFR_{myo}$  (Pijls & de Bruyne 1998). When multiple stenoses on the epicardial segment investigated are present, another formulation of  $FFR_{myo}$  is required, to measure the respective contribution of each stenosis [De Bruyne, personal communication]. Finally, the assumption of a linear relationship between the pressure gradient and flow is a simplification of a complex fluid dynamic process (de Jong et al. 1986).

## 10.4 Optimization of a percutaneous intervention

### *QCA, IVUS or functional assessment?*

In the PICTURE study (Peters et al. 1997) no IVUS criteria has been found significantly correlated to the restenosis rate ( $DS > 50\%$ ) among 200 patients after PTCA. On the other hand, Mintz et al. found that the residual plaque burden

measured with IVUS was an independent predictor of restenosis (Mintz et al. 1996). The GUIDE trial has also showed the predictive value of IVUS plaque area and minimal lumen cross-section (The GUIDE Trial Investigators 1996). It has been demonstrated that based on IVUS, it was safe to increase the nominal balloon-to-artery ratio (Stone et al. 1997), and a low rate (12%) of clinical events at one year has been reported in a mono-center, non-randomized study of 144 patients where the balloon sizes were based on the external elastic membrane diameters (Haase et al. 1998). For stenting, a very recent pooled analysis of trials (n=800 patients) has demonstrated that the IVUS criteria minimum lumen cross sectional area (CSA), mean in-stent lumen area, stent length and lumen diameter were predictors of 6 month in-stent restenosis (de Feyter et al. 1999), in agreement with other reports which demonstrated also the predictive value of an ostial lesion location, the preinterventional and residual lesion site plaque burden (Hoffman et al. 1998; Kasaoka et al. 1998; Prati et al. 1999; Hong et al. 1999). However, it remains controversial that IVUS guidance may decrease in-stent restenosis and improve the event-free survival after an intervention (Moussa et al. 1999).

In a study matching patients between two centers, one performing IVUS guidance, and the other one using only angiography, there was only a significant decrease of the restenosis rate (9.2% vs. 22.3%) in an early phase where the IVUS criteria implied aggressive dilatation using oversized balloons (Albiero et al. 1997), which lead to a high incidence of vessel ruptures. When IVUS criteria were modified, no more difference in the outcome of the patients was found. IVUS guidance improved in-stent CSA at the end of the intervention in the MUSIC trial, and comparison of angiographic data with earlier studies demonstrated that the improvement of the MLD (2.9 mm vs. 2.5 mm) was associated with a lower restenosis rate (9.7% vs. 20%, respectively for the MUSIC and Benestent I trials) (de Jaegere et al. 1998; Serruys & Deshpande 1998a). When the IVUS criteria for optimal stent expansion are met, the restenosis rate is lower (Blasini et al. 1998). However, these criteria cannot be met in all the patients, and the results of two randomized trials (RESIST and OPTICUS) comparing IVUS versus angiographic guidance today show no difference in clinical and angiographic outcome at 6-month follow-up (Schiele et al. 1998; Mudra et al. 1998). On the other hand, it has been demonstrated that the rate of target vessel revascularization in the randomized CRUISE trial was reduced from 15.3% to 8.5% ( $P < 0.05$ ) in the arm with IVUS-guided stent implantation.

Additional results from ongoing studies are pending and should clarify the remaining question: does IVUS guidance for stent deployment improve the clinical outcome? However, these studies compare quantitative IVUS with visual assessment of the angiographic results. There is no large study that has compared QCA versus IVUS guidance. Recently, Hannekamp et al. have investigated stent implantation in 30 patients, using a stepping pressure inflation protocol (8 to



14 atm). During the step-up procedure, a total of 81 paired IVUS and coronary pressure measurements were performed, of which 91% yielded concordant results. On the contrary, QCA showed a low concordance rate with IVUS and  $FFR_{myo}$  (48% and 46%, respectively). The following criteria were used: for IVUS: (1) complete apposition of all stent struts against the vessel wall, (2) symmetry index of  $> 0.7$ , and (3) in-stent minimal CSA  $> 90\%$  of the average reference CSA or  $> 100\%$  of the smallest reference segment CSA (Di Mario et al. 1998); for QCA: on the average of 2 orthogonal views, residual DS  $< 10\%$ ; for  $FFR_{myo}$ :  $> 0.94$ .

Investigating the predictive value of  $FFR_{myo}$  after PTCA, Bech et al. (1999b) have reported in 60 consecutive patients with single-vessel disease that a successful angioplasty result, defined as a residual DS  $< 50\%$ , was achieved in 58 patients. In these patients, DS and  $FFR_{myo}$ , measured 15 minutes after PTCA, were analyzed in relation to clinical outcome. In those 26 patients with both optimal angiographic (residual DS  $\leq 35\%$ ) and functional ( $FFR \geq 0.90$ ) results, event-free survival rates at 12 and 24 months were  $92 \pm 5\%$  and  $88 \pm 6\%$ , respectively, versus  $69 \pm 8\%$  and  $59 \pm 9\%$ , respectively, in the remaining 32 patients in whom the angiographic or functional result or both were suboptimal ( $P = 0.028$  and  $P = 0.014$ , respectively). Therefore, there is a complementary value of coronary angiography and coronary pressure measurement in the evaluation of PTCA result.

The concordance between morphological parameters and intracoronary flow velocity reserve has also been largely investigated, and the more controversial data might reflect the limitations of CFR to differentiate between the true effect of an epicardial stenosis and an alteration of the microvascular bed. Moses et al., studying 41 patients pre-intervention, showed that single cross-sectional anatomic measurements, either by QCA or by IVUS, have only a weak relation to CFR (Moses et al. 1998). On the contrary, in Washington, the evaluation of 86 consecutive patients before and/or after intervention showed a linear relation between CFR and (1) IVUS minimum lumen CSA ( $R = 0.771$ ,  $P < 0.0001$  for the 112 available measurements); (2) QCA DS ( $R = 0.47$ ,  $P < 0.0001$ ); (3) QCA MLD ( $R = 0.57$ ,  $P < 0.0001$ ). When only the preintervention data were analyzed, results were slightly improved. Overall, an IVUS minimum lumen CSA  $\geq 4.0 \text{ mm}^2$  had a diagnostic accuracy of 89% in identifying a CFR  $\geq 2.0$ . This diagnostic accuracy increased also slightly to 92% when only the preintervention observations were considered. Using multivariate linear regression analysis, the independent determinants of the CFR were IVUS minimum lumen CSA, QCA lesion length and diabetes mellitus.

The DEBATE I trial (Serruys et al. 1997) demonstrated in 225 patients with an angiographically successful PTCA, that the postprocedural distal CFR and QCA DS were correlated with symptoms and/or ischemia, with the need for target lesion revascularization and with angiographic restenosis. A DS  $\leq 35\%$  and a CFR  $> 2.5$  were found the best criteria for the prediction of these clinical events

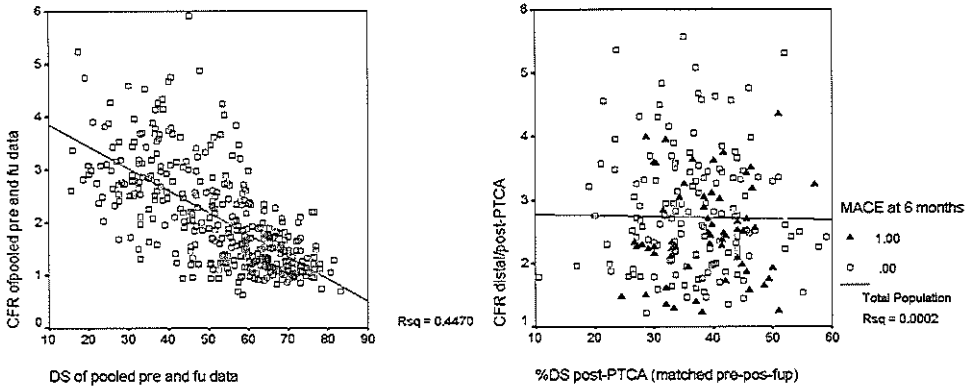


**Figure 10.2:** Left panel: pooling the measurements pre-intervention and at 6-month follow up of the 225 patients of DEBATE I, a correlation was found between a morphological assessment of the stenosis (diameter stenosis DS by quantitative angiography) and the coronary flow reserve (CFR) ( $R^2=0.447$ ). On the contrary, the right panel demonstrates that there was no correlation between DS and CFR measured after the angioplasty. The patients who presented a major cardiac adverse event (MACE) are plotted with ( $\blacktriangle$ ), those free of event with ( $\square$ ). The lowest incidence of MACE was found when  $DS \leq 35\%$  and  $CFR > 2.5$ .

at 6 month. A distal CFR after angioplasty  $> 2.5$  associated to a residual  $DS \leq 35\%$  identified lesions with a low incidence of recurrence of symptoms (23% versus 47%,  $P = 0.005$ ), a low need for reintervention (16% versus 34%,  $P = 0.024$ ), and a low restenosis rate (16% versus 41%,  $P = 0.002$ ), compared with patients who did not meet these criteria. The predictive value of DS and CFR was nevertheless modest. This may be partially explained by the complex mechanism occurring after PTCA, and the inherent inability to assess microvascular dysfunction with only CFR measurements. This is reflected in the results of an in-depth analysis we recently performed of the velocity profile observed in this cohort (Albertal et al. 2002): it appears that the patients unable to achieve an optimal  $CFR > 2.5$  after angioplasty had similar QCA results (MLD  $1.76 \pm 0.40$  vs.  $1.80 \pm 0.37$  mm, NS), but a higher baseline APV ( $22 \pm 9$  vs.  $15 \pm 5$  cm/s,  $P < 0.05$ ) associated to a lower APV in hyperemia ( $43 \pm 16$  vs.  $50 \pm 17$  cm/s,  $P < 0.05$ ). At 6-month follow-up, baseline APV tended to decrease in the suboptimal group but still remained slightly higher than in the group with optimal CFR post-angioplasty ( $19.9 \pm 11$  vs.  $16 \pm 7$  cm/s,  $P < 0.05$ ). However, hyperemic APV were then comparable ( $42 \pm 20$  vs.  $45 \pm 18$ , NS). This confirms an observation on a smaller group of patients reported by van Liebergen et al. (1998) and shows probably the influence of a slow recovery of autoregulation of the microvascular bed. Figure 10.2 shows for these patients that CFR and DS by QCA were well correlated when analyzing stabilized conditions in this population (pre-intervention and 6-month follow-up data pooled,  $R^2=0.447$ , left panel), but not after the intervention (right panel).

This poor correlation has also been reported by Kern et al. who could further demonstrate the beneficial effect of stenting, associated to an increase in lumen dimension: in 42 patients, DS by QCA decreased from  $84\pm 13\%$  to  $37\pm 18\%$  after angioplasty and to  $8\pm 8\%$  after stenting (both  $P < 0.05$ ). CFR was minimally changed from  $1.70\pm 0.79$  at baseline to  $1.89\pm 0.56$  ( $P = \text{NS}$ ) after angioplasty, but increased to  $2.49\pm 0.68$  after stent placement ( $P < 0.01$  vs. before and after angioplasty) (Kern et al. 1997b). Following DEBATE I, 3 independent studies have randomized patients to elective stenting or to a strategy of balloon angioplasty and provisional stenting when QCA and CFR measurements were suboptimal. Preliminary data presented (de Bruyne et al. 1998; Di Mario & al. 1999; Lafont & al. 1999), but not yet published, demonstrate that when optimal angiographic and physiologic end-points are met after PTCA, clinical outcome is equivalent to the outcome observed after elective stent implantation: the 1 year event-free survival in DEBATE II is 85.6% vs. 86.6% (respectively for provisional stenting and elective stenting) (Serruys et al. 2000). It is at 6-month 84.4% vs. 82.8% in DESTINI, and 84.1% vs. 83.4% in FROST. The limitation of a provisional stenting strategy is that only a minority ( $\sim 40\%$ ) of patients could achieve the pre-determined end-points of optimal PTCA results. Furthermore, the specific second randomization protocol of DEBATE II could demonstrate that additional stenting for patient with optimal PTCA decreases the incidence of major adverse cardiac events (15.9% to 6.5%,  $P = 0.066$ ).

## 10.5 Future directions

A new intracoronary volumetric blood flow measurement method with IVUS has recently been developed in our laboratory, based on a decorrelation analysis of IVUS radiofrequency signals (Li et al. 1998b). Over the cross-sectional arterial lumen area, blood velocity is estimated in small ( $\sim 200 \mu\text{m}$ ) consecutive range windows and superimposed on the conventional IVUS image, using a color scale. Flow is obtained by spatiotemporal integration. With intravenous administration of adenosine, it is possible to derive CFR measurements (Fig. 10.3). This method has been initially evaluated with a mechanical transducer (30 MHz Princeps<sup>TM</sup>, JOMED/Du-Med), and good correlations between Doppler-derived and IVUS-derived flow and CFR were found in a carotid porcine model (Céspedes et al. 1998a) and in patients (Carlier et al. 1998b, 1998d).

Presently, this method is under implementation with a solid-state array transducer (20 MHz Vision 64F/X<sup>TM</sup>, JOMED Inc.). The recent availability of a combined device (JoSonics<sup>TM</sup>, JOMED A.B., Helsingborg) of a stent delivery system with an IVUS transducer mounted proximally to the balloon offer an ideal combination of immediate morphological assessment of the optimal stent implantation,

together with the possibility to assess physiological parameters such as the CFR. Further studies are required to investigate the merit of this approach, as well as the limitation related *e.g.* to the presence of a rather large device (3.5 Fr) in the arterial lumen in which the CFR is measured.

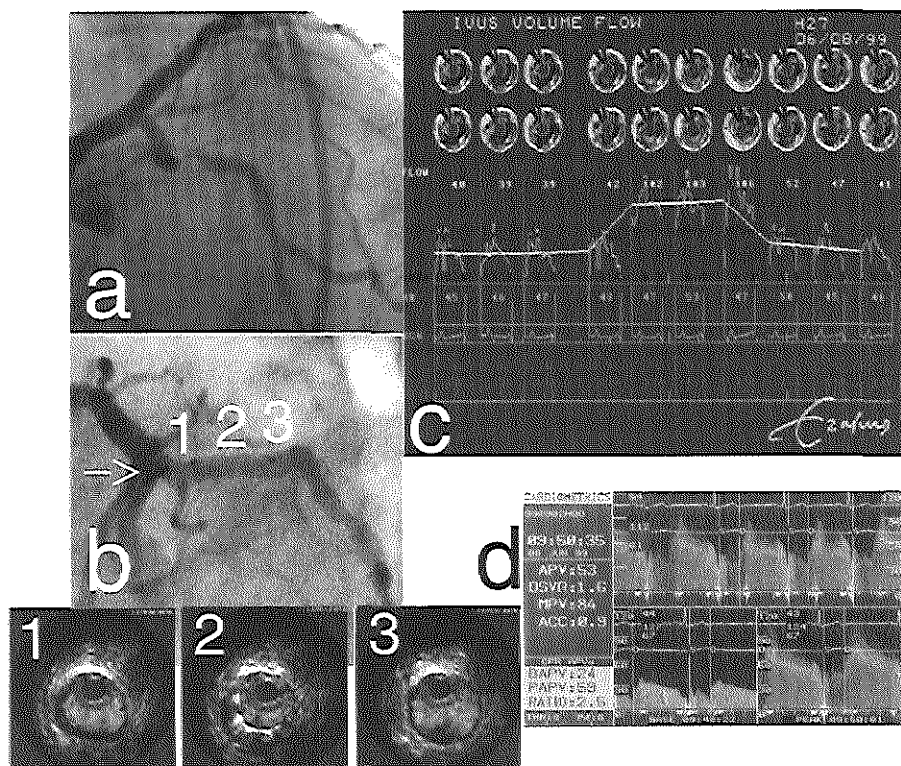


**Figure 10.3:** Panel a: Severe lesion in a circumflex artery which could be directly stented (panel b) with the JoSonics device, combining a stent delivery system (between 2 distal markers) and a phased-array IVUS transducer (arrow). Immediate morphological assessment of the implementation is possible, by advancing this combined catheter distally. IVUS images show (1) the proximal reference segment, (2) sub-optimal stent implantation and (3) distal reference segment. Lumen is colored by the qualitative Chromaflow<sup>TM</sup> algorithm, which detects flowing blood. Quantitative flow assessment by processing the Radio Frequency (RF) IVUS signal is demonstrated on panel c. For each short RF IVUS sequence recorded (one heart beat), velocities are superimposed on the lumen (upper part), and the mean flow is indicated and plotted below (yellow line). Storage time permits only the acquisition of one heart beat every 12 seconds. Mean baseline flow was 40 cc/min (*with this new catheter, presently, the calibration of these absolute flow values is still under investigation*). Successive columns ( $\sim 12$  seconds apart) show the increase of flow during an intravenous infusion of adenosine (140  $\mu\text{g}/\text{kg}/\text{min}$ ). Peak flow reached 103 cc/min, which correspond to a CFR of 2.6. The CFR measured with a Doppler Flowire (panels d) was 2.5.

## 10.6 Conclusions

With the development of miniaturized coronary Doppler and pressure probes and of new approaches to the interpretation of intracoronary hemodynamic measurements, a complex technique, reserved to a few research laboratories in the past, has been transformed into a reliable diagnostic tool that can be used for the physiological assessment of stenoses severity and for the evaluation of the results of coronary interventions. Combined flow and imaging ultrasound can be applied for measurement of absolute coronary flow as well as for the simultaneous study of morphological and functional characteristics of the coronary system. Presently, with the refinements of pressure and Doppler guide wire technology, the superiority of one technique is not established, because pressure and flow represent the two sides of the same complex interaction between fluid dynamic and physiological regulation. Ambiguous values obtained with one technique can be reduced or eliminated using the corresponding alternative method. In the 25% of the current angioplasty population with stable chest pain syndromes in whom evidence of ischemia is lacking, using coronary physiology, one might modify a widely practiced dictum, "When in doubt, dilate" to "When in doubt, measure and decide" (Kern et al. 1997a).



# Chapter 11

## Discussion and Conclusions

### 11.1 Discussion

Recent research resulted in the capability to measure of transverse blood velocity and the quantification of arterial volume blood flow using a correlation-based method with a rotating single-element intravascular catheter (Li et al. 1997, 1998b). Transverse blood flow velocity and quantitative volume blood flow can be measured using a time domain correlation-based method in a burst of ultrasound beams transmitted in the same direction at a short time interval. The use of mechanically rotated transducer to measure flow requires compensation for the intrinsic decorrelation due to rotation. This could be cumbersome if the rotation is not uniform. Intravascular Ultrasound (IVUS) array catheters are not hampered by rotational problems. The array transducer is capable of transmitting and receiving many echoes at a fixed angle. The array is scanned electronically (Eberle 1997). In the present study, the correlation-based method has been developed for the IVUS array catheter. Fundamental decorrelation properties have been studied using computer modeling and *in vitro* experiments. Methods have been validated using *in vitro* and animal models, and patient recordings.

### 11.2 Computer simulations

As a first step of the present study, the characteristics of the ultrasound beam from the IVUS array catheter for measuring transverse blood velocity and quantitative blood flow were investigated by means of computer simulations. First, the decorrelation patterns for a scattering medium formed by single red blood cells (RBCs) and aggregates of RBCs were studied and compared with the auto-convolution of the acoustical beam. The auto-convolution of the acoustical beam was used as a reference curve. The RF decorrelation patterns were in agreement with the reference curve when the scattering medium was formed by single RBCs.

When aggregates of RBCs were aligned with the flow, the decorrelation pattern showed to be influenced by the length of the aggregates. The longer the aggregates of RBCs the lower the rate of decorrelation. However, the decorrelation curves for aggregates of random lengths and organization were very close to those from single RBCs.

Secondly, the influence on the correlation-based method by blood velocity profiles such as random spread of flow, linear velocity gradients and parabolic flow was studied. This study was performed for the Radio Frequency (RF) and envelope signals and for transverse and axial flow. For the RF and envelope signals, transverse blood flow is not significantly influenced by random spread of flow velocity, linear velocity gradient or parabolic flow. A similar result can be seen for axial flow and for the RF signals when random spread flow was considered. However, the envelope mean decorrelation pattern for axial spread of blood velocity was faster than the one for axial plug flow.

The correlation-based method is highly influenced by the presence of noise in the RF signals. Correction for noise is crucial for measuring intravascular transverse blood flow; if no correction for noise is applied, an overestimation of the blood velocity will occur. The noise within the RF signals is system-dependent and is band-limited, which has an impact on the shape of the correlation function especially the correlation coefficients at lag 0 (Ledoux et al. 1998). The method for noise correction presented in this study is easy to implement and not computational time consuming. The method uses the fact that the correlation pattern should be 1 at lag 0; however, this does not occur when noise is present in the RF signals. The correlation coefficients at lag 0 is estimated by curve fitting to measure the shift in the correlation pattern. Adding 1 minus the intercept value at lag 0 to each correlation value corrects the correlation pattern for noise. The set of RF signals were windowed and since the decorrelation due to noise was estimated and corrected per window, the noise correction method is dynamic and not dependent on previous measurements.

### 11.3 *In vitro* experiments

As previously described during the present study, the correlation-based method needs a calibration file in order to convert the correlation coefficients as a function of time into blood velocity (*e.g.* cm/sec). Since close agreements were found between the auto-convolution of the acoustical beam and decorrelation patterns for single RBCs and aggregates of RBCs at random angles and lengths, the auto-convolution of the acoustical beam was used as a calibration of the method during the present study. Therefore, measurements of the ultrasound beam from several IVUS array catheters were performed to produce the calibration file for the correlation-based method.



IVUS blood flow measurements were performed using a flow setup in a controlled environment and a calibrated Electromagnetic Flowmeter (EMF) as a reference. Human blood and a tissue mimicking flow phantom were used during the experiments. Good linear relationships were found between IVUS flow measurements and those from the EMF with high correlation ( $R^2 > 0.96$ ). The slopes were close to 1 and offsets lower than 3 cc/min were measured.

Using a Couette system and whole human blood, the effect of linear blood velocity gradient and aggregation of RBCs on the correlation-based method was studied. Blood from healthy and patient volunteers was used in the present study. Changing the shear rate of the Couette system modified the level of aggregation of RBCs. The experiments revealed that linear velocity gradients will not influence the velocity estimation using the correlation-based method even when a large window is used for the calculations. In this case, a large spread of velocities is included. However, most of velocity estimators use a window length close to the wavelength of the used ultrasound transducer. Aggregation of RBCs showed no effect on the decorrelation patterns, except at very low shear rates and for high aggregating blood (*i.e.* large aggregates of RBCs). Overall, for the high shear rate present in coronary arteries, the correlation-based method for blood flow estimation should not be influenced by these phenomena when a small window length is used for the evaluations. This experiments also confirmed previous simulation on aggregation of RBCs.

## 11.4 In animal experiments

IVUS quantitative blood flow measurements were performed in Yorkshire pigs. A shunt was made from the carotid to the jugular on the right side of the pigs, where the Electromagnetic Flowmeter was connected in line with the shunt. Good linear relationships ( $R^2 > 0.85$ ) were found between IVUS flow measurements and those from the calibrated EMF; slopes close to 1 were found. These experiments showed the correlation-based method capable to measure quantitative volume blood flow *in vivo*, which means blood flow measurements performed in an artery, under pulsatile flow, and the inevitable motion of the catheter due to breathing and heart beating. Although individual flow measurements have a large spread, mean IVUS flow per cardiac cycle showed a linear relationship (slope close to 1) and high correlation with the flow measurements from the EMF.

## 11.5 In patient recordings

The technique was advanced to coronary applications in patients. Absolute coronary blood flow is the optimal parameter for intracoronary physiological studies. However, intracoronary flow measurements have been simplified for clinical prac-

tice. The most useful index at the end of an intervention such as a stent implantation is the coronary flow reserve estimated from the ratio of the maximum flow velocity measured with a Doppler Flowire<sup>TM</sup> during hyperemia to the baseline velocity (Serruys et al. 2000; Di Mario et al. 2000). Results for CFR in patients based on IVUS blood flow compared to the CFR based on Doppler blood velocity were presented in close agreement; the hyperemia cycle can be followed by both methods. However, one should realize that IVUS blood flow measurements were acquired every 30 sec, which could lead to miss the peak of the hyperemia cycle and thus produce the underestimation.

## 11.6 Limitations and Future directions

This study revealed some limitations of the correlation-based method to assess transverse blood velocity and volume blood flow. Aggregation of RBCs under very low shear rates ( $< 20 \text{ s}^{-1}$ ) showed to have an influence on the correlation-based method producing an underestimation of the flow. Motion of the catheter in and out of plane produces erroneous measurements since the correlation-based method is not capable of detecting the direction of blood velocity across the ultrasound beam. Then, transverse forward and backward blood flow will be considered as blood flow, which may produce an overestimation of the flow in the presence of back flow. Although ring-down obscuring can be considered as a limiting factor for quantitative blood flow, the technique introduced in the present study proved to estimate the blood flow in the ring-down well. The presence of the IVUS catheter might act as a significant stenosis and produces large axial pressure drops. Consequently, hyperemic flow conditions might be not presented correctly despite accurate measurements of flow (Krams et al. 1999).

Finite element modeling can be implemented in order to assess how the blood flow profile develops in a realistic situation when the IVUS catheter is present in the lumen vessel. The essential boundary conditions needed for such a study can be provided by our method since only quantitative blood flow and flow profile at the entrance is needed. Previous studies showed the IVUS catheter to help on reducing the secondary flow -flow around the IVUS catheter- when a straight and curve tube was considered and the IVUS catheter was located at the inner, outer and top curve of the tube (Krams et al. 1999). However, in most of the cases, the IVUS catheter goes from an inner position to an outer position along the curvature of the vessel. Therefore, the blood flow profile will change along the curvature producing different wall shear stress and changes in the secondary flow pattern at each position within the vessel. Since secondary flow cannot be discriminated from primary flow by the correlation-based technique, it can be considered as a limitation of the method. Furthermore, pulsatile flow produces

movement of the IVUS catheter within the vessel producing extra changes in the flow profile.

Quantitative IVUS blood flow is currently an off-line technique as implemented in software; the computer program is capable to produce frames with blood flow information at a rate of about 2 frames per second when the frame rate of the used IVUS echo system is 11 frames per second. However, with the advances in technology, hardware implementation could improve the speed of processing and real-time IVUS blood flow measurements could be achievable. Once the technique is implemented for real-time calculations, a robust method for lumen contour detection can also be based on this technique.

## 11.7 Conclusions

Quantitative IVUS blood flow is a recently introduced technique capable of measuring quantitative volume blood flow from cross-sectional images of a vessel under different flow conditions. The technique was validated during *in vitro*, in animal and in patient recordings. Aggregation of RBCs and different blood velocity profiles showed to have no impact on the volume blood flow measurements under most conditions. Although there is a combined deleterious effect from the ring-down and noise present in the RF signals, the technique showed to be capable to measure absolute quantitative blood flow *in vitro* and in animal recordings. Absolute IVUS blood flow measurement is now possible for intracoronary physiological studies in patients. However, intracoronary flow measurements have been simplified for clinical practice; coronary flow reserve is a useful index at the end of an intervention such as a stent implantation. Further research on signal processing -to speed up computer signal processing- and validation are needed to improve the technique for in patient recordings.



# Appendix A

## Derivation of the Reference Curves

This appendix describes the method to obtain the  $A$  (Amplitude) and the  $E$  (Energy) reference curves. The scattering target, a point scatterer for the 1-D reference curves and a line of point scatterers for the 2-D reference curves, crossed transversally the acoustical beam centered with respect to the origin of the coordinate system (Fig. 3.1). For the 1-D curves, the  $y$ -coordinates were set to zero and thus the point scatterer crossed through the center of the acoustical beam. For the 2-D curves, the  $y$ -coordinates for the point scatterers were determined using the -20 dB beam-width (Wendling et al. 1992). These reference curves were obtained for the near field and for the far field, separately; the  $z$ -coordinate of the scattering target was set to 1 mm for the near field and 3 mm for the far field.

For the 1-D reference curves, the backscattered RF signals  $e_d(P_1, n)$  were auto-convolved over the displacements  $d$  at each sample time  $n$ :

$$e_u(P_1, n) = e_d(P_1, n) \otimes e_d(P_1, n) \text{ for } n = 0, 1, 2 \dots N, \quad (\text{A.1})$$

where  $d=0, 1, \dots, D$  and  $u=0, 1, \dots, (2D-1)$ . The symbol " $\otimes$ " means convolution process. Next, the signals  $e_u(P_1, n)$  were summed in time and normalized by the maximum value to obtain the  $A_{1D}$  reference curve as follows:

$$A_u = \sum_{n=1}^N e_u(P_1, n), \quad (\text{A.2})$$

$$A_{1D} = \frac{A_u}{\max(A_u)}. \quad (\text{A.3})$$

The point scatterer coordinates  $P_1$  was removed from the  $A_u$  to present the result as the reference curve  $A_{1D}$ ; this will apply for all the reference curves.

For the  $E_{1D}$ , the energy from the backscattered RF signal at each displacement was calculated as follows:

$$E_d(P_1) = \sum_{n=1}^N (e_d(P_1, n))^2, \quad (\text{A.4})$$

when  $d=0, 1, \dots, D$ . Next, the squared root of the energy curve was auto-convolved and then normalized to obtain the  $E_{1D}$  reference curve:

$$E_u = \left( \sqrt{E_d(P_1)} \otimes \sqrt{E_d(P_1)} \right), \quad (\text{A.5})$$

$$E_{1D} = \frac{E_u}{\max(E_u)}. \quad (\text{A.6})$$

The 2-D reference curves were obtained in similar way to the first ones, however, the backscattered RF signals came from a line of point scatterers. Thus, the function for the point scatterers coordinates was considered and  $K_{line}$  was the number of point scatterers which was determined using the -20 dB beam-width criterion. So, the total number of RF signals depended on  $K_{line}$  and on the displacements  $D$ . The distance between the point scatterers forming the line was half a wavelength ( $\lambda/2$ ). Thus the backscattered RF signals  $e_d(P_k, n)$  were auto-convolved over the displacements  $d$  at each sample time  $n$ :

$$e_u(P_k, n) = e_d(P_k, n) \otimes e_d(P_k, n) \text{ for } n = 0, 1, 2 \dots N, \quad (\text{A.7})$$

where  $k=1, 2 \dots K_{line}$ ,  $d=0, 1, \dots, D$  and  $u=0, 1 \dots (2D-1)$ . Next, the signals  $e_u(P_k, n)$  were summed respect to the number of point scatterers and then respect to the time  $n$ :

$$A_u = \sum_{n=1}^N \sum_{k=1}^{K_{line}} e_u(P_k, n), \quad (\text{A.8})$$

and normalized to obtain the  $A_{2D}$  reference curve:

$$A_{2D} = \frac{A_u}{\max(A_u)}. \quad (\text{A.9})$$

For the  $E_{2D}$  reference curve, a line of  $K_{line}$  point scatterers was used and the energy values for the point scatterers were:

$$E_d(P_k) = \sum_{n=1}^N (e_d(P_k, n))^2, \quad (\text{A.10})$$

for  $k=1,2\dots K_{line}$  when  $d=0,1,\dots D$ .

After this, the squared root of  $E_d$  was auto-convolved respect to number of displacements  $d$ :

$$E_u(P_k) = \sqrt{E_d(P_k)} \otimes \sqrt{E_d(P_k)}, \quad (\text{A.11})$$

when  $k=1,2\dots K_{line}$  and  $u=0,1\dots(2D-1)$ . Next, these values from  $E_u$  were summed respect to the number of point scatterer  $k$  and then normalized by the maximum value:

$$E_u = \sum_{k=1}^{K_{line}} E_u(P_k), \quad (\text{A.12})$$

$$E_{2D} = \frac{E_u}{\max(E_u)}. \quad (\text{A.13})$$

The *Envelope*<sub>2D</sub> reference curve was obtained for a line of  $K_{line}$  point scatterers transversally moved across the ultrasound beam. The envelope from the backscattered RF signals was calculated as follows:

$$Envelope_d(P_k, n) = |Hilbert(e_d(P_k, n))|, \quad (\text{A.14})$$

when  $k=1,2\dots K_{line}$  and  $d=0,1,\dots D$ . The  $||$  means the squared root of the summation of the squared real part and squared imaginary part of the Hilbert transform. After this, the *Envelope*( $P_k, n$ ) was auto-convolved respect to number of displacements  $d$ :

$$Envelope_u(P_k, n) = Envelope_d(P_k, n) \otimes Envelope_d(P_k, n) \quad (\text{A.15})$$

for  $n = 0, 1, 2 \dots N$ ,

where  $u=0,1\dots(2D-1)$ . Next, the *Envelope*( $P_k, n$ ) values were summed respect to the number of point scatterer  $k$  and respect to the time  $n$ :

$$Envelope_u = \sum_{n=0}^N \sum_{k=1}^{K_{line}} Envelope_u(P_k, n), \quad (\text{A.16})$$

and normalized to obtain the *Envelope*<sub>2D</sub> as follows:

$$Envelope_{2D} = \frac{Envelope_u}{\max(Envelope_u)}. \quad (\text{A.17})$$





## Appendix B

# The Fisher-Z transform

The correlation coefficients can be transformed to a normal distribution using the Fisher-Z transform as defined by (Fisher 1970):

$$z = 0.5 * [\ln(1 + \rho) - \ln(1 - \rho)] \quad (\text{B.1})$$

Thus, the mean decorrelation and the 95% confidence interval can be calculated in  $z$  domain which can be transformed to the time domain by computing the inverse of the Fisher-Z transform *viz.*:

$$\rho = \frac{e^{2z} - 1}{e^{2z} + 1} \quad (\text{B.2})$$



# Bibliography

- Abizaid, A., Kornowski, R., Mintz, G. S., Hong, M. K., Pichard, A. D., Kent, K. M., Satler, L. F., Popma, J. J., Bramwell, O. & Leon, M. B. (1997). Influence of guiding catheter selection on the measurement of coronary flow reserve. *American Journal of Cardiology*, 79, 703-704.
- Abreu, A., Mahmarian, J. J., Nishimura, S. & Verani, M. S. (1991). Tolerance and safety of pharmacologic coronary vasodilation with adenosine in association with thallium 201 scintigraphy in patients with suspected coronary artery disease. *American Journal of Cardiology*, 18, 730.
- Agatston, A. S., Janowitz, W. R., Hildner, F. J., Zusmer, N. R., Viamonte, M. J. & Detrano, R. (1990). Quantification of coronary artery calcium using ultrafast computed tomography. *Journal of the American College of Cardiology*, 15(4), 827-832.
- Albertal, M., Regar, E., Van Langenhove, G., Carlier, S. G., Serrano, P., Boersma, E., de Bruyne, B., Di Mario, C., Piek, J. & Serruys, P. W. (2002). Flow velocity and predictors of a suboptimal coronary flow velocity reserve after coronary balloon angioplasty. *European Heart Journal*, 23(2), 133-138.
- Albiero, R., Rau, T., Schluter, M., Di Mario, C., Reimers, B., Mathey, D. G., Tobias, J. M., Schofer, J. & Colombo, A. (1997). Comparison of immediate and intermediate-term results of intravascular ultrasound versus angiography-guided Palmaz-Schatz stent implantation in matched lesions. *Circulation*, 96(9), 2997-3005.
- Anderson, H. V., Roubin, G. S., Leimgruber, P. P., Cox, W. R., Douglas, J. S., King, S. B. & Grntzig, A. R. (1986). Measurement of transtenotic pressure gradient during percutaneous transluminal coronary angioplasty. *Circulation*, 73(3), 1223-1230.
- Bacon, D. R. (1982). Characteristics of a pvdf membrane hydrophone for use in the range 1-100 MHz. *IEEE Transactions on Ultrasonics, Ferroelectrics, and Frequency Control*, SU-29, 18-25.

- Baptista, J., Di Mario, C., Ozaki, Y., Escaned, J., Gil, R., de Feyter, P. J., Roelandt, J. R. T. C. & Serruys, P. W. (1996). Impact of plaque morphology and composition on the mechanisms of lumen enlargement using intracoronary ultrasound and quantitative angiography after balloon angioplasty. *American Journal of Cardiology*, 77, 115-121.
- Bartunek, J., Marwick, T. H., Rodrigues, A. C. T., Vincent, M., Van Schuerbeeck, E., Sys, S. U. & de Bruyne, B. (1996). Dobutamine-induced wall motion abnormalities: correlations with myocardial fractional flow reserve and quantitative coronary angiography. *Journal of the American College of Cardiology*, 27(6), 1429-1436.
- Bartunek, J., Sys, S. U., Heyndrickx, G. R., Pijls, N. H. & de Bruyne, B. (1995). Quantitative coronary angiography in predicting functional significance of stenoses in an unselected patient cohort. *Journal of the American College of Cardiology*, 26(2), 328-334.
- Baumgart, D., Haude, M., Goerge, G., Ge, J., Vetter, S., Dagues, N., Heusch, G. & Erbel, R. (1998a). Improved assessment of coronary stenosis severity using the relative flow velocity reserve. *Circulation*, 98(1), 40-46.
- Baumgart, D., Haude, M., Liu, F., Ge, J., Goerge, G. & Erbel, R. (1998b). Current concepts of coronary flow reserve for clinical decision making during cardiac catheterization. *American Heart Journal*, 136(1), 136-149.
- Bech, G. J. W., de Bruyne, B. & Pijls, N. H. J. (1999a). Comparison of deferral versus performance of PTCA based upon fractional flow reserve: the defer study. *Journal of the American College of Cardiology*, 33((Abst Suppl)), 89A.
- Bech, G. J. W., Pijls, N. H., de Bruyne, B., Peels, K. H., Michels, H. R., Bonnier, H. J. & Koolen, J. J. (1999b). Usefulness of fractional flow reserve to predict clinical outcome after balloon angioplasty. *Circulation*, 99(7), 883-888.
- Bell, M. R., Lerman, L. O. & Rumberger, J. A. (1999). Validation of minimally invasive measurement of myocardial perfusion using electron beam computed tomography and application in human volunteers. *Heart*, 81(6), 628-635.
- Bendat, J. S., & Piersol, A. C. (1986). *Random data: analysis and measurement* (2 ed.). New York: Wiley and Sons.
- Berman, D. S., Kiat, H., Van Train, K. F., Friedman, J., Garcia, E. V. & Madhavi, J. (1990). Comparison of SPECT using technetium-99m agents and thallium-201 and pet for the assessment of myocardial perfusion and viability. *American Journal of Cardiology*, 66(13), 72E-79E.

- Blasini, R., Neumann, F. J., Schmitt, C., Bokenkamp, J. & Schomig, A. (1997). Comparison of angiography and intravascular ultrasound for the assessment of lumen size after stent placement: impact of dilation pressures. *Catheter Cardiovasc Diag*, 42(2), 113-119.
- Blasini, R., Neumann, F. J., Schmitt, C., Walter, H. & Schomig, A. (1998). Restenosis rate after intravascular ultrasound-guided coronary stent implantation. *Cathet Cardiovasc Diagn*, 44(4), 380-386.
- Bom, N., Hoff, H. ten, Lancée, C. T., Gussenhoven, W. J. & Bosch, J. G. (1989). Early and recent intraluminal ultrasound devices. *International Journal of Cardiac Imaging*, 4(2-4), 79-88.
- Bom, N., Lancée, C. T. & van Egmond, F. C. (1972). An ultrasonic intracardiac scanner. *Ultrasonics*, 10, 72-76.
- Bom, N., Li, W., van der Steen, A. F. W., Lancée, C. T., Céspedes, E. I., Slager, C. J. & de Korte, C. L. (1998). Novel developments in intravascular imaging. *European Journal of Ultrasound*, 7(1), 9-14.
- Borsboom, J. M. G., Céspedes, E. I., van der Steen, A. F. W., Lancée, C. T. & Deprettere, E. F. (2000). Simulation of cylindrical intravascular ultrasound transducer. *Journal of the Acoustical Society of America*, 108(2), 827-835.
- Braunwald, E. (1971). Control of myocardial oxygen consumption: physiologic and clinical considerations. *American Journal Cardiology*, 27(4), 416-432.
- Bridal, S. L., Fornes, P., Bruneval, P. & Berger, G. (1997a). Correlation of ultrasonic attenuation (30 to 50 MHz) and constituents of atherosclerotic plaque. *Ultrasound in Medicine and Biology*, 23(5), 691-703.
- Bridal, S. L., Fornes, P., Bruneval, P. & Berger, G. (1997b). Parametric (integrated backscatter and attenuation) images constructed using backscattered radio frequency signals (25-56 MHz) from human aortae *in vitro*. *Ultrasound in Medicine and Biology*, 23(2), 215-229.
- Briguori, C., Anzuini, A., Airolidi, F., Gimelli, G., Nishida, T., Adamian, M., Corvaja, N., Di Mario, C. & Colombo, A. (2001). Intravascular ultrasound criteria for the assessment of the functional significance of intermediate coronary artery stenoses and comparison with fractional flow reserve. *American Journal of Cardiology*, 87(2), 136-141.
- Budoff, M. J., Oudiz, R. J., Zalace, C. P., Bakhsheshi, H., Goldberg, S. L., French, W. J., Rami, T. G. & Brundage, B. H. (1999). Intravenous three-dimensional coronary angiography using contrast enhanced electron beam computed tomography. *American Journal of Cardiology*, 83(6), 840-845.

- Cannon, R. O., Schenke, W. H., Leon, M. B., Rosing, D. R., Urquhart, J. & Epstein, S. E. (1987). Limited coronary flow reserve after dipyridamole in patients with ergonovine-induced coronary vasoconstriction. *Circulation*, *75*, 163-174.
- Cannon, R. O. d., Watson, R. M., Rosing, D. R. & Epstein, S. E. (1983). Angina caused by reduced vasodilator reserve of the small coronary arteries. *Journal of the American College of Cardiology*, *1*(6), 1359-1373.
- Carlier, S. G., Céspedes, E. I., Li, W., Mastik, F., van der Steen, A. F. W., Bom, N. & Serruys, P. W. (1998a). Blood flow assessment using IVUS. *Cardiovascular Interventions Online*, *2*.
- Carlier, S. G., Céspedes, E. I., Li, W., Mastik, F., van der Steen, A. F. W., Bom, N. & Serruys, P. W. (1998b). Blood flow assessment with intravascular ultrasound catheters: the ideal tool for simultaneous assessment of the coronary haemodynamics and vessel wall? *Seminars in Interventional Cardiology*, *3*, 21-29.
- Carlier, S. G., Céspedes, E. I., Li, W., van der Steen, A. F. W., van Meegen, J. R., Mastik, F., Honkoop, J., Serruys, P. W. & Bom, K. (1997). *In vivo* validation of a new intracoronary volumetric blood flow measurement method with intravascular ultrasound. *Circulation*, *96*(8 (Suppl I)), I-703 (abst).
- Carlier, S. G., Di Mario, C., Kern, M. & Serruys, P. W. (1998c). Intracoronary Doppler and pressure monitoring. In E. Topol (Ed.), *Textbook of interventional cardiology (3rd ed)* (p. 748-781). Philadelphia: W.B.Saunders Company.
- Carlier, S. G., Gordov, E., Gailly, E., Van Camp, G., Cosyns, B., Geschwind, H. & Vandenbossche, J. L. (1996). Acquisition of raw intracoronary Doppler signal for better characterization of flows. *Computers in Cardiology*, 221-224.
- Carlier, S. G., Li, W., Céspedes, E. I., van der Steen, A. F. W., Hamburger, J. N., Bom, N. & Serruys, P. W. (1998d). Simultaneous morphological and functional assessment of a renal artery stent intervention with intravascular ultrasound. *Circulation*, *97*, 2575-2576.
- Carlier, S. G., van Langenhove, G., Lupotti, F. A., Albertal, M., Mastik, F., Bom, N. & Serruys, P. S. (1999). Coronary flow reserve versus geometric measurements of coronary dimensions: Advantages and limitations of the functional stenosis assessment. *Journal of Interventional Cardiology*, *12*(6), 411-424.

- Céspedes, E. I. (1993). *Elastography: imaging of biological tissue elasticity*. Ph.d. dissertation, University of Houston.
- Céspedes, E. I., Carlier, S. G., Li, W., Mastik, F., van der Steen, A. F. W., Bom, N., Verdouw, P. D. & Serruys, P. W. (1998a). Blood flow assessment using a mechanical intravascular ultrasound catheter: initial evaluation *in vivo*. *Journal of Vascular Investigation*, 4(1), 39-44.
- Céspedes, E. I., Carlier, S. G., Sabate, M., Ligthart, J. & Serruys, P. W. (1998b). Angiographically undetected stent mal-apposition resolved by intravascular ultrasound and flow imaging. *Journal of Vascular Investigation*, 4, 81-84.
- Céspedes, E. I., de Korte, C. L. & van der Steen, A. F. W. (1997a). Intravascular ultrasonic palpation: assessment of local wall compliance. *IEEE Ultrasonics Symposium*, 1079-1082.
- Céspedes, E. I., de Korte, C. L. & van der Steen, A. F. W. (1999). Echo decorrelation from displacement gradients in elasticity and velocity estimation. *IEEE Transactions on Ultrasonics, Ferroelectrics, and Frequency Control*, 46(4), 791-801.
- Céspedes, E. I., de Korte, C. L. & van der Steen, A. F. W. (2000). Intraluminal ultrasonic palpation: assessment of local and cross-sectional tissue stiffness. *Ultrasound in Medicine and Biology*, 26(3), 385-396.
- Céspedes, E. I., de Korte, C. L., van der Steen, A. F. W., von Birgelen, C. & Lancée, C. T. (1997b). Intravascular elastography: principles and potentials. *Seminars in Interventional Cardiology*, 2(1), 55-62.
- Céspedes, E. I., Li, W., Mastik, F., van der Steen, A. W. F., Carlier, S. G., van Bremen, R. H. & Eberle, M. (1997c). Intravascular power flow imaging: theory and potentials for planimetry. *IEEE Ultrasonics Symposium*, 1273-1276.
- Céspedes, E. I., Ophir, J. & Alam, S. K. (1997d). The combined effect of signal decorrelation and random noise on the variance of time delay estimation. *IEEE Transactions on Ultrasonics, Ferroelectrics, and Frequency Control*, 44(1), 220-225.
- Chabanel, A., Horellou, M. H., Conard, J. & Samama, M. M. (1994). Red blood cell aggregability in patients with a history of leg vein thrombosis: influence of post-thrombotic treatment. *British Journal of Haematology*, 88(1), 174-179.

- Chauhan, A., Mullins, P. A., Petch, M. C. & Schofield, P. M. (1994). Is coronary flow reserve in response to papaverine really normal in syndrome X? *Circulation*, *89*(5), 1998-2004.
- Chien, S. (1974). Biophysical behavior of red cells in suspensions. In D. M. Surgenor (Ed.), *The red blood cell* (p. 1021-1133). San Francisco: Academic Press.
- Chien, S., Usami, S., Dellenback, R. J. & Gregersen, M. I. (1970). Shear-dependent interaction of plasma proteins with erythrocytes in blood rheology. *American Journal of Physiology*, *219*(1), 143-153.
- Chou, T. M., Sudhir, K., Iwanaga, S., Chatterjee, K. & Yock, P. G. (1994). Measurement of volumetric coronary blood flow by simultaneous intravascular two-dimensional and Doppler ultrasound: Validation in an animal model. *American Heart Journal*, *128*(2), 237-243.
- Christensen, D. A. (1988). In *Ultrasonic bioinstrumentation*. New York: John Wiley & Sons Ed., Chap. 8.
- Cloutier, G., & Qin, Z. (2000). Shear rate dependence of ultrasound backscattering from blood samples characterized by different levels of erythrocyte aggregation. *Annals of Biomedical Engineering*, *28*, 399-407.
- Cloutier, G., & Shung, K. K. (1993). Study of red cell aggregation in pulsatile flow from ultrasonic Doppler power measurements. *Biorheology*, *30*, 443-461.
- Crowe, J. R., Shapo, B. M., Stephens, D. N., Bleam, D., Eberle, M. J., Céspedes, E. I., Wu, C. C., Muller, D. W. M., Kovatch, J. A., Lederman, R. J. & O'Donnell, M. (2000). Blood speed imaging with an intraluminal array. *IEEE Transactions on Ultrasonics, Ferroelectrics, and Frequency Control*, *47*(3), 672-681.
- Crowe, J. R., Shapo, B. M., Stephens, D. N., Bleam, D., Eberle, M. J., Wu, C. C., Muller, D. W. M., Kovatch, J. A., Lederman, R. J. & O'Donnell, M. (1996). Coronary artery flow imaging with an intraluminal array. *IEEE Ultrasonics Symposium*, *2*, 1481-1484.
- de Bruyne, B., Bartunek, J., Sys, S. U. & Heyndrickx, G. R. (1995). Relation between myocardial fractional flow reserve calculated from coronary pressure measurements and exercise-induced myocardial ischemia. *Circulation*, *92*(1), 39-46.
- de Bruyne, B., Bartunek, J., Sys, S. U., Pijls, N. H. J., Heyndrickx, G. R. & Wijns, W. (1996). Simultaneous coronary pressure and flow velocity mea-



- surements in humans. Feasibility, reproducibility and hemodynamic dependence of coronary flow velocity reserve, hyperemic flow versus pressure slope index and fractional flow reserve. *Circulation*, *94*(8), 1842-1849.
- de Bruyne, B., Baudhuin, T., Melin, J. A., Pijls, N. H. J., Sys, S. U., Bol, A., Paulus, W. J., Heyndrickx, G. R. & Wijns, W. (1994). Coronary flow reserve calculated from pressure measurements in humans. Validation with positron emission tomography. *Circulation*, *89*(3), 1013-1022.
- de Bruyne, B., Pijls, N. H. J., Heyndrickx, G. R., Hodeige, D., Kirkeeide, R. & Gould, K. L. (2000). Pressure-derived fractional flow reserve to assess serial epicardial stenoses: theoretical basis and animal validation. *Circulation*, *101*(15), 1840-1847.
- de Bruyne, B., Pijls, N. H. J., Smith, L., Wievegg, M. & Heyndrickx, G. R. (2001). Coronary thermodilution to assess flow reserve. Experimental validation. *Circulation*, *104*, 2003-2006.
- de Bruyne, B., Serruys, P. W. & al. et. (1998). Debate II: a randomized study to evaluate provisional stenting after guided balloon angioplasty. *Circulation*, *98*(17), I-498.
- de Feyter, P. J., Disco, C., Serruys, P. & al. et. (1999). Reference chart derived from post-stent-implantation intravascular ultrasound predictors of 6-month expected restenosis on quantitative coronary angiography. *Circulation*, *100*, 1777-1783.
- de Feyter, P. J., Nieman, K., van Ooijen, P. & Oudkerk, M. (2000). Non-invasive coronary artery imaging with electron beam computed tomography and magnetic resonance imaging. *Heart*, *84*(4), 442-448.
- de Jaegere, P., Mudra, H., Figulla, H., Almagro, Y., Doucet, S., Penn, I., Colombo, A., Hamm, C., Bartorelli, A., Rothman, M., Nobuyoshi, M., Yamaguchi, T., Voudris, V., Di Mario, C., Makovski, S., Hausmann, D., Rowe, S., Rabinovich, S., Sunamura, M. & van Es, G. A. (1998). Intravascular ultrasound-guided optimized stent deployment. immediate and 6 months clinical and angiographic results from the multicenter ultrasound stenting in coronaries study (MUSIC study). *Journal of European Heart*, *19*(8), 1214-1223.
- de Jong, J. P., Westerhof, N. & Elzinga, G. (1986). How to quantify an arterial stenosis: a study on the femoral arteries of dog and man. *Cardiovasc Res*, *20*(2), 134-144.
- de Korte, C. L. (1999). intravascular ultrasound elastography. *PhD Thesis Erasmus University Rotterdam*.

- de Korte, C. L., Pasterkamp, G., van der Steen, A. F. W., Woutman, H. A. & Bom, N. (2000). Characterization of plaque components using intravascular ultrasound elastography in human femoral and coronary arteries *in vitro*. *Circulation*, *102*, 617-623.
- de Korte, C. L., van der Steen, A. F. W., Céspedes, E. I. & Pasterkamp, G. (1998). Intravascular ultrasound elastography in human arteries: initial experience *in vitro*. *Ultrasound in Medicine and Biology*, *24*(3), 401-408.
- de Kroon, M. G. M., Slager, C. J., Gussenhoven, W. J., Serruys, P. W., Roelandt, J. R. T. C. & Bom, N. (1991). Cyclic changes of blood echogenicity in high-frequency ultrasound. *Ultrasound in Medicine and Biology*, *17*, 723-728.
- Derode, A., & Fink, M. (1998). Correlation length of ultrasonic speckle in anisotropic random media: Application to coherent echo detection. *Journal of the Acoustical Society of American*, *103*(1), 73-82.
- Di Mario, C., & al. et. (1999). Doppler and QCA guided aggressive PTCA has the same target lesion revascularization of stent implantation: 6-month-results of the DESTINI study. *Journal of the American College of Cardiology*, *33*(2), 47A.
- Di Mario, C., Gil, R. & Serruys, P. W. (1995). Long-term reproducibility of coronary flow velocity measurements in patients with coronary artery disease. *American Journal of Cardiology*, *75*, 1177-1180.
- Di Mario, C., Gorge, G., Peters, R., Kearney, P., Pinto, F., Hausmann, D., von Birgelen, C., Colombo, A., Mudra, H., Roelandt, J. R. T. C. & Erbel, R. (1998). Clinical application and image interpretation in intracoronary ultrasound. Study Group on Intracoronary Imaging of the Working Group of Coronary Circulation and of the Subgroup on Intravascular Ultrasound of the Working Group of Echocardiography of the European Society of Cardiology. *European Heart Journal*, *19*(2), 207-209.
- Di Mario, C., Moses, J. W., Anderson, T. J., Bonan, R., Muramatsu, T., Jain, A. C., Suarez de Lezo, J., Cho, S. Y., Kern, M., Meredith, I. T., Cohen, D., Moussa, I. & Colombo, A. (2000). Randomized comparison of elective stent implantation and coronary balloon angioplasty guided by on-line quantitative angiography and intracoronary Doppler. DESTINI Study Group (Doppler Endpoint STenting INternational Investigation). *Circulation*, *102*(24), 2938-2944.
- Di Mario, C., The, S. H. K., Madrestma, S., van Suylen, R. J., Wilson, R. A., Bom, N., Serruys, P. W., Gussenhoven, E. J. & Roelandt, J. R. T. C.

- (1992). Detection and characterization of vascular lesions by intravascular ultrasound: and *in vitro* study correlated with histology. *Journal of American Society Echocardiography*, 5(2), 135-146.
- Doppler, J. C. (1843). Ueber das farbige lichth der doppelsterne und einiger anderer gestirne des himmels. *Abhandl. Konigl. Bohm. Ges. Ser.*, 2, 465-482.
- Doriot, P., Dorsaz, P., Dorsaz, L. & Chatelain, P. (2000). Accuracy of coronary flow measurements performed by means of Doppler wires. *Ultrasound in Medicine and Biology*, 26(2), 221-228.
- Doucette, J. W., Corl, P. D., Payne, H. M., Flynn, A. E., Goto, M., Nassi, M. & Segal, J. (1992). Validation of a Doppler guide wire for intravascular measurement of coronary artery flow velocity. *Circulation*, 85, 1899-1911.
- Doyley, M. M., Mastik, F., de Korte, C. L., Carlier, S. G., Céspedes, E. I., Serruys, P. W., Bom, N. & van der Steen, A. F. W. (2001). Advancing intravascular ultrasonic palpation toward clinical applications. *Ultrasound in Medicine and Biology*, 27(11), 1471-1480.
- Eberle, M. J. (1997). The latest in electronic imaging. *Seminars in Interventional Cardiology*, 2(1), 19-23.
- Embree, P. M., & O'Brien, W. D. (1990). Volumetric blood flow via time-domain correlation: Experimental verification. *IEEE Transactions on Ultrasonics, Ferroelectrics, and Frequency Control*, 37(2), 176-189.
- Erbel, R., Ge, J., Bockisch, A., Kearney, P., Gorge, G., Haude, M., Schumann, D., Zamorano, J., Rupprecht, H. J. & Meyer, J. (1996). Value of intracoronary ultrasound and Doppler in the differentiation of angiographically normal coronary arteries: a prospective study in patients with angina pectoris. *European Heart Journal*, 17, 880-889.
- Fayad, Z. A., Fallon, J. T., Shinnar, M., Wehrli, S., Dansky, H. M., Poon, M., Badimon, J. J., Charlton, S. A., Fisher, E. A., Breslow, J. L. & Fuster, V. (1998a). Noninvasive *in vivo* high-resolution magnetic resonance imaging of atherosclerotic lesions in genetically engineered mice. *Circulation*, 98, 1541-1547.
- Fayad, Z. A., Fuster, V., Fallon, J. T., Jayasundera, T., Worthley, S. G., Helft, G., Aguinaldo, J. G., Badimon, J. J. & Sharma, S. K. (2000). Noninvasive *in vivo* human coronary artery lumen and wall imaging using black-blood magnetic resonance imaging. *Circulation*, 102, 506-510.

- Fayad, Z. A., Tamana, N., Badimon, J. J. & et, a. l. (1998b). *In vivo* MRI characterization of plaques in the thoracic aorta. *Circulation*, 98((suppl I):I-515), Abstract.
- Ferrara, K. W., & Algazi, V. R. (1994). A statistical analysis of the received signal from blood during laminar flow. *IEEE Transactions on Ultrasonics, Ferroelectrics, and Frequency Control*, 41(2), 185-198.
- Ferrari, M., Schnell, B., Werner, G. S. & Figulla, H. R. (1999). Safety of deferring angioplasty in patients with normal coronary flow velocity reserve. *Journal of the American College of Cardiology*, 33(1), 82-87.
- Fisher, R. A. (1970). *Statistical methods for research workers* (4th edition ed.). Edinburgh: Oliver and Boyd.
- Fitzgerald, P. J., Takagi, A., Moore, M. P., Hayase, M., Kolodgie, F. D., Corl, D., Nassi, M., Virmani, R. & Yock, P. G. (2001). Intravascular sonotherapy decreases neointimal hyperplasia after stent implantation in swine. *Circulation*, 103(14), 1828-1831.
- Foster, F. S., Ohara, H., Bloomfield, T., Ryan, L. K. & Lockwood, G. (1994). Ultrasound backscatter from blood in the 30 to 70 MHz frequency range. *IEEE Ultrasonics Symposium*, 3, 1599-1602.
- Foster, S. G., Embree, P. M. & O'Brien, W. D. (1990). Flow velocity profile via time-domain correlation: error analysis and computer simulation. *IEEE Transactions on Ultrasonics, Ferroelectrics, and Frequency Control*, 37(2), 164-175.
- Friemel, B. H., Bohs, L. N., Nightingale, K. R. & Trahey, G. E. (1998). Speckle decorrelation due to two-dimensional flow gradients. *IEEE Transactions on Ultrasonics, Ferroelectrics, and Frequency Control*, 45(2), 317-327.
- Fung, Y. C. (1993). The flow properties of blood. In *Biomechanics: mechanical properties of living tissues* (2nd ed.). New York: Springer-Verlag.
- Ganz, W., Donoso, R., Marcus, H. S., Forrester, J. S. & Swan, H. J. (1971a). A new technique for measurement of cardiac output by thermodilution in man. *Am J Cardiol*, 27(4), 392-396.
- Ganz, W., Tamura, K., Marcus, H. S., Donoso, R., Yoshida, S. & Swan, H. J. (1971b). Measurement of coronary sinus blood flow by continuous thermodilution in man. *Circulation*, 44(2), 181-195.
- George, N., Christensen, C. R., Bennett, J. S. & Guenther, B. D. (1976). Speckle noise in displays. *Journal of Optic Society of America*, 66(11), 1282-1290.

- Glagov, S., Weisenberg, E. & Zarins, C. K. (1987). Compensatory enlargement of human atherosclerotic coronary arteries. *New England Journal Medicine*, *316*, 1371-1375.
- Goldsmith, H. L., & Mason, S. G. (1962). The flow of suspensions through tubes I. Single spheres, rods and discs. *Journal of Colloid Science*, *17*, 448-476.
- Gould, K., Kelley, K. & Bolson, E. (1982). Experimental validation of quantitative coronary arteriography for determining pressure-flow characteristics of coronary stenosis. *Circulation*, *66*(5), 930-937.
- Gould, K. L., Kirkeeide, R. L. & Buchi, M. (1990). Coronary flow reserve as a physiologic measure of stenosis severity. *Journal of the American College of Cardiology*, *15*, 459.
- Gould, K. L., Lipscomb, K. & Hamilton, G. W. (1974). Physiologic basis for assessing critical coronary stenosis. Instantaneous flow response and regional distribution during coronary hyperemia as measures of coronary flow reserve. *American Journal of Cardiology*, *33*(1), 87-94.
- Grüntzig, A. R., Senning, A. & Slegenthaler, W. E. (1979). Nonoperative dilatation of coronary-artery stenosis: percutaneous transluminal coronary angioplasty. *New England Journal Medicine*, *301*, 61-68.
- Haase, K. K., Athanasiadis, A., Mahrholdt, H., Treusch, A., Wullen, B., Jaramillo, C., Baumbach, A., Voelker, W., Meisner, C. & Karsch, K. R. (1998). Acute and one year follow-up results after vessel size adapted PTCA using intracoronary ultrasound. *Eur Heart J*, *19*(2), 263-272.
- Hamburger, J. N., Gijsbers, G. H., Ozaki, Y., Ruygrok, P. N., de Feyter, P. J. & Serruys, P. W. (1997). Recanalization of chronic total coronary occlusions using a laser guide wire: a pilot study. *Journal of the American College of Cardiology*, *30*(3), 649-656.
- Harrison, D. G., White, C. W., Hiratzka, L. F., Eastham, C. L. & Marcus, M. L. (1984). The value of lesional cross-sectional area determined by quantitative coronary angiography in assessing the physiologic significance of proximal left anterior descending coronary artery stenoses. *Circulation*, *69*, 111.
- Hartley, C., & Cole, J. (1974). An ultrasonic pulsed Doppler system for measuring blood flow in small vessels. *Journal of Applied Physiology*, *37*, 626.
- Hasdai, D., Holmes, J., D. R., Higano, S. T. & Lerman, A. (1998). Effect of basal epicardial tone on endothelium-independent coronary flow reserve measurement. *Cathet Cardiovasc Diagn*, *44*(4), 392-396.

- He, X., & Ku, D. N. (1996). Pulsatile flow in the human left coronary artery bifurcation: average conditions. *Journal of Biomechanical Engineering*, *118*(1), 74-82.
- Hodgson, J., Reddy, D., Suneja, R., Nair, R., Lesnefsky, E. & Sheehan, H. (1993). Intracoronary ultrasound imaging: correlation of plaque morphology with angiography, clinical syndrome and procedural results in patients undergoing coronary angioplasty. *Journal of the American College of Cardiology*, *21*, 35-44.
- Hodgson, J. M., Reinert, S., Most, A. S. & Williams, D. O. (1986). Prediction of long-term clinical outcome with final translesional pressure gradient during coronary angioplasty. *Circulation*, *74*, 563-566.
- Hoeks, A. P. G., Arts, T. G. J., Brands, P. J. & Reneman, R. S. (1993). Comparison of the performance of the rf cross correlation and Doppler autocorrelation technique to estimate the mean velocity of simulated ultrasound signals. *Ultrasound in Medicine and Biology*, *19*(9), 727-740.
- Hoeks, A. P. G., Arts, T. G. J., Brands, P. J. & Reneman, R. S. (1994). Processing scheme for velocity estimation using ultrasound rf cross correlation techniques. *European Ultrasound Journal*, *1*, 171-182.
- Hoffman, J. I., & Spaan, J. A. (1990). Pressure-flow relations in coronary circulation. *Physiol Rev*, *70*(2), 331-390.
- Hoffman, R., Mintz, G. S., Mehran, R., Pichard, A. D., Kent, K. M., Satler, L. F., Popma, J. J., Hongsheng, W. & Leon, M. B. (1998). Intravascular ultrasound predictors of angiographic restenosis in lesions treated with Palmaz-Schatz stents. *Journal of the American College of Cardiology*, *31*(1), 43-49.
- Holdright, D. R., Lindsay, D. C., Clarke, D., Fox, K., Poole-Wilson, P. A. & Collins, P. (1993). Coronary flow reserve in patients with chest pain and normal coronary arteries. *British Heart Journal*, *70*, 513-519.
- Hong, M. K., Mintz, G. S., Pichard, A. D., Satler, L. F., Kent, K. M., Popma, J. J. & Leon, M. B. (1999). Intravascular ultrasound predictors of target lesion revascularization after stenting of protected left main coronary artery stenoses. *American Journal of Cardiology*, *83*(2), 175-179.
- Hongo, M., Nakatsuka, T., Watanabe, N., Takenada, H., Tanaka, M., Kinoshita, O., Okubo, S. & Sekiguchi, M. (1994). Effects of heart rate on phasic coronary blood flow pattern and flow reserve in patients with normal coronary arteries: a study with an intravascular Doppler catheter and spectral analysis. *American Heart Journal*, *127*, 545-551.

- Houbouyan, L. L., Delamaire, M., Beauchet, A., Gentil, M., Cauchois, G., Tac-coen, A., Yvert, J. P., Montredon, N., Roudaut, M. F., Zhao, S., Goguel, A., Potron, G., Boisseau, M. & Stoltz, J. F. (1997). Multicenter study of an erythro-aggregometer: quality control and standardization. *Clin. Hemorheology*, 17, 299-306.
- Hozumi, T., Yoshida, K., Ogata, Y., Akasaka, T., Asami, Y., Takagi, T. & Morioka, S. (1998). Noninvasive assessment of significant left anterior descending coronary artery stenosis by coronary flow velocity reserve with transthoracic color Doppler echocardiography. *Circulation*, 97(16), 1557-1562.
- Hutchison, S. J., Soldo, S. J., Gadallah, S., Kawanishi, D. T. & Chandraratna, P. A. (1997). Determination of coronary flow measurements by trans-esophageal echocardiography: dependence of flow velocity reserve on the location of stenosis. *American Heart Journal*, 133(1), 44-52.
- Isner, J. M., Kaufman, J., Rosenfield, K., Pieczek, A., Schainfeld, R., Ramaswamy, K. & Kosowsky, B. D. (1993). Combined physiologic and anatomic assessment of percutaneous revascularization using a Doppler guidewire and ultrasound catheter. *American Journal of Cardiology*, 71(14), 70D-86D.
- Jenni, R., Buchi, M., Jakob, M. & Ritter, M. (1998a). Position control of intravascular Doppler guidewire: concept of a tracking indicator and its clinical implications. *Cathet Cardiovasc Diagn*, 44(1), 28-33.
- Jenni, R., Buchi, M., Zweifel, H. J. & Ritter, M. (1998b). Impact of Doppler guidewire size and flow rates on intravascular velocity profiles. *Cathet Cardiovasc Diagn*, 45(1), 96-100.
- Joye, J. D., Schulman, D. S., Lasorda, D., Farah, T., Donohue, B. C. & Reichek, N. (1994). Intracoronary Doppler guide wire versus stress single-photon emission computed tomographic thallium-201 imaging in assessment of intermediate coronary stenoses. *Journal of the American College of Cardiology*, 24(4), 940-947.
- Kasaoka, S., Tobis, J. M., Akiyama, T., Reimers, B., Di Mario, C., Wong, N. D. & Colombo, A. (1998). Angiographic and intravascular ultrasound predictors of in-stent restenosis. *Journal of the American College of Cardiology*, 32(6), 1630-1635.
- Kern, M. J., Bach, R. G., Mechem, C. J., Caracciolo, E. A., Aguirre, F. V., Miller, L. W. & Donohue, T. J. (1996). Variations in normal coronary vasodilatory reserve stratified by artery, gender, heart transplantation and

- coronary artery disease. *Journal of the American College of Cardiology*, 28(5), 1154-1160.
- Kern, M. J., de Bruyne, B. & Pijls, N. H. J. (1997a). From research to clinical practice: current role of intracoronary physiologically based decision making in the cardiac catheterization laboratory. *Journal of the American College of Cardiology*, 30, 613-620.
- Kern, M. J., Deligonul, U., Aguirre, F. & Hilton, T. C. (1991). Intravenous adenosine: Continuous infusion and low dose bolus administration for determination of coronary vasodilator reserve in patients with and without coronary artery disease. *Journal of the American College of Cardiology*, 18, 718.
- Kern, M. J., Donohue, T. J., Aguirre, F. V., Bach, R. G., Caracciolo, E. A., Wolford, T., Mechem, C. J., Flynn, M. S. & Chaitman, B. (1995). Clinical outcome of deferring angioplasty in patients with normal translesional pressure-flow velocity measurements. *Journal of the American College of Cardiology*, 25, 178-187.
- Kern, M. J., Dupouy, P., Drury, J. H., Aguirre, F. V., Aptekar, E., Bach, R. G., Caracciolo, E. A., Donohue, T. J., Rande, J. L., Geschwind, H. J., Mechem, C. J., Kane, G., Teiger, E. & Wolford, T. L. (1997b). Role of coronary artery lumen enlargement in improving coronary blood flow after balloon angioplasty and stenting: a combined intravascular ultrasound Doppler flow and imaging study. *Journal of the American College of Cardiology*, 29(7), 1520-1527.
- Kilpatrick, D., & Webber, S. (1986). Intravascular blood velocity in simulated coronary angioplasty. *Cathet Cardiovasc Diagn*, 12(5), 317-323.
- King III, S. B., Williams, D. O., Chougule, P., Klein, J. L., Waksman, R., Hilstead, R., MacDonald, J., Andersberg, K. & Crocker, I. R. (1998). Endovascular beta-radiation to reduce restenosis after coronary balloon angioplasty: results of the Beta Energy Restenosis Trial (BERT). *Circulation*, 97, 2025-2030.
- Kitamura, H., Sigel, B., Machi, J., Feleppa, E. J., Sokil-Melgar, J., Kalisz, A. & Justin, J. (1995). Roles of hematocrit and fibrinogen in red cell aggregation determined by ultrasonic scattering properties. *Ultrasound in Medicine and Biology*, 21, 827-832.
- Klocke, F. J. (1987). Measurements of coronary flow reserve: Defining pathophysiology versus making decisions about patient care. *Circulation*, 76, 245.



- Krams, R., Wentzel, J. J., Céspedes, E. I., Vinke, R., Carlier, S., van der Steen, A. F. W., Lancee, C. T. & Slager, C. J. (1999). Effect of catheter placement on 3-D velocity profiles in curved tubes resembling the human coronary system. *Ultrasound in Medicine and Biology*, 25(5), 803-810.
- Lafont, A., & al. et. (1999). The French Optimal Stenting Trial (FROST): a multicenter, prospective randomized study comparing systematic stenting to angiography and coronary flow reserve guided stenting: 6 month clinical and angiographic follow-up. *Journal of the American College of Cardiology*, 89A(2), 89A.
- Le Devehat, C., Vimeux, M., Bondoux, G. & Khodabandehlou, T. (1990). Red blood cell aggregation in diabetes mellitus. *Int Angiol*, 9(1), 11-15.
- Ledoux, L. A. F., Willigers, J. M., Brands, P. J. & Hoeks, A. P. G. (1998). Experimental verification of the correlation behavior of analytic ultrasound radiofrequency signals received from moving structures. *Ultrasound in Medicine and Biology*, 24(9), 1383-1396.
- Lee, B. K., Kwon, H. M., Hong, B. K., Park, B. E., Suh, S. H., Cho, M. T., Lee, C. S., Kim, M. C., Kim, C. J., Yoo, S. S. & Kim, H. S. (2001). Hemodynamic effects on atherosclerosis-prone coronary artery: wall shear stress/rate distribution and impedance phase angle in coronary and aortic circulation. *Yonsei Medical Journal*, 42(4), 375-383.
- Legrand, V., Mancini, G., Bates, E., Hodgson, J., Gross, M. & Vogel, R. (1986). Comparative study of coronary flow reserve, coronary anatomy and results of radionuclide exercise tests in patients with coronary artery disease. *Journal of the American College of Cardiology*, 8(5), 1022-1032. (limitations of QCA for physiologic assessment)
- Li, W., Lancée, C. T., Céspedes, E. I., van der Steen, A. F. W. & Bom, N. (1997). Decorrelation of intravascular echo signals: Potentials for blood velocity estimation. *Journal of the Acoustical Society of America*, 102(6), 3785-3794.
- Li, W., Lancée, C. T., Céspedes, E. I., van der Steen, A. F. W. & Bom, N. (1998a). Decorrelation properties of intravascular echo signals. *Journal of the Acoustical Society of America*, 102(6), 3785-3794.
- Li, W., van der Steen, A. F. W. & Lancee, C. T. (1996). Temporal correlation of blood scattering signals *in vivo* from radio frequency intravascular ultrasound. *Ultrasound in Medicine and Biology*, 22(5), 583-590.

- Li, W., van der Steen, A. F. W., Lancée, C. T., Céspedes, E. I. & Bom, N. (1998b). Blood flow imaging and volume flow quantitation with intravascular ultrasound. *Ultrasound in Medicine and Biology*, *24*(2), 203-214.
- Linderkamp, O., Ozanne, P., Wu, P. Y. & Meiselman, H. J. (1984). Red blood cell aggregation in preterm and term neonates and adults. *Pediatr Res*, *18*(12), 1356-1360.
- Lupi, A., Buffon, A., Finocchiaro, M. L., Conti, E., Maseri, A. & Crea, F. (1997). Mechanisms of adenosine-induced epicardial coronary artery dilatation. *European Heart Journal*, *18*(4), 614-617.
- Marcus, M., Wright, C., Doty, D., Eastham, C., Laughlin, D., Krumm, P., Fastenow, C. & Brody, M. (1981a). Measurements of coronary velocity and reactive hyperemia in the coronary circulation of humans. *Circ Res*, *49*(4), 877-891.
- Marcus, M. L., Gascho, J. A., Mueller, T. M., Eastham, C., Wright, C. B., Doty, D. B. & Hiratzka, L. F. (1981b). The effects of ventricular hypertrophy on the coronary circulation. *Basic Res Cardiol*, *76*(5), 575-581.
- McGinn, A. L., White, C. W. & Wilson, R. F. (1990). Interstudy variability of coronary flow reserve. *Circulation*, *81*(4), 1319-1330. (Doppler 3F)
- Mehran, R., Dangas, G., Mintz, G. S., Waksman, R., Abizaid, A., Satler, L. F., Pichard, A. D., Kent, K. M., Lansky, A. J., Stone, G. W. & Leon, M. B. (2000). Treatment of in-stent restenosis with excimer laser coronary angioplasty versus rotational atherectomy: comparative mechanisms and results. *Circulation*, *101*(21), 2484-2489.
- Meier, P., & Zierler, K. L. (1954). On the theory of the indicator-dilution method for measurement of blood flow and volume. *Journal of Applied Physiology*, *6*, 731-734.
- Miller, D., Donohue, T., Younis, L., Bach, R., Aguirre, F., Wittry, M., Goodgold, H., Chaitman, B. & Kern, M. (1994). Correlation of pharmacological 99mTc-sestamibi myocardial perfusion imaging with poststenotic coronary flow reserve in patients with angiographically intermediate coronary artery stenoses. *Circulation*, *89*(5), 2150-2160.
- Miller, D. D., Donohue, T. J., Wolford, T. L., Kern, M. J. & Bergmann, S. R. (1996). Assessment of blood flow distal to coronary artery stenosis. *Circulation*, *94*, 2447-2454.
- Milnor, W. R. (1989). *Hemodynamics* (Second Edition ed.). Baltimore: Waverly Press, Inc., USA.

- Mintz, G. S., Popma, J. J., Pichard, A. D., Kent, K. M., Satler, L. W., Wong, S. C., Hong, M. K., Kovach, J. A. & Leon, M. B. (1996). Arterial remodeling after coronary angioplasty. a serial intravascular ultrasound study. *Circulation*, *94*, 35-43.
- Morse, P. M., & Ingard, K. U. (1968). The scattering of sound. In *Theoretical acoustics*. New York: McGraw-Hill Book Company.
- Moses, J. W., Undermir, C., Strain, J. E., Kreps, E. M., Higgins, J. E., Gleim, G. W. & Kern, M. J. (1998). Relation between single tomographic intravascular ultrasound image parameters and intracoronary Doppler flow velocity in patients with intermediately severe coronary stenoses. *American Heart Journal*, *135*(6 Pt 1), 988-994.
- Moussa, I., Moses, J., Di Mario, C., Albiero, R., De Gregorio, J., Adamian, M., Di Francesco, L. & Colombo, A. (1999). Does the specific intravascular ultrasound criterion used to optimize stent expansion have an impact on the probability of stent restenosis? *American Journal of Cardiology*, *83*(7), 1012-1017.
- Mudra, H., Macaya, C., Zahn, R. & al. et. (1998). Interim analysis of the "OPTimization with ICUS to reduce stent restenosis" (OPTICUS) trial. *Circulation*, *98*(17), I-363.
- Muzik, O., Duvernoy, C., Beanlands, R. S., Sawada, S., Dayanikli, F., Wolfe, J., E. R. & Schwaiger, M. (1998). Assessment of diagnostic performance of quantitative flow measurements in normal subjects and patients with angiographically documented coronary artery disease by means of nitrogen-13 ammonia and positron emission tomography. *Journal of the American College of Cardiology*, *31*(3), 534-540.
- Narayanan, V. M., Shankar, P. M. & Reid, J. M. (1994). Non-rayleigh statistics of ultrasound backscattered signals. *IEEE Transactions on Ultrasonics, Ferroelectrics, and Frequency Control*, *41*(6), 845-852.
- Neumann, F. J., Katus, H. A., Hoberg, E., Roebruck, P., Braun, M., Haupt, H. M., Tillmanns, H. & Kbler, W. (1991). Increased plasma viscosity and erythrocyte aggregation: indicators of an unfavourable clinical outcome in patients with unstable angina pectoris. *British Heart Journal*, *66*, 425-430.
- Neumann, F. J., Schmid-Schonbein, H. & Ohlenbusch, H. (1987). Temperature-dependence of red cell aggregation. *Pflugers Arch - European Journal of Physiology*, *408*(5), 524-530.

- Nishikawa, T., & Dohi, S. (1993). Haemodynamic changes associated with thermodilution cardiac output determination during metabolic acidosis or hypoxic hypoxia in dogs. *European Journal of Anaesthesiology*, *10*(5), 321-329.
- Nissen, S., & Yock, P. (2001). Intravascular ultrasound. Novel pathophysiological insights and current clinical applications. *Circulation*, *103*, 604-616.
- O'Donnell, M., Eberle, M. J., Stephens, D. N., Litzza, J. L., San Vicente, K. & Shapo, B. M. (1997a). Synthetic phased arrays for intraluminal imaging of coronary arteries. *IEEE Transactions on Ultrasonics, Ferroelectrics, and Frequency Control*, *44*(3), 714-721.
- O'Donnell, M., Eberle, M. J., Stephens, D. N., Litzza, J. L., Shapo, B. M., Crowe, J. R., Choi, C. D., Chen, J. J., Muller, D. M. W., Kovach, J. A., Lederman, R. L., Ziegenbein, R. C., Wu, C. C., San Vicente, K. & Bleam, D. (1997b). Catheter arrays: can intravascular ultrasound make a difference in managing coronary artery disease? In *IEEE Ultrasonics Symposium* (Vol. 2, p. 1447-1456). Toronto, Canada.
- Ofili, E. O., Kern, M. J., Labovitz, A. J., St Vrain, J. A., Segal, J., Aguirre, F. & Castello, R. (1992). Analysis of coronary blood flow velocity dynamics in angiographically normal and stenosed arteries before and after endoluminal enlargement by angioplasty. *Journal of the American College of Cardiology*, *21*, 308.
- Passariello, R., & De Santis, M. (1998). Magnetic resonance imaging evaluation of myocardial perfusion. *American Journal of Cardiology*, *81*(12A), 68G-73G.
- Peters, R. J. G., Kok, W. E. M., Di Mario, C., Serruys, P. W., Bar, F., Pasterkamp, G., Borst, C., Kamp, O., Bronzwaer, J., Visser, C., Piek, J. J., Panday, R., Jaarsma, W., Savalle, L. & Bom, N. (1997). Prediction of restenosis after coronary balloon angioplasty. Results of PICTURE (Post-intracoronary Treatment Ultrasound Result Evaluation), a prospective multicenter intracoronary ultrasound imaging study. *Circulation*, *95*, 2254-2261.
- Pijls, N. H., & de Bruyne, B. (1998). Coronary pressure measurement and fractional flow reserve. *Heart*, *80*(6), 539-542.
- Pijls, N. H. J., de Bruyne, B., Bech, G. J., Liistro, F., Heyndrickx, G. R., Bonnier, H. J. & Koolen, J. J. (2000). Coronary pressure measurement to assess the hemodynamic significance of serial stenoses within one coronary artery: validation in humans. *Circulation*, *102*(19), 2371-2377.

- Pijls, N. H. J., de Bruyne, B., Peels, K., Van der Voort, P., Bonnier, H. J. R. M., Bartunek, J. & Koolen, J. J. (1996). Measurement of fractional flow reserve to assess the functional severity of coronary artery stenoses. *New England Journal of Medicine*, 334(26), 1703-1708.
- Pijls, N. H. J., Van Gelder, B., Van der Voort, P., Peels, K., Bracke, F. A. L. E., M, B. H. J. R. & El Gamal, M. I. H. (1995). Fractional flow reserve. A useful index to evaluate the influence of an epicardial coronary stenosis on myocardial blood flow. *Circulation*, 92(11), 3183-3193.
- Pijls, N. H. J., van Son, J. A. M., Kirkeeide, R. L., de Bruyne, B. & Gould, K. L. (1993). Experimental basis of determining maximum coronary, myocardial, and collateral blood flow by pressure measurements for assessing functional stenosis severity before and after percutaneous transluminal coronary angioplasty. *Circulation*, 86(4), 1354-1367.
- Porenta, G., Schima, H., Pentaris, A., Tsangaris, S., Moertl, D., Probst, P., Maurer, G. & Baumgartner, H. (1999). Assessment of coronary stenoses by Doppler wires: a validation study using *in vitro* modeling and computer simulations. *Ultrasound in Medicine and Biology*, 25(5), 793-801.
- Prati, F., Di Mario, C., Moussa, I., Reimers, B., Mallus, M. T., Parma, A., Lioy, E. & Colombo, A. (1999). In-stent neointimal proliferation correlates with the amount of residual plaque burden outside the stent: an intravascular ultrasound study. *Circulation*, 99(8), 1011-1014.
- Proudfit, W. L., Shirey, E. K. & Sones, J., F. M. (1966). Selective cine coronary arteriography. Correlation with clinical findings in 1,000 patients. *Circulation*, 33(6), 901-910.
- Qin, Z., Durand, L. G., Allard, L. & Cloutier, G. (1998a). Effects of a sudden flow reduction on red blood cell rouleau formation and orientation using rf backscattered power. *Ultrasound in Medicine and Biology*, 24(4), 503-511.
- Qin, Z., Durand, L. G. & Cloutier, G. (1998b). Kinetics of the "black holes" phenomenon in ultrasound backscattering measurements with red blood cell aggregation. *Ultrasound in Medicine and Biology*, 24(2), 245-256.
- Rayford, C. R., Khouri, E. M., Lewis, F. B. & Gregg, D. E. (1959). Evaluation of use of left coronary inflow and O<sub>2</sub> content of coronary sinus blood as a measure of left ventricular metabolism. *Journal of Applied Physiology*, 14, 817-.
- Razavian, S. M., Del Pino, M., Simon, A. & Levenson, J. (1992). Increase in erythrocyte disaggregation shear stress in hypertension. *Hypertension*, 20(2), 247-252.

- Rensing, B. J., Vos, J., Smits, P. C., Foley, D. P., van den Brand, M. J., van der Giessen, W. J., de Feijter, P. J. & Serruys, P. W. (2001). Coronary restenosis elimination with a sirolimus eluting stent: first european human experience with 6-month angiographic and intravascular ultrasonic follow-up. *European Heart Journal*, 22(22), 2125-2130.
- Roelandt, J. R. T. C., Gussenhoven, E. J. & Bom, N. (Eds.). (1993). *Intravascular ultrasound*. The Netherlands: Kluwer Academic Publishers.
- Ropers, D., Moshage, W., Daniel, W. G., Jessl, J., Gottwik, M. & Achenbach, S. (2001). Visualization of coronary artery anomalies and their anatomic course by contrast-enhanced electron beam tomography and three-dimensional reconstruction. *American Journal of Cardiology*, 87(2), 193-197.
- Rossen, J. D., & Winniford, M. D. (1993). Effects of increases in heart rate and arterial pressure on coronary flow reserve in humans. *Journal of the American College of Cardiology*, 21(2), 343-348.
- Rothman, M. T., Baim, D. S., Simpson, J. B. & Harrison, D. C. (1982). Coronary hemodynamics during percutaneous transluminal coronary angioplasty. *American Journal of Cardiology*, 49(7), 1615-1622.
- Rubin, J. M., Tuthill, T. A. & Fowlkes, J. B. (2001). Volume flow measurement using Doppler and grey-scale decorrelation. *Ultrasound in Medicine and Biology*, 27(1), 101-109.
- Ryan, T. J., Bauman, W. B., Kennedy, J. W., Kereiakes, D. J., King, S. B. d., McCallister, B. D., Smith, J., S. C. & Ulliyot, D. J. (1993). Guidelines for percutaneous transluminal coronary angioplasty. A report of the American Heart Association/American College of Cardiology Task Force on Assessment of Diagnostic and Therapeutic Cardiovascular Procedures (Committee on Percutaneous Transluminal Coronary Angioplasty). *Circulation*, 88(6), 2987-3007.
- Schatz, R. A. (1989). A view of vascular stents. *Circulation*, 79(2), 445-457.
- Schiele, F., Meneveau, N. & Vuillemont, A. (1998). Impact of intravascular ultrasound guidance in stent deployment on 6-month restenosis rate: a multicenter, randomized study comparing two strategies - with and without intravascular ultrasound guidance. *Journal of American College in Cardiology*, 32, 320-328.
- Schneider, B., & Shung, K. K. (1996). Quantitative analysis of pulsed ultrasonic beam patterns using a shlieren system. *IEEE Transactions on Ultrasonics, Ferroelectrics, and Frequency Control*, 43(6), 1181-1186.

- Schwartz, R. S., Topol, E. J., Serruys, P. W., Sangiorgi, G. & Holmes, D. R. (1998). Artery size, neointima, and remodeling. time for some standards. *Journal of American College in Cardiology*, 32(7), 2087-2094.
- Schwarzacher, S. P., Fitzgerald, P. J. & Yock, P. G. (1997a). Clinical use of intravascular ultrasound. *Seminars in Interventional Cardiology*, 2(1), 1-9.
- Schwarzacher, S. P., Metz, J. A., Yock, P. G. & Fitzgerald, P. J. (1997b). Vessel tearing at the edge of intracoronary stents detected with intravascular ultrasound imaging. *Cardiovasc Diag*, 40(2), 152-155.
- Segers, P., Stergiopoulos, N., Verdonck, P. & Verhoeven, R. (1997). Assessment of distributed arterial network models. *Med Biol Eng Comput*, 35(6), 729-736.
- Serruys, P., Di Mario, C., Piek, J., Schroeder, E. & al. et. (1997). Prognostic value of intracoronary flow velocity and diameter stenosis in assessing the short and long term outcome of coronary balloon angioplasty: the DEBATE study. *Circulation*, 96(10), 3369-3377.
- Serruys, P. W., de Bruyne, B., Carlier, S., Sousa, J. E., Piek, J., Muramatsu, T., Vrints, C., Probst, P., Seabra-Gomes, R., Simpson, I., Voudris, V., Gurne, O., Pijls, N. H. J., Belardi, J., van Es, G. A., Boersma, E., Morel, M. A. & van Hout, B. (2000). Randomized comparison of primary stenting and provisional balloon angioplasty guided by flow velocity measurement. Doppler Endpoints Balloon Angioplasty Trial Europe (DEBATE) II Study Group. *Circulation*, 102(24), 2930-2937.
- Serruys, P. W., & Deshpande, N. V. (1998a). Is there MUSIC in IVUS guided stenting? is this MUSIC going to be a MUST? Multicenter Ultrasound Stenting in Coronaries study. *European Heart Journal*, 19(8), 1122-1124.
- Serruys, P. W., Di Mario, C., Meneveau, N., de Jaegere, P., Strikwerda, S., Feijter, P. J. de & Emanuelsson, H. (1993). Intracoronary pressure and flow velocity with sensor-tip guidewires. A new methodological comprehensive approach for the assessment of coronary hemodynamics before and after coronary interventions. *American Journal of Cardiology*, 71, 41D.
- Serruys, P. W., Emanuelsson, H., van der Giessen, W. & al. et. (1996). Heparin-coated Palmaz-Schatz stents in human coronary arteries. Early outcome of the Benestent-II Pilot study. *Circulation*, 93, 412-422.
- Serruys, P. W., Regar, E. & Carter, A. J. (2002). Rapamycin eluting stent: the onset of a new era in interventional cardiology. *Heart*, 87(4), 305-307.

- Serruys, P. W., van Hout, B., Bonnier, H., Legrand, V., Garcia, E., Macaya, C., Sousa, J. E., van der Giessen, W. J., Colombo, A., Seabra-Gomes, R., Kiemeneij, F., Ruygrok, P., Ormiston, J., Emanuelsson, H., Fajadet, J., Haude, M., Klugmann, S. & Morel, M. A. (1998b). Randomized comparison of implantation of heparin-coated stents with balloon angioplasty in selected patients with coronary artery disease (BENESTENT II). *Lancet*, *352*(9129), 673-681.
- Serruys, P. W., Wijns, W., Reiber, J. H. C., de Feyter, P. J., van den Brand, M., Piscione, F. & Hugenholtz, P. G. (1985). Values and limitations of transstenotic pressure gradients measured during percutaneous coronary angioplasty. *Herz*, *10*(337).
- Sgura, F. A., & Di Mario, C. (2001). New methods of coronary imaging II. Intracoronary ultrasonography in clinical practice. *Ital Heart J*, *2*(6), 579-592.
- Siegel, R. J. (Ed.). (1998). *Intravascular ultrasound imaging in coronary artery disease*. Los Angeles, California: Marcel Dekker, Inc.
- Slager, C. J., Essed, C. E., Schuurbiers, J. C., Bom, N., Serruys, P. W. & Meester, G. T. (1985). Vaporization of atherosclerotic plaques by spark erosion. *Journal of the American College of Cardiology*, *5*(6), 1382-1386.
- Slager, C. J., Wentzel, J. J., Schuurbiers, J. C., Oomen, J. A., Kloet, J., Krams, R., von Birgelen, C., van der Giessen, W. J., Serruys, P. W. & de Feyter, P. J. (2000). True 3-dimensional reconstruction of coronary arteries in patients by fusion of angiography and IVUS (ANGUS) and its quantitative validation. *Circulation*, *102*(5), 511-516.
- Smith, S. W., Trahey, G. E., Hubbard, S. M. & Wagner, R. F. (1988). Properties of acoustical speckle in the presence of phase aberration part II: correlation lengths. *Ultrasonic Imaging*, *10*(1), 29-51.
- Sonoda, S., Takeuchi, M., Nakashima, Y. & Kuroiwa, A. (1998). Safety and optimal dose of intracoronary adenosine 5'-triphosphate for the measurement of coronary flow reserve. *American Heart Journal*, *135*(4), 621-627.
- Spaan, J. A. E. (1991). Structure and function of the coronary arterial tree. In J. A. E. Spaan (Ed.), *Coronary blood flow: mechanics, distribution and control* (p. 37-67). Boston: Kluwer Academic Publishers.
- Spencer, T., Ramo, M. P., Salter, D. M., Anderson, T., Kearney, P. P., Sutherland, G. R., Fox, K. A. A. & McDicken, W. N. (1997a). Assessment of regional vascular distensibility in deceased iliofemoral arteries by intravascular ultrasound. *Ultrasound in Medicine and Biology*, *20*(6), 529-542.



- Spencer, T., Ramo, M. P., Slater, D. M., Anderson, T., Kearney, P. P., Sutherland, G. R., Fox, K. A. & McDicken, W. N. (1997b). Characterization of atherosclerotic plaque by spectral analysis of intravascular ultrasound: an *in vitro* study with histological and radiological validation. *Ultrasound in Medicine and Biology*, 23(2), 191-203.
- Stone, G. W., Hodgson, J. M., St. Goar, F. G., Frey, A., Mudra, H., Sheehan, H. & Linnermeier, T. J. (1997). Improved procedural results of coronary angioplasty with intravascular ultrasound-guided balloon sizing: the CLOUT Pilot Trial. *Circulation*, 95, 2044-2052.
- Strauer, B. E. (1990). The significance of coronary reserve in clinical heart disease. *Journal of the American College of Cardiology*, 15(4), 775-783.
- Sudhir, K., MacGregor, J. S., Barbant, S. D., Foster, E., Fitzgerald, P. J., Chatterjee, K. & Yock, P. G. (1993). Assessment of coronary conductance and resistance vessel reactivity in response to nitroglycerin, ergonovine and adenosine: *in vivo* studies with simultaneous intravascular two-dimensional and Doppler ultrasound. *Journal of the American College of Cardiology*, 21(5), 1261-1268.
- Sugawara, M. (1989). Stenosis: Theoretical background. In M. Sugawara, F. Kajiyama, A. Kitabatake & H. Matsuo (Eds.), *Blood flow in the heart and large vessels* (p. 91). Tokyo-Berlin-New York: Springer-Verlag.
- The GUIDE Trial Investigators. (1996). IVUS-determined predictors of restenosis in PTCA and DCA: final report from the GUIDE trial, phase II. *Journal of the American College of Cardiology*, 27(supplA), 156A.
- Thomas, A. C., Davies, M. J., Dilly, N. & et, a. l. (1986). Potential errors in the estimation of coronary arterial stenoses from clinical arteriography with reference to the shape of the coronary arterial lumen. *British Heart Journal*, 55, 129-139.
- Tobis, J. M., Mahon, D. J., Goldberg, S. L. & al., e. (1993). Lessons from intravascular ultrasonography: observations during interventional angioplasty procedures. *Journal of Clinical Ultrasound*, 21, 589-607.
- Tobis, J. M., & Yock, P. G. (Eds.). (1992). *Intravascular ultrasound imaging*. New York: Churchill Livingstone.
- Topol, E. J., Ellis, S. G., Cosgrove, D. M., Bates, E. R., Muller, D. W., Schork, N. J., Schork, M. A. & Loop, F. D. (1993). Analysis of coronary angioplasty practice in the united states with an insurance-claims data base. *Circulation*, 87(5), 1489-1497.

- Topol, E. J., & Nissen, S. E. (1995). Our preoccupation with coronary luminology: the dissociation between clinical and angiographic findings in ischemic heart disease. *Circulation*, *92*, 2333-2342.
- Toussaint, J. F., LaMuraglia, G. M., Southern, J. F., Fuster, V. & Kantor, H. L. (1996). Magnetic resonance images lipid, fibrous, calcified, hemorrhagic, and thrombotic components of human atherosclerosis *In vivo*. *Circulation*, *94*, 932-938.
- Uren, N. G., Melin, J. A., de Bruyne, B., Wijns, W., Baudhuin, T. & Camici, P. G. (1994). Relation between myocardial blood flow and the severity of coronary artery stenosis. *New England Journal in Medicine*, *330*, 1782-1788.
- Uren, N. G., Schwarzacher, S. P., Whitbourn, R., Hayase, M., Kernoff, R. S., Yeung, A., Fitzgerald, P. J. & Yock, P. G. (1997). Fractional vs coronary flow reserve: comparison of guidewire-based measurements of coronary stenosis. *Journal of the American College of Cardiology*, *29* (Suppl A), 125A.
- van der Heiden, M. S., de Kroon, M. G. M., Bom, N. & Borst, C. (1995). Ultrasound backscatter at 30 MHz from human blood: influence of rouleau size affected by blood modification and shear rate. *Ultrasound in Medicine and Biology*, *21*(6), 817-826.
- van der Steen, A. F. W., Céspedes, E. I., Carlier, S. G., Mastik, F., Lupotti, F. A., Borsboom, J. M. G., Li, W., Serruys, P. W. & Bom, N. (2000). Flow estimation using an intravascular imaging catheter. *Ultrasonics*, *38*(1-8), 363-368.
- van der Steen, A. F. W., Céspedes, E. I., de Korte, C. L., Carlier, S. G., Li, W., Mastik, F., Lancée, C. T., Borsboom, J. M. G., Lupotti, F. A., Krams, R., Serruys, P. W. & Bom, N. (1998a). Novel developments in intravascular imaging. *IEEE Ultrasonics Symposium*, *2*, 1733-1742.
- van der Steen, A. F. W., de Korte, C. L. & Céspedes, E. I. (1998b). Intravascular ultrasound elastography. *Ultraschall in Med.*, *19*(5), 196-201.
- van der Steen, A. F. W., Li, W., Céspedes, E. I., Carlier, S., Eberle, M., Verdouw, P. D., Serruys, P. W. & Bom, N. (1997). *In vivo* validation of blood flow estimation using the decorrelation of radiofrequency intravascular echo signals. *IEEE ultrasonics symposium*, 1247-1250.
- van Liebergen, R. A., Piek, J. J., Koch, K. T., Winter, R. J. de & Lie, K. I. (1998). Immediate and long-term effect of balloon angioplasty or stent implantation on the absolute and relative coronary blood flow velocity reserve. *Circulation*, *98*(20), 2133-2140.

- von Birgelen, C., Kutryk, M. J. B. & Serruys, P. W. (1998). Three-dimensional Intravascular Ultrasound Analysis of Coronary Stent Deployment and In-Stent Neointimal Volume: Current Clinical Practice and the Concepts of TRAPIST, ERASER, and ITALICS. *J Invas Cardiol*, 10(1), 17-26.
- Voudris, V., Manginas, A., Vassilikos, V., Koutelou, M., Kantzis, J. & Cokkinos, D. V. (1996). Coronary flow velocity changes after intravenous dipyridamole infusion: measurements using intravascular Doppler guide wire. A documentation of flow inhomogeneity. *Journal of the American College of Cardiology*, 27(5), 1148-1155.
- Wagner, R. F., Insana, M. F. & Smith, S. W. (1988). Fundamental correlation lengths of coherent speckle in medical ultrasonic images. *IEEE Transactions on Ultrasonics, Ferroelectrics, and Frequency Control*, 35(1), 34-44.
- Wagner, R. F., Smith, S. W., Sandrik, J. M. & Lopez, H. (1983). Statistic of speckle in ultrasound B-scans. *IEEE Transactions on Sonics and Ultrasonics*, 30(3), 156-163.
- Walker, R. D., Smith, R. E., Sherriff, S. B. & Wood, R. F. M. (1999). Time-averaged mean velocity for volumetric blood flow measurements: an *in vitro* model validation study using physiological femoral artery flow waveforms. *Ultrasound in Medicine and Biology*, 25(4), 577-582.
- Waller, B. F. (1989). Crackers, breakers, stretchers, drillers, scrapers, shavers, burners, welders and melters. The future treatment of atherosclerotic coronary artery disease. *Journal of the American College of Cardiology*, 13, 969-987.
- Wardeh, A. J., Albiero, R., Kay, I. P., Knook, A. H., Wijns, W., Kozuma, K., Nishida, T., Ferrero, V., Levendag, P. C., van der Giessen, W. J., Colombo, A. & Serruys, P. W. (2002). Angiographical follow-up after radioactive "cold ends" stent implantation: a multicenter trial. *Circulation*, 105(5), 550-553.
- Wellnhofer, E., Wahle, A., Mugaragu, I. & et, a. l. (1999). Validation of an accurate metho for three-dimensional reconstruction and quantitative assessment of volumes, lengths and diameters of coronary vascular branches and segments from biplane angiographic projections. *Int J Card Imaging*, 15, 339-353.
- Wendling, F., Jones, S. A. & Giddens, D. P. (1992). Simulation of Doppler ultrasound signals for a laminar, pulsatile, nonuniform flow. *Ultrasound in Medicine and Biology*, 18(2), 179-193.

- Weng, X., Cloutier, G., Beaulieu, R. & Roederer, G. O. (1996). Influence of acute-phase proteins on erythrocyte aggregation. *American Journal of Physiology*, *271* (*Heart Circ. Physiol.* *40*), H2346-H2352.
- Weng, X., Roederer, G. O., Beaulieu, R. & Cloutier, G. (1998). Contribution of acute-phase proteins and cardiovascular risk factors to erythrocyte aggregation in normolipidemic and hyperlipidemic individuals. *Thromb Haemost*, *80*, 903-908.
- Wentzel, J. J., Krams, R., van der Steen, A. F. W., Li, W., Céspedes, E. I., Bom, N. & Slager, C. J. (1997). Disturbance of 3D velocity profiles induced by an IVUS catheter evaluation with computational fluid dynamics. *Computers in Cardiology*, *24*, 597-599.
- White, C. W., Wright, C. B., Doty, D. B., Hiratza, L. F., Eastham, C. L., Harrison, D. G. & Marcus, M. L. (1984). Does visual interpretation of the coronary arteriogram predict the physiologic importance of a coronary stenosis? *New England Journal in Medicine*, *310*(13), 819-824.
- Whorlow, R. W. (1980). *Rotational viscometers*. Chichester: Ellis Horwood Ltd.
- Wilson, R. F., Laughlin, D. E., Ackell, P. H. & al. et. (1985). Transluminal, sub-selective measurement of coronary artery blood flow velocity and vasodilator reserve in man. *Circulation*, *72*, 82.
- Wilson, R. F., Marcus, M. L. & White, C. W. (1987). Prediction of the physiologic significance of coronary arterial dimensions by quantitative lesion geometry in patients with limited coronary artery disease. *Circulation*, *75*, 723-732.
- Wilson, R. F., & White, C. W. (1986). Intracoronary papaverine: An ideal coronary vasodilator for studies of the coronary circulation in conscious humans. *Circulation*, *73*, 444.
- Wilson, R. F., Wyche, K., Christensen, B. V., Zimmer, S. & Laxson, D. D. (1990). Effects of adenosine on human coronary circulation. *Circulation*, *82*(5), 1595-1606.
- Worthley, S. G., Helft, G., Fuster, V., Fayad, Z. A., Fallon, J. T., Osende, J. I., Roque, M., Shinnar, M., Zaman, A. G., Rodriguez, O. J., Verhallen, P. & Badimon, J. J. (2000). High resolution *ex vivo* magnetic resonance imaging of *in situ* coronary and aortic atherosclerotic plaque in a porcine model. *Atherosclerosis*, *150*(2), 321-329.
- Wright, C. B., Doty, D. B. & Eastham, C. L. (1980). Measurement of coronary reactive hyperemia with a Doppler probe: Intraoperative guide to hemody-

- namically significant lesions. *Journal of Thoracic Cardiovascular Surgery*, 80, 888.
- Yock, P. G., & Linker, D. T. (1990). Intravascular ultrasound. Looking below the surface of vascular disease. *Circulation*, 81(5), 1715-1718.
- Zagzebski, J. A., Madsen, E. L. & Goodsitt, M. M. (1985). Quantitative tests of a three-dimensional model for gray-scale texture. *Ultrasound Imaging*, 7(3), 252-263.
- Zannad, F., Voisin, P., Brunotte, F., Bruntz, J. F., Stoltz, J. F. & Gilgenkrantz, J. M. (1988). Haemorheological abnormalities in arterial hypertension and their relation to cardiac hypertrophy. *Journal of Hypertension*, 6(4), 293-297.



# Summary

Intravascular ultrasound (IVUS) has been used for many purposes as it provides real-time cross-sectional images of blood vessels at a high-resolution. Radio Frequency (RF)-data processing has significantly enhanced the potential of IVUS and aims now at obtaining information concerning vessel wall and mechanical plaque properties. In addition, IVUS has been applied to measure blood velocity and volumetric blood flow. To measure blood flow a burst of ultrasound signals is emitted, transverse to the blood flow. The decorrelation of the RF-signals in this burst has proven to be proportional to the transverse blood flow velocity. The principle of blood flow assessment is based on lateral decorrelation, which depends on the beam profile of the transducer. More specifically, decorrelation is related to the auto-convolution of the acoustical beam in the direction of blood flow. All information can be obtained from regular cross-sectional IVUS RF signals.

The technique was initially implemented using an IVUS rotating single element catheter; however, the use of mechanically rotated transducer to measure flow requires compensation for the intrinsic decorrelation due to rotation. This could be cumbersome if the rotation is not uniform. The use of array technology in IVUS applications removes this limitation in the intravascular measurements of blood flow. This thesis describes the development and evaluation of the correlation-based technique for blood velocity estimation as has been implemented for an IVUS array catheter. The technique was evaluated by computer modeling, *in vitro* and in animal measurements. Preliminary results from patient recordings demonstrate the potential of quantitative IVUS blood flow in the clinical environment. The usefulness and additional diagnostic value of this technique are also described in this thesis.

As a first step of this study, the characteristics of the acoustical beam from the IVUS array catheter for measuring transverse blood velocity and quantitative blood flow were investigated by means of computer simulations. First, the decorrelation patterns for a scattering medium formed by single red blood cells (RBCs) and aggregates of RBCs were studied and compared with the auto-convolution of the acoustical beam. This auto-convolution of the acoustical beam is used as a reference curve. The RF decorrelation patterns were in agreement with the

reference curve when the scattering medium was formed by single RBCs and, by a more realistic situation, aggregates of RBCs at random angles and lengths. However, when aggregates of RBCs were aligned with the flow, the decorrelation pattern showed to be influenced by the length of the aggregates. The longer the aggregates of RBCs the lower the rate of decorrelation; this would result in an underestimation of the blood flow velocity

The influence on the correlation-based method by blood velocity profiles such as random spread of flow, linear velocity gradients and parabolic flow was also studied by means of computer simulations. This study was performed for the RF and envelope signals and for transverse and axial flow. For the RF and envelope signals, transverse blood flow is not significantly influenced by random spread of flow velocity, linear velocity gradient or parabolic flow. Similar results were found for axial flow and for the RF signals when random spread flow was considered. However, the envelope mean decorrelation pattern for axial spread of blood velocity was faster than the one for axial plug flow.

The correlation-based method is highly influenced by the presence of noise in the RF signals. Correction for noise is crucial for measuring intravascular transverse blood flow; if no correction for noise is applied, an overestimation of the blood velocity will occur. The noise within the RF signals is system-dependent and band-limited, which has an impact on the shape of the correlation function especially the correlation coefficients at lag 0. A new method for noise correction is presented in this study, which is easy to implement and computationally not time consuming. The method uses the fact that the correlation pattern should be 1 at lag 0; however, when noise is present in the RF signals a correlation value smaller than 1 is observed. By fitting a curve through the data, the effect of noise on the decorrelation is determined. Since the decorrelation due to noise was estimated and corrected per window, the noise correction method is dynamic and not dependent on previous measurements.

The ring-down of the IVUS catheter (formed by ultrasound reverberations from the array transducer) and the influence of the catheter eccentricity were studied by means of numerical simulation. The ring-down obscures a part of the vessel lumen and affects the blood flow measurements; the level of obscuring is dependent on the ring-down length and on the eccentricity of the IVUS catheter -as defined as the distance between the center of the lumen and the center of the IVUS catheter divided by the radius of the lumen-. A method, was derived to estimate the blood flow that cannot be measured in the ring-down, assuming a parabolic blood flow profile. The results showed that this method can correct for the ring-down artifact.

A calibration for the correlation-based method is needed in order to convert the correlation coefficients as a function of time into blood velocity (*e.g.* cm/sec). Therefore, measurements of the acoustical beam from several IVUS array catheters were performed to produce the calibration file. A Gaussian fit



of the auto-convolution of the acoustical beam was used as a calibration of the method. To evaluate the correction for noise and ring-down obscuring methods, and the calibration of the technique, IVUS blood flow measurements were performed using a flow setup in a controlled environment. Human blood and a tissue mimicking flow phantom were used during the experiments. These results showed that after correction for noise and ring-down, and using the calibration as produced by a Gaussian fit, the blood flow can be estimated well.

The influence of linear blood velocity gradient and aggregation of RBCs on the correlation-based method was studied using a Couette system and whole human blood from healthy and patient volunteers. Changing the shear rate of the Couette system modified the level of aggregation of RBCs. The experiments, using washed RBCs, revealed that linear velocity gradients will not influence the velocity estimation using the correlation-based method. *In vitro* results from aggregation of RBCs also showed close agreements between the mean decorrelation pattern and the theoretical values at all shear rates, for the normal and disease blood groups, except during very low shear rates (1 and 5 s<sup>-1</sup>) and for high aggregating blood (*i.e.* large aggregates of RBCs)

IVUS quantitative blood flow measurements were also performed in Yorkshire pigs using the correction for noise and ring-down, the mean auto-convolution of the acoustical beam was used as a calibration. These experiments showed the correlation-based method capable to measure quantitative volume blood flow *in vivo*, which means blood flow measurements performed in an artery, under pulsatile flow, and the inevitable motion of the catheter due to breathing and heart beating (from 100 to 120 beats/min).

Finally, the technique was advanced to coronary application in patients. Absolute coronary blood flow is the optimal parameter for intracoronary physiological studies. Quantitative IVUS blood flow is up to now the only technique capable to measure the blood velocity and vessel lumen area at the same cross-section simultaneously, to produce blood flow. Furthermore, mean blood flow per cardiac cycle can be calculated and used for other purposes such as Coronary Flow Reserve (CFR), which is a useful index to evaluate the outcome of an intervention such as a stent implantation. CFR is estimated from the ratio of the maximum flow at peak hyperemia to the baseline flow. The hyperemia is induced by the injection of adenosine. Results for CFR practiced in patients based on IVUS blood flow measurements showed a good relationship when compared to those based on Doppler blood velocity measurements. The results presented in this thesis demonstrated the feasibility of IVUS blood flow to be applied in a clinical environment.



# Samenvatting

Intravasculair ultrageluid (IVUS) wordt voor vele doeleinden gebruikt, omdat het doorsnedebeelden van bloedvaten levert met een hoge resolutie. De verwerking van Radio Frequentie (RF) data heeft de toepassingsmogelijkheden van IVUS in belangrijke mate uitgebreid en richt zich nu op het verkrijgen van informatie over de pathologische toestand van de vaatwand en de mechanische eigenschappen van plaque. Verder wordt IVUS gebruikt om bloedstroomsnelheid te meten en volumetrische bloeddorstroming. Om blood flow te meten wordt een serie ultrageluidssignalen uitgezonden loodrecht op de bloedstroom. De decorrelatie van de RF-signalen is proportioneel aan de transversale bloedstroomsnelheid. Het principe van schatting van de bloeddorstroming is gebaseerd op laterale decorrelatie, welke afhangt van het bundelprofiel van de gebruikte transducent. Meer specifiek is decorrelatie gerelateerd aan auto-convolutie van de geluidsbundel in de richting van de bloedstroom. Alle informatie kan verkregen worden uit RF-signalen van normale IVUS dwarsdoorsneden. Aanvankelijk werd bij deze techniek een catheter met een enkel roterend element gebruikt. Echter, toepassing van een mechanisch aangedreven roterende catheter voor het vaststellen van de bloeddorstroming vereist compensatie voor de door die rotatie veroorzaakte decorrelatie. Dit kan lastig zijn als de rotatie niet uniform is. Het gebruik van array technologie bij IVUS toepassingen heft deze beperking bij het intravasculair meten van de blood flow op.

Dit proefschrift beschrijft ontwikkeling en evaluatie van de op decorrelatie gebaseerde techniek voor het berekenen van de bloedsnelheid met gebruik van een IVUS array catheter. De techniek is geëvalueerd aan de hand van computermodellen, *in vitro* en in proefdieren. Eerste resultaten van opnamen in patiënten tonen de waarde voor de kliniek aan van kwantitatieve schatting met IVUS van de bloeddorstroming. Het nut en de toegevoegde diagnostische waarde worden ook in dit proefschrift beschreven.

Als eerste stap in deze studie werden door middel van computersimulaties de eigenschappen bestudeerd van de geluidsbundel van de IVUS array catheter bij het meten van de transversale bloedstroomsnelheid en de kwantitatieve bloeddorstroming. Eerst werden de decorrelatiepatronen van een reflecterend medium, gevormd door enkelvoudige rode bloedcellen (RBC's), en van een aggregaat van

RBC's bestudeerd en vergeleken met de auto-convolutie van de geluidsbundel, welke laatste als referentiecurve werd gebruikt. De RF decorrelatiepatronen kwamen overeen met de referentiecurve wanneer het reflecterende medium gevormd werd door enkelvoudige RBC's en, in een meer realistische situatie, wanneer het aggregaten van RBC's betrof met een willekeurige lengte en onder een willekeurige hoek. Wanneer de lengterichting van de RBC aggregaten echter overeenkwam met de stroomrichting van het bloed, bleek het decorrelatiepatroon beïnvloed door de lengte van het aggregaat. Hoe langer het aggregaat, des te lager de decorrelatie. Dit resulteert in een onderschatting van de bloedstroomsnelheid.

De invloed op de correlatiemethode van bloedsnelheidsprofielen zoals willekeurige spreiding van de stroomsnelheid, lineaire snelheidsgradienten en parabolische stroomsnelheid werd ook bestudeerd door middel van computersimulaties. Deze studie werd gedaan voor de RF- en videosignalen en voor transversale en axiale bloedstroom. Voor wat betreft de RF- en videosignalen, werd de transversale bloedstroom niet significant beïnvloed door willekeurige spreiding van de stroomsnelheid, een lineaire snelheidsgradient of een parabolisch stroomprofiel. Een dergelijk resultaat werd ook gevonden voor de axiale stroomsnelheid en voor de RF-signalen wanneer willekeurig gespreide stroomsnelheid in aanmerking werd genomen. Het gemiddelde decorrelatiepatroon van het videosignaal was echter bij axiale spreiding van de bloedstroomsnelheid sneller dan bij axiale propstrooming.

De op decorrelatie gebaseerde methode wordt sterk beïnvloed door de aanwezigheid van ruis in de RF-signalen. Correctie voor ruis is uitermate belangrijk bij het intravasculair meten van transversale bloedstroomsnelheid. Als er niet wordt gecorrigeerd voor ruis, wordt die snelheid overschat. De ruis in het RF-signaal is systeem-afhankelijk en beperkt door de bandbreedte, hetgeen van invloed is op de vorm van de correlatie-functie, vooral op de correlatie-coëfficiënten bij interval 0. In deze studie wordt een nieuwe methode gepresenteerd voor het corrigeren van ruis, welke gemakkelijk is te implementeren en weinig computertijd vergt. Deze methode maakt gebruik van het feit dat de correlatie 1 zou moeten zijn bij interval 0; echter, als er ruis aanwezig is in het RF-signaal, wordt een waarde kleiner dan 1 waargenomen. Door de datapunten door middel van een curve te verbinden, wordt het effect van ruis op de decorrelatie vastgesteld. Aangezien de door ruis veroorzaakte decorrelatie per venster werd geschat en gecorrigeerd, is deze methode om ruis te corrigeren dynamisch en niet afhankelijk van eerdere metingen.

Ring-down van de IVUS catheter (gevormd door reverberatie van het ultrageluid uit de array transducer) en de invloed van een eccentriche positie van de catheter werden bestudeerd door middel van numerieke simulatie. Door de ring-down kan uit een deel van het vaatlumen geen signaal ontvangen worden. Dit is dus van invloed op de bloedstroommeting. De mate waarin geen signalen ontvangen kunnen worden is afhankelijk van de lengte van de ring-down en van de eccentriciteit van de IVUS catheter, gedefinieerd als de afstand tussen het

middelpunt van het lumen en het middelpunt van de catheter, gedeeld door de straal van het lumen. Een methode, waarbij het bloedstroomprofiel parabolisch werd verondersteld, werd afgeleid om een indruk te krijgen van de bloedstroom die tijdens de ring-down niet kan worden gemeten. De resultaten toonden aan, dat deze methode kan corrigeren voor het ring-down artefact.

Om de correlatiecoëfficiënten als functie van de tijd te herleiden tot bloedstroomsnelheid (in b.v. cm/s) is een calibratie nodig. Om een calibratiebestand op te bouwen, werden metingen gedaan aan de geluidsbundels van verscheidene IVUS array catheters. Een fit van de auto-convolutie van de geluidsbundel in een Gauss-curve werd gebruikt als calibratie voor de methode. Om de correctie voor ruis en ring-down en de calibratie van de methode te evalueren, werden er IVUS bloeddorstromingsmetingen gedaan, waarbij gebruik werd gemaakt van een flow opstelling in een gecontroleerde omgeving. Bij deze experimenten werden menselijk bloed en een zich als weefsel gedragend fantoom gebruikt. De resultaten lieten zien dat na correctie voor ruis en ring-down, en gebruik makende van de calibratie verkregen door inpassing in een Gauss-curve, de bloeddorstroming goed geschat kan worden.

De invloed van een lineaire bloedsnelheidsgradient en aggregatie van RBC's op de op correlatie gebaseerde methode werd bestudeerd met gebruikmaking van een Couette systeem en onbewerkt menselijk bloed, vrijwillig afgestaan door gezonde proefpersonen en patiënten. Verandering van de afschuifspanning van het Couette systeem veranderde ook de mate van aggregatie van de RBC's. De experimenten, waarbij gewassen RBC's werden gebruikt, maakten duidelijk dat lineaire snelheidsgradiënten de correlatie-gebaseerde snelheidsschatting niet beïnvloeden. *In vitro* resultaten voor aggregatie van RBC's lieten ook grote overeenkomst zien tussen het gemiddelde decorrelatiepatroon en alle theoretische waarden van de afschuifspanning, zowel voor het bloed van de normalen als van de patiënten, behalve bij zeer lage afschuifspanning ( $1$  en  $5 \text{ s}^{-1}$ ) en voor sterk geaggregeerd bloed (d.w.z. grote aggregaten van RBC's).

IVUS kwantitatieve bloedstroommetingen werden ook gedaan in Yorkshire varkens met correctie voor ruis en ring-down; de gemiddelde auto-convolutie van de geluidsbundel werd gebruikt als calibratie. Deze experimenten toonden aan dat met de op correlatie gebaseerde methode kwantitatieve volumetrische bloeddorstromingsmetingen *in vivo* mogelijk zijn en dus ook in een slagader met pulserende bloedstroom en de onvermijdelijke beweging van de catheter veroorzaakt door ademhaling en hartslag (van 100 tot 120 slagen per minuut).

Tenslotte werd de techniek ook toegepast in de coronairarteriën van patiënten. Absolute coronaire bloeddorstroming is de optimale parameter voor intracoronaire fysiologische studies. Kwantitatieve benadering met IVUS van de bloeddorstroming is tot nu toe de enige techniek die in staat is tegelijkertijd de bloedstroomsnelheid en de oppervlakte van dezelfde dwarsdoorsnede van het vat te meten, waardoor bloedstroomsnelheidsmeting mogelijk wordt.

Voorts kan de gemiddelde bloedstroom per hartcyclus worden berekend en gebruikt voor andere doeleinden zoals Coronary Flow Reserve (CFR), een nuttige index om het resultaat van een interventie, zoals een stent implantatie, te beoordelen. CFR is de verhouding van de bloeddorstrooming bij piekbelasting en die in rust. De verhoogde belasting wordt opgewekt door een injectie met adenosine. Resultaten voor CFR toegepast in patiënten en gebaseerd op IVUS metingen van de bloeddorstrooming toonden een goede overeenkomst bij vergelijking met Doppler bloedsnelheidsmetingen. De in dit proefschrift gepresenteerde uitkomsten tonen de bruikbaarheid van IVUS bloeddorstroomingsmetingen voor toepassing in de kliniek.

# Acknowledgements

In January 1998, I was given the opportunity to join in the Experimental Echocardiography department as a visitor for a period of 6 months. A brand new, and the fastest, computer was given to me. I was really impressed by the laboratory and how things were organized. In the mean time, I realized that this was the opportunity to chase my Ph.D. degree.

*Prof. N. Bom*, as my promotor, I would like to thank you for your support on my research and I must congratulate you for the laboratory you have created and conducted over the past 30 years and how you pushed the Experimental Echocardiography lab to the leading edge of research in ultrasound.

*Prof. A.F.W. van der Steen*, "Ton", my supervisor and promotor, thanks for giving me the chance to obtain my Ph.D. degree. Your constant support on my research and planning of my publications as well as the reviewing of manuscripts were very important to accomplish my Ph.D. degree. Thanks for being such a nice person not only inside but also outside work.

I would like to specially thank *E. Ignacio Céspedes*, who introduced me to *Prof. A.F.W. van der Steen* that 3<sup>rd</sup> of September 1997 in Buenos Aires and pushed him to bring me to Rotterdam. That 3<sup>rd</sup> of September made a turn on my life that I will never forget. *Ignacio*, although we worked together for only 6 months, I learned a lot from you and our friendship grew fast and still grows.

*Chris L. de Korte*, thanks for your brilliant ideas and for your help on improving the quality of my papers as well as for fixing my tax forms (I still own you the 10% commission for that). I learned from you an important Dutch custom: "planning to go on holidays, so then visit a friend". *Peter J. A. Frinking*, thanks for being my official translator and supporter as well as for letting me to taste the "fantastisch" Dutch food, the famous "boerenkool met worst".

*Frits Mastik*, we have been working closely together for the last 3 years to make the volume blood flow using the IVUS array catheter true. This has resulted

in a significant contribution to this thesis from your part. *Stephane G. Carlier*, you gave us the opportunity to perform patient recordings in the catheterization laboratory as well as help on performing the *in vitro* and in animal measurements. Thanks for trust on my skills to make volume blood flow method actually work (as you said it in your thesis).

Special thanks to *Prof. Patrick W. Serruys*, *Dr. Pim de Feyter*, and *Dr. Willem J. van der Giessen* from the Interventional Cardiology department, Thoraxcenter, that also allowed us to perform the patient recordings as well as for the help from *Jurgen Lighart*, *Emile Onderwater*, *Guio Matrijk*, and the rest of the team.

*Ayache Bouakaz* and *Peggy Palanchon*, thanks for improving my international taste with those burning *Ayache's* buffalo wings and Couscous, and for the delicious *Peggy's* French cuisine. I want to acknowledge the help of *Charles T. Lancée*, who was always ready to give me a hand with the correlation-based method for blood velocity estimation. *Jan Honkoop*, as our specialist on sexing babies using ultrasound, thanks for the help in all electronics.

*Frans van Egmond*, thanks for keeping my computer as new as possible and for organizing those exciting lab days, which nobody knows where we go and where the weather is also a surprise. The more recent help from *Roland van Lindt* on computer problems was also very helpful. *Leo Bekkering* and *Wim van Alphen*, thanks for taking care of all technical developments related to *in vitro* measurements.

*Nico de Jong*, *Michiel Postema*, *Annemieke van Wamel*, "*Cash*" *Chien Ting Chin*, *Jerome Borsboom*, *Martijn Frijlink*, *Marco Voormolen*, *Boudewijn Krenning*, *Egon Merks*, *Antoinette ten Have* and *Fokko P. Wieringa*, thanks for teaching us new techniques on contrast imaging, intravascular ultrasound, 3D imaging and thermography.

*Johannes A. Schaar*, we had interesting discussions about our friends in common, thanks for being a volume blood flow believer. *Radj A. Baldewsing*, keep on collecting ADV hours so then take a sabbatical year; finally after 2 years of waiting you could take over my desk in the lab. *Marvin M. Doyley*, my brother, since you left, the lab has no sticky chairs and no spot of coffee is found on the floor (this is now boring).

I sincerely thank *Ms. Corrie Eefting* (muchas gracias por todo) and *Ms. Riekje Daane*, for their assistance in preparing so many documents such as application forms and letters, during my Ph.D..



I acknowledge *Prof. P.D. Verdouw* and *Dr. D. Duncker*, and the group from the Experimental Echocardiology department, *Elza van Deel*, *Maarten Punt*, *Ilona Peters*, *Miranda Hartevelde*, *Rob van Bremen*, *Helene van Beusekom* and many others, for their support in carrying out animal experiments.

I would like to thank *Prof. G. Cloutier* and his group, *Audrey Zimmer*, *Michel Daronat* and *Isabelle Fontaine*, from the University of Montreal, Montreal, Canada for giving me an excellent opportunity to perform the *in vitro* experiments on aggregation of red blood cells and shear rate described in this thesis.

Well, to all the Exp. Echo. group, nothing can explain how grateful I feel, and hope that all working places are as nice and comfortable as this one.

I would like to thank the teachers from the Faculty of Engineering, Bioengineering, from the National University of Entre Ríos, Argentina, who put all their efforts on teaching everything they know to the students.

At last but not least, I especially thank my wife, *María*, for her full support and for leaving everything she had to follow me. To my parents who are always interested in my work and to whom I owe everything.



# Curriculum Vitae

Fermín Armando Lupotti was born in October 14, 1969 in Santa Fe, Argentina. He completed his high school education at the La Salle Jobson, Santa Fe, Argentina. He went to the Faculty of Engineering, Bioengineering, National University of Entre Ríos, Argentina, where he obtained his M.Sc. degree in Biomedical Engineering. His graduation project was carried out at the department of Images in Medicine from the Faculty of Engineering. The topic of his graduation project was "Digital Processing of Ultrasound Images and 3D Reconstruction of the Vascular System".

In January 1998, he came to the Experimental Echocardiography Department at the Erasmus University Rotterdam, the Netherlands, headed by Prof. dr. ir. N. Bom, as a visiting guest for a period of 6 months. The same year he started his Ph.D. at the same department under the supervision of Prof. dr. ir. A.F.W. van der Steen. Since then he is employed by the Interuniversity Cardiology Institute of the Netherlands (ICIN) as a researcher and has been participating in the Intravascular Ultrasound project supported by ICIN 18 and 32.



# List of Publications

## International publications

- S. G. Carlier, G. van Langenhove, F. A. Lupotti, M. Albertal, F. Mastik, N. Bom, and P. S. Serruys, "Coronary Flow Reserve versus Geometric Measurements of Coronary Dimensions: Advantages and Limitations of the Functional Stenosis Assessment", *Journal of Interventional Cardiology*, vol. 12, pp. 411-424, 1999.
- A. F. W. van der Steen, E. I. Céspedes, S. G. Carlier, F. Mastik, F. A. Lupotti, J. M. G. Borsboom, W. Li, P. W. Serruys, and N. Bom, "Flow estimation using an intravascular imaging catheter", *Ultrasonics*, vol. 38, Issue 1-8, pp. 363-368, 2000.
- F. A. Lupotti, E. I. Céspedes, and A. F. W. van der Steen, "Decorrelation Characteristics of Transverse Blood Flow along an Intravascular Array Catheter," *IEEE Transactions on Ultrasonics, Ferroelectrics, and Frequency Control*, vol. 47, No. 6, pp. 1582-1592, 2000.
- F. A. Lupotti, E. I. Céspedes, and A. F. W. van der Steen, "Decorrelation Characteristics of Transverse Blood Flow along an Intravascular Array Catheter: Effects of Aggregation of Red Blood Cells," *Ultrasound in Medicine and Biology*, Vol. 27, No. 3, pp. 409-417, 2001.
- F. A. Lupotti, A. F. W. van der Steen, F. Mastik and C. L. de Korte, "Decorrelation-based Blood Flow Velocity estimation: Effect of Spread of Flow Velocity, Linear Flow Velocity Gradients, and Parabolic Flow," *IEEE Transactions on Ultrasonics, Ferroelectrics, and Frequency Control*, Vol. 49, No. 6, pp. 705-714, 2002.
- F. A. Lupotti, E. I. Céspedes, F. Mastik and A. F. W. van der Steen, "IVUS Flow measurements: Line Spread Function and Decorrelation Pattern", *Ultrasonics*, Vol. 40, pp. 843-847, 2002.

- F. A. Lupotti, F. Mastik, C. L. de Korte and A. F. W. van der Steen, "Dynamic Noise Suppression for Transverse Blood Flow: Methods and numerical validation", *accepted for publication in Ultrasound in Medicine and Biology*, 2002.
- F. A. Lupotti, F. Mastik, C. L. de Korte, S. G. Carlier, W. J. van der Giessen, P. W. Serruys and A. F. W. van der Steen, "Quantitative IVUS Blood Flow: Validation *in vitro*, in animals and in patients", *Ultrasound in Medicine and Biology*, *submitted*, 2002.
- F. A. Lupotti, A. Zimmer, M. Daronat, F. S. Foster, A. F. W. van der Steen and G. Cloutier, "Effects of Aggregation of Red Blood Cells and Linear Velocity Gradients on the Correlation-based method for Quantitative IVUS Blood Flow at 20 MHz", *Ultrasound in Medicine and Biology*, *submitted*, 2002.

## Award

- F. A. Lupotti, F. Mastik, S. G. Carlier, E. I. Céspedes, A. F. W. van der Steen, "Quantitative IVUS Blood Flow using an Array Catheter", finalist of the *Rosanna Degani Young Investigator Award*, *Computers in Cardiology*, *Rotterdam, The Netherlands*, 2001.

## Conference proceedings

- A. F. W. van der Steen, E. I. Céspedes, C. L. de Korte, S. G. Carlier, W. Li, F. Mastik, C. T. Lancée, J. M. G. Borsboom, F. A. Lupotti, R. Krams, P. W. Serruys, and N. Bom, "Novel developments in Intravascular Imaging," *IEEE Ultrasonics Symposium, Japan*, Vol. 2, pp. 1733-1742, 1998.
- F. A. Lupotti, E. I. Céspedes, and A. F. W. van der Steen, "Computer Modelling of Decorrelation Patterns of Transverse Blood Flow", *IEEE Ultrasonics Symposium, Lake Tahoe, USA*, Vol. 2, pp. 1485-1488, 1999.
- F. A. Lupotti and A. F. W. van der Steen, "Computer Modeling of Spread of Blood-Flow Velocity and Blood-Flow Velocity Gradients during Transverse Blood Flow along an Intravascular Array Catheter", *IEEE Ultrasonics Symposium, San Juan de Puerto Rico, Puerto Rico*, Vol. 2, pp. 1465-1468, 2000.
- F. A. Lupotti, F. Mastik, S. G. Carlier, E. I. Céspedes, A. F. W. van der Steen, "Quantitative IVUS Blood Flow using an Array Catheter", *Computers in Cardiology, Rotterdam, The Netherlands*, Vol. 28, pp. 5-8, 2001.

- F. A. Lupotti, F. Mastik, C. L. de Korte and A. F. W. van der Steen, "IVUS Transverse Blood Flow: Dynamic Noise Suppression", *IEEE Ultrasonics Symposium, Atlanta, USA*, Vol. 2, pp. 1457-1460, 2001.
- F. A. Lupotti, A. Zimmer, M. Daronat, F. S. Foster, A. F. W. van der Steen and G. Cloutier, "Experiments on Effects of Aggregation of Red Blood Cells and Linear Velocity Gradients on Decorrelation-based Transverse Blood Flow Estimation", *IEEE Ultrasonics Symposium, Munich, Germany*, 2002.
- A.F.W. van der Steen, C.L. de Korte, F. Mastik, F.A. Lupotti, J.A. Schaar, E.I. Céspedes, C.J. Slager, C.T. Lancée, P.W. Serruys, N. Bom, "Intravascular Ultrasound Probes and Their Clinical Applications" *IEEE Ultrasonics Symposium, Munich, Germany*, 2002.

## Conference abstracts

- J. Borsboom, E. I. Céspedes, A. F. W. van der Steen, F. A. Lupotti, and E. F. Deprettere, "Simulation of a miniature cylindrical array transducer for transcatheter imaging," *23rd International Symposium on Ultrasonic Imaging and Tissue Characterization, Arlington-Virginia, USA*, 1998.
- A. F. W. van der Steen, E. I. Céspedes, C. L. de Korte, S. G. Carlier, W. Li, F. Mastik, C. T. Lancée, J. M. G. Borsboom, F. A. Lupotti, R. Krams, P. W. Serruys, and N. Bom, "Novel developments in intravascular imaging," *IEEE Ultrasonics Symposium, Japan*, 1998.
- F. A. Lupotti, E. I. Céspedes, and A. F. W. van der Steen, "Computer modeling of decorrelation patterns of transverse blood flow", *IEEE Ultrasonics Symposium, Lake Tahoe, USA*, 1999.
- F. A. Lupotti and A. F. W. van der Steen, "Computer Modeling of Spread of Blood-Flow Velocity and Blood-Flow Velocity Gradients during Transverse Blood Flow along an Intravascular Array Catheter", *IEEE Ultrasonics Symposium, San Juan de Puerto Rico, Puerto Rico*, 2000.
- S. G. Carlier, F. A. Lupotti, F. Mastik, A. F. W. van der Steen, N. Bom, P. W. Serruys, "In vitro validation of coronary flow reserve measurement with a array IVUS transducer", *European Society of Cardiology, Stockholm, Sweden*, Vol. 22, p. 239, 2001.
- F. A. Lupotti, E. I. Céspedes, F. Mastik and A. F. W. van der Steen, "IVUS Flow measurements: Line Spread Function and Decorrelation Pattern along an Intravascular Array Catheter", *Ultrasonics International, Delft, The Netherlands*, 2001.

- F. A. Lupotti, F. Mastik, S. G. Carlier, E. I. Céspedes, A. F. W. van der Steen, "Quantitative IVUS Blood Flow using an Array Catheter", *Computers in Cardiology, Rotterdam, The Netherlands*, 2001.
- F. A. Lupotti, F. Mastik, C. L. de Korte and A. F. W. van der Steen, "Dynamic Noise Suppression in Blood during Measurement of Transverse Blood Flow along an Intravascular Array Catheter", *IEEE Ultrasonics Symposium, Atlanta, USA*, 2001.
- F. A. Lupotti, A. Zimmer, M. Daronat, F. S. Foster, A. F. W. van der Steen and G. Cloutier, "Experiments on Effects of Aggregation of Red Blood Cells and Linear Velocity Gradients on Decorrelation-based Transverse Blood Flow Estimation", *IEEE Ultrasonics Symposium, Munich, Germany*, 2002.
- A.F.W. van der Steen, C.L. de Korte, F. Mastik, F.A. Lupotti, J.A. Schaar, E.I. Céspedes, C.J. Slager, C.T. Lancée, P.W. Serruys, N. Bom, "Intravascular Ultrasound Probes and Their Clinical Applications" *IEEE Ultrasonics Symposium, Munich, Germany*, 2002.